

Process Oscillations in Continuous Ethanol Fermentation
with *Saccharomyces cerevisiae*

by
Fengwu Bai

A thesis
presented to the University of Waterloo
in fulfillment of the
thesis requirement for the degree of
Doctor of Philosophy
in
Chemical Engineering

Waterloo, Ontario, Canada, 2007

© Fengwu Bai, 2007

I hereby declare that I am the sole author of this thesis. This is a true copy of the thesis, including any required final revisions, as accepted by my examiners.

I understand that my thesis may be made electronically available to the public.

Fengwu Bai

ABSTRACT

Based on ethanol fermentation kinetics and bioreactor engineering theory, a system composed of a continuously stirred tank reactor (CSTR) and three tubular bioreactors in series was established for continuous very high gravity (VHG) ethanol fermentation with *Saccharomyces cerevisiae*. Sustainable oscillations of residual glucose, ethanol, and biomass characterized by long oscillation periods and large oscillation amplitudes were observed when a VHG medium containing 280 g l⁻¹ glucose was fed into the CSTR at a dilution rate of 0.027 h⁻¹. Mechanistic analysis indicated that the oscillations are due to ethanol inhibition and the lag response of yeast cells to ethanol inhibition.

A high gravity (HG) medium containing 200 g l⁻¹ glucose and a low gravity (LG) medium containing 120 g l⁻¹ glucose were fed into the CSTR at the same dilution rate as that for the VHG medium, so that the impact of residual glucose and ethanol concentrations on the oscillations could be studied. The oscillations were not significantly affected when the HG medium was used, and residual glucose decreased significantly, but ethanol maintained at the same level, indicating that residual glucose was not the main factor triggering the oscillations. However, the oscillations disappeared after the LG medium was fed and ethanol concentration decreased to 58.2 g l⁻¹. Furthermore, when the LG medium was supplemented with 30 g l⁻¹ ethanol to achieve the same level of ethanol in the fermentation system as that achieved under the HG condition, the steady state observed for the original LG medium was interrupted, and the oscillations observed under the HG condition occurred. The steady state was gradually restored after the original LG medium replaced the modified one. These experimental results confirmed that ethanol, whether produced by yeast cells during fermentation or externally added into a fermentation system, can trigger oscillations once its concentration approaches to a criterion.

The impact of dilution rate on oscillations was also studied. It was found that oscillations occurred at certain dilution rate ranges for the two yeast strains. Since ethanol production is tightly coupled with yeast cell growth, it was speculated that the impact of the dilution rate on the oscillations is due to the synchronization of the mother and daughter cell growth rhythms. The difference in the oscillation profiles exhibited by the two yeast strains is due to their difference in ethanol tolerance.

For more practical conditions, the behavior of continuous ethanol fermentation was studied using a self-flocculating industrial yeast strain and corn flour hydrolysate medium in a simulated tanks-in-series fermentation system. Amplified oscillations observed at the dilution rate of 0.12 h^{-1} were postulated to be due to the synchronization of the two yeast cell populations generated by the continuous inoculation from the seed tank upstream of the fermentation system, which was partly validated by oscillation attenuation after the seed tank was removed from the fermentation system. The two populations consisted of the newly inoculated yeast cells and the yeast cells already adapted to the fermentation environment.

Oscillations increased residual sugar at the end of the fermentation, and correspondingly, decreased the ethanol yield, indicating the need for attenuation strategies. When the tubular bioreactors were packed with $\frac{1}{2}$ " Intalox ceramic saddles, not only was their ethanol fermentation performance improved, but effective oscillation attenuation was also achieved. The oscillation attenuation was postulated to be due to the alleviation of backmixing in the packed tubular bioreactors as well as the yeast cell immobilization role of the packing.

The residence time distribution analysis indicated that the mixing performance of the packed tubular bioreactors was close to a CSTR model for both residual glucose and ethanol, and the assumed backmixing alleviation could not be achieved. The impact of yeast cell immobilization was further studied using several different packing materials. Improvement in ethanol fermentation performance as well as oscillation attenuation was achieved for the wood chips, as well as the Intalox ceramic saddles, but not for the porous polyurethane particles, nor the steel Raschig rings. Analysis for the immobilized yeast cells indicated that high viability was the mechanistic reason for the improvement of the ethanol fermentation performance as well as the attenuation of the oscillations.

A dynamic model was developed by incorporating the lag response of yeast cells to ethanol inhibition into the pseudo-steady state kinetic model, and dynamic simulation was performed, with good results. This not only provides a basis for developing process intervention strategies to minimize oscillations, but also theoretically support the mechanistic hypothesis for the oscillations.

ACKNOWLEDGES

I would like to express my sincere gratitude and appreciation to the following:

- My supervisors, Professors W. A. Anderson and M. Moo-Young for their assistance, guidance, advice and ideas.
- Committee members, Professors J. M. Scharer, R. Legge, K. Ma for their valuable comments on the project and thesis.
- Professor Y. H. Lin at the University of Saskatchewan for his willingness to be my external examiner and for his valuable comments on the thesis.
- Professors E. Jervis and P. Chou as well as Visiting Professor F. Alani for their inspirational discussion.
- Jana Otruba, Ralph Dickhout, Ron Neil and Dennis Herman for their various technical support.
- Pat Anderson, Liz Bevan, Debbie Loney and Ingrid Sherrer for their help within the duration of my study.
- My colleagues, Lijie Chen and Yali Xu, for their kind collaboration in the preliminary research of this project.
- My colleagues at Dalian University of Technology, China, especially Mr. Lingwei Chen, Ms. Lei Yang and Mr. Tiejun Xu for their help in the experimental work, as well as Dr. Xumeng Ge for his great assistance in the kinetic data treatment and dynamic simulations.
- My friend, Victoria Zhang, for her encouragement and support during my thesis writing.
- My wife, Li Dong, for her understanding, patience and sacrifice. My son, Yun Bai, for his excellent performance in his secondary and high school studies, although without me with him.

TABLE OF CONTENTS

ABSTRACT	iv
ACKNOWLEDGEMENTS	vi
LIST OF TABLES	xi
LIST OF FIGURES	xii
NOMENCLATURE	xxi

1 General Introduction

1.1 Project Background	1
1.2 Research Objectives	6
1.3 Research Approach	7
1.4 Thesis Outline	8

2 Literature Review

2.1 Glycolytic Pathway and Ethanol Fermentation	9
2.2 Microorganisms Used for Ethanol Production	12
2.2.1 <i>Saccharomyces cerevisiae</i>	12
2.2.2 <i>Zymomonas mobilis</i>	15
2.3 Kinetics and Process Design	17
2.3.1 Steady State and Instantaneous Kinetics	18
2.3.2 Process Design	22
2.4 Mechanisms of Ethanol Inhibition	25
2.5 Yeast Cell Immobilization	29
2.6 VHG Ethanol Fermentation	31
2.7 Oscillation and Dynamic Kinetics	33
2.8 Summary	36

3 Background Research: Continuous VHG Ethanol Fermentation

3.1 Introduction	38
------------------------	----

3.2 Materials and Methods	38
3.2.1 Strain, medium, and pre-culture	38
3.2.2 Bioreactor system	39
3.2.3 Analytical methods	41
3.3 Results and Discussion	42
3.3.1 Process state	42
3.3.2 Mechanistic discussion	57
3.3.2 Oscillation attenuation	61
3.4 Conclusions	65
4 Impacts of Added Ethanol, Dilution Rate and Strain on Oscillations	
4.1 Introduction	67
4.2 Materials and Methods	68
4.2.1 Strain, medium, and pre-culture	68
4.2.2 Bioreactor	68
4.2.3 Analytical methods	68
4.2.4 Measurement of ethanol tolerance	69
4.3 Results and Discussion	69
4.3.1 Influence of added ethanol on oscillations	69
4.3.2 Impact of dilution rate on oscillations	71
4.3.3 Evaluation of ethanol tolerance	82
4.3.4 Continuous VHG ethanol fermentation with <i>S. cerevisiae</i> 6508	83
4.4 Conclusions	89
5 Oscillations of continuous ethanol fermentation with self-flocculating yeast in a tanks-in-series system	
5.1 Introduction	91
5.2 Materials and Methods	92
5.2.1 Strain, medium, and pre-culture	92
5.2.2 Bioreactor system	94

5.2.3 Analytical methods	96
5.3 Results and Discussion	97
5.3.1 Continuous fermentation in the tanks-in-series system with the seed tank.....	97
5.3.2 Continuous fermentation in the tanks-in-series system without the seed tank	122
5.4 Conclusions	129

6 Oscillation Attenuation Strategies and Mechanisms

6.1 Introduction	130
6.2 Materials and Methods	131
6.2.1 Strain, medium, and pre-culture	131
6.2.2 Packing selection	131
6.2.3 Bioreactor system	132
6.2.3 Analytical methods	134
6.2.3.1 Glucose, ethanol and biomass analysis	134
6.2.3.2 RTD analysis	134
6.2.3.3 Evaluation of yeast cell immobilization effect	134
6.2.3.4 Viability analysis of immobilized yeast cells	134
6.3 Results and Discussion	135
6.3.1 Mixing performance of tubular bioreactors	135
6.3.2 Exploration of the attenuation mechanisms	142
6.3.2.1 Impact of the packing on the backmixing of the tubular bioreactors ..	142
6.3.2.2 Yeast cell immobilization and its impact on oscillation attenuation	147
6.3.3.3 Impact of cell immobilization methods on oscillation attenuation.....	152
6.3.3.4 Impact of the shift of dilution rate on oscillation attenuation	164
6.4 Conclusions	164

7 Kinetics and Dynamic Simulations

7.1 Introduction	166
7.2 Materials and Methods	167
7.2.1 Strain, medium, and pre-culture	167

7.2.2 Bioreactor system	167
7.2.3 Analytical methods	167
7.3 Models	167
7.3.1 Pseudo-steady state kinetic models	167
7.3.2 Dynamic models	171
7.4 Results and Discussion	173
7.4.1 Pseudo-steady kinetics	173
7.4.2 Dynamic simulations	180
7.5 Conclusions	183
8 Thesis Conclusions and Recommendations	
9.1 Conclusions	185
9.2 Recommendations	186
References	188
Appendixes	
Appendix A: Evaluation of ethanol yield under oscillations	200
Appendix B: Validation of the reproducibility of oscillations	201
Appendix C: Mathematical derivation of Equation (7.23)	202
Appendix D: MATLAB Programs	
Appendix D1: Evaluation of Pseudo-steady State Kinetic Parameters	204
Appendix D2: Dynamic Simulations	210

LIST OF TABLES

Table 4.1	Ethanol tolerance of <i>S. cerevisiae</i> ATCC4126 and <i>S. cerevisiae</i> 6508	82
Table 5.1	Comparison of the oscillation parameters of the first fermentor, $D = 0.12 \text{ h}^{-1}$	126
Table 6.1	Impact of the packings on yeast cell immobilization	159
Table 6.2	Impact of the packings on fermentation performance and cell viability	160
Table 7.1	Pseudo-steady state kinetic data of continuous ethanol fermentation by <i>S. cerevisi</i>	174
Table 7.2	Values of the pseudo-steady state kinetic parameters.....	175
Table 7.3	Dynamic data of continuous VHG ethanol fermentation by <i>S. cerevisiae</i> ATCC 4126, $S_0 = 280 \text{ g l}^{-1}$ and $D = 0.027 \text{ h}^{-1}$	181

LIST OF FIGURES

Figure 1.1	Ethanol production capacity in the United States from 1980 to 2006	1
Figure 1.2	Typical production costs for fuel ethanol from starch materials	2
Figure 1.3	Energy consumptions for fuel ethanol production from starch materials.....	3
Figure 2.1	Metabolic pathways of ethanol fermentation in <i>S. cerevisiae</i>	11
Figure 2.2	Diagram of the asymmetric budding cycle of <i>S. cerevisiae</i>	13
Figure 2.3	Environmental stresses exerted on <i>S. cerevisiae</i> during ethanol fermentation	14
Figure 2.4	Carbohydrate metabolic pathways in <i>Z. mobilis</i>	16
Figure 2.5	Possible sites of ethanol attack in yeast cells	26
Figure 3.1	Diagram of the bioreactor system for continuous VHG ethanol fermentation with <i>S. cerevisiae</i>	40
Figure 3.2	Time-courses of the residual sugar, ethanol, and biomass of the CSTR. The initial glucose concentration in the VHG medium: $S_0 = 280 \text{ g l}^{-1}$ and the dilution rate: $D = 0.027 \text{ h}^{-1}$	44
Figure 3.3	Time-courses of the residual sugar and ethanol of the first tubular bioreactor. The initial glucose concentration in the VHG medium: $S_0 = 280 \text{ g l}^{-1}$ and the dilution rate of the CSTR: $D = 0.027 \text{ h}^{-1}$	47
Figure 3.4	Time-courses of the residual sugar and ethanol of the second tubular bioreactor. The initial glucose concentration in the VHG medium: $S_0 = 280 \text{ g l}^{-1}$ and the dilution rate of the CSTR: $D = 0.027 \text{ h}^{-1}$	48
Figure 3.5	Time-courses of the residual sugar and ethanol of the third tubular bioreactor. The initial glucose concentration in the VHG medium: $S_0 = 280 \text{ g l}^{-1}$ and the dilution rate of the CSTR: $D = 0.027 \text{ h}^{-1}$	49

Figure 3.6 Ethanol yield of the continuous fermentation. Initial glucose concentration in the VHG medium: $S_0 = 280 \text{ g l}^{-1}$, and the dilution rate of the CSTR: $D = 0.027 \text{ h}^{-1}$	50
Figure 3.7 Time courses of the residual glucose, ethanol, and biomass of the CSTR, sampling at an interval of 4 hours. The initial glucose concentration of the VHG medium: $S_0 = 280 \text{ g l}^{-1}$, $D = 0.027 \text{ h}^{-1}$	52
Figure 3.8 Time courses of the residual glucose, ethanol, and biomass of the CSTR sampling at an interval of 4 hours. The initial glucose concentration of the HG medium: $S_0 = 200 \text{ g l}^{-1}$, the dilution rate: $D = 0.027 \text{ h}^{-1}$	55
Figure 3.9 Time courses of the ethanol and biomass of the CSTR, sampling at an interval of 4 hours. The initial glucose concentration of the LG medium: $S_0 = 120 \text{ g l}^{-1}$, the dilution rate: $D = 0.027 \text{ h}^{-1}$	56
Figure 3.10 Impacts of the packing on the ethanol fermentation performance and Oscillatory behaviors of the first tubular bioreactor. The VHG medium containing 280 g l^{-1} glucose was fed into the CSTR at the dilution rate of 0.027 h^{-1}	62
Figure 3.11 Impacts of the packing on the ethanol fermentation performance and oscillatory behaviors of the second tubular bioreactor. The VHG medium containing 280 g l^{-1} glucose was fed into the CSTR at the dilution rate of 0.027 h^{-1}	63
Figure 3.12 Impacts of the packing on the ethanol fermentation performance and oscillatory behaviors of the third tubular bioreactor. The VHG medium containing 280 g l^{-1} glucose was fed into the CSTR at the dilution rate of 0.027 h^{-1}	64

Figure 4.1	Time courses of the residual glucose, ethanol, and biomass of the CSTR. Initial glucose concentration of the LG medium: $S_0 = 120 \text{ g l}^{-1}$, the dilution rate: $D = 0.027 \text{ h}^{-1}$. The LG medium supplemented with 30 g l^{-1} ethanol was fed into the fermentation system at the day 6.5, and the original LG medium was restored in the day 26.5	70
Figure 4.2	Impact of dilution rates on the residual glucose of the continuous VHG ethanol fermentation with <i>S. cerevisiae</i> ATCC4126 The initial glucose concentration in the medium: $S_0 = 280 \text{ g l}^{-1}$	72
Figure 4.3	Impact of dilution rates on the ethanol profiles of the continuous VHG ethanol fermentation with <i>S. cerevisiae</i> ATCC4126. The initial glucose concentration in the medium: $S_0 = 280 \text{ g l}^{-1}$	70
Figure 4.4	Impact of dilution rates on the biomass profiles of the continuous VHG ethanol fermentation with <i>S. cerevisiae</i> ATCC4126. The initial glucose concentration in the medium: $S_0 = 280 \text{ g l}^{-1}$	74
Figure 4.5	Oscillation profiles of the residual glucose, ethanol, and biomass of the continuous ethanol fermentation with <i>S. cerevisiae</i> ATCC4126 at the dilution rate of 0.012 h^{-1} . The initial glucose concentration in the medium: $S_0 = 280 \text{ g l}^{-1}$	78
Figure 4.6	Oscillation profiles of the residual glucose, ethanol, and biomass of the continuous ethanol fermentation with <i>S. cerevisiae</i> ATCC4126 at the dilution rate of 0.021 h^{-1} . The initial glucose concentration in the medium: $S_0 = 280 \text{ g l}^{-1}$	79
Figure 4.7	Oscillation profiles of the residual glucose, ethanol, and biomass of the continuous ethanol fermentation with <i>S. cerevisiae</i> ATCC4126 at the dilution rate of 0.027 h^{-1} . The initial glucose concentration in the medium: $S_0 = 280 \text{ g l}^{-1}$	80

Figure 4.8	Oscillation profiles of the residual glucose, ethanol, and biomass of continuous ethanol fermentation with <i>S. cerevisiae</i> ATCC4126 at the dilution rate of 0.036 h^{-1} . The initial glucose concentration in the medium: $S_0 = 280 \text{ g l}^{-1}$	81
Figure 4.9	Residual glucose profiles of the continuous VHG ethanol fermentation with <i>S. cerevisiae</i> 6508. The initial glucose concentration in the medium $S_0 = 280 \text{ g l}^{-1}$	84
Figure 4.10	Ethanol profiles of the continuous VHG ethanol fermentation with <i>S. cerevisiae</i> 6508. The initial glucose concentration in the medium $S_0 = 280 \text{ g l}^{-1}$	85
Figure 4.11	Biomass profiles of the continuous VHG ethanol fermentation with <i>S. cerevisiae</i> 6508. The initial glucose concentration in the medium $S_0 = 280 \text{ g l}^{-1}$	86
Figure 5.1	Diagram of the tanks-in-series bioreactor system for the continuous ethanol fermentation with a self-flocculating yeast fusant SPSC and the hydrolysate of corn flour	95
Figure 5.2	Performance of the first fermentor of the SPSC fermentation system at the dilution rate of 0.05 h^{-1} . The initial sugar concentration in the hydrolysate medium: $S_0 = 220 \text{ g l}^{-1}$	98
Figure 5.3	Performance of the second fermentor of the SPSC fermentation system at the dilution rate of 0.05 h^{-1} . The initial sugar concentration in the hydrolysate medium: $S_0 = 220 \text{ g l}^{-1}$	99
Figure 5.4	Performance of the third fermentor of the SPSC fermentation system at the dilution rate of 0.05 h^{-1} . The initial sugar concentration in the hydrolysate medium: $S_0 = 220 \text{ g l}^{-1}$	100

Figure 5.5	Performance of the first fermentor of the SPSC fermentation system at the dilution rate of 0.10 h^{-1} . The initial sugar concentration in the hydrolysate medium: $S_0 = 220 \text{ g l}^{-1}$	102
Figure 5.6	Performance of the second fermentor of the SPSC fermentation system at the dilution rate of 0.10 h^{-1} . The initial sugar concentration in the hydrolysate medium: $S_0 = 220 \text{ g l}^{-1}$	103
Figure 5.7	Performance of the third fermentor of the SPSC fermentation system at the dilution rate of 0.10 h^{-1} . The initial sugar concentration in the hydrolysate medium: $S_0 = 220 \text{ g l}^{-1}$	104
Figure 5.8	Performance of the first fermentor of the SPSC fermentation system at the dilution rate of 0.15 h^{-1} . The initial sugar concentration in the hydrolysate medium: $S_0 = 220 \text{ g l}^{-1}$	106
Figure 5.9	Performance of the second fermentor of the SPSC fermentation system at the dilution rate of 0.15 h^{-1} . The initial sugar concentration in the hydrolysate medium: $S_0 = 220 \text{ g l}^{-1}$	107
Figure 5.10	Performance of the third fermentor of the SPSC fermentation system at the dilution rate of 0.15 h^{-1} . The initial sugar concentration in the hydrolysate medium: $S_0 = 220 \text{ g l}^{-1}$	108
Figure 5.11	Performance of the first fermentor of the SPSC fermentation system at the dilution rate of 0.12 h^{-1} . The initial sugar concentration in the hydrolysate medium: $S_0 = 220 \text{ g l}^{-1}$	110
Figure 5.12	Performance of the second fermentor of the SPSC fermentation system at the dilution rate of 0.12 h^{-1} . The initial sugar concentration in the hydrolysate medium: $S_0 = 220 \text{ g l}^{-1}$	111

Figure 5.13 Performance of the third fermentor of the SPSC fermentation system at the dilution rate of 0.12 h^{-1} . The initial sugar concentration in the hydrolysate medium: $S_0 = 220 \text{ g l}^{-1}$	112
Figure 5.14 Residual sugar profiles of the SPSC fermentation system at the dilution of 0.12 h^{-1} . The initial total sugar concentration of the hydrolysate medium: $S_0 = 220 \text{ g l}^{-1}$	115
Figure 5.15 Ethanol profiles of the SPSC fermentation system at the dilution of 0.12 h^{-1} . The initial total sugar concentration of the hydrolysate medium: $S_0 = 220 \text{ g l}^{-1}$	116
Figure 5.16 Biomass profiles of the SPSC fermentation system at the dilution of 0.12 h^{-1} . The initial total sugar concentration of the hydrolysate medium: $S_0 = 220 \text{ g l}^{-1}$	117
Figure 5.17 Residual sugar profiles of the continuous SPSC ethanol fermentation system with the seed fermentor. The initial sugar concentration in the hydrolysate medium: $S_0 = 220 \text{ g l}^{-1}$	119
Figure 5.18 Ethanol profiles of the continuous SPSC ethanol fermentation system with the seed fermentor. The initial sugar concentration in the hydrolysate medium: $S_0 = 220 \text{ g l}^{-1}$	120
Figure 5.19 Biomass profiles of the continuous SPSC ethanol fermentation system with the seed fermentor. The initial sugar concentration in the hydrolysate medium: $S_0 = 220 \text{ g l}^{-1}$	121
Figure 5.20 Residual sugar profiles of the continuous SPSC ethanol fermentation system without the seed fermentor. The initial sugar concentration in the hydrolysate medium: $S_0 = 220 \text{ g l}^{-1}$	123
Figure 5.21 Ethanol profiles of the continuous SPSC ethanol fermentation system without the seed fermentor. The initial sugar concentration in the hydrolysate medium: $S_0 = 220 \text{ g l}^{-1}$	124

Figure 5.22 Biomass profiles of the continuous SPSC ethanol fermentation system without the seed fermentor. The initial sugar concentration in the hydrolysate medium: $S_0 = 220 \text{ g l}^{-1}$	125
Figure 6.1 Sampling diagram along the axial direction of a tubular bioreactor	133
Figure 6.2 Residual glucose concentrations along the axial directions of the tubular bioreactors. The VHG medium containing 280 g l^{-1} glucose was fed into the CSTR at the dilution rate of 0.027 h^{-1}	136
Figure 6.3 Ethanol concentrations along the axial directions of the tubular bioreactors. The VHG medium containing 280 g l^{-1} glucose was fed into the CSTR at the dilution rate of 0.027 h^{-1}	137
Figure 6.4 Biomass concentrations along the axial direction of the first tubular bioreactor. The VHG medium containing 280 g l^{-1} glucose was fed into the CSTR at the dilution rate of 0.027 h^{-1}	138
Figure 6.5 Biomass concentrations along the axial direction of the second tubular bioreactor. The VHG medium containing 280 g l^{-1} glucose was fed into the CSTR at the dilution rate of 0.027 h^{-1}	139
Figure 6.6 Biomass concentrations along the axial direction of the third tubular bioreactor. The VHG medium containing 280 g l^{-1} glucose was fed into the CSTR at the dilution rate of 0.027 h^{-1}	140
Figure 6.7 Response of the tank to the step input. Xylose was used as a tracer and added into the medium at a concentration of 20 g l^{-1} . The VHG medium containing 280 g l^{-1} glucose was fed into the tank fermentor at a dilution rate of 0.027 h^{-1}	143
Figure 6.8 Response of the tank and first tubular bioreactor to the step input. Xylose was used as a tracer and added into the medium at a concentration of 20 g l^{-1} . The VHG medium containing 280 g l^{-1} glucose was fed into the tank fermentor at the dilution rate of 0.027 h^{-1}	144

Figure 6.9	Response of the tank, first and second tubular bioreactors to the step input. Xylose was used as a tracer and added into the medium at a concentration of 20 g l ⁻¹ . The VHG medium containing 280 g l ⁻¹ glucose was fed into the tank fermentor at the dilution rate of 0.027 h ⁻¹	145
Figure 6.10	Response of the whole bioreactor system to the step input. Xylose was used as a tracer and added into the medium at a concentration of 20 g l ⁻¹ . The VHG medium containing 280 g l ⁻¹ glucose was fed into the tank fermentor at the dilution rate of 0.027 h ⁻¹	146
Figure 6.11	Biomass in the effluent from the first tubular bioreactor before and after it was packed with the Intalox ceramic saddles. The VHG medium containing 280 g l ⁻¹ glucose was fed into the tank at a dilution rate of 0.027 h ⁻¹	148
Figure 6.12	Biomass in the effluent from the second tubular bioreactor before and after it was packed with the Intalox ceramic saddles. The VHG medium containing 280 g l ⁻¹ glucose was fed into the tank at a dilution rate of 0.027 h ⁻¹	149
Figure 6.13	Biomass in the effluent from the third tubular bioreactor before and after it was packed with the Intalox ceramic saddles. The VHG medium containing 280 g l ⁻¹ glucose was fed into the tank at a dilution rate of 0.027 h ⁻¹	150
Figure 6.14	Impact of the packings on the fermentation performance of the first tubular bioreactor. The VHG medium containing 280 g l ⁻¹ glucose was fed into the tank at a dilution rate of 0.027 h ⁻¹	154
Figure 6.15	Impact of the packings on the fermentation performance of the second tubular bioreactor. The VHG medium containing 280 g l ⁻¹ glucose was fed into the tank at a dilution rate of 0.027 h ⁻¹	156

Figure 6.16 Impact of the packings on the fermentation performance of the third tubular bioreactor. The VHG medium containing 280 g l ⁻¹ glucose was fed into the tank at a dilution rate of 0.027 h ⁻¹	158
Figure 7.1 Comparison of the experimental data with the model predictions for yeast cell growth (A linear correlation: $y = x$, $R^2 = 0.9744$).....	178
Figure 7.2 Comparison of the experimental data with the model predictions for ethanol production (A linear correlation: $y = x$, $R^2 = 0.9289$)	179
Figure 7.3 Dynamic simulations of the oscillations of residual glucose, ethanol and biomass for continuous VHG fermentation with <i>S. cerevisiae</i> ATCC 4126. The VHG medium containing 280 g l ⁻¹ glucose was fed into the tank at a dilution rate of 0.027 h ⁻¹	182

NOMENCLATURE

Abbreviations

LG low gravity

A LG medium contains 12 % (w/v) sugar so that lower ethanol concentration can be achieved to study the impact of ethanol concentration on process oscillations.

HG high gravity

A HG medium contains 18-22 % (w/v) sugar so that 10-13 % (v/v) ethanol can be achieved at the end of the fermentation. The HG medium is widely used in the fuel ethanol production from starch and sugar materials.

VHG very high gravity

A VHG medium contains more than 25% (w/v) sugar so that at least 15 % (v/v) ethanol can be achieved at the end of the fermentation.

CSTR continuously stirred tank reactor/bioreactor

PFR plug flow reactor/bioreactor

SPSC name of a yeast fusant developed by the protoplast fusion technology from *Schizosaccharomyces pombe* and *Saccharomyces cerevisiae*

TB tubular bioreactor

Symbols

C tracer concentration in the effluent, g l^{-1}

C_0 tracer concentration in the medium, g l^{-1}

D dilution rate, h^{-1}

F_t total medium flow rate of the SPSC fermentation system, ml h^{-1}

F_1 medium flow rate of the first tank of the SPSC fermentation system, ml h^{-1}

F_S medium flow rate of the seed fermentor of the SPSC fermentation system, ml h^{-1}

S	residual glucose (sugar) concentration, g l^{-1}
S_0	glucose (sugar) concentration in the media, g l^{-1}
P	ethanol concentration, g l^{-1}
P_t	ethanol concentration of the SPSC fermentation system, g l^{-1}
P_S	ethanol concentration in the seed culture of the SPSC fermentation system, g l^{-1}
P_{max}	maximum ethanol concentration at which cell growth is completely inhibited, g l^{-1}
q	ethanol productivity, $\text{g l}^{-1} \text{h}^{-1}$
R^2	correlation coefficient
V	working volume of the tank fermentor in the SPSC fermentation system, ml
t	time, h
X	biomass, g (DCW) l^{-1}
K_S	Monod parameter for cell growth, g l^{-1}
K_S^*	Monod parameter for ethanol production, g l^{-1}
K_I	substrate inhibition parameter for cell growth, g l^{-1}
K_I^*	substrate inhibition parameter for ethanol production, g l^{-1}
V_G	intermediate variable defined in Equation (7.24)
V_P	intermediate variable defined in Equation (7.28)
$Y_{P/S}$	ethanol yield based on substrate consumption
α	inhibition index for cell growth
β	inhibition index for ethanol production
μ	specific growth rate, h^{-1}
μ_{max}	maximum specific growth rate, h^{-1}
μ_{cal}	calculated specific growth rate by the pseudo-steady state kinetics, h^{-1}

μ_{exp}	measured specific growth rate, h^{-1}
μ_0	modification factor to specific growth rate when the residual sugar of a continuous ethanol fermentation system is below a criterion, h^{-1}
ν	specific ethanol production rate, h^{-1}
ν_{max}	maximum specific ethanol production rate, h^{-1}
ν_{cal}	calculated specific ethanol production rate by the pseudo-steady state kinetics, h^{-1}
ν_{exp}	measured specific ethanol production rate, h^{-1}
ν_0	modification factor to specific ethanol production rate when the residual sugar of a continuous ethanol fermentation system is below a criterion, h^{-1}
ω	time delay factor defined in Equation (7.19), h^{-1}
τ	time history, h
Ω	dynamic specific growth rate, h^{-1}
Φ	dynamic specific ethanol production rate, h^{-1}

Chapter 1

General introduction

1.1 Project Background

The gradual depletion of crude oil and the environmental deterioration resulting from the over consumption of petroleum-derived transportation fuels have garnered great attention again across the whole world, which makes it urgent to develop alternatives that are both renewable and environmentally friendly. Ethanol, produced from renewable biomass such as sugar and starch materials at present and possibly lignocellulosic materials in the future, is believed to be one of these alternatives, and its production capacity has been undergoing rapid expansion since the beginning of this new millennium. Figure 1.1 illustrates the increasing trend of fuel ethanol production capacity in the United States since 1980.

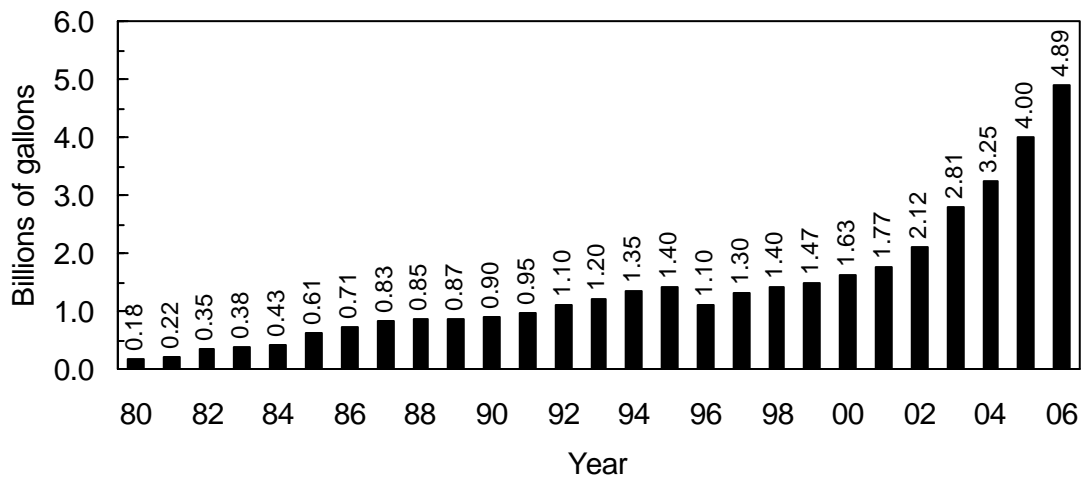


Figure 1.1 Ethanol production capacity in the United States from 1980 to 2006

(Data from the website of ACE, www.ethanol.org/production.html)

Compared with the production capacity of 1.63 billion gallons in 2000, it was trebled at the end of 2006! It was reported by ACE (American Coalition for Ethanol, www.ethanol.org) that the total ethanol production capacity of more than 100 existing facilities in the United States was approaching 6.0 billion gallons in March, 2007, and another 70 more new facilities with a total production capacity of 5.4 billion gallons are under construction. Other countries, such as China and India, are following this trend. Three new large-scale fuel ethanol plants with a total annual production capacity of 1.2 million tons were put into operation in China in 2005.

For such a bulk product, any technology improvements, especially the major fermentation technologies, will be economically very attractive. Figure 1.2 illustrates the current production costs of fuel ethanol from starch materials.

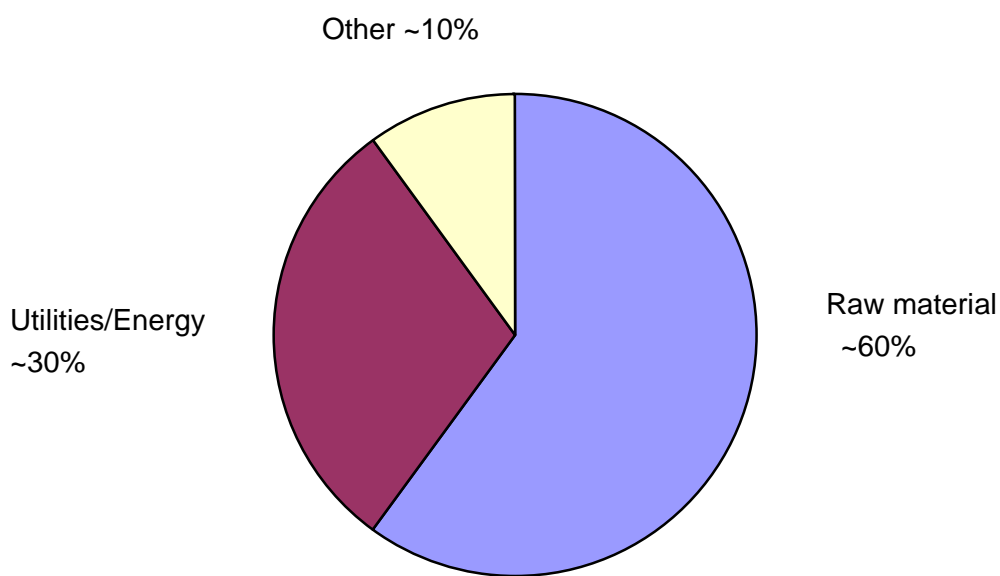


Figure 1.2 Typical production costs for fuel ethanol from starch materials

(Data from BBKA, Anhui Province, East China, 2006)

As can be seen, about 60% of the production cost is from raw material consumption, which drives the R & D of lignocellulosic biomass for ethanol production. Although some breakthroughs have been made within the past few years, it is still economically problematic to replace sugar and starch materials in the near-, even long-term (Bungay, 2004). Energy consumption cost is the second largest, about 30% of the total production cost. It can be seen from Figure 1.3 that about 80% of the energy consumption is from the downstream processes after fermentation, mainly in the distillation of dilute broth as well as in the treatment of large amount of waste distillate by the multiple evaporation technology.

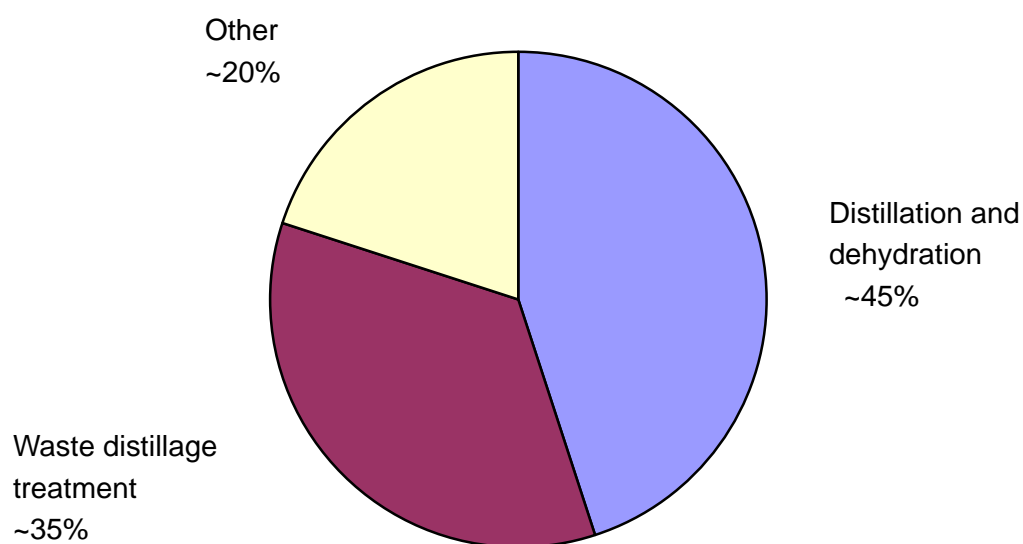


Figure 1.3 Energy consumptions of fuel ethanol production from starch materials

(Data from BBKA, Anhui Province, East China, 2006)

The fermented broth containing low ethanol concentration not only makes the ethanol purification by distillation highly energy-intensive, but also generates more waste distillate that needs to be treated by multistage evaporation, costing even more energy. As a result,

many attempts have been made to achieve higher ethanol concentration at the end of fermentation, such as coupling pervaporation membrane into ethanol fermentation, vacuum fermentation, extractive fermentation, and so on. Unfortunately, although high ethanol concentration can be achieved, these technologies have been proven to be not economically practical because of high extra costs resulting from either high energy consumption or high capital investment for the facilities.

High gravity (HG) ethanol fermentation technologies were proposed in the 1980s and successfully applied in the ethanol fermentation industry thereafter, which made the ethanol concentration at the end of fermentation increase dramatically from previously 6-8% (w/v) to currently 10-12% (w/v). Research in yeast physiology has revealed that many strains in the genus of *Saccharomyces cerevisiae* can tolerate far higher ethanol concentration than assumed (Casey and Ingledew, 1986; Thomas and Ingledew, 1992), usually without any conditioning or genetic modifications that risk making the modified strains lose some of their original traits. Therefore, very high gravity (VHG) ethanol fermentation technologies using media containing sugar in excess of 250 g l⁻¹ in order to achieve more than 15% (v/v) ethanol were proposed in the middle of the 1990s (Thomas et al., 1996).

VHG fermentation technologies, perhaps, are most promising for commercialization. On the one hand, energy cost is the second largest in ethanol production, only after that of raw material consumption, and it increases continuously with the increase in energy prices. On the other hand, the availability of the VHG media in a large quantity is now economically feasible because the enzyme industry can provide high efficiency enzymes with low cost for ethanol production use, such as α -amylases, glucoamylases and proteases. Furthermore, the concept of the biorefinery requires the separation of most raw material residues in the pretreatment processes, especially for those fermentation plants with large processing capacities, which further guarantees a reliable supply of the VHG media. However, both the fundamental research and applied technology development in the VHG ethanol

fermentation area have not been given enough attention within the past decade.

Oscillatory behaviors have been observed and reported for the continuous aerobic cultures of *S. cerevisiae*. Biomass, glucose, ethanol, dissolved oxygen, pH, and some intracellular storage materials oscillate periodically under certain conditions (Chen and McDonald, 1990a, b; Beuse et al., 1998, 1999). The synchronization of the asymmetric cell budding cycles of the mother and daughter cells of *S. cerevisiae* was believed to be the mechanistic reason for these oscillations (Duboc et al., 1996; Patnaik, 2003). In our preliminary research in the continuous VHG ethanol fermentation with *S. cerevisiae*, significant oscillations of residual glucose, ethanol and biomass were also observed, and the mechanistic analysis indicated these oscillations seem more complicated than those oscillations observed in the continuous aerobic cultures of *S. cerevisiae* caused by the synchronization of the asymmetric cell budding cycles of the mother and daughter cells, because much longer oscillation periods and much larger oscillation amplitudes were observed. These problems have never been explored before since the continuous ethanol fermentation with *S. cerevisiae* was believed to be at steady state.

As the cost of fuel ethanol production is mainly from raw material consumption (Figure 1.2), the residual sugar at the end of fermentation is strictly controlled at a level of 0.1–0.2% (w/v) in industry. The oscillatory behaviors observed in the continuous VHG ethanol fermentation are highly problematic for increasing the residual sugar level at the end of the fermentation, which not only increases raw material consumption, but also increase the difficulties of process control if no economically acceptable attenuation strategies are developed.

1.2 Research Objectives

A comprehensive literature review on ethanol fermentation technologies as well as the understanding of current economical and technological status of fuel ethanol production generated several critical aspects that need to be addressed for continuous VHG ethanol fermentation, one of the most promising technologies in fuel ethanol production from sugar and starch materials.

1. How to design a bioreactor system to effectively alleviate the strong product inhibition as well as the potential substrate inhibition.
2. Currently, steady states have been assumed for the continuous ethanol fermentation using media containing sugar at 18-22% (w/v) through which 10-13% (v/v) ethanol can be achieved at the end of the fermentation. Is the steady state assumption still true under a VHG condition?
3. Given that unsteady states and oscillations have been observed for the continuous VHG ethanol fermentation in our preliminary research, what is the mechanistic reason(s) triggering these unsteady states and oscillations?
4. How can these unsteady states and oscillations affect ethanol fermentation performance, and what kind of strategies should be developed to deal with these problems?

Therefore, the objectives of this research are:

1. Design a bioreactor system suitable for the continuous VHG ethanol fermentation using a general strain of *S. cerevisiae*, and evaluate its long-term operating performance.
2. Investigate the mechanism(s) triggering the unsteady states and oscillatory

behaviors observed in the continuous VHG ethanol fermentation.

3. Evaluate the impact of these unsteady states and oscillatory behaviors on the continuous VHG ethanol fermentation performance.
4. According to the impact of these unsteady states and oscillatory behaviors on the fermentation performance, develop corresponding strategies to augment or attenuate them.
5. Establish kinetic and dynamic models to simulate these unsteady states and oscillations.

1.3 Research Approach

The approach for this research is based on a comprehensive examination of the mechanisms proposed for the oscillations observed in the continuous productions of ethanol by *Zymomonas mobilis* (Daugulis et al., 1997), reuterin by *Lactobacillus reuteri* (Rasch et al., 2002), and 1, 3-propanediol by *Klebsiella pneumonia* (Zeng et al., 1996; Ahrens et al., 1998; Menzel et al., 1996, 1998), and in the continuous aerobic culture of *S. cerevisiae* (Bellgardt, 1994a, b), as well as in our preliminary research in which oscillations were observed for the continuous ethanol fermentation by *S. cerevisiae* in a bioreactor system composed of a CSTR and three tubular bioreactors in series, and the effective oscillation attenuation was achieved by packing the tubular bioreactors.

Thus, it is hypothesized:

1. The mechanistic reasons for the unsteady states and oscillatory behaviors observed in the continuous VHG ethanol fermentation are due to ethanol inhibition and lag response of yeast cells to the ethanol inhibition.

2. The lethal effect of ethanol on yeast cells toward the end of VHG fermentation will exaggerate the unsteady states and oscillatory behaviors, and so does the synchronization of the mother and daughter cell cycles of *S. cerevisiae*, if occurring.
3. The mechanisms of the oscillation attenuation by packing are due to the reduction of backmixing in the packed tubular bioreactors as well as the yeast cell immobilization role of the packing.

1.4 Thesis Outline

This thesis comprises eight chapters and is organized as follows: Chapter 1, general introduction, introduces the research background and objectives as well as theoretical hypotheses that penetrate through the whole research. Chapter 2 gives a comprehensive literature review of ethanol fermentation. Chapter 3, the preliminary research, studies the continuous VHG ethanol fermentation using a bioreactor system composed of a CSTR and three tubular bioreactors in series, reports the unsteady states and oscillatory behaviors, and analyzes their mechanistic reasons. Chapter 4 investigates the impact of dilution rate and strain characteristics on the unsteady states and oscillations, providing more complete mechanistic understanding. Chapter 5 further exploits the oscillatory behaviors of continuous ethanol fermentation using an industrial self-flocculating yeast strain and a simulated tanks-in-series fermentation system, evaluating the impact of the oscillations on ethanol fermentation performance. Chapter 6 develops the oscillation attenuation strategy through packing the tubular bioreactors and elucidates the corresponding mechanisms. Chapter 7 establishes the models through which the dynamic simulations are done. And finally, Chapter 8 summarizes the whole research and presents conclusions and some recommendations for future work.

Chapter 2

Literature review

2.1 Glycolytic Pathway and Ethanol Fermentation

Metabolic pathway analysis is a prerequisite for investigating how changing environmental conditions affect metabolism, a key for process control and optimization. This technique has been widely used in the culture of recombinant organisms for pharmaceuticals and other high value-added products since it was created at the beginning of 1990s (Bailey, 1991). However, ethanol fermentation, the oldest biotechnology that has benefited humans for thousands of years, is far behind those modern biotechnologies in applying this useful tool for improving its efficiency. For example, the relatively low ethanol concentration currently achieved at the end of fermentation makes the ethanol purification by distillation highly energy-intensive and produce more waste distillate that needs to be treated by multi-stage evaporation, in which yet more energy is consumed. The high ethanol-tolerant strains that technically can be developed by metabolic engineering are still not available for industrial applications. This is one of the reasons why the science and engineering technologies of ethanol fermentation are not as well applied as those of the raw material handling and post-fermentation processing. From the point view of engineering design, ethanol fermentation is still “an art” or “a black box” in this seemingly very mature industry through which billions of gallons of ethanol are being produced annually across the world (Ingledeew, 1999).

The main metabolic pathway involved in the ethanol fermentation of yeast is glycolysis through which one molecule of glucose is metabolized and two molecules of pyruvate are produced (Madigan et al., 2000), as illustrated in Figure 2.1. Under an anaerobic condition, the pyruvate is further reduced to ethanol with the release of CO₂. Theoretically, the yield is 0.511 for ethanol and 0.499 for CO₂ on the basis of 1 g glucose metabolized. Two ATPs

produced in glycolysis are used to drive yeast cell biosynthesis, including a variety of energy-requiring reactions under the anaerobic condition. Therefore, ethanol fermentation is tightly coupled with the growth of yeast cells, which means that yeast in the amount of 1-3% of ethanol must be produced as a co-product of ethanol fermentation. Without the continuous consumption of ATPs by the growth of yeast cells or other endoergic reactions, the glycolytic metabolism of glucose would be interrupted immediately because of the intracellular accumulation of ATPs.

Some intermediates in glycolysis can be diverted to yeast cell biomass synthesis, but the percentage is very low, normally less than 5% on the basis of glucose metabolized, because many other nutrients supplemented in the media in both laboratory research and industrial production can be degraded into the building blocks through catabolism and used for the biomass synthesis through anabolism (Ingledew, 1999).

Three key regulation sites in glycolysis are highlighted in Figure 2.1. The first is the initial reaction involving the phosphorylation of glucose at the sixth carbon by hexokinase (HK). HK is inhibited by glucose-6-phosphate, through which the reaction is regulated. The phosphorylation of fructose-6-phosphate is the second regulation site. ATP is an allosteric inhibitor of phosphofructokinase (PFK) and the enzymatic reaction rate decreases dramatically when the intracellular ATP is accumulated. This is the most important and effective regulation site in the glycolytic pathway and acts as the “valve” controlling the rate of glycolysis. The last is the conversion of phosphoenolpyruvate to pyruvate with one molecule of ATP produced because the enzyme, pyruvate kinase (PYK), possesses allosteric sites for numerous effectors. In addition to these regulation sites in the glycolytic pathway, the last reaction catalyzed by alcohol dehydrogenase (ADH) is also a regulation site. These key regulation sites, regulation enzymes, and corresponding intermediate metabolites can be exploited when the mechanisms triggering the unsteady states and parameter oscillations in the continuous VHG ethanol fermentation are investigated.

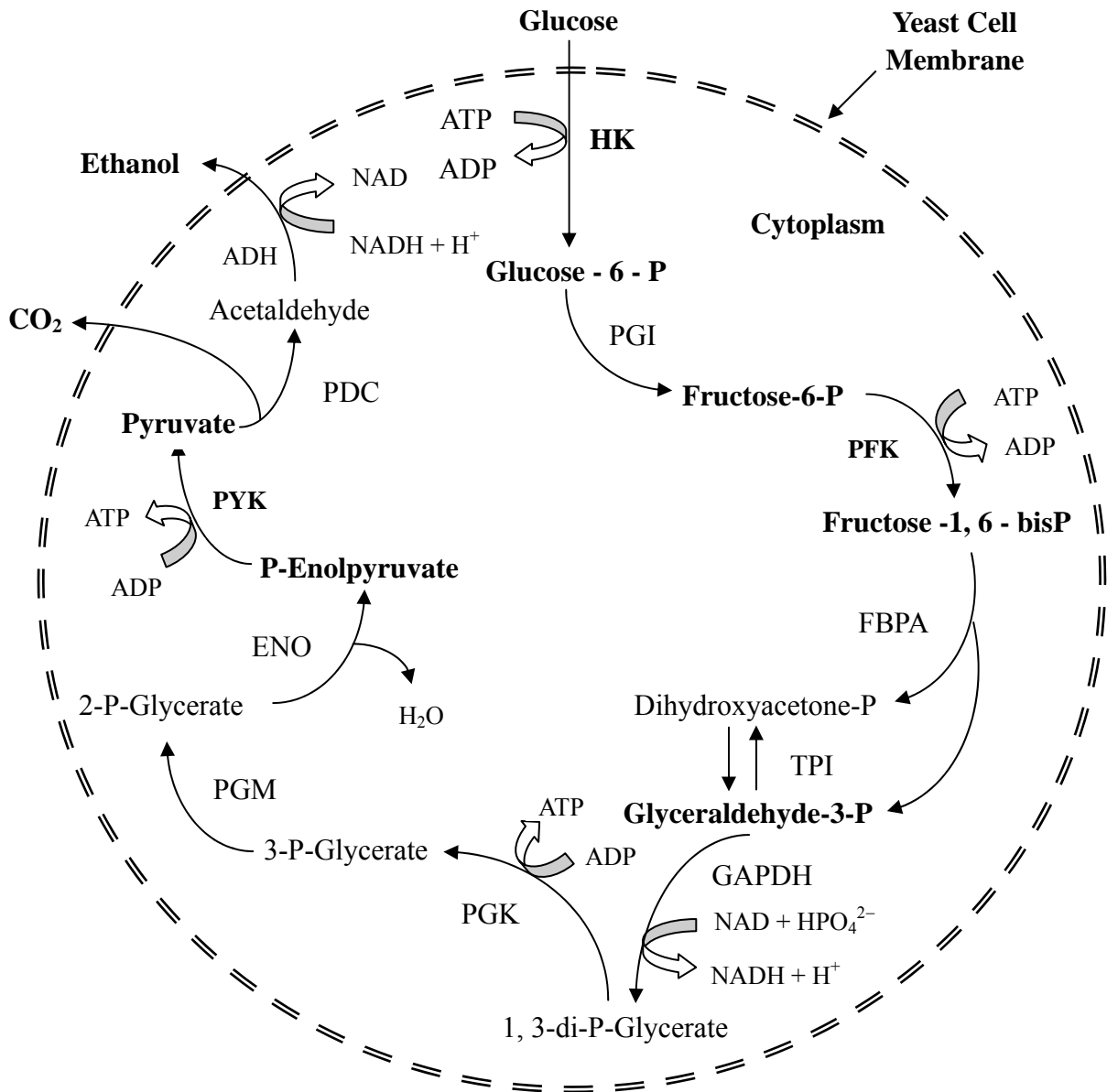


Figure 2.1 Metabolic pathways of ethanol fermentation in *S. cerevisiae*

Abbreviations: HK: hexokinase, PGI: phosphoglucosomerase, PFK: phosphofructokinase, FBPA: fructose bisphosphate aldolase, TPI: triose phosphate isomerase, GAPDH: glyceraldehydes-3-phosphate dehydrogenase, PGK: phosphoglycerate kinase, PGM: phosphoglyceromutase, ENO: enolase, PYK: pyruvate kinase, PDC: pyruvate decarboxylase, ADH: alcohol dehydrogenase.

2.2 Microorganisms Used for Ethanol Production

Among many microorganisms being exploited for ethanol production, the genus of *Saccharomyces cerevisiae* still remains as the prime species. Currently, almost all ethanol, either alcoholic beverage or industrial fuel, is being produced by fermentations using *S. cerevisiae*. *Zymomonas mobilis* is another of the most intensively investigated species within the past three decades because it possesses some “superior characteristics” compared to its counterpart *S. cerevisiae*.

2.2.1 *Saccharomyces cerevisiae*

S. cerevisiae, as a model of eukaryotic cells, has been extensively studied in fundamental biological science. Its genome sequencing was completed in 1996 and about 6000 potential protein-coding genes were identified (Goffeau et al., 1996), which provides a unique tool for molecular microbiologists to better understand this species at its molecular level and develop modified strains with new metabolic pathways, such as the recombinants capable of metabolizing pentose and fermenting lignocellulosic hydrolysates (Ho et al., 1998). It also allows biochemical engineers to operate their fermentation plants more efficiently and economically by manipulating this biocatalyst at its process-control level and improve its product yield that is extremely important for those bulk fermentation products, ethanol as an instance.

The production of ethanol, a typical primary metabolite, is tightly associated with the growth of yeast cells. Therefore, many considerations involved in ethanol fermentation processes, including fermentation kinetics and process optimization that will be discussed later, are based on the growth of yeast cells. *S. cerevisiae* propagates by budding, which is an asymmetric process and schematically illustrated in Figure 2.2 (Patnaik, 2003). The parent and daughter cells can be distinguished and show different behaviors during the reproduction cycle. It is known that the size of the buds at division, the new-born daughter

cells, is smaller than their parents, and they need a longer time to be ready for budding than that their parents require. Hartwell and Unger (1977) investigated the unequal division in *S. cerevisiae* and control mechanism for the cell cycle. Later research further found that the cell cycling characteristics of *S. cerevisiae* can be smoothly explained by the concept of critical cell mass for the initiation of division (Bellgardt, 1994a, b). According to this concept, the generation time of the newly born daughter cells is longer than that of their parent cells, because they need to accumulate more cell mass. This specific growth pattern of *S. cerevisiae* was believed to be the intrinsic mechanism triggering the sustained oscillations of biomass, sugar, dissolved oxygen, evolved CO₂, and so on during the continuous aerobic cultures of *S. cerevisiae*.

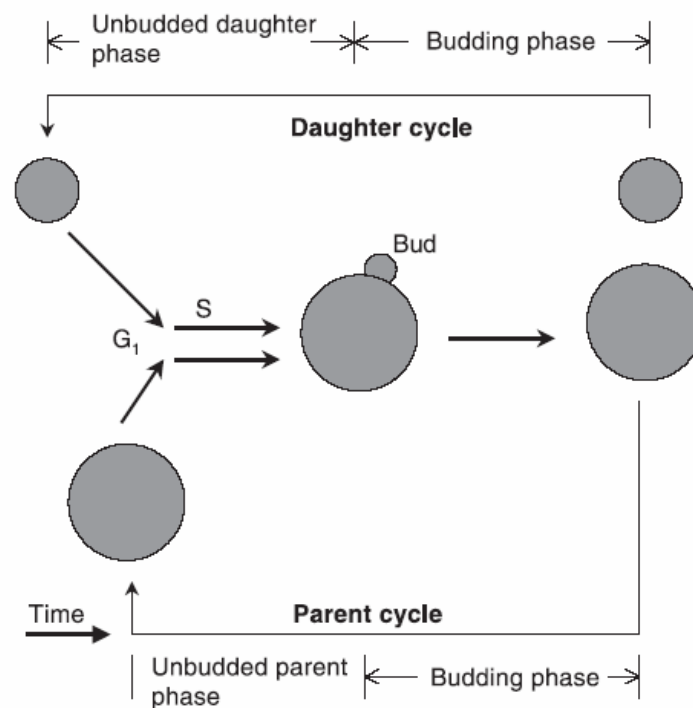


Figure 2.2 Diagram of the asymmetric budding cycle of *S. cerevisiae* (Patnaik, 2003)

However, under anaerobic ethanol fermentations, yeast cells suffer from various stresses. Some of them are environmental, while the others are generated by the yeast cells

themselves, for example ethanol accumulation, and correspondingly strong inhibition on yeast cell growth and ethanol fermentation. The yeast cells in ethanol fermentations are under harsh conditions compared with their aerobic cultures in which the process parameters are optimized with optimum pH, sufficient nutrients and very low ethanol that does not exert inhibition. Their metabolic activities are seriously affected, especially under industrial conditions in which the optimum conditions for growth and fermentation are overwhelmed by pursuing economic benefits. Figure 2.3 illustrates some stresses that yeast cells could experience in ethanol fermentations. Many of them are synergistic, which will exacerbate their negative impacts on yeast cells simultaneously. Stresses, especially ethanol inhibition, and the lag response of yeast cells to it is assumed to be the main reason triggering the parameter oscillations during the continuous ethanol fermentation under a VHG condition.

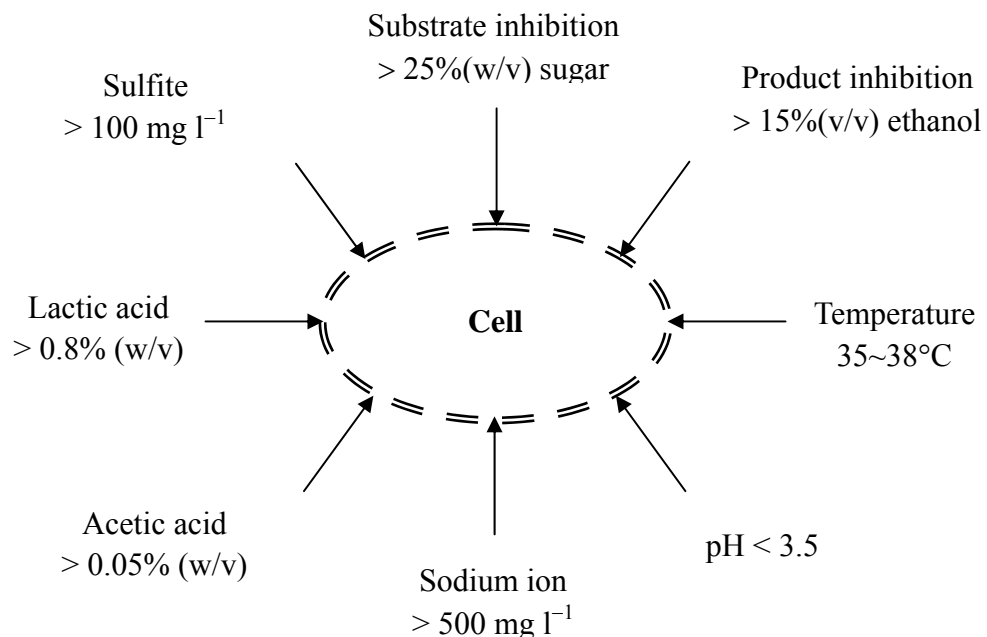


Figure 2.3 Environmental stresses exerted on *S. cerevisiae* during ethanol fermentation

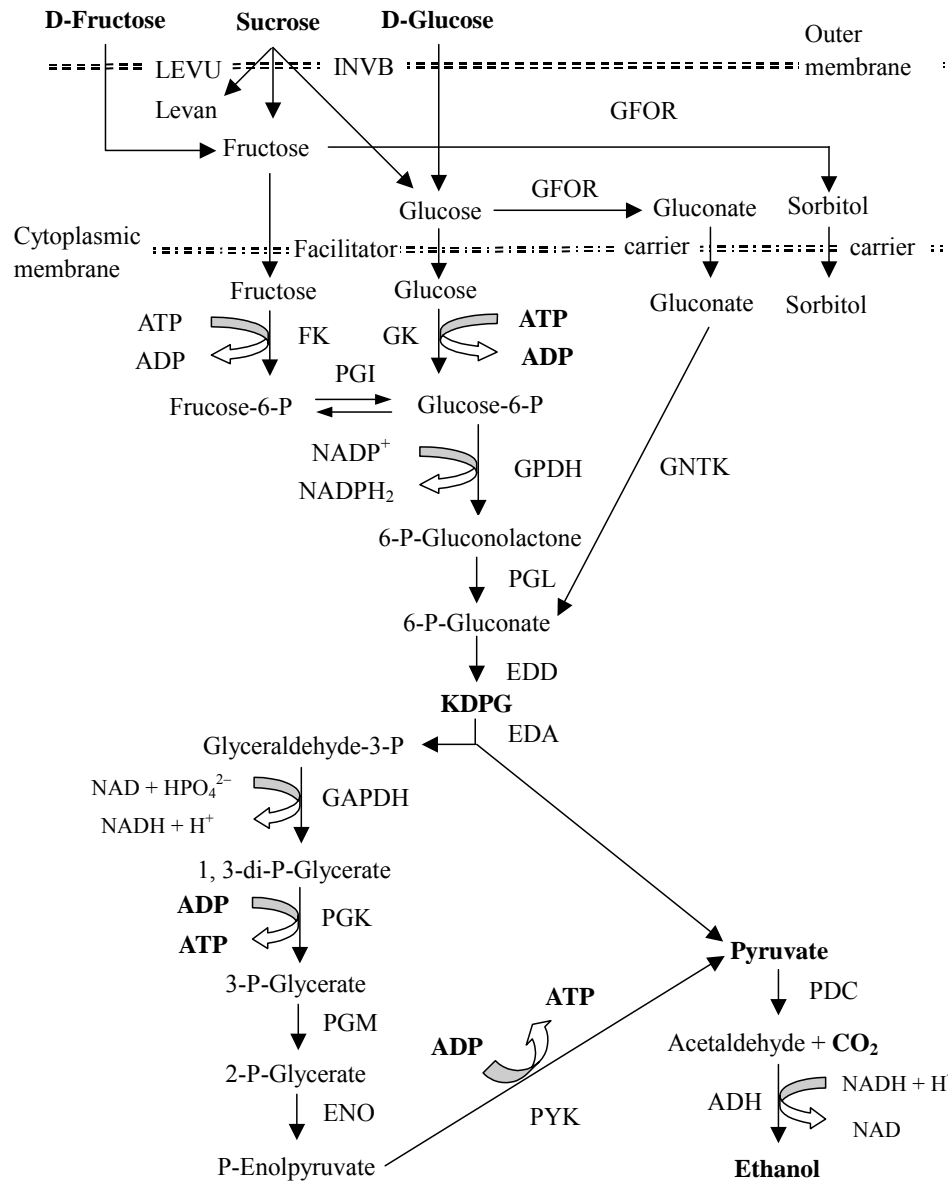
(Ingledew, 1999)

2.2.2 *Zymonomas mobilis*

Z. mobilis is an anaerobic and gram-negative bacterium producing ethanol from glucose *via* the Entner-Doudoriff (ED) pathway (Conway, 1992) in conjunction with the enzymes PDC and ADH, as illustrated in Figure 2.4. This microorganism was originally discovered in fermenting sugar-rich plant saps, e.g., in the traditional pulque drink of Mexico, palm wines of tropical African, or ripening honey (Swings and Deley, 1977).

Z. mobilis catabolizes only three sugars, D-glucose, D-fructose and sucrose, as its sole carbon and energy sources. Its growth on sucrose is accompanied by the extracellular formation of the fructose oligomers (levan) and sorbitol with a significant reduction in its yield of ethanol production, which makes it unsuitable for the ethanol productions using molasses materials. Meanwhile, it can only ferment glucose in the hydrolysate of starch materials but cannot utilize other sugars like the species of *S. cerevisiae*, making it unsuitable for ethanol production using starch materials.

Compared with the EMP that involves cleavage of fructose-1, 6-bisphosphate by FBPA to yield one molecule each of glyceraldehydes-3-phosphate and dihydroxyacetone phosphate, the ED pathway forms glyceraldehydes-3-phosphate and pyruvate by cleavage of 2-keto-3-deoxy-6-phosphogluconate (KDPG) by 2-keto-3-deoxy-gluconate aldolase (EDA), which yields only one mole ATP per molecule glucose rather than two moles as the EMP does. As a consequence, *Z. mobilis* produces less biomass than *S. cerevisiae* and more carbon can be funneled to ethanol production. It was reported that the yield of ethanol from glucose could be as high as 97% of the theoretical yield of 0.511 (Sprenger, 1996), while only 90-93% was reported for *S. cerevisiae* (Ingledeew, 1999). Also, as a consequence of the low ATP yield, *Z. mobilis* maintains high glucose flux, which guarantees its high ethanol fermentation productivity, normally 3-5 fold higher than *S. cerevisiae* (Sprenger, 1996).



Abbreviations: LEVU: levansucrase, INVB: invertase, GFOR: glucose-fructose oxidoreductase, FK: fructokinase, GK: glucokinase, GPDH: glucose-6-phosphate dehydrogenase, PGL: phosphogluconolactonase, EDD: 6-phosphogluconate dehydratase, KDPG: 2-keto-3-deoxy-6-phosphogluconate, EDA: 2-keto-3-deoxy-gluconate aldolase, GNTK: gluconate kinase. See Figure 2.1 for PGI, GAPDH, PGK, PGM, ENO, PYK, PDC and ADH.

Figure 2.4 Carbohydrate metabolic pathways in *Z mobilis*. (Conway, 1992)

Despite its above advantages as an ethanologen species, *Z. mobilis* is not suitable for ethanol production from industrial materials, currently sugar and starch materials, and in the future maybe lignocellulosic materials, because of its narrow substrate spectrum. Ethanol fermentation in industry can never use pure glucose as its raw material as many researchers have done in their laboratories. Obviously, many investigations involving the ethanol fermentation using *Z. mobilis* with so-called promising industrial application prospects were too optimistic. Some researchers who concluded this species could replace *S. cerevisiae* in ethanol fermentations are lacking considerations of the industrial constraints.

Another drawback associated with the continuous ethanol fermentation by *Z. mobilis* is the peculiar occurrence of oscillations or repeated cycles of sugar, ethanol and biomass concentrations under certain conditions, which may be caused by its faster metabolic rate and higher ethanol productivity. However, this species may be a good contrast model to elucidate the mechanism triggering the oscillations observed in the continuous VHG ethanol fermentation by *S. cerevisiae*.

2.3 Kinetics and Process Design

The scale-up of ethanol fermentation process seems to be much easier than those for aerobic processes such as penicillin fermentation, which attracted many scholars and engineers in the 1940s, established scale-up theories and technologies, and founded modern biochemical engineering (Bailey and Ollis, 1986). However, when we examine today's ethanol fermentation industry, we are surprised at finding that for such an old industry, its engineering design and plant operation are far behind other fermentations such as organic acids, amino acids, antibiotics, and needless to say, modern recombinant pharmaceuticals.

2.3.1 Steady State and Instantaneous Kinetics

It is well known that ethanol is inhibitory to both yeast cell growth and ethanol fermentation. Also, the production of ethanol is tightly coupled with the growth of yeast cells under an anaerobic condition. Aiba et al. (1968) first reported their research results in ethanol fermentation kinetics. A chemostat fermentation system was established and run at 30 °C, the media with the initial glucose concentrations of 10 and 20 g l⁻¹ were fed at different dilution rates, and ethanol was added into the fermenter to reach different concentration levels to investigate their inhibitions on both yeast growth and ethanol production as the ethanol concentration produced by yeast cells themselves was too low to exert inhibition. The following steady state kinetic models were proposed and correlated.

$$\mu = \mu_0 e^{-k_1 p} \frac{S}{K_S + S} \quad (2.1)$$

$$\nu = \nu_0 e^{-k_2 p} \frac{S}{K_S^* + S} \quad (2.2)$$

where μ and ν are the specific rates for growth and ethanol production, subscript “0” designates the specific rates when the ethanol concentration is zero, K_S and K_S^* are the Monod constants for growth and ethanol production, S is the limiting substrate concentration, and p is the ethanol concentration (produced and added in total).

Although the inhibition of ethanol on yeast growth and ethanol production is reflected in Aiba’s models, mathematically, these models predict that infinite ethanol concentration can be approached when yeast growth and ethanol production are completely inhibited ($\mu = 0$, $\nu = 0$) at the condition of constant S . Obviously, it is unreasonable. On the other hand, when continuous ethanol fermentation is run at a low dilution rate, especially when feeding with medium containing lower initial sugar concentration, the limiting substrate concentration can be too low to be detectable ($S \approx 0$). Both the specific rates for growth and ethanol

production predicted by the Equations (2.1) and (2.2) are zero, which is also wrong as the broth containing yeast cells and ethanol is continuously produced, and both yeast cell growth and ethanol fermentation occur. No scholars addressed these problems or corrected these errors, but cited these models in their own research. Aiba's article had been cited over two hundred times before it was reprinted in *Biotechnology and Bioengineering* in 2000. Recently, we reported our preliminary research on the kinetics of continuous VHG ethanol fermentation in which some modifications were introduced (Chen et al., 2005).

In the middle of the 1980s, Luong summarized the research progress in the kinetics of ethanol inhibition and pointed out that the inhibition of ethanol on yeast cell growth is noncompetitive, similar to that of enzymatic reactions. The following kinetic models were proposed (Luong, 1985).

$$\frac{\mu}{\mu_0} = 1 - \left(\frac{P}{P_m}\right)^\alpha \quad (2.3)$$

$$\frac{v}{v_0} = 1 - \left(\frac{P}{P_m'}\right)^\beta \quad (2.4)$$

where P_m and P_m' are maximum ethanol concentrations at which yeast cell growth and ethanol production are completely inhibited, α and β are model parameters.

Levenspiel (1980) proposed a generalized nonlinear equation to account for the influence of ethanol inhibition. A few other expressions were also proposed such as the linear models (Holzberg et al., 1967) and the parabolic models (Bazua and Wilke, 1977). However, these kinetic models seemed to be not appreciated by researchers compared with Aiba's and Luong's.

Some scholars found that added ethanol was less toxic than ethanol produced by yeast cells themselves (Nagodawithana and Steinkraus, 1976), while others believed that the inhibition effect of ethanol, whether it is added or produced, is the same because of the excellent

permeability of ethanol across the yeast cell membrane system (Guijarro and Lagunas, 1984). The reliable kinetic models for process design and optimization should be established under real fermentation conditions in which a HG medium is used and high ethanol concentration is produced by fermentation rather than by addition.

In addition to ethanol inhibition, biomass was found to be another inhibitor when very high biomass density was achieved through cell immobilization, cell retention by membranes, and cell recycle after centrifugation. Lee and Chang (1987) established a continuous ethanol fermentation system coupled with a membrane unit to retain yeast cells. Both the kinetic models for yeast growth and ethanol production were correlated with the biomass concentration. They extrapolated and obtained the maximum yeast concentrations of 255 g (DCW) l⁻¹ and 640 g (DCW) l⁻¹, at which the yeast cell growth and ethanol production were completely inhibited, respectively, which seems implausible. Porto et al. (1987) also investigated the impact of yeast cell biomass on ethanol production rate in a fermentation system similar to Chang's and an exponential correlation between specific ethanol production rate and yeast cell concentration was established.

Although some researchers noticed that the maximum ethanol concentration at which yeast cell growth was completely inhibited was different from that at which ethanol production was completely inhibited, no reasonable explanations were given until Groot et al. (1992a) introduced the concept of maintenance into ethanol fermentation systems and proposed that ethanol is continuously produced until the maximum P_{max}' at which ethanol production is completely inhibited, after the maximum ethanol concentration, P_{max} , is approached at which yeast cell growth is completely inhibited ($P_{max}' > P_{max}$). They further developed a quantitative relation between substrate consumption/ethanol production and maintenance through the continuous ethanol fermentation experiment that was run at different dilution rates, fed with the media containing different initial glucose concentrations from 120 g l⁻¹ to 280g l⁻¹, achieving different ethanol levels rather than adding ethanol into the

fermentation system. This treatment seems to be more reasonable, but has been neglected in the past.

Substrate inhibition was not taken into account in both Aiba's and Luong's models as well as in many others. Apparently, these models deviate from the real ethanol fermentation situations in which substrate inhibition tends to occur, especially when a VHG medium is used in order to achieve higher ethanol concentration at the end.

Substrate inhibition is a common phenomenon, not only in ethanol fermentation, but also in many others when substrate concentrations are increased to the corresponding criteria of various strains, normally around 20-30 g l⁻¹ for yeasts. Andrews (1968) generalized Boon and Laudelout's work (1962) in the nitrite oxidation by *Nitrobacter winogradskyi*, simulated the impact of substrate inhibition through batch and continuous fermentations, and proposed the following model.

$$\mu = \mu_{max} \frac{S}{K_S + S + S^2/K_I} \quad (2.5)$$

where K_S is Monod constant, numerically equivalent to the substrate concentration at which the specific growth rate is equal to one-half the maximum in the absence of substrate inhibition, and K_I is the inhibition constant, reflecting the inhibition effect of high concentration substrate.

Unfortunately until now, kinetic investigations involving substrate inhibition in ethanol fermentations, especially in the genus of *S. cerevisiae*, are still very limited. This may be because simultaneous saccharification and fermentation technologies have been widely used in the ethanol fermentation using starch materials in which substrate inhibition is not serious. However, substrate inhibition is surely occurring in the ethanol fermentation using molasses, especially for those main fermentors where high sugar concentrations exist.

Compared with *S. cerevisiae*, the kinetics of *Z. mobilis* have been heavily studied within the

past three decades. On the one hand, this species was discovered relatively late in the early 1960s. On the other hand, since then it has been highly anticipated as the industrial species for ethanol production in place of *S. cerevisiae* because of its much faster fermentation rate and somewhat higher ethanol yield from its ED pathway, compared to the EMP of *S. cerevisiae*. However, this species has been shown to be not economically competitive with *S. cerevisiae* in ethanol production because of its narrow substrate spectrum, as discussed in Section 2.2.2.

In most studies involving ethanol fermentations using *Z. mobilis*, glucose was the only carbon source. In order to achieve higher ethanol concentrations, HG media were used, which resulted in substrate inhibition. But reliable quantitative kinetic models are still very limited. Huang and Chen (1988) studied the kinetics of *Z. mobilis* through batch fermentation using a HG medium containing glucose of 200 g l^{-1} , and proposed the kinetic models characterized by both substrate and product inhibitions. As *Z. mobilis* can tolerate higher temperature than *S. cerevisiae*, the impact of temperature on its kinetic performance has also been studied (Fieschko and Humphrey, 1983; Stevsborg et al., 1986).

2.3.2 Process Design

The kinetics of ethanol fermentations are characterized by strong product inhibition, especially under VH and VHG conditions. *In situ* removal of ethanol seems to be the best way to decrease the inhibiting impact of ethanol, thus increasing the fermentation rates of yeasts and the productivities of fermentors (Roffler et al., 1984). Among the many technologies technically feasible for removing ethanol *in situ* from fermentation systems, pervaporation-fermentation has been widely investigated (Groot et al., 1992b; O'Brien and Craig, 1996; Ikegami et al., 2002).

O'Brien et al. (2000) analyzed the economic feasibility of coupling pervaporation with ethanol fermentation by comparing this technology with a typical dry-milling ethanol

fermentation process, and pointed out that the cost of the fermentation-pervaporation process is higher. Considering the problem of membrane fouling in handling the fermented mash with high concentration of solid raw material residues, this technology is impractical for use in dry-milling fuel ethanol production. Probably, it could be a possibility for the wet-milling process, in which most of raw material residues are separated prior to fermentation and a cleaner liquid mash is pumped into fermentors. However, the flux of the pervaporation membranes currently available is still not high enough to satisfy the large ethanol production capacity of the wet-milling process. Meanwhile, membrane fouling by yeast cells is still problematic.

Vacuum fermentation can also decrease the ethanol concentration inside the fermentors. This technology was investigated in ethanol fermentations using both *S. cerevisiae* and *Z. mobilis* (Cysewski and Wilke, 1977; Lee et al., 1981; Ghose et al., 1983). However, it is also impractical for ethanol fermentors with working volumes of hundreds, even thousands, of cubic meters to be operated at vacuum conditions. Both the capital cost for tank manufacture and the energy cost for tank operation are prohibitive in industry.

Taylor et al. (2000) reported on their pilot plant operation in which the ethanol fermentation was coupled with a stripping column and a condenser. Ethanol was stripped by recycled CO₂ in the stripping column and the ethanol enriched CO₂ went into a low temperature condenser where ethanol was absorbed by the circulated dilute ethanol condensate. The dry-milling corn mash containing 31% in total solids was continuously fed at a flowrate of 3.4 kg h⁻¹ into the fermentor in which the ethanol concentration was decreased to 4.8%. The condensate containing 27% ethanol was pumped out of the system at a flowrate of 0.88 kg h⁻¹. Meanwhile, the fermenting mash containing 4.8% ethanol was also pumped out of the system at a flowrate of 2.8 kg h⁻¹ to maintain its mass balance. The biggest disadvantage of such a system is the complexities in both its process design and operation, which makes it economically unattractive. Meanwhile, the fermenting mash containing 4.8

% ethanol was mixed with the condensate containing 27% ethanol, and the resulting mixture with a lower ethanol concentration was distilled, which seriously compromised the technical advantages.

In the event that economically feasible technologies, which can remove ethanol *in situ* and alleviate ethanol inhibition, are not available, the bioreaction engineering strategies that can decrease ethanol inhibition through decreasing the fermentor backmixing could be an alternative. Theoretically, batch bioreactors (BBR) and plug flow bioreactors (PFR) are the best selections because of no backmixing inside these two type bioreactors, which effectively minimizes production inhibition (Levenspiel, 1999). Indeed, BBRs have been widely used in conventional ethanol fermentations, especially in plants with small production capacities. Now, due to the dramatically increasing market demand for fuel ethanol, large scale ethanol fermentation plants with annual production capacities of several hundred thousand tons are being planned and established, in which fermentors are required with working volumes of over one thousand cubic meters. The disadvantage of the BBR's long operational downstream time required by mash addition, broth harvesting, and tank and pipeline cleaning makes it not suitable for large scale fermentation plants. As an average fermentation time of 48-72 hours is normally required to achieve a final ethanol concentration of 10-12% (w/v), and PFRs with very high superficial flow rate are also difficult to design and operate efficiently.

The chemical reaction engineering theory indicates that, compared with a single continuously stirred tank bioreactor (CSTR), a tanks-in-series system can effectively minimize product inhibition (Levenspiel, 1999). It is known that a system with an infinite number of CSTRs in series is equal to a PFR. Actually, this strategy has been practiced in ethanol fermentations for many years. Generally, tanks-in-series systems, composed of four to six tanks depending on their production capacity requirements, are preferred in industry because these designs tend to achieve the best balance between fermentation kinetics and

the capital investment for fermentor manufacture.

For VHG fermentations, product inhibition is more severe than the regular fermentations and substrate inhibition also likely occurs, especially for those tanks at the start of the cascade fermentation systems. Special considerations for their process design need to be addressed.

2.4 Mechanisms of Ethanol Inhibition

Ethanol is inhibitory, and the microbial cells exposed to ethanol respond to this inhibition and correspondingly adjust their intracellular metabolisms. Not only are the steady and instantaneous kinetics inhibited by ethanol but also the dynamic behaviors, which are unusual to be triggered by the delayed responses of cells to ethanol inhibition. Understanding the mechanisms through which toxic ethanol inhibits yeast cells is a prerequisite to better exploit potentials of the strains in use as well as to optimize process control to alleviate the negative impact of ethanol inhibition. Ethanol inhibition is multiple and very complicated. Figure 2.5 shows some possible sites in yeast cells at which ethanol could attack (D'Amore and Stewart, 1987).

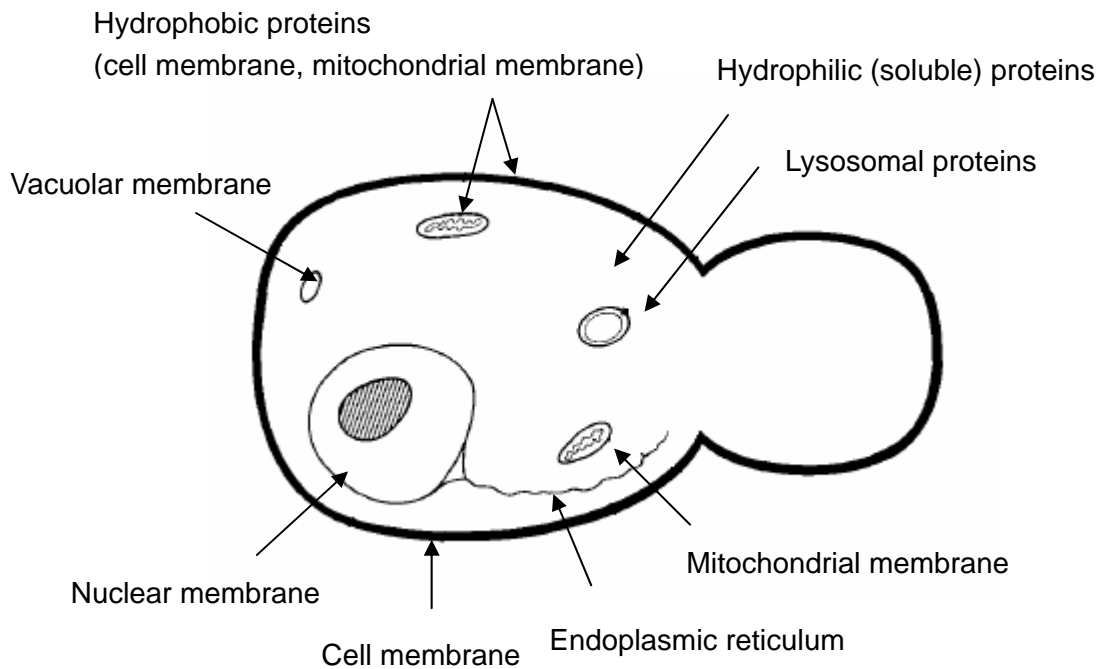


Figure 2.5 Possible sites of ethanol attack in yeast cells (D'Amore and Stewart, 1987)

Some key enzymes in the glycolytic pathway of yeast cells such as HK and ADH may be affected by ethanol, and ethanol may also affect nutrient uptake and membrane potential through decreasing the activity of the plasma membrane ATPase (Larue et al., 1984; Casey and Ingledew, 1986). Although discrepancies still exist among the many studies on the mechanisms of ethanol inhibition, it has been commonly accepted that the membranes of cells and some organelles are the main targets for ethanol attack (D'Amore and Stewart, 1987). In many cases, the inhibition by ethanol is exacerbated by the synergistic roles of other fermentation by-products such as acetaldehyde and other stresses such as high temperature (Jones, 1989).

Fatty acids, especially unsaturated fatty acids, like palmitoleic acid (C16: 1) and oleic acid, (C18: 1) of yeast cell membranes are the key components that overcome ethanol inhibition

by means of increasing the fluidity of the plasma membrane and compensating for the decrease of the plasma membrane fluidity resulting from the presence of ethanol. The levels of these two unsaturated fatty acids were measured to be higher for those ethanol tolerant strains or significantly increased after ethanol stress was exerted (You et al., 2003). They are synthesized in *S. cerevisiae* by the catalysis of the oxygen- and NADH-dependent desaturase of palmitric acid (C16: 0) and stearic acid (C18: 0). Therefore, a small amount of oxygen is required for yeast cells to synthesize these unsaturated fatty acids under an anaerobic fermentation condition. Actually, the role of a small amount of oxygen in improving the ethanol tolerance of yeast cells was investigated and already practiced in industry (Ryu et al., 1984). It is predicted that under VHG fermentation conditions the role of small amount of oxygen supply in improving ethanol tolerance will be more significant.

The trans-membrane proton flow that drives the secondary active transport of many nutrients has been found to be sensitive to ethanol inhibition. The dissipation of the proton gradient induced by ethanol was proposed to be involved in both the increase of the plasma membrane permeability (Pascual et al., 1988) and the inhibition of the proton-pumping plasma membrane ATPase activity (Salguero et al., 1988). It was therefore pointed out that the plasma membrane ATPase is a key membrane protein whose activity could be directly related to the ethanol tolerances of strains (Cartwright et al., 1987). Rosa and Sa-Correia reported that ethanol activated the plasma membrane ATPase of *S. cerevisiae* and *K. marxianus* at its lower levels while exerting inhibition at its higher levels (Rosa and Sá-Correia, 1992). Obviously, the adequate activity of the plasma membrane ATPase is a basis for yeast cells to maintain their intracellular physiological pH because the H^+ produced in fermentations needs to be continuously pumped out of cells by the proton motive force driven by the ATPase. The ethanol inhibition on yeast cells undergoing VHG fermentation is expected to be alleviated by properly neutralizing environmental H^+ and decreasing the H^+ gradient across the membranes when the plasma membrane ATPase is

inhibited by high ethanol concentration and cannot provide enough driving force to drive the H^+ out.

The pH values inside the rear fermentors of the cascade fermentation systems used in industry are observed to be higher than those inside the upstream fermentors. The main reason may be the increase of the plasma membrane permeability and decrease of the activity of ATPase caused by ethanol inhibition rather than by the by-product metabolism such as the uptake of organic acids produced during main fermentation under the depletion of sugar, because ethanol concentration as high as 12% (v/v) is normal in industry, which exerts strong inhibition on yeast cells, while the residual sugar at the level of 0.1-0.2 % (w/v) at the end of fermentation is actually not being depleted.

Indeed, the mechanisms of ethanol inhibition are still not clear in many aspects, especially at the genetic level and the investigations in this field are still ongoing. Many factors, such as temperature and nutrients, directly or indirectly affect the ethanol tolerance of the same strain, and either exacerbate or alleviate it. Many strategies have been developed and new research progress is continuously being made. Some of these strategies are scientifically meaningful, but may be not practical in industry because of their economic disadvantages. Just as in achieving ethanol inhibition alleviation through optimizing the mixing performance of fermentors, the engineering strategies might include adding a small amount of oxygen by aeration to stimulate the synthesis of unsaturated fatty acids, and feeding ammonia to the rear fermentors to improve their nutritional conditions as well as to neutralize some organic acids produced in the preceding main fermentors so that the proton gradient across the cell membrane can be decreased to compensate for the decrease of the activity of ATPase caused by ethanol inhibition. These strategies will likely be more economically practical in industry.

2.5 Yeast Cell Immobilization

The concept of whole cell immobilization was proposed in the 1970's (Kierstan and Bucke, 1977). It was adopted from the concept of enzyme immobilization and aimed at simplifying those complicated bioreactions catalyzed by intracellular multiple enzyme systems involving cofactors or coenzymes. It was predicted to be more economically competitive than those separated individual enzymatic bioreactions. However, because cells, whether living or dormant, are far more complicated than any enzymes, immobilized cells, in many cases, could not work as efficiently as they were initially predicted.

Theoretically, cell immobilization is more reasonable for secondary metabolites than for primary metabolites whose production is coupled with cell growth. When cells are immobilized, they are generally constrained by the supporting materials, and their growth is seriously compromised by such factors as the depletion of nutrients and accumulation of metabolites because of potential mass transfer limitation. Nevertheless, the growing cells are difficult to remove from immobilized cell systems, especially when cells are immobilized by gel entrapment, one of the most commonly used technologies.

Ethanol is a primary metabolite and its production is tightly coupled with yeast cell growth. The ethanol fermentation rate of the non-growing yeast cells is at least 30 fold slower than that of growing ones (Ingledeew, 1999), because the accumulation of ATP strongly inhibits the activity of PFK, one of the most important enzymes in glycolytic pathway. While a lot of studies have been done on ethanol fermentations using gel-entrapped immobilized yeast and bacterial cells within the past three decades, no commercial applications have been reported since Nagashima et al. (1984) established their pilot plant in 1984. Apparently this research trend had been misdirected in the past and may still be misdirected at present, both technically and economically, because the energy cost to achieve high ethanol productivities at the price of sacrificing ethanol concentrations adopted in those

immobilized yeast cell systems was actually increased.

Some yeast cell immobilization techniques, especially by surface adsorption, seem to be more reasonable than those by gel and microcapsule entrapments, as well as those using membrane retention through which yeast cells are almost completely immobilized in which the growth of yeast cells is seriously compromised. When yeast cells are immobilized by surface adsorption, the growth of yeast cells is not significantly affected and some yeast cells can be washed out because the adsorption of the yeast cells onto the surfaces of the supporting materials is generally very loose.

As discussed previously, the yeast cell membranes are the main targets at which toxic ethanol attacks. When yeast cells are confined by supporting inert matrixes, they have surfaces to attach as well as more opportunities to be closely aggregated. This not only provides better protection to the damaged membranes, but also facilitates the synergistic roles among individual yeast cells to overcome ethanol stress and enhances their ethanol tolerance. Jirku investigated *S. cerevisiae* immobilized by gel entrapment and found that the leakage of UV-absorbing intracellular substances significantly decreased compared with that of free yeast cells. Further analysis of the membrane composition of immobilized cells indicated that fatty acids (saturated and unsaturated), phospholipids, and sterols increased for the immobilized yeast cells and therefore provided better protection for the cell membranes under ethanol attack (Jirku, 1999). Desimone et al. (2002) also reported that the specific death rate for gel immobilized yeast cells decreased to one tenth of that of free yeast cells when both two groups were exposed to 50% (v/v) ethanol for 15 minutes. Recently, the research progress in the ethanol fermentation using self-flocculating yeast also showed similar results. The ethanol tolerance could be improved significantly when the yeast cells self-flocculated and formed the flocs on a millimeter scale from their free cells on a micrometer scale. Not only did the membrane composition change result from their self-flocculation, but also the potential synergism of the yeast cells flocculating

together contributed to their ethanol tolerance improvements (Hu et al., 2005).

The cell immobilization that aims to decrease ethanol fermentation time and increase the ethanol productivity of fermentors is likely to fail in the regular ethanol fermentations. However, this technology has new potential in improving the ethanol tolerance of yeast cells and may be helpful in attenuating the oscillations caused by the strong ethanol inhibition under VHG fermentation conditions, which needs to be exploited.

2.6 VHG Ethanol Fermentation

As discussed previously in Chapter 1, VHG fermentation technology can significantly save energy consumption for fuel ethanol production, especially for the downstream distillation and waste distillage treatment after fermentation. However, when a VHG medium is used, the strong inhibition on yeast cells: the substrate inhibition at the beginning and the product inhibition toward the end of the fermentation, will be present, negatively affecting the performance of such a fermentation system (Devantier et al., 2005).

Research has revealed that the ability for a yeast strain to achieve high ethanol concentration strongly depends on its nutritional conditions and protective functions that some special materials can provide. Assimilable nitrogen is the most important component of fermentation media and has been reported to be the limiting nutrient in the VHG ethanol fermentation using wheat mash. Thomas and Ingledew (1990) fermented wheat mash with 35% dissolved solids and produced 17.1% (v/v) ethanol in 8 days at 20 °C. When supplemented with 0.9% yeast extract, the fermentation time was reduced to 3 days to achieve the same ethanol concentration. Considering yeast extract is too costly for industry use, Jones and Ingledew (1994a, b) further studied the possibility of replacing yeast extract with industrial nutrient supplements and found urea could be an alternative. When protease

was used, the proteins in the mash were hydrolyzed and free amino acids and small peptides were released, which provided better nutrients for the yeast cells and the fermentation performance was improved significantly.

Glycine was found to be an effective osmoprotectant, which helped to maintain the high viability of yeast cells compared with no protection (Thomas et al., 1994). Reddy (2005, 2006) reported that horse gram (*Dolichos biflorus*) and finger millet (*Eleusine coracana*) improved the fermentability of *S. cerevisiae* under VHG conditions because of their double roles as both nutrients and osmoprotectants.

In addition to product and substrate inhibition, other stresses may also exist. Under a VHG condition, the fermentation is worsened by high temperature, which is always being pursued by industry because the fermentation plants operated at high temperature can save on energy consumption for fermenter cooling. Jones and Ingledew (1994c) investigated the impact of temperature on VHG fermentation and found that the fermentation time was extended dramatically when temperature increased from 17°C to 33°C.

No matter what factors are investigated, the most important is that their contributions to improving the performance of VHG fermentations are economically feasible and acceptable in industry. Many nutrients supplemented into the media in laboratory research, such as amino acids, vitamins, sterols, unsaturated fatty acids and so on, are too expensive to be used in industry. Probably engineering improvements that can help optimize physiological environments for the yeast cells under a variety of stresses could be more economically feasible. For example, increasing the number of the tanks in series for new plant construction or adding baffles inside the tanks in use to partition them can effectively decrease the backmixing of fermentors and alleviate ethanol inhibitions.

For large-scale fuel ethanol production, continuous fermentations have been approved to be more economically competitive than batch models. However, up till now, almost all

research involving VHG ethanol fermentation technologies has been carried out in batch models except that Bayrock and Ingledew (2001) as well as Lin et al. (2002) reported continuous VHG ethanol fermentation in a multistage fermentation system, through which process state and fermentation performance were studied. Steady states were claimed for residual glucose, ethanol, and yeast cell biomass.

2.7 Oscillation and Dynamics

All kinetic models currently available in *S. cerevisiae* ethanol fermentations are steady-state for continuous fermentations, or instantaneous for batch ones. Although unsteady states and oscillations are common phenomena in almost all continuous biological systems, and many studies in the oscillations of the glycolytic pathway in *S. cerevisiae* have been reported (Ghosh and Chance, 1964; Ghosh et al., 1971; Danø et al., 1999; Wolf and Heinrich, 2000; Madsen et al., 2005), only Borzani (2001) reported the oscillations of residual sugar, ethanol and biomass in the continuous ethanol fermentation using *S. cerevisiae* and molasses. More recently, our preliminary studies observed and validated the sustainable oscillations characterized by long oscillation periods and large oscillation amplitudes for residual glucose, ethanol, and biomass in the continuous ethanol fermentation using *S. cerevisiae* and a VHG medium (Bai et al., 2004a).

The oscillations of continuous ethanol fermentation were first reported by Lee et al. (1979) in the late 1970s when they studied the continuous ethanol fermentation by *Z. mobilis* using 10, 15, and 20% glucose media, and found that although steady states presented for glucose, ethanol, and biomass at the low gravity medium (10% glucose) condition, oscillations of the fermentation system were observed when the media containing 15 and 20% glucose were used. Later, when Ghommidh et al. (1989) reported the oscillatory behaviors in the continuous ethanol fermentation using *Z. mobilis*, they questioned: “**why such phenomena**

have never been reported with yeast?”

However, if we carefully examine the industrial processes of ethanol fermentation, such oscillations do exist but have been neglected. For example, residual sugar, ethanol and biomass concentrations within the main fermentors of four to six tanks in series systems oscillate up and down around their average levels, but are gradually dampened as the fermented broth goes through the rear fermentors, and are finally attenuated in the last one or two fermentors. Much longer fermentation time is required to attenuate these oscillations and achieve quasi-steady state at the end of fermentation, especially for the final residual sugar that must be controlled at no more than 0.25%(w/v) to guarantee the ethanol yield that is calculated on the basis of the total sugar in the medium, without the deduction of the residual sugar in the final broth. Generally, an average fermentation time of 50-70 hours is required for starch materials to achieve the ethanol concentration of only 10-12% (w/v) at the end of fermentation when no centrifuges are used to separate yeast cells and recycle the part of condensed yeast cream back to the main fermentors (Bothast and Schlicher, 2005).

In the case of oscillations, dynamic kinetics rather than steady-state kinetics are required to explain, predict, and optimize fermentation processes. A mechanistic analysis is a prerequisite to develop such kinds of dynamic models. Although there are many investigations involving oscillations in the continuous cultures of *S. cerevisiae* (Chen and McDonald, 1990a, b; Duboc et al., 1996; Beuse et al., 1998, 1999; Patnaik, 2003), the oscillation patterns observed in the continuous ethanol fermentations using both *S. cerevisiae* in our preliminary research (Bai et al., 2004a) and Borzani's work (2001) and *Z. mobilis* (Lee et al., 1979; Bruce et al., 1991; Jarzebski, 1992) are significantly different from the oscillations reported for the continuous aerobic cultures of *S. cerevisiae*, in which the synchronization of the rhythms of the mother and daughter cells is believed to be the mechanistic reason. Therefore, the mechanisms triggering such oscillations could be different, correspondingly.

Jöbses et al. (1986) analyzed the sustained oscillations in biomass, ethanol and glucose concentrations in the continuous ethanol fermentation using *Z. mobilis* and pointed out that the theoretical possibility of such a system is a delayed response of *Z. mobilis* on ethanol inhibition. This hypothesis can be imagined if ethanol inhibition does not directly act on fermentation and its production, but indirectly on it by inhibiting what is coupled with its production, say, the growth of biomass.

For dynamic ethanol fermentation systems, the inhibition of ethanol involves two aspects, the history of ethanol concentration and the rate of change of ethanol concentration. Lee et al. (1995) carefully designed their experiments on the ethanol fermentation by *Z. mobilis* and revealed that the latter, the rate of change of ethanol concentration and especially the upward rate of change, exerts stronger inhibition than the history of ethanol concentration that reflects the time period that the cells experience a corresponding ethanol concentration. Furthermore, they developed dynamic models incorporating the time delay and predicted the oscillatory behaviors of *Z. mobilis* (Daugulis et al., 1997; McLellan et al., 1999). No similar work is available for the continuous ethanol fermentations using *S. cerevisiae*!

Rasch et al. (2002) studied the continuous production of reuterin in a chemostat system by *Lactobacillus reuteri* and observed sustainable oscillations of biomass, glucose, reuterin, and the by-products of glucose and glycerol metabolisms such as acetic acid, lactic acid, and 1,3-propanediol. Compared with the oscillations observed in the ethanol fermentation by *Z. mobilis* (Daugulis et al., 1997; McLellan et al., 1999) as well as by *S. cerevisiae* (Borzani, 2001), the oscillation profiles of the reuterin fermentation were different, and the rapid increase and decrease of the oscillatory parameters were observed. For example, after the biomass concentration maintained at its lowest level of 0.06 for a relatively longer period of time, it dramatically increased to its highest level of 3.0, then, immediately decreased to the lowest again, and the concentration of reuterin oscillated in the same

pattern with that of the biomass. The reason for this special oscillation pattern was speculated and partly validated to be the acute cell lysis caused by the lethal effect of reuterin on its host cells. A similar situation was also observed in our preliminary studies within the tubular bioreactors, in which a very high ethanol concentration was achieved and the lethal effect of high concentration ethanol on the yeast cells affected the oscillation patterns of the tubular bioreactors (Bai et al., 2004b).

Menzel et al. (1996) reported the oscillation behavior of the continuous production of 1,3-propanediol by *Klebsiella pneumoniae* from glycerol. Glycerol, biomass, 1,3-propanediol, and many other metabolites including CO₂, H₂, formate, acetic acid, and ethanol were oscillatory during the fermentation. In their later series of articles (Zeng et al., 1996; Ahrens et al., 1998; Menzel et al., 1998), the mechanism inciting these oscillations was studied through metabolite flux analysis as well as the analysis and comparison of the key enzyme activities in the glycerol dissimilation pathway. It was concluded that the reason for the oscillations lies in an unstable regulation of three enzymes in the pyruvate metabolism pathway triggered by substrate excess and drastic change(s) of environmental conditions. It was reported that these oscillations could improve the productivity of 1,3-propanediol as the stresses exerted on the cells was alleviated during the oscillations (Yang and Su, 1993). Substrate excess definitely presents in continuous VHG ethanol fermentation, and might affect its process state and oscillation profile.

2.8 Summary

Although ethanol fermentations have been heavily studied in both its fundamentals and applied technologies, many aspects are still open, as Ingledew named it “a black box” in his book: *The Alcohol Textbook* (Ingledew, 1999).

The VHG fermentation technology can save energy and utility consumption not only for the post-fermentation such as distillation and waste distillage treatment, but also for the fermentation itself as well as for the pretreatment involving mash preparation for fuel ethanol production from starch materials. The success of the VHG fermentation technology lies in the deep understanding of ethanol fermentation pathways of yeast cells, especially the inhibitions exerted by the VHG medium at the initial stage of the fermentation and the high ethanol concentration toward the end. However, developing the corresponding engineering strategies to bridge the fundamental research and industrial application is more important. From a comprehensive literature review, the following needs to be studied to improve this energy-saving ethanol fermentation technology:

1. From the point view of large scale fuel ethanol production, a more effective continuous VHG ethanol fermentation model rather than the batch ones currently established should be developed.
2. Unsteady state and oscillatory behavior were observed in the continuous ethanol fermentation by *Z. mobilis* as well as in the continuous fermentations of other microbial products which are inhibitory to their host cells, similar to the inhibition of ethanol on yeast cells. Theoretically, similar unsteady state and oscillation should occur in the continuous ethanol fermentation by yeast cells under a VHG condition, but have been rarely reported until now.
3. Unsteady-state and oscillation have been observed for the continuous VHG ethanol fermentation in our preliminary research, and the corresponding mechanism has been postulated. But, more understanding is needed based on established knowledge in the ethanol fermentation field as well as new insights into the VHG fermentation system in order to develop practical engineering strategies to deal with these phenomena, and to improve the efficiency of the VHG fermentation system.

Chapter 3 Project background: Continuous VHG ethanol fermentation

The work in this chapter was published in *Biotechnol Bioeng*, 2004, 88, 558-566 and *J Biotechnol*, 2004, 110, 287-293, respectively.

3.1 Introduction

Ethanol fermentation is a typical product-inhibited process. When a VHG medium containing more than 250 g l⁻¹ sugar is used in order to achieve more than 15% (v/v) ethanol at the end of the fermentation, not only can strong product inhibition develop as the fermentation is proceeding and high ethanol concentration is approached, but substrate inhibition is also inevitable at the early stage of the fermentation. No single bioreactor is suitable for the VHG fermentation without encountering these inhibitions. A bioreactor system composed of a CSTR and three-stage tubular bioreactors in series was established and examined for its VHG ethanol fermentation performance. Both the substrate and product inhibitions were expected to be alleviated because of the different mixing patterns of these two types of bioreactors.

3.2 Materials and Methods

3.2.1 Strain, medium, and pre-culture

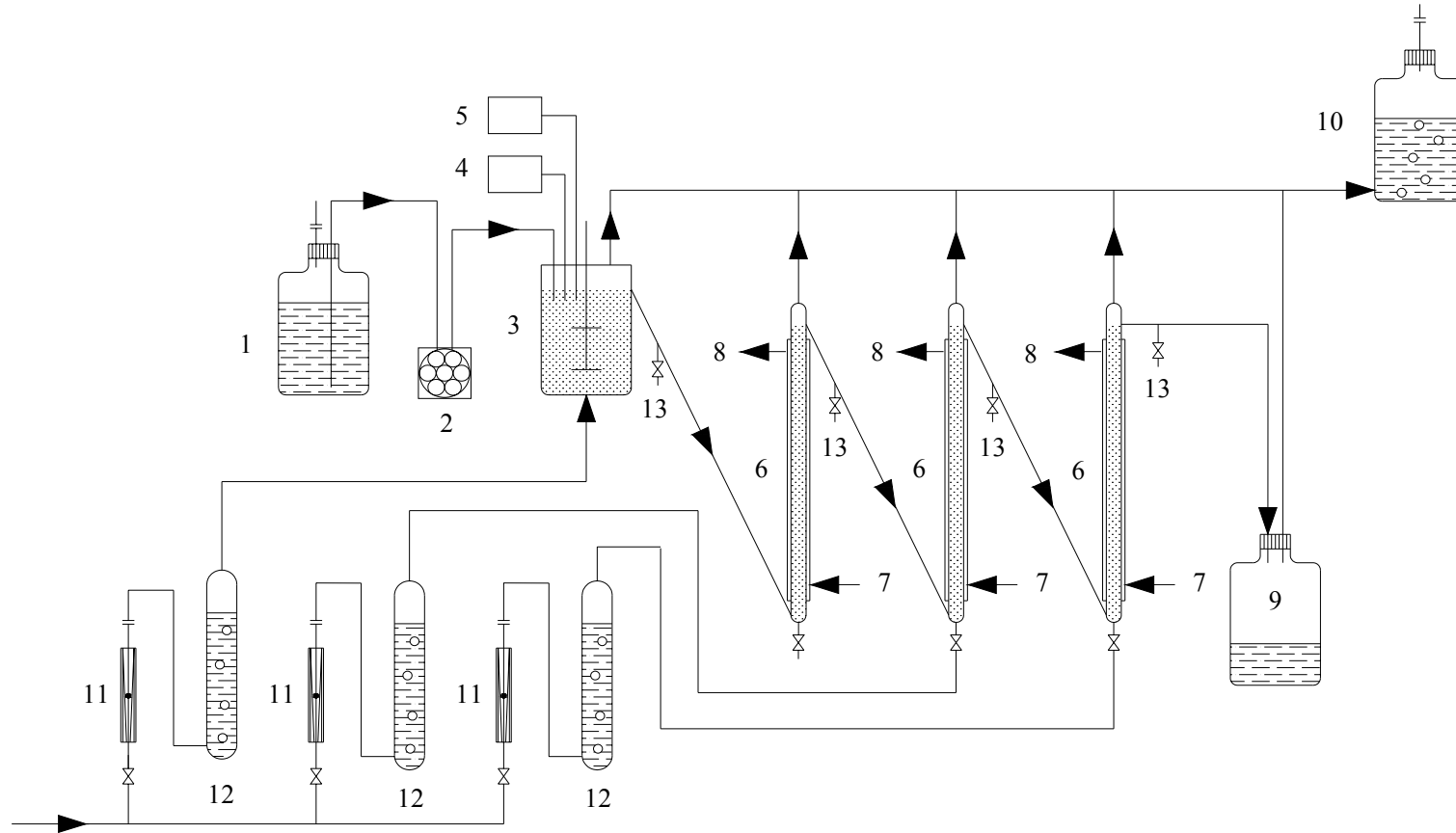
A yeast strain, *Saccharomyces cerevisiae* ATCC 4126, was used as a model strain. Pre-culture was carried out in 250 ml Erlenmeyer flasks containing 100 ml medium composed of (g l⁻¹) glucose, 30, yeast extract, 5 and peptone, 3. The rotary shaker speed and temperature were controlled at 150 rpm and 30 °C, respectively. The overnight growth

culture was used to inoculate the fermentor with a working volume of 1500 ml and containing the medium composed of (g l^{-1}) glucose, 120, yeast extract, 5 and peptone 3. After inoculation, a batch culture was carried out until the glucose was exhausted. Then, continuous ethanol fermentation was initiated by feeding the VHG medium containing 280 g l^{-1} glucose at the designated dilution rate. The high gravity (HG) medium containing 200 g l^{-1} glucose and the low gravity (LG) medium containing 120 g l^{-1} glucose were used to achieve different ethanol and residual glucose scenarios within the fermentor so that the impact of ethanol and residual glucose on the fermentation process could be studied. Yeast extract and peptone were added to all media at the concentrations of 5 g l^{-1} and 3 g l^{-1} , respectively.

Several 5000 ml flasks were used as medium reservoirs. The sterilization of the media was carried out by heating the flasks to 121°C for 10 minutes, then immediately cooling down to room temperature to avoid inhibitor formation.

3.2.2 Bioreactor system

The bioreactor system was a 1500 ml Bioflo fermentor (New Brunswick Scientific, New Brunswick, NJ, USA) followed by three tubular bioreactors, as illustrated in Figure 3.1. The diameter of the tubular bioreactor was 36 mm. The volumes of the first, second, and third tubular bioreactors were measured to be 600, 610 and 620 ml, respectively. The fermentor was validated to be a CSTR when its stirring speed was adjusted at 300 rpm. This bioreactor system was operated in two modes: empty columns or packed with 1/2" Intalox ceramic saddles, and fed with the VHG medium at a constant dilution rate, which was selected to achieve the lowest residual glucose in the final effluent. After being packed, the volumes of the first, second, and third tubular bioreactors were measured to be 460, 470, and 480 ml, respectively.



1 Substrate tank, 2 Peristaltic pump, 3 Stirred tank, 4 and 5 pH and temperature control units, 6 Tubular bioreactors, 7 and 8 Thermostat water inlets and outlets, 9 Effluent tank, 10 Exhaust gas washing tank, 11 Air flowmeters, 12 Humidifiers, 13 Sampling ports

Figure 3.1 Diagram of the bioreactor system for continuous VHG ethanol fermentation with *S. cerevisiae*.

A small amount of oxygen was supplied to the CSTR by aerating it at 0.025 vvm. The pH value of the CSTR was controlled at 4.5 by automatically adding 1 N NaOH, and the natural pH values were maintained for the tubular bioreactors. The temperature for the whole bioreactor system was controlled at 30 °C. In order to calculate the ethanol yield, the exhaust gas was washed by bubbling it into a de-ionized water storage tank to recover volatilized ethanol.

For the empty tubular bioreactors, as the residual glucose concentrations within the second and third ones were too low to produce enough CO₂ to suspend yeast cells (especially when the yeast cells aggregated under the poor nutrient and high ethanol conditions), they were aerated at a flowrate of 0.005 vvm to improve the suspension of the yeast cells. The aeration was discontinued for the packed columns.

The empty tubular bioreactors were naturally inoculated at the fermentation dilution rate by the overflow of the broth containing yeast cells from the CSTR. The packed ones were inoculated by feeding the LG medium at a higher dilution rate of 0.1 h⁻¹ to eliminate ethanol inhibition, facilitate fermentation, and generate more CO₂ within the bioreactors to prevent yeast cells from depositing within the small chambers formed by the packing.

3.2.3 Analytical methods

After sampling, the sample was filtered immediately using a 0.2 µm filter to remove yeast cells. The supernatant was collected and refrigerated for 2-3 days during which 16-24 samples could be collected for glucose and ethanol analysis.

In order to guarantee the ethanol concentration of the analytical sample was in the linear range, the supernatant sample was diluted ten times by the internal standard solution containing 10 g l⁻¹ isopropanol by adding 100 µl supernatant sample to 900 µl internal standard solution. Then, ethanol was analyzed by gas chromatography (HP 5890: Solid phase: crossbonded phenylmethyl polysiloxane, helium carrier gas, 70°C isothermal

capillary column, 150°C injector temperature, 250°C Flame ionization detector temperature, Peaksimple Data Handling System). Duplicates were applied to all samples. Meanwhile, for every batch analysis, a verification standard was prepared to check the accuracy of the analysis. The analytical error was validated to be no more than $\pm 1.5\%$.

Glucose was analyzed by an enzymatic method (Sigma Glucose Diagnostic Kit, Catalog No. 115-A). Triplicates were applied to all samples. The analytical error for glucose analysis was validated to be no more than $\pm 3.0\%$.

The dry weight gravimetric method was used to measure biomass concentration, where a 1 ml sample was centrifuged, washed 3 times by deionized water, dried at 85 °C for 24 hours, and then weighed. Three parallel samples were collected simultaneously to assure the reliability of analytical results. The analytical error for the biomass measurement was validated to be no more than $\pm 5.0\%$.

A 0.1% methylene blue water solution was used to qualitatively evaluate the viability of yeast cells after samples were properly diluted with deionized water.

3.3 Results and Discussion

3.3.1 Process State

Currently, the medium containing no more than 22% (w/v) sugar is used in the ethanol fermentation industry, from which 12~13% (v/v) ethanol is produced at the end of fermentation. Both batch and continuous models can be found, but continuous fermentation is widely used in large-scale fuel ethanol production in which steady state is assumed. Only Borzani (2001) reported oscillatory behaviors of residual sugar, ethanol, and biomass in continuous ethanol fermentation by *S. cerevisiae* when diluted sugar-cane molasses containing 17% (w/v) sugar was fed into a small CSTR at a dilution rate of 0.032 h^{-1} .

For the VHG medium described in Section 3.2.1 and the bioreactor system illustrated in Figure 3.1, when the CSTR was operated at a medium flowrate of 40.5 ml h^{-1} , the lowest average residual glucose was achieved in the effluent from the third tubular bioreactor. The corresponding medium dilution rate was 0.027 h^{-1} . Then, the bioreactor system was operated at this dilution rate to evaluate its long-term continuous VHG fermentation performance. Within the whole experiment duration, the dilution rate was calibrated twice daily by measuring the flowrate of the fermented broth discharged from the last tubular bioreactor, and the fluctuation of the flowrate was validated to be no more than $\pm 2.5\%$, guaranteeing that a constant dilution rate was applied to the fermentation system. Three weeks were required for the bioreactor system to complete the transition from its inoculation. After that, residual glucose and ethanol in the effluent out of each bioreactor reasonably matched the initial glucose in the VHG medium feeding into the CSTR.

Figure 3.2 illustrates the time-courses of the residual glucose, ethanol and biomass of the CSTR. It can be seen that these parameters fluctuated significantly, and true steady states could not be established within the duration of 40 days. The fluctuation ranges of the residual glucose, ethanol and biomass were $106.3\sim 129.7 \text{ g l}^{-1}$, $64.4\sim 76.1 \text{ g l}^{-1}$ and $3.3\sim 5.1 \text{ g(DCW) l}^{-1}$, and the corresponding absolute fluctuation amplitudes* were 23.4 g l^{-1} , 11.7 g l^{-1} , and $1.8 \text{ g (DCW) l}^{-1}$. The averages of residual glucose, ethanol, and biomass were 117.2 g l^{-1} , 70.3 g l^{-1} , and $4.1 \text{ g(DCW) l}^{-1}$, making the corresponding relative fluctuation amplitudes $\pm 10.0\%$, $\pm 8.3\%$, and $\pm 22.0\%$, respectively, which were much larger than the analytical errors, $\pm 3\%$ for glucose, $\pm 1.5\%$ for ethanol and $\pm 5\%$ for biomass. In addition, these fluctuations were observed to be sustainable and periodic oscillations, with oscillation periods of 7~10 days. The oscillation of the biomass was not in phase or out of phase with the oscillations of ethanol or residual glucose, which are always out of phase in ethanol fermentation.

* The absolute and relative amplitudes were defined as the difference between the fluctuation peak and trough, and the percentage of the fluctuation peak and trough to the fluctuation average, respectively.

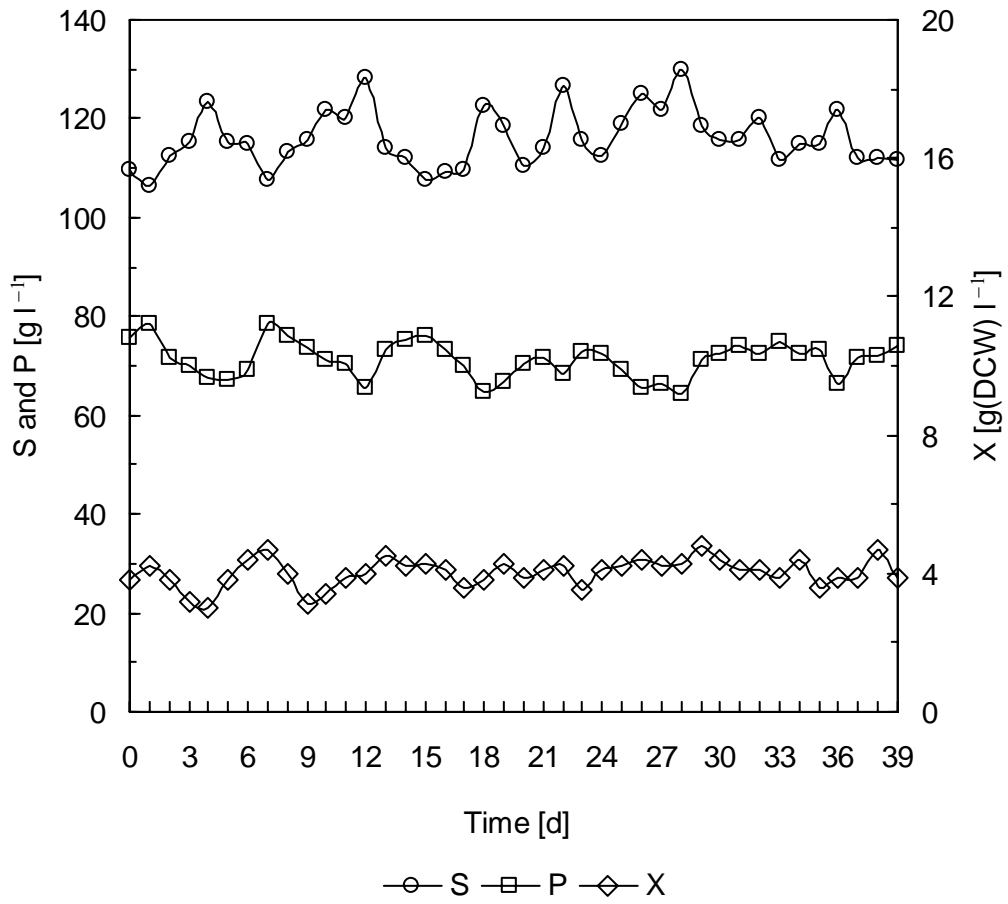


Figure 3.2 Time-courses of the residual sugar, ethanol, and biomass of the CSTR. Initial glucose concentration in the VHG medium: $S_0 = 280 \text{ g l}^{-1}$, and the dilution rate: $D = 0.027 \text{ h}^{-1}$.

As 15% (v/v) ethanol concentration is believed to be a physiological barrier for general yeast strains, VHG fermentation is not commonly accepted in both academia and industry. Thomas and Ingledew (1992) studied fermentation physiology of *S. cerevisiae*, pointed out that most strains from *S. cerevisiae*, without any modifications, can tolerate much stronger ethanol inhibition and achieve as high as 21% (v/v) ethanol concentration, and initiated VHG fermentation in the early 1990s. It is true that ethanol tolerance of yeast strains can be improved by optimizing their nutritional conditions and fermentation parameters, and ethanol concentration achieved at the end of fermentation has been continuously increased in the ethanol fermentation industry within the past two decades.

Until recently, almost all VHG ethanol fermentations were carried out in batch models. Bayrock and Ingledew (2001) reported on a continuous VHG ethanol fermentation using a multistage continuous fermentation system. A VHG medium containing 31.2% (w/v) glucose supplemented with 2% corn steep flour and 20 mM $(\text{NH}_4)_2\text{HPO}_4$ was used, and a maximum ethanol concentration of 16.7% (v/v) was achieved when the fermentation system was operated at a dilution rate of $8.6 \times 10^{-3} \text{ h}^{-1}$ based on the fermentation system's total working volume of 16.2 l or a dilution rate of 0.028 h^{-1} based on the first fermentor with a working volume of 5 l, in order to control the residual glucose in the final effluent to be no more than 3 g l^{-1} . The ethanol yield was calculated to be 0.421, equivalent to 82.3% of the theoretical value of the ethanol-to-glucose yield of 0.511.

The equilibration time for Bayrock and Ingledew's fermentation system was one week when the dilution rate change was made and steady state was claimed when the glucose concentration variation was less than 5% over a three-day sampling period. Given the low dilution rate of $8.5 \times 10^{-3} \text{ h}^{-1}$ and the corresponding average fermentation time of 116 h, it was highly possible that the one-week equilibration time was too short to truly equilibrate the fermentation system.

Figures 3.3~3.5 further illustrate the time-courses of the residual glucose and ethanol of the tubular bioreactors. The residual glucose and ethanol within the tubular bioreactors were validated to be well-mixed, but the biomass concentration was not because dead yeast cells caused by the toxicity of high ethanol concentration tended to aggregate and deposit in the lower sections of the tubular bioreactors, and axial biomass concentration gradients were observed. The mixing performance of the tubular bioreactors was studied by measuring their axial concentration distributions of the residual glucose, ethanol, and biomass as well as the residence time distributions (RTDs) later in Chapter 6. It can be seen that these tubular bioreactors were also oscillatory.

For the first tubular bioreactor, its absolute oscillation amplitudes were 28.1 g l^{-1} for residual glucose and 13.8 g l^{-1} for ethanol with the corresponding oscillation averages of 60.1 g l^{-1} and 93.4 g l^{-1} . Given the ethanol productivity of $1.49 \text{ g l}^{-1} \text{ h}^{-1}$, slightly lower than the ethanol productivity of $1.89 \text{ g l}^{-1} \text{ h}^{-1}$ of the CSTR, these oscillations were almost at the same scales, and the oscillation periods were not changed significantly. The absolute oscillation amplitudes of residual glucose and ethanol were 24.8 g l^{-1} and 13.6 g l^{-1} for the second tubular bioreactor, and 23.5 g l^{-1} and 16.5 g l^{-1} for the third tubular bioreactor, respectively. The corresponding averages of residual glucose and ethanol were 31.7 g l^{-1} and 106.8 g l^{-1} for the second tubular bioreactor, and 17.9 g l^{-1} and 114.0 g l^{-1} for the third tubular bioreactor. Taking into account the ethanol productivities of $0.88 \text{ g l}^{-1} \text{ h}^{-1}$ for the second tubular bioreactor and $0.54 \text{ g l}^{-1} \text{ h}^{-1}$ for the third tubular, their oscillations were significantly exaggerated.

Ethanol yield was further evaluated for the whole bioreactor system and illustrated in Figure 3.6 and Appendix A. As can be seen, although each of those bioreactors was oscillatory, their ethanol yield was relatively constant within the duration of 40 days, at the averages of 0.433, 0.425, 0.430, and 0.434 for the CSTR, first, second, and third tubular bioreactors.

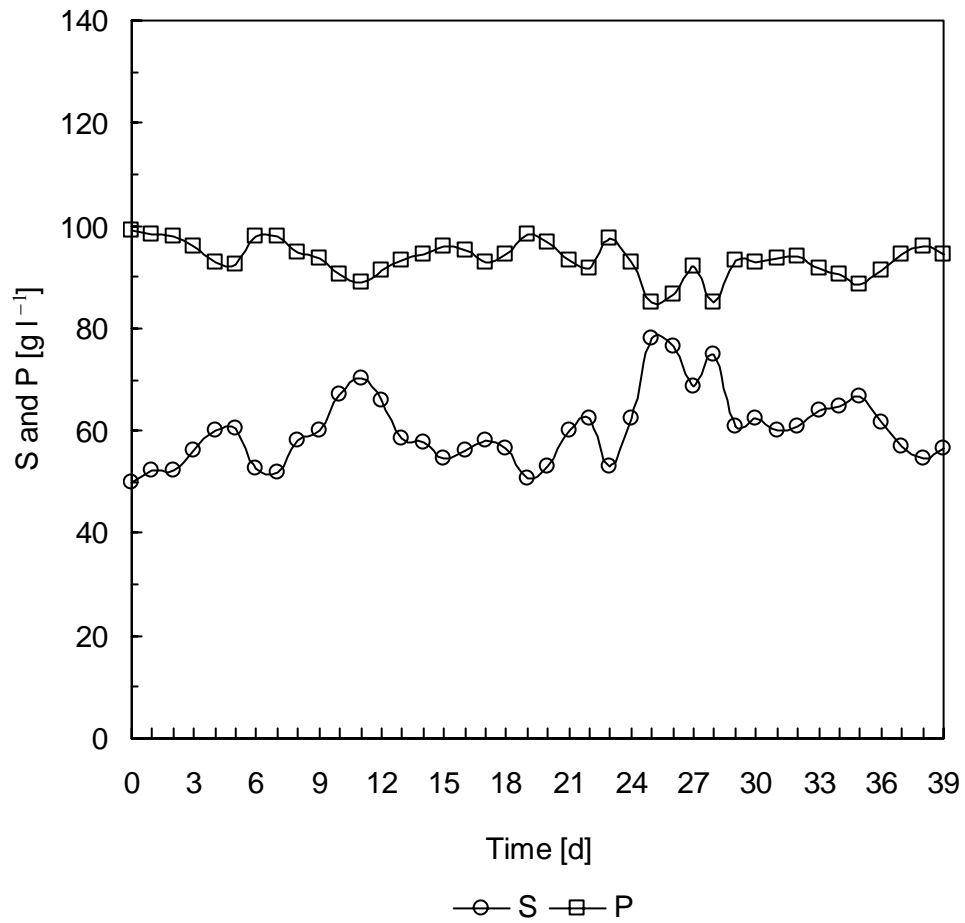


Figure 3.3 Time-courses of the residual sugar and ethanol of the first tubular bioreactor. Initial glucose concentration in the VHG medium: $S_0 = 280 \text{ g l}^{-1}$, and the dilution rate of the CSTR: $D = 0.027 \text{ h}^{-1}$.

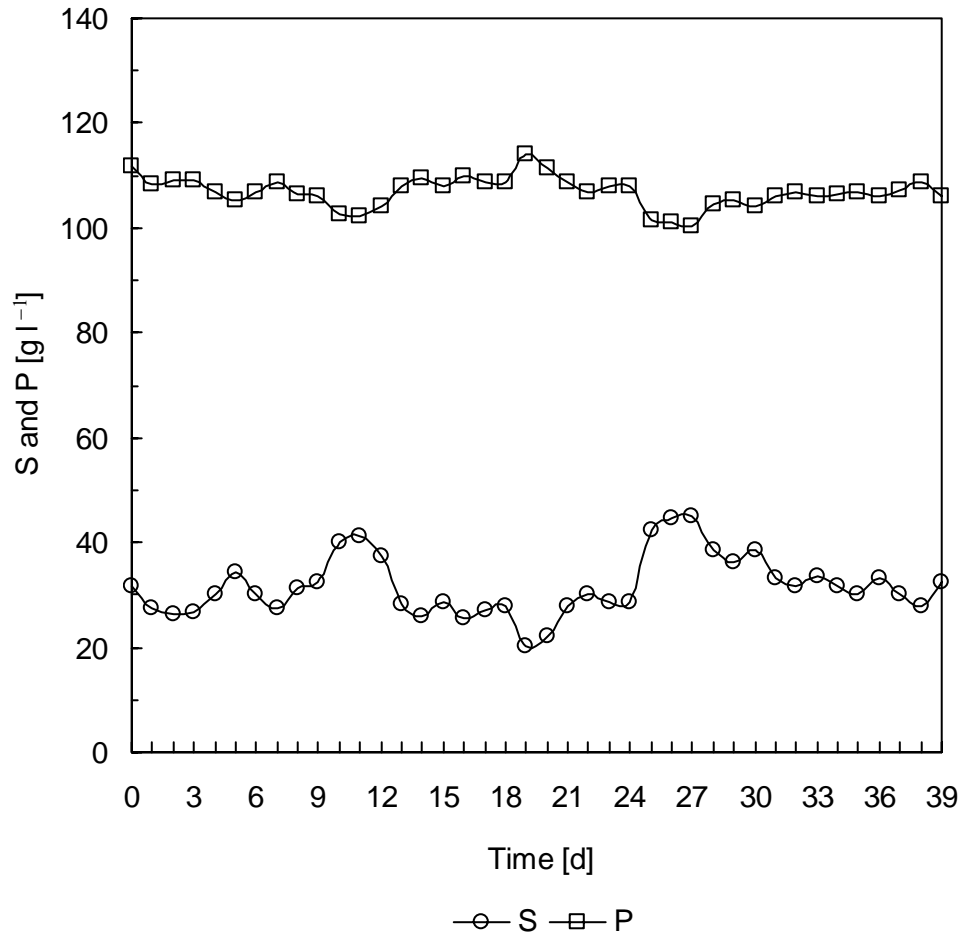


Figure 3.4 Time-courses of the residual sugar and ethanol of the second tubular bioreactor.

Initial glucose concentration in the VHGM medium: $S_0 = 280 \text{ g l}^{-1}$, and the dilution rate of the CSTR: $D = 0.027 \text{ h}^{-1}$.

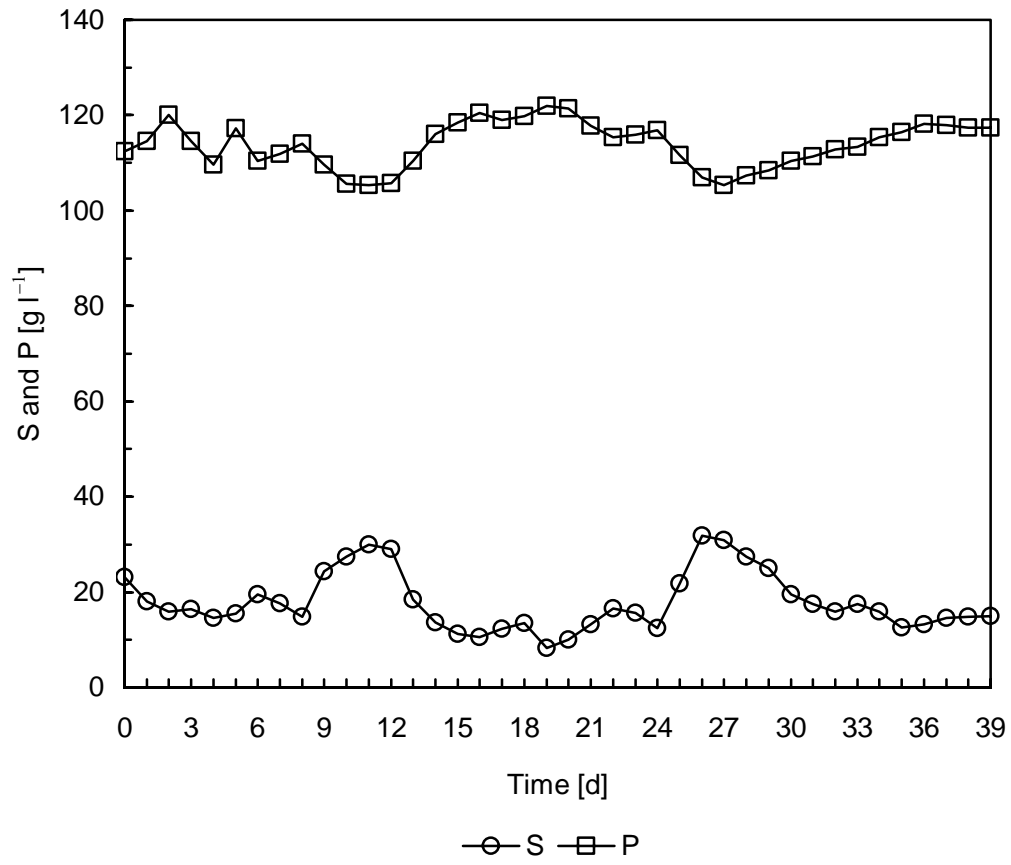


Figure 3.5 Time-courses of the residual sugar and ethanol of the third tubular bioreactor.

Initial glucose concentration in the VHG medium: $S_0 = 280 \text{ g l}^{-1}$, and the dilution rate of the CSTR: $D = 0.027 \text{ h}^{-1}$.

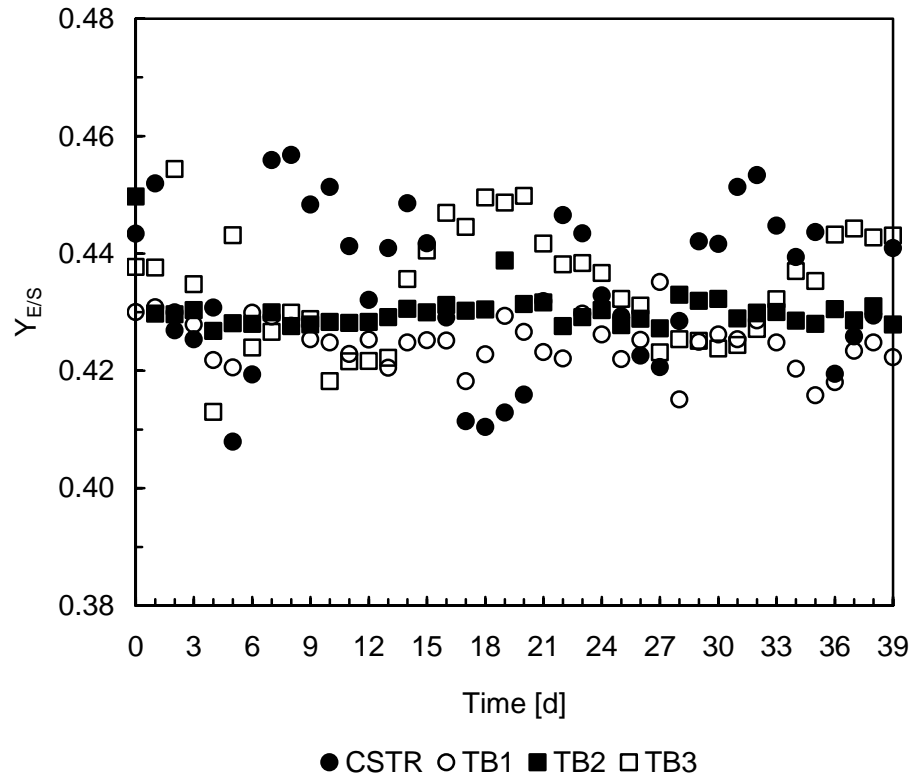


Figure 3.6 Ethanol yield of the continuous fermentation. Initial glucose concentration in the VH medium: $S_0 = 280 \text{ g l}^{-1}$, and the dilution rate of the CSTR: $D = 0.027 \text{ h}^{-1}$.

If the ethanol loss caused by evaporation with the exhaust gas during the fermentation was taken into account, the ethanol yield of the whole bioreactor system was calibrated to be 0.465, about 91% of the theoretical value of the ethanol-to-glucose yield of 0.511*.

Initially, the continuous VHG ethanol fermentation was expected to be operated at steady state, and samples were taken on a daily basis. After oscillatory behaviors were observed, the sampling interval was shortened to four hours to ensure that some intrinsic phenomena which might be masked by the longer sampling interval could be revealed.

As illustrated in Figure 3.7, two different fluctuation profiles for residual glucose, ethanol and biomass were further observed. First, these parameters fluctuated within small ranges, and lasted for a relatively longer period of time, about three to four days. At this stage, quasi-steady states were developed, but these quasi-steady parameters were toward one direction, either upward or downward. It was possible that the experimental data in literature which supported the claims for steady or quasi-steady state in continuous ethanol fermentations were collected at this stage. Then, another kind of process state occurred, which was characterized by large fluctuations and the changes of fluctuation directions, but lasted for a short period of time, only several hours. At this stage, the oscillation peaks and troughs illustrated in Figure 3.2 were observed.

* The experimentally measured ethanol loss caused by the evaporation with the exhaust gas was about 6.5% of the ethanol produced under the experimental conditions.

Ethanol yield was calculated by

$$Y_{P/S} = \frac{P_2 - P_1}{S_1 - S_2}$$

where P_1 and P_2 are ethanol concentrations in the effluents into and out of each bioreactor of the fermentation system, and S_1 and S_2 are the corresponding glucose concentrations.

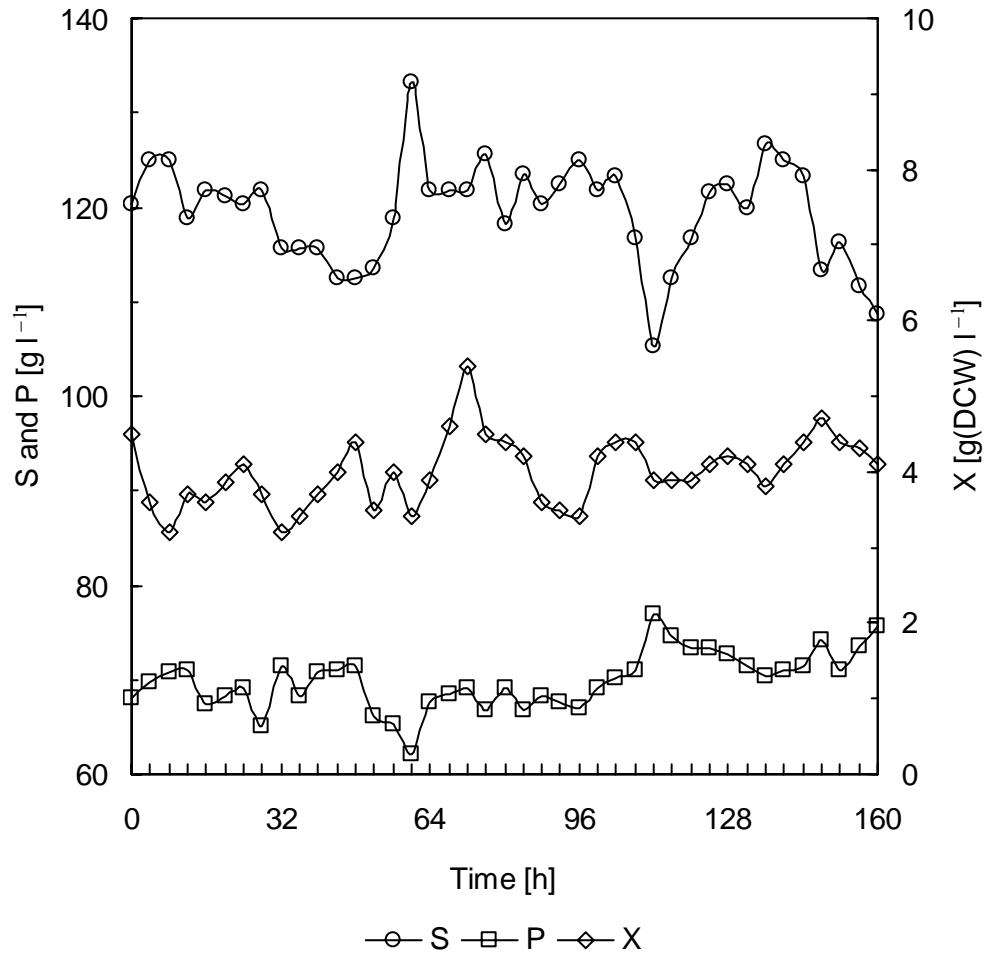


Figure 3.7 Time courses of the residual glucose, ethanol, and biomass of the CSTR, sampling at an interval of 4 hours. Initial glucose concentration of the VHGM medium: $S_0 = 280 \text{ g l}^{-1}$; $D = 0.027 \text{ h}^{-1}$.

The correlation between ethanol inhibition and the response of yeast cells to ethanol inhibition could be qualitatively analyzed from the experimental data illustrated in Figure 3.6. From the 8th hour to the 24th hour, the biomass concentration increased, indicating the increase of the specific growth rate of the yeast cells, which could be caused by the previous lower ethanol concentration and less ethanol inhibition. From the 24th hour to the 32nd hour, the biomass concentration decreased, which was possibly caused by the increase of ethanol from the beginning to the 12th hour. Then, from the 32nd hour to the 48th hour, the biomass concentration increased again, which was caused by the decrease of ethanol from the 12th hour to the 28th hour. The biggest biomass increase occurred from the 60th hour to the 72nd hour, which was caused by the biggest ethanol decrease from the 48th hour to the 60th hour. These experimental data indicated that the lag response of the yeast cells to the change of ethanol concentration occurred.

When the VHG medium containing 280 g l^{-1} glucose was used, both residual glucose and ethanol were high, exerting inhibition on yeast cells simultaneously. For ethanol fermentation, residual sugar cannot be completely dissociated from the ethanol generated from sugar during the fermentation except external ethanol is added into the fermentation system as widely adopted earlier in ethanol fermentation kinetic research (Aiba et al., 1968). However, different residual sugar and ethanol concentration scenarios can be obtained by adjusting medium gravity, and the impact of residual glucose and ethanol on ethanol fermentation can be studied.

When the HG medium containing 200 g l^{-1} glucose was fed into the fermentation system at the same dilution rate of 0.027 h^{-1} , the residual glucose in the effluent decreased to the average of 36.5 g l^{-1} from the average of 119.4 g l^{-1} under the VHG condition, which did not exert significant inhibition on yeast cells. But the ethanol in the effluent increased only slightly to the average of 70.8 g l^{-1} from the average of 70.3 g l^{-1} under the VHG condition, exerting the same level of inhibition on yeast cells. The residual glucose, ethanol, and

biomass were still oscillatory, as illustrated in Figure 3.8. The absolute oscillation amplitudes were 38.5 g l^{-1} , 17.5 g l^{-1} and $2.1 \text{ g(DCW) l}^{-1}$ for the residual glucose, ethanol, and biomass, respectively, and the corresponding relative amplitudes were $\pm 52.7\%$, $\pm 12.3\%$, and $\pm 21.9\%$ *

Compared with the oscillation profiles observed under the VH condition, the oscillations under the HG condition were not damped although the residual glucose decreased significantly, which indicates that although the high residual glucose under the VH condition exerted inhibition on yeast cells, it could not be the main reason triggering the quasi-steady state and oscillation.

Then, the LG medium containing 120 g l^{-1} glucose was fed into the fermentation system, and the dilution rate was still maintained at the level of 0.027 h^{-1} . No residual glucose was detected in the effluent, and the ethanol concentration decreased to an average of 49.3 g l^{-1} . In this situation, although glucose inhibition was completely eliminated, it could be safely concluded that its impact on the process state, compared with the average residual glucose of 36.5 g l^{-1} under the HG condition, was negligible. However, the impact of ethanol inhibition alleviation was more significant as the ethanol concentration decreased significantly from the average of 70.8 g l^{-1} under the HG condition to the average of 49.3 g l^{-1} . As illustrated in Figure 3.9, both ethanol and biomass fluctuated within very small ranges, $\pm 3\%$ for the ethanol and $\pm 5\%$ for the biomass based on their average levels of 49.3 g l^{-1} and $6.3 \text{ g(DCW) l}^{-1}$, and quasi-steady states were achieved.

These experimental results clearly indicated that high ethanol concentration produced by yeast cells during the fermentations was the main factor triggering the unsteady state and oscillation in continuous ethanol fermentation with *S. cerevisiae* ATCC 4126.

* The average biomass concentration was $4.8 \text{ g(DCW) l}^{-1}$.

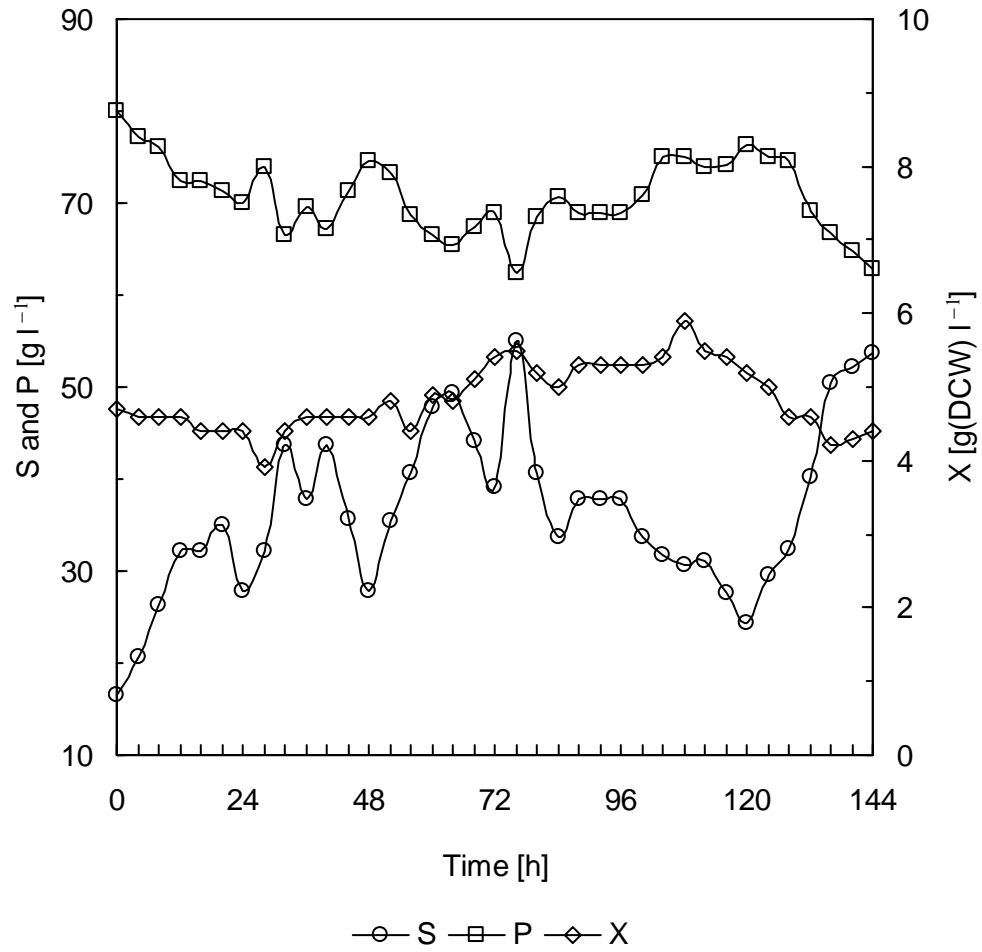


Figure 3.8 Time courses of the residual glucose, ethanol, and biomass of the CSTR, sampling at an interval of 4 hours. The initial glucose concentration of the HG medium: $S_0 = 200 \text{ g l}^{-1}$, the dilution rate: $D = 0.027 \text{ h}^{-1}$.

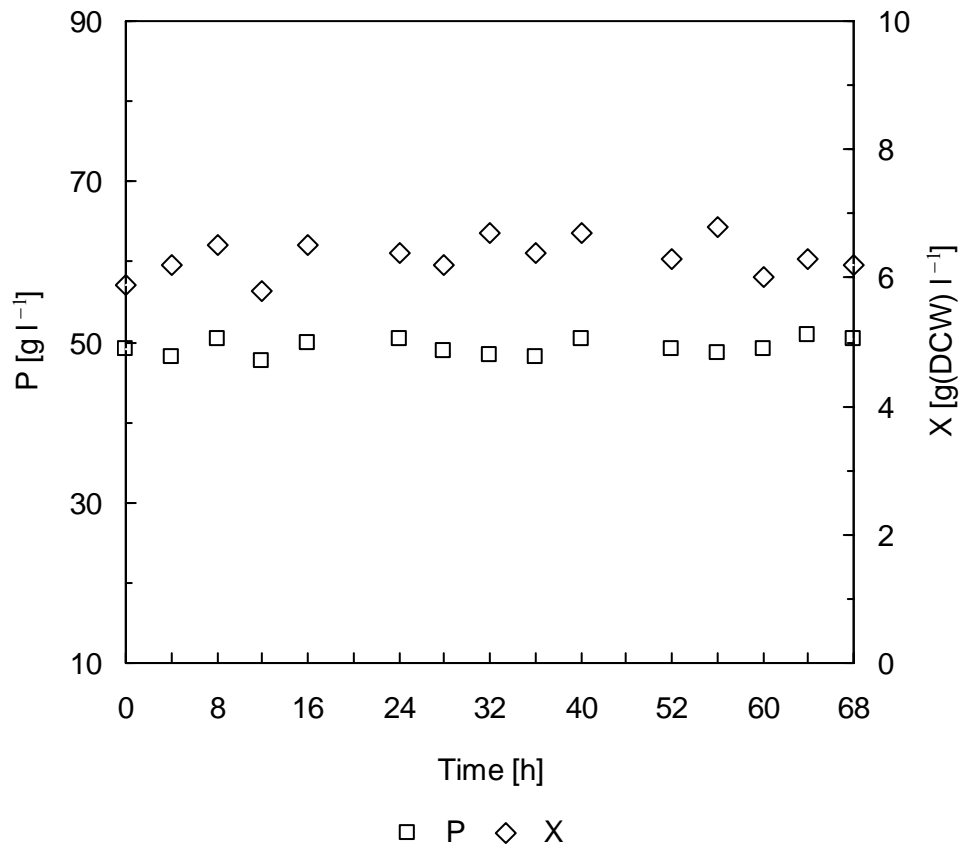


Figure 3.9 Time courses of the ethanol and biomass of the CSTR, sampling at an interval of 4 hours. The initial glucose concentration of the LG medium: $S_0 = 120 \text{ g l}^{-1}$, the dilution rate: $D = 0.027 \text{ h}^{-1}$.

3.3.2 Mechanism Discussion

Oscillatory behaviors were reported in the continuous aerobic cultures of *S. cerevisiae* as well as in a few continuous microbial fermentations involving the production of ethanol by *Zymomonas mobilis*, 1,3-propanediol by *Klebsiella pneumoniae*, and reuterin by *Lactobacillus reuteri*, and the corresponding mechanisms were proposed to explain these oscillation cases.

The synchronization of the mother and daughter cells of *S. cerevisiae* has been elucidated to be the mechanistic reason for the oscillations observed in the continuous aerobic cultures of *S. cerevisiae* because of the asynchronous budding growth pattern of this species, through which two different cell populations, the mother cells with relatively short generation time and the daughter cells with much longer generation time (in order to build up enough intracellular cell mass required by their budding) are created. Under specific conditions, the synchronization of the cell cycles of these two types of yeast cells can occur, triggering oscillations. Although ethanol is also produced in the continuous aerobic cultures of *S. cerevisiae* in case of the excess of glucose supply, its concentration is too low to affect the oscillation patterns (Chen and McDonald, 1990; Beuse et al., 1998).

Our experimental results illustrated that unsteady state and oscillation occurred in the continuous ethanol fermentation by *S. cerevisiae*, and only when ethanol concentration decreased below 60 g l^{-1} , was steady state established. Compared with the oscillatory behaviors observed in continuous aerobic cultures of *S. cerevisiae*, in which the oscillation amplitudes were at the scale no more than 0.1 g l^{-1} for glucose and 0.3 g l^{-1} for ethanol and the oscillation periods were on a scale of only several hours (Chen and McDonald, 1990; Beuse et al., 1998), much bigger oscillation amplitudes and much longer oscillation periods were observed in the continuous ethanol fermentations under the HG and VH conditions. For example, the absolute oscillation amplitudes were 23.4 g l^{-1} , $11.7.0 \text{ g l}^{-1}$, and 1.8 g l^{-1} .

(DCW) l^{-1} for the residual glucose, ethanol, and biomass of the CSTR when it was fed with the VHG medium at the dilution of 0.027 h^{-1} , and the oscillation periods were 8-10 days, which indicated that there are mechanistic differences between these two kinds of oscillations happening for *S. cerevisiae*. The synchronization of the mother and daughter cells, which is responsible for the oscillatory behaviors in continuous cultures of *S. cerevisiae*, could happen and affect the oscillation patterns to some extent because yeast cells are still growing in the same pattern in ethanol fermentation as that in their aerobic cultures. This impact will be studied in Chapter 4 through changing the dilution rate of the fermentation system.

For the continuous cultures and fermentations using bacteria such as the species of *Zymomonas mobilis*, *Klebsiella pneumoniae* and *Lactobacillus reuteri* which grow in the pattern of binary fission, there is no asynchronous growth because their cell materials are equally partitioned into their daughter cells. The mechanisms triggering the oscillatory behaviors of these species are species-dependent. For the ethanologen bacterium, *Z. mobilis*, ethanol inhibition and the lag response of this species to ethanol inhibition were proposed to be the main reasons for its oscillatory behaviors (Jöbses et al., 1986; Daugulis et al., 1997; McLellan et al., 1999). Likewise the lethal effect of reuterin, an antimicrobial compound, on *L. reuteri* was believed to be the reason for oscillations during the continuous production of reuterin (Rasch et al., 2002). The oscillatory behaviors of *K. pneumoniae* in the continuous production of 1,3-propanediol involved another mechanism, the excess of substrate and corresponding intracellular metabolism regulations (Menzel et al., 1996; Zeng et al., 1996; Menzel et al., 1998a, b).

The oscillation amplitudes of $20 \sim 110 \text{ g l}^{-1}$ for residual glucose, $50 \sim 90 \text{ g l}^{-1}$ for ethanol and $1.5 \sim 3.5 \text{ g (DCW) l}^{-1}$ for biomass, as well as the oscillation periods of $40 \sim 60$ hours observed in the continuous ethanol fermentation by *Z. mobilis*, are comparable to the oscillation profiles observed in the continuous ethanol fermentation by *S. cerevisiae*, which

indicates some similarities in their oscillation mechanisms. Likewise ethanol inhibition and the lag response of *S. cerevisiae* to ethanol inhibition can be applied to analyze and explain the oscillatory behaviors observed in the continuous ethanol fermentation by *S. cerevisiae*, which were supported by the analysis of the relationship between the oscillation profiles of ethanol and biomass illustrated in Figure 3.7.

This mechanism can be understood in the following way. The energy released during ethanol fermentation can not be utilized immediately for the anaerobic biosynthesis of yeast cells, and the yeast cells require some time to adjust their intracellular metabolisms to adapt to ethanol inhibition and respond to it effectively. Therefore, it can be further speculated that the slower the response, the longer the oscillation periods will be. As the response of *S. cerevisiae* to ethanol inhibition is much slower than that of *Z. mobilis*, its oscillatory periods should be longer. This inference was supported by our own experimental data as well as by the studies in continuous ethanol fermentation by *Z. mobilis* (Daugulis et al., 1997; McLellan et al., 1999). At the same time, no quasi-steady state observed in the continuous ethanol fermentation by *S. cerevisiae* was observed for *Z. mobilis*, which might indicate that the faster response of *Z. mobilis* to ethanol stress made this transitional quasi-steady state too unstable to be detected.

Ethanol is toxic to yeast cells, and when the yeast cells are under ethanol inhibition, they adjust their intracellular metabolisms to try to adapt to this environmental stress. At this stage, the intracellular dynamic balance tends to be established. It is proposed that at this stage, the quasi-steady state is developed for the continuous ethanol fermentation by *S. cerevisiae* during which the fermentation parameters change slowly in a one-way direction. Furthermore, once this dynamic balance is disrupted, the oscillation peak and trough are present. If the oscillation is toward a higher ethanol direction, the time would be short as the higher ethanol exerts stronger inhibition on yeast cells, decreasing their growth rate and resulting in the decrease of ethanol production rate, since ethanol production is tightly

associated with growth. If the oscillation is toward a lower ethanol direction, the inhibition of ethanol on yeast cells is alleviated, the growth of yeast cells is stimulated, and ethanol production rate increases. Therefore, no matter which direction the oscillation is toward, it tends to return to quasi steady state and cannot remain at the oscillation peak or trough. These assertions are in correspondence with our experimental results.

The lethal effect that is responsible for the oscillation in the continuous production of reuterin by *L. reuteri* is also useful in explaining the oscillatory behavior observed in the continuous ethanol fermentation by *S. cerevisiae* because the ethanol produced by yeast cells during fermentation is lethal to yeast cells when its concentration is high enough. But this lethal effect of ethanol to yeast cells could not be the main reason for the oscillation of the CSTR because its maximum ethanol concentration was 76.1 g l^{-1} , not high enough to cause the death of the yeast cells. However, as the fermentation went through the tubular bioreactors, the ethanol concentration dramatically increased to the averages of 93.4 g l^{-1} , 106.8 g l^{-1} , and 114.0 g l^{-1} for the first, second, and third tubular bioreactors, and the highest ethanol concentration achieved within the third tubular bioreactor was 121.9 g l^{-1} , high enough to make some yeast cells lose their fermentability, and even kill them.

The viability-loss and death of yeast cells were observed during microscopic examinations for the tubular bioreactors, especially for the second and third ones. Therefore, the lethal effect of ethanol on yeast cells could be used to analyze and explain the oscillation profiles observed for these tubular bioreactors. For example, when the preceding bioreactor experienced its ethanol oscillation peak, the ethanol concentration in the input stream to the tubular bioreactor was high, and the ethanol concentration inside the tubular bioreactor increased, correspondingly, making more yeast cells lose their viability, the increase rate of ethanol concentration slow down, but the ethanol concentration approach its maximum, then decrease. Thus, oscillation occurred. The oscillation of each of these tubular bioreactors tended to be synchronous with the oscillation occurring in the preceding

bioreactor, which resulted in an exaggeration effect, as illustrated in Figures 3.4 and 3.5.

3.3.3 Oscillation Attenuation

As illustrated in Figures 3.3~3.5, the tubular bioreactors were still oscillatory, making the residual glucose in the effluent from the third tubular bioreactor as high as 17.9 g l^{-1} . The reason might be the backmixing resulting from CO_2 produced during ethanol fermentation for the first tubular bioreactor and the aeration for the second and third tubular bioreactors. The bioreactor engineering theory indicates that a tanks-in-series system is equivalent to a plug flow reactor when the number of the tanks is infinite. If the tubular bioreactors were partitioned into an infinite number of small reaction chambers by packing, their backmixing was expected to be alleviated. Therefore, $\frac{1}{2}$ " Intalox ceramic saddles were packed into the tubular bioreactors.

Figures 3.10~3.12 illustrate the fermentation performance of the packed tubular bioreactors as well as the comparisons with the empty columns. It can be seen that not only lower residual glucose and higher ethanol concentrations were achieved for these packed tubular bioreactors, but the oscillations of their residual glucose and ethanol previously observed in the empty columns were effectively attenuated.

For the first tubular bioreactor, the averages of residual glucose and ethanol were 43.9 g l^{-1} and 102.1 g l^{-1} after it was packed, compared with the averages of 60.2 g l^{-1} and 93.5 g l^{-1} observed for the empty column. Although it was still oscillatory, its oscillation ranges for residual glucose and ethanol were decreased to $35.0\sim 50.0 \text{ g l}^{-1}$ and $98.8\sim 106.5 \text{ g l}^{-1}$ from $50.0\sim 78.1 \text{ g l}^{-1}$ and $85.1\sim 98.9 \text{ g l}^{-1}$, making the absolute oscillation amplitudes correspondingly decrease to 15.0 g l^{-1} and 7.7 g l^{-1} from 28.1 g l^{-1} and 13.8 g l^{-1} .

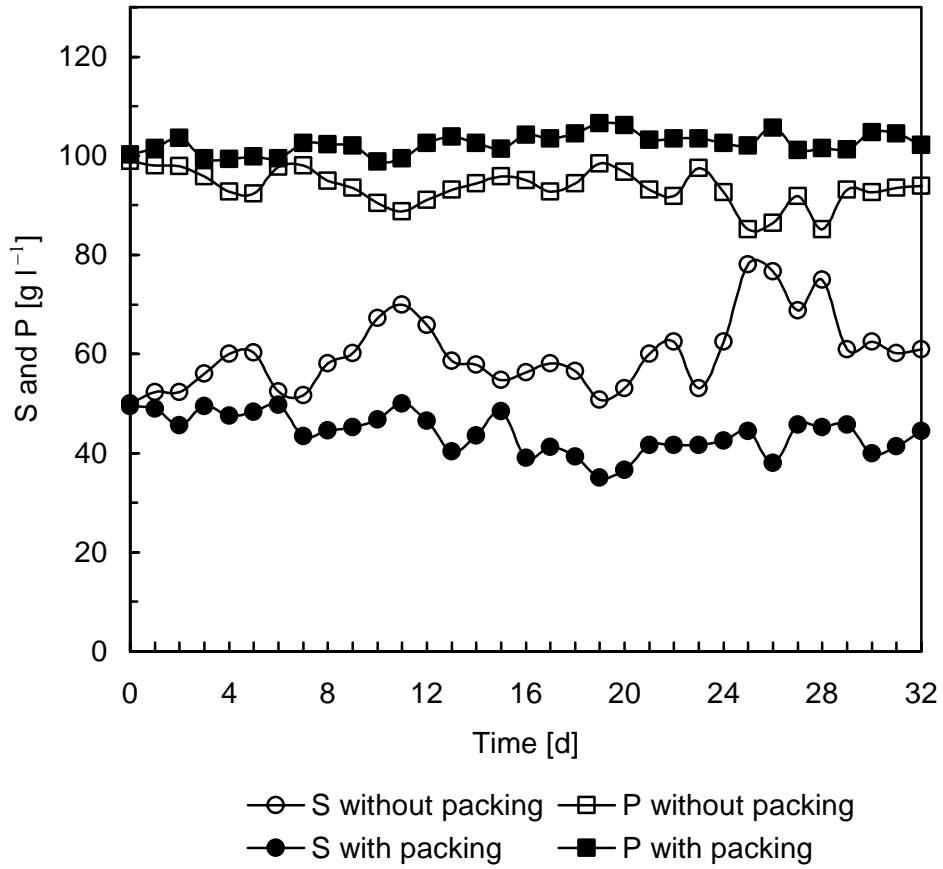


Figure 3.10 Impact of the packing on the ethanol fermentation performance and oscillatory behavior of the first tubular bioreactor. The VHG medium containing 280 g l⁻¹ glucose was fed into the CSTR at the dilution rate of 0.027 h⁻¹.

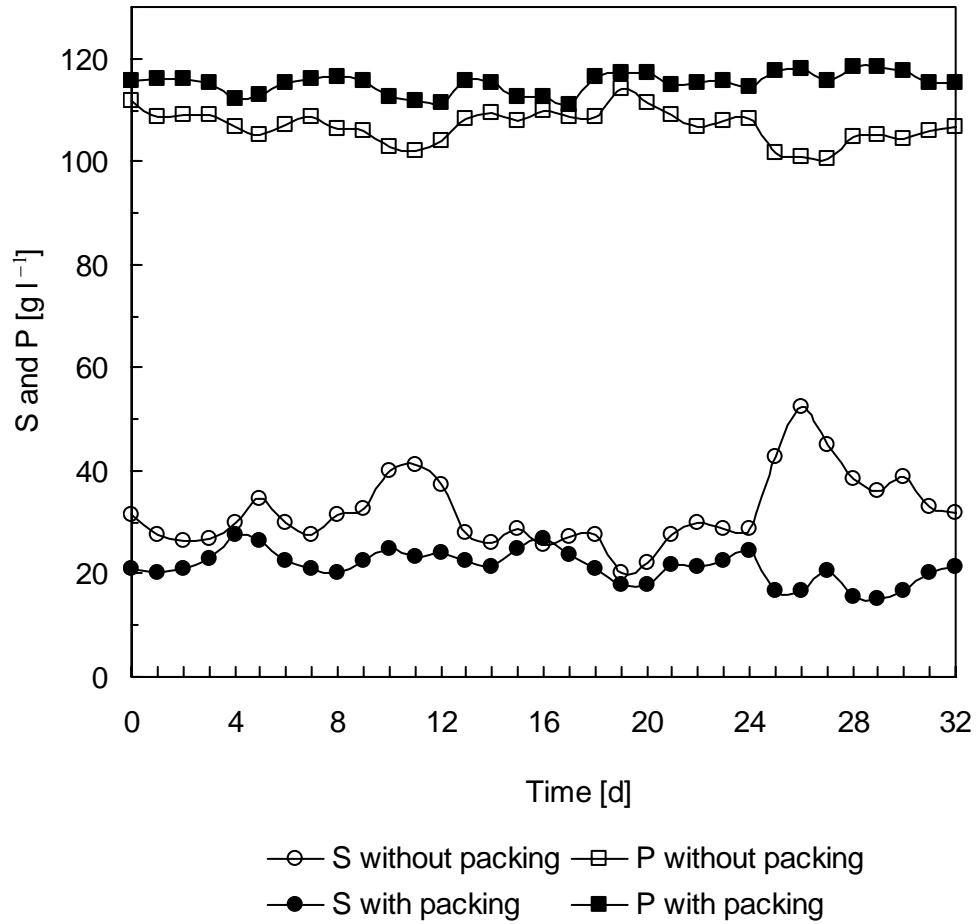


Figure 3.11 Impact of the packing on the ethanol fermentation performance and oscillatory behavior of the second tubular bioreactor. The VHG medium containing 280 g l⁻¹ glucose was fed into the CSTR at the dilution rate of 0.027 h⁻¹.

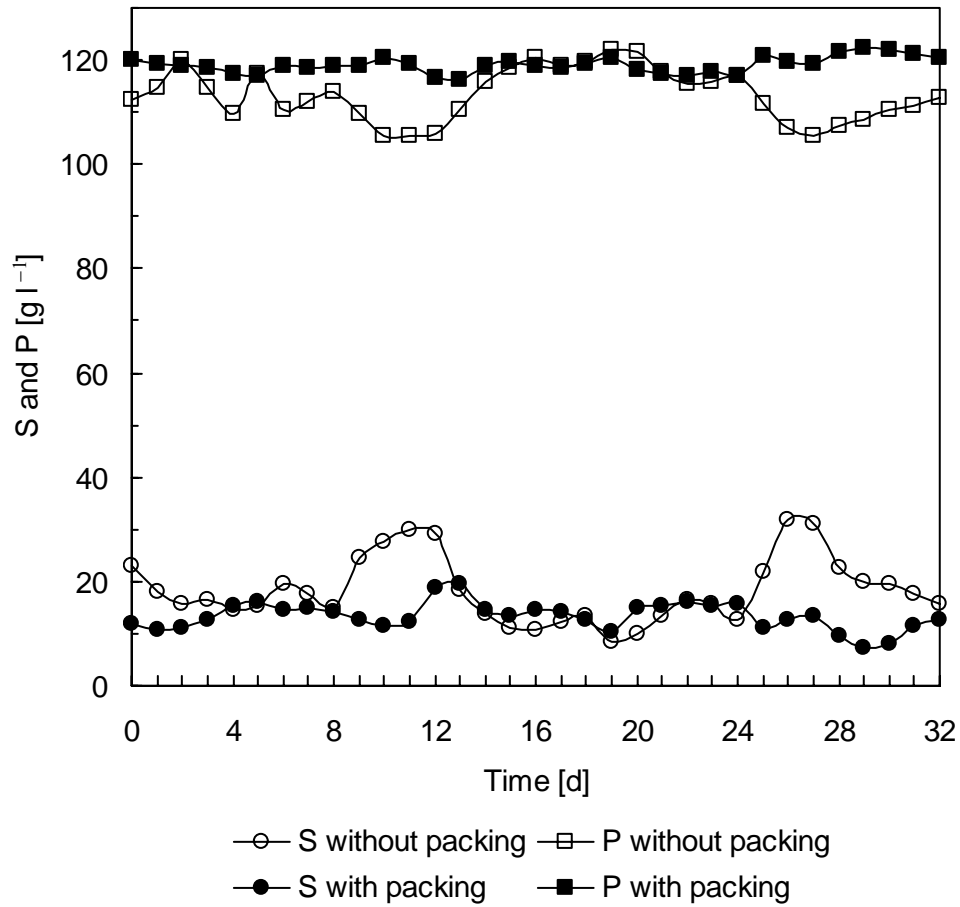


Figure 3.12 Impact of the packing on the ethanol fermentation performance and oscillatory behavior of the third tubular bioreactor. The VHG medium containing 280 g l^{-1} glucose was fed into the CSTR at the dilution rate of 0.027 h^{-1} .

Similar to the first tubular bioreactor, the packing also significantly improved the ethanol fermentation performance of the second and third tubular bioreactors. The average residual glucose concentrations were decreased to 21.3 g l⁻¹ and 13.3 g l⁻¹, respectively, from 32.0 g l⁻¹ and 18.3 g l⁻¹ before they were packed, whereas the average ethanol concentrations were increased to 115.2 g l⁻¹ and 119.1 g l⁻¹, correspondingly, from 106.9 g l⁻¹ and 113.3 g l⁻¹. Most importantly, the oscillations of residual glucose and ethanol were completely attenuated after the broth flowed through the third packed tubular bioreactor, and quasi-steady state over the whole experiment duration was achieved at the end of the fermentation.

3.4 Conclusions

Continuous VHG ethanol fermentation was carried out using a general yeast strain, *S. cerevisiae* ATCC 4126 and a bioreactor system composed of a CSTR and three tubular bioreactors in series. Experimental results illustrated unsteady state and oscillation instead of steady state that was expected. The reasons for triggering the unsteady state and oscillation were studied, and the following can be concluded:

1. Ethanol was the main factor triggering the unsteady state and oscillatory behavior in the continuous ethanol fermentation with *S. cerevisiae* ATCC4126.
2. Ethanol inhibition and the lag response of yeast cells to ethanol inhibition were speculated and partly validated to be the mechanistic reasons for the unsteady state and oscillation of the CSTR, while the lethal effect of high ethanol concentration on yeast cells was responsible for the exaggerated oscillations observed in the tubular bioreactors.

3. Packing significantly improved the ethanol fermentation performance of the tubular bioreactors and attenuated their oscillations, but the corresponding oscillation attenuation mechanism needs to be further examined.

Chapter 4

Impacts of Added Ethanol, Dilution Rate and Strain on Oscillations

A manuscript has been prepared for submission based on the work presented in this chapter.

4.1 Introduction

Oscillations were observed in the continuous VHG fermentation with *S. cerevisiae* ATCC 4126 when the CSTR was operated at a dilution rate of 0.027 h^{-1} , and the mechanisms triggering the oscillations were proposed and partly validated to be ethanol inhibition and lag response of yeast cells to ethanol inhibition.

However, early research in which steady state was claimed for continuous ethanol fermentation with *S. cerevisiae* such as the pioneering work of Aiba et al. in ethanol fermentation kinetics (Aiba et al., 1968) was done by adding ethanol into fermentation systems to generate different ethanol concentrations to study ethanol inhibition effect. Therefore, the effect of ethanol externally added into the fermentation system in the oscillations needs to be examined to further complete the mechanistic analysis.

Furthermore, based on the mechanistic analysis, the oscillations can be affected by dilution rate, one of the most important operating parameters in continuous fermentations, which affects both the specific growth rate of cells and the production rate and concentration of primary metabolites such as ethanol. Nevertheless, ethanol tolerance, which reflects the response of cells to toxic ethanol, is strain-dependent, and therefore, different strains should exhibit different oscillation profiles.

In this chapter, the influence of added ethanol was studied by feeding the LG medium

supplemented with ethanol into the fermentation system. Then, the impacts of dilution rate and strain on the oscillations were further studied.

4.2 Materials and Methods

4.2.1 Strain, Medium, and Pre-culture

S. cerevisiae ATCC4126 was described in Section 3.2.1. The strain *S. cerevisiae* 6508 was kindly donated by Dr. G. Stewart, formerly of Labatt Brewery, London, Ontario, Canada. The culture media, pre-culture, inoculation and fermentation procedures of *S. cerevisiae* 6508 were the same as those for *S. cerevisiae* ATCC 4126, which were described in Section 3.2.1. A self-flocculating yeast strain developed by the protoplast fusion technology from *Schizosaccharomyces pombe* and *Saccharomyces cerevisiae* (SPSC) was kindly provided by Ms. Ning Li, Dalian University of Technology, China, which was also used to further study the impact of strain on the process state as well as to explore some practical aspects. Currently, this strain is used in the fuel ethanol production at BBKA, China.

4.2.2 Bioreactor

The CSTR illustrated previously in Figure 3.1 was used to study the impact of dilution rates on the oscillatory behaviors of the strains, *S. cerevisiae* ATCC4126 and *S. cerevisiae* 6508. The same VHG medium described in Section 3.2.1 was used for these two strains.

4.2.3 Analytical methods

Ethanol and biomass analysis were described in Section 3.2.3. Glucose was analyzed by a glucose analyzer (SBA-50B, Shandong, China).

4.2.4 Measurement of ethanol tolerance

The ethanol tolerance of the three yeast strains was examined through ethanol shock experiments. The 250 ml flasks containing 100 ml medium composed of 30 g l⁻¹ glucose, 5 g l⁻¹ yeast extract, and 3 g l⁻¹ peptone were prepared and sterilized at 121 °C for 15 minutes. After cooling, 10 ml fresh culture of each strain was inoculated and incubated overnight at 30 °C and 150 rpm. Then, ethanol shock was exerted onto the cultures by adding 20 ml ethanol into each of these cultures, making the ethanol concentration about 15% (v/v). The cultures were incubated at 30 °C and 150 rpm for two hours, and the percentage of viable cells was counted by the regular methylene blue stain and chamber counting techniques. If the ethanol tolerance of the strains could not be distinguished, the concentration of ethanol shock was increased to 18% (v/v).

4.3 Results and Discussion

4.3.1 Influence of added ethanol on oscillations

In Chapter 3, it was shown that ethanol produced by yeast cells during fermentation is the main factor triggering unsteady steady state and oscillation in continuous ethanol fermentation. In order to further study the impact of added ethanol, ethanol was added into the LG medium, making its initial ethanol concentration of 30 g l⁻¹, so that ethanol concentration in the fermentation system could approach the same level as that of the HG medium at which unsteady states and oscillations of residual glucose, ethanol, and biomass were observed, as illustrated in Figure 3.7. The same dilution rate of 0.027 h⁻¹ was applied to the fermentation system, and the experimental results are illustrated in Figure 4.1.

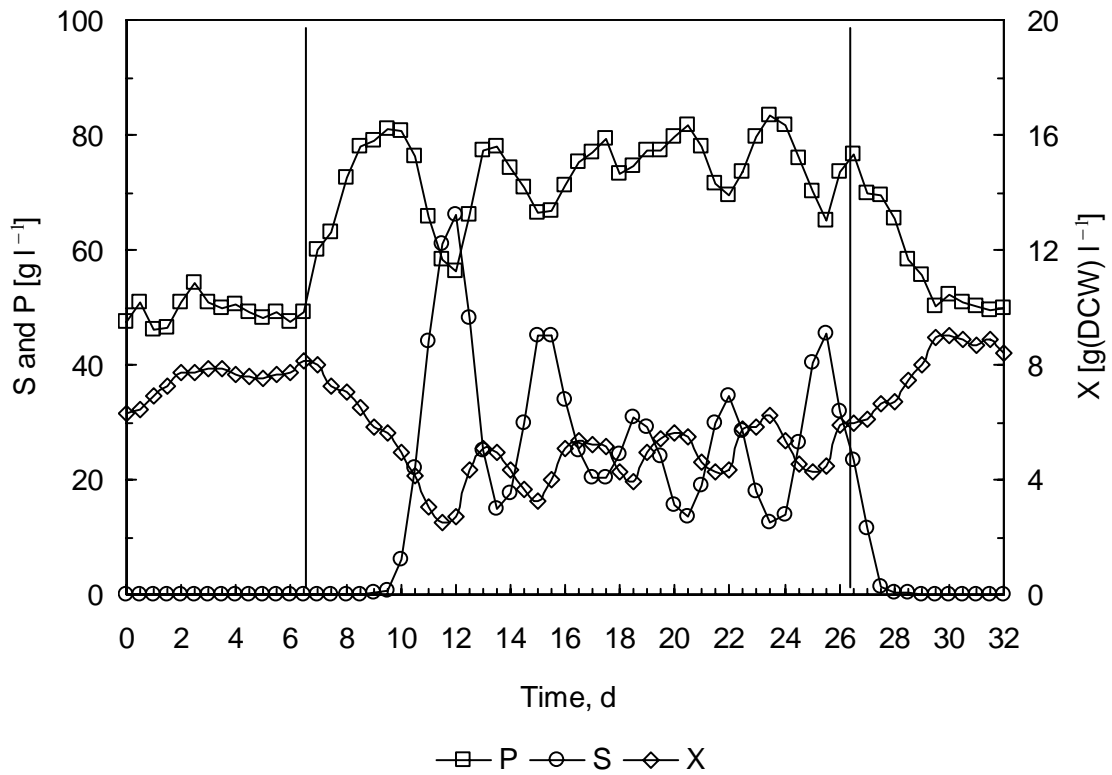


Figure 4.1 Time courses of the residual glucose, ethanol, and biomass of the CSTR. Initial glucose concentration of the LG medium: $S_0 = 120 \text{ g l}^{-1}$, the dilution rate: $D = 0.027 \text{ h}^{-1}$. The LG medium supplemented with 30 g l^{-1} ethanol was fed into the fermentation system at the day 6.5, and the original LG medium was restored in the day 26.5.

As can be seen, the quasi-steady states of ethanol and biomass observed for the original LG medium were interrupted immediately after the LG medium supplemented with ethanol was fed into the fermentation system in the day 6.5 and the ethanol concentration in the effluent increased, correspondingly. But the residual glucose did not increase till the day 9.5, which once again validated the lag response of yeast cells to ethanol inhibition. After the fermentation system experienced about 5 days' transition, oscillations similar to those previously observed for the original HG medium were observed within a 12 days' duration. The oscillation ranges of residual glucose, ethanol, and biomass were 12.5~45.0 g l⁻¹, 66.3~83.2 g l⁻¹ and 3.5~6.2 g(DCW) l⁻¹, respectively, and the corresponding absolute oscillation amplitudes were 32.5 g l⁻¹, 16.9 g l⁻¹, and 2.7 g(DCW) l⁻¹, at the same scales as those observed for the original HG medium. After the original LG medium was restored in the day 26.5 and the ethanol concentration of the fermentation system decreased, these oscillations gradually disappeared and the steady states for ethanol and biomass were also restored in four days.

These experimental results indicated that ethanol, whether added into fermentation systems or produced by yeast cells during fermentation, can trigger oscillation.

4.3.2 Impact of dilution rate on oscillations

Using the strain *S. cerevisiae* ATCC4126, four dilution rates (0.012, 0.012, 0.027 and 0.036 h⁻¹) were selected to study their impact on process oscillation. Ten days to two weeks were required for each dilution rate adjustment to achieve the system equilibrium from its inoculation, which was judged by matching the residual glucose and ethanol in the effluent with the initial glucose in the VHG medium. Then samples were taken daily, and two or three weeks were maintained for each dilution rate, depending on the corresponding process state, making the duration longer than one intact oscillation period. The experimental results are illustrated in Figures 4.2-4.4.

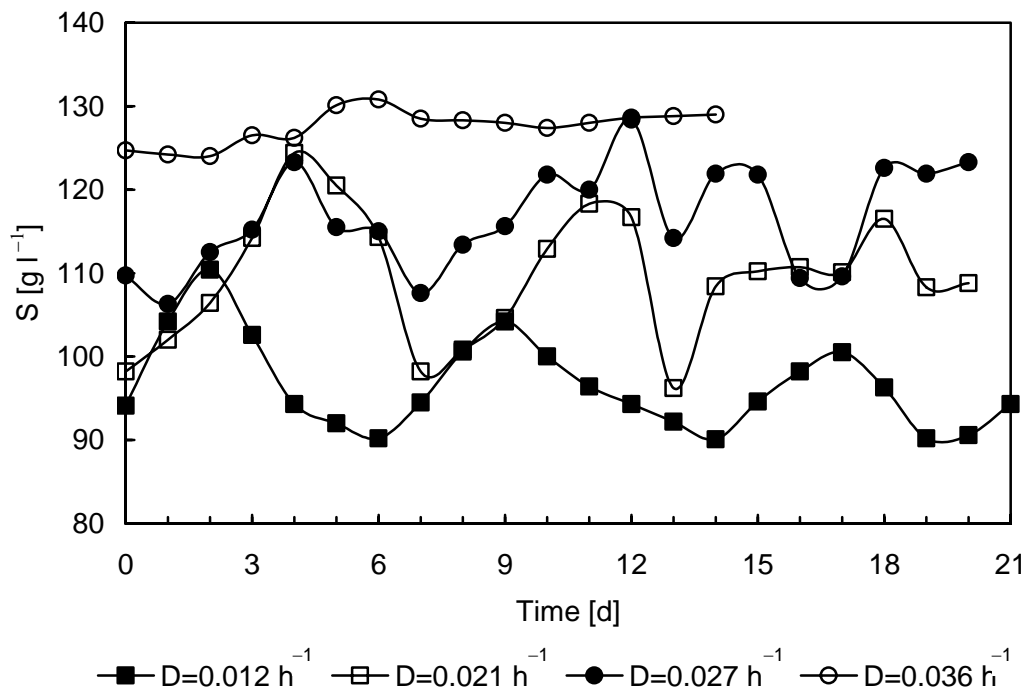


Figure 4.2 Impact of dilution rates on the residual glucose of the continuous VHG ethanol fermentation with *S. cerevisiae* ATCC4126. Initial glucose concentration in the medium: $S_0 = 280 \text{ g l}^{-1}$.

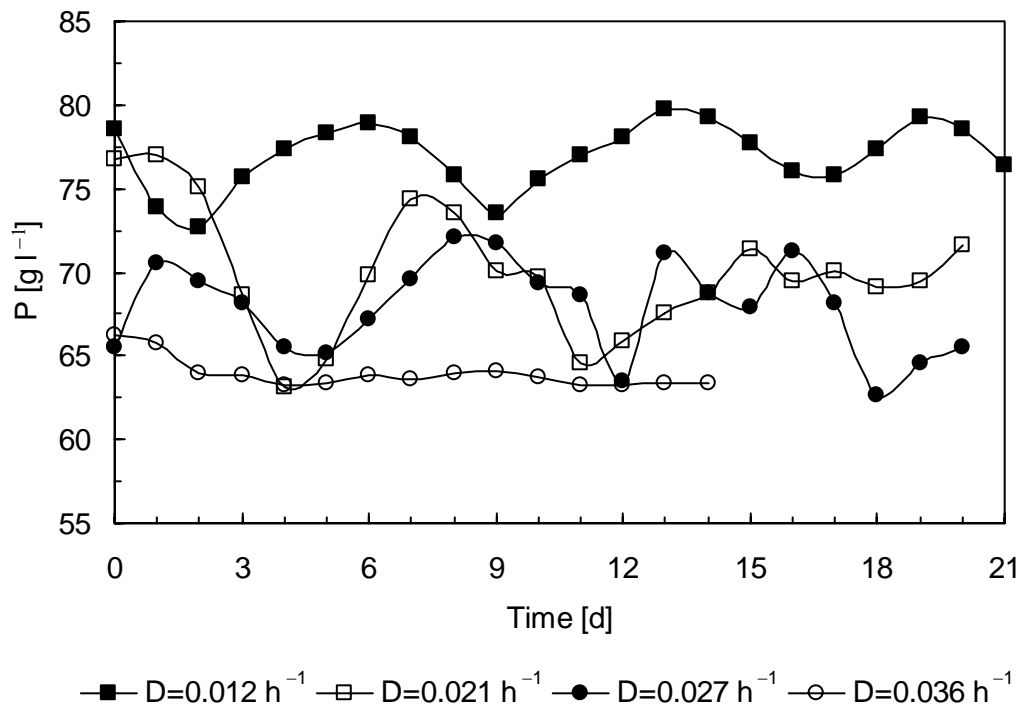


Figure 4.3 Impact of dilution rates on the ethanol profiles of the continuous VHG ethanol fermentation with *S. cerevisiae* ATCC4126. Initial glucose concentration in the medium: $S_0 = 280 \text{ g l}^{-1}$.

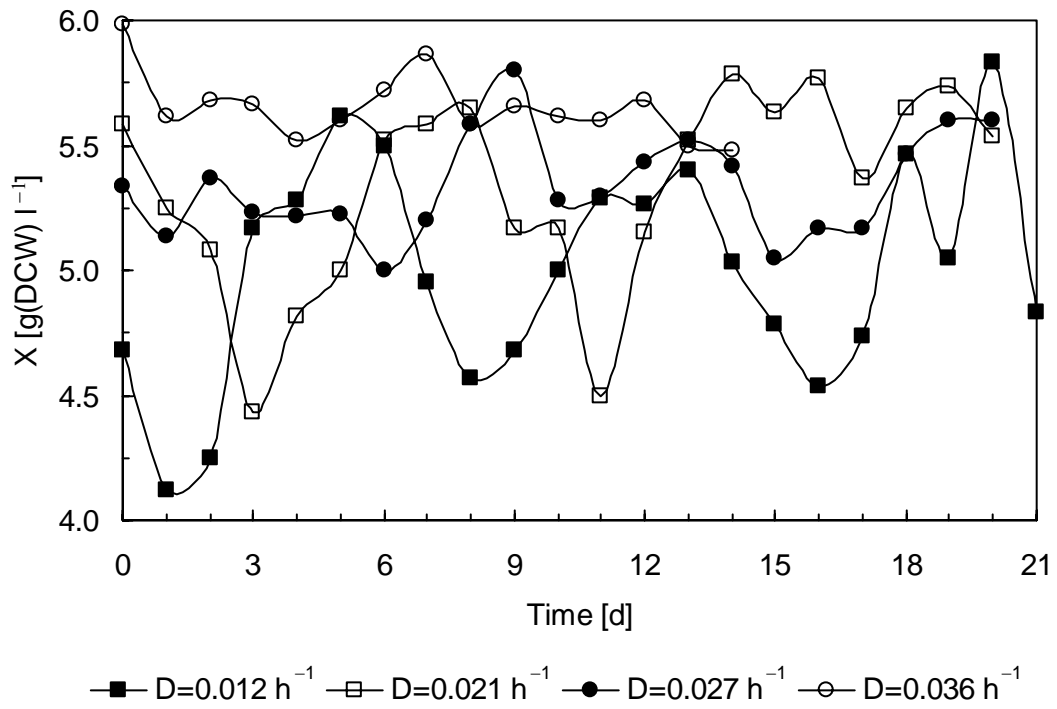


Figure 4.4 Impact of dilution rates on the biomass profiles of the continuous VHG ethanol fermentation with *S. cerevisiae* ATCC4126. Initial glucose concentration in the medium: $S_0 = 280 \text{ g l}^{-1}$.

Oscillations similar to those observed and discussed in Chapter 3 were observed at the dilution rate of 0.012 h^{-1} . The oscillation ranges of residual glucose, ethanol and biomass were $90.1\sim 110.4 \text{ g l}^{-1}$, $72.7\sim 79.8 \text{ g l}^{-1}$ and $4.1\sim 5.8 \text{ g(DCW) l}^{-1}$, respectively, making their absolute oscillation amplitudes 20.3 g l^{-1} , 7.1 g l^{-1} , and $1.7 \text{ g(DCW) l}^{-1}$. The averages of residual glucose, ethanol, and biomass were 96.6 g l^{-1} , 77.0 g l^{-1} , and $5.0 \text{ g(DCW) l}^{-1}$, and the corresponding relative oscillation amplitudes were $\pm 10.5\%$, $\pm 5.0\%$, and $\pm 17.0\%$, respectively. The oscillation periods were observed to be 7~8 days for all of these fermentation parameters.

At the dilution rate of 0.021 h^{-1} , the average residual glucose increased to 109.6 g l^{-1} , the average ethanol decreased to 70.0 g l^{-1} , and the average biomass slightly increased to $5.3 \text{ g(DCW) l}^{-1}$. The ethanol fermentation was still oscillatory. The oscillation ranges were $96.2\sim 124.4 \text{ g l}^{-1}$, $63.2\sim 77.0 \text{ g l}^{-1}$ and $4.4\sim 5.8 \text{ g(DCW) l}^{-1}$ for residual glucose, ethanol, and biomass, making their absolute oscillation amplitudes 28.2 g l^{-1} , 13.8 g l^{-1} , and $1.4 \text{ g(DCW) l}^{-1}$, respectively. The relative oscillation amplitudes were $\pm 13.0\%$ for residual glucose, $\pm 10.0\%$ for ethanol, and $\pm 13.0\%$ for biomass. Compared with the oscillation profiles observed at the dilution rate of 0.012 h^{-1} , the oscillations of residual glucose and ethanol seemed to be increased, but the oscillation periods were not significantly changed.

When the dilution rate was increased to 0.027 h^{-1} , the average residual glucose increased to 116.6 g l^{-1} , the average ethanol decreased to 67.9 g l^{-1} , and the average biomass was still $5.3 \text{ g(DCW) l}^{-1}$. The oscillation ranges were $106.3\sim 128.4 \text{ g l}^{-1}$, $62.6\sim 72.1 \text{ g l}^{-1}$, and $5.0\sim 5.8 \text{ g(DCW) l}^{-1}$ for residual glucose, ethanol, and biomass, the corresponding absolute oscillation amplitudes were 22.1 g l^{-1} , 9.5 g l^{-1} , and $0.8 \text{ g (DCW) l}^{-1}$, and the relative oscillation amplitudes were $\pm 9.0\%$, $\pm 7.0\%$, and $\pm 7.5\%$. Compared with the oscillations observed at the dilution rate of 0.021 h^{-1} , the oscillation profiles of residual glucose and ethanol seemed to be damped to the same scales as those oscillations observed at the

dilution rate of 0.012 h^{-1} . In fact, the experimental data at this dilution rate also confirmed that the oscillatory behaviors previously observed at the same dilution rate of 0.027 h^{-1} and discussed in Chapter 3 were reproducible. The oscillation periods were still 7-8 days.

As the dilution rate was increased to 0.036 h^{-1} , the average residual glucose increased to 127.5 g l^{-1} , the average ethanol decreased to 63.9 g l^{-1} , and the average biomass increased to $5.7 \text{ g (DCW) l}^{-1}$. These fermentation parameters were not significantly oscillated, but only slightly fluctuated. The fluctuation ranges were $124.0\sim 130.8 \text{ g l}^{-1}$, $63.2\sim 66.2 \text{ g l}^{-1}$, and $5.0\sim 6.0 \text{ g(DCW) l}^{-1}$ for residual glucose, ethanol, and biomass, and the absolute fluctuation amplitudes were 6.8 g l^{-1} for residual glucose and 3.0 g l^{-1} for ethanol, and the relative fluctuation amplitudes were only $\pm 2.7\%$ for residual glucose and $\pm 2.4\%$ for ethanol. In fact, quasi-steady states were achieved for residual glucose and ethanol because these variations were almost within their analytical errors. The fluctuation of biomass seemed a little bigger, with its absolute fluctuation amplitude of $1.5 \text{ g (DCW) l}^{-1}$ and relative fluctuation amplitude of $\pm 13.2\%$.

The mechanistic analysis discussed in Chapter 3 indicates that ethanol inhibition and the lag response of yeast cells to ethanol inhibition were the mechanistic reasons triggering these oscillatory behaviors. However, the experimental data showed two impacts of dilution rate on oscillation profile. On the one hand, the difference between the average ethanol concentrations at which the process state shifted from oscillation at the dilution rate of 0.027 h^{-1} to quasi-steady state at the dilution rate of 0.036 h^{-1} was only 6.0 g l^{-1} , which indicated the onset of oscillation is imminent when a continuous ethanol fermentation system is operated close to its critical dilution rate, at which the oscillation can be triggered. For *S. cerevisiae* ATCC 4126 and the VHG medium described in Section 3.2.1, the critical oscillation dilution rate is around 0.027 h^{-1} . On the other hand, for the three dilution rates of 0.012 h^{-1} , 0.021 h^{-1} , and 0.027 h^{-1} at which oscillation occurred, the dilution rate of 0.021 h^{-1} exhibited the biggest oscillation which was characterized by both its absolute and

relative amplitudes, indicating the impact of dilution rate on oscillation is more complicated than its direct impact on ethanol concentration because the higher ethanol concentration achieved at the lower dilution rate of 0.012 h^{-1} did not enhance the oscillation as predicted by our previous mechanistic analysis.

Figures 4.5~4.8 further illustrate the profiles of residual sugar, ethanol, and biomass at each of the four dilution rates applied to the fermentation system. It can be seen that for the three dilution rates at which oscillation happened, the oscillation of residual glucose was out of phase with the oscillation of ethanol, but some phase angles were observed with the oscillation of biomass. This more clearly indicated the lag response of yeast cells to ethanol inhibition, that is, the current growth of yeast cells and biomass concentration profile were affected by the previous ethanol concentration and its corresponding inhibition. At the dilution rate of 0.36 h^{-1} , quasi-steady state was established.

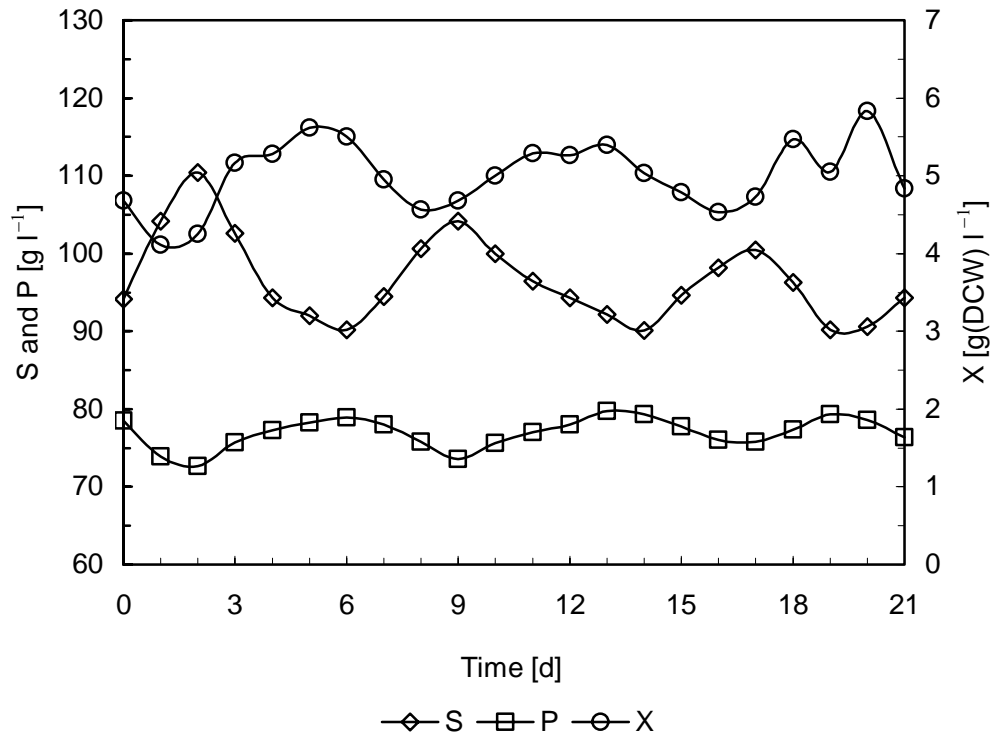


Figure 4.5 Oscillation profiles of the residual glucose, ethanol, and biomass of the continuous ethanol fermentation with *S. cerevisiae* ATCC4126 at the dilution rate of 0.012 h^{-1} . Initial glucose concentration in the medium: $S_0 = 280 \text{ g l}^{-1}$.

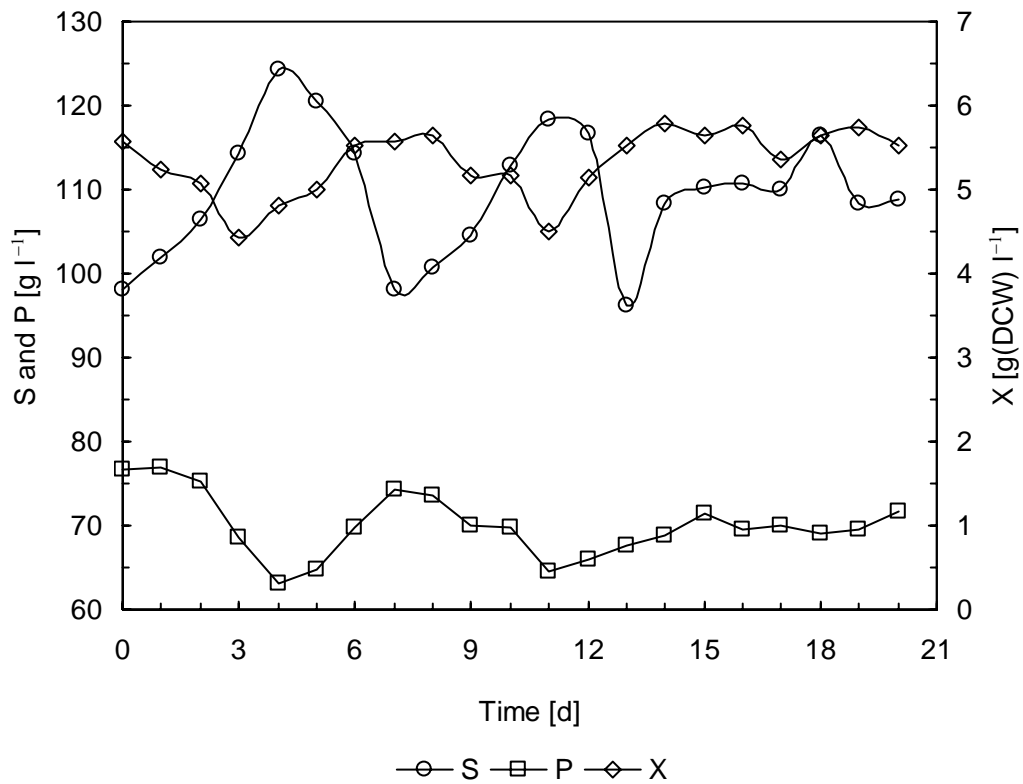


Figure 4.6 Oscillation profiles of the residual glucose, ethanol, and biomass of the continuous ethanol fermentation with *S. cerevisiae* ATCC4126 at the dilution rate of 0.021 h^{-1} . Initial glucose concentration in the medium: $S_0 = 280 \text{ g l}^{-1}$.

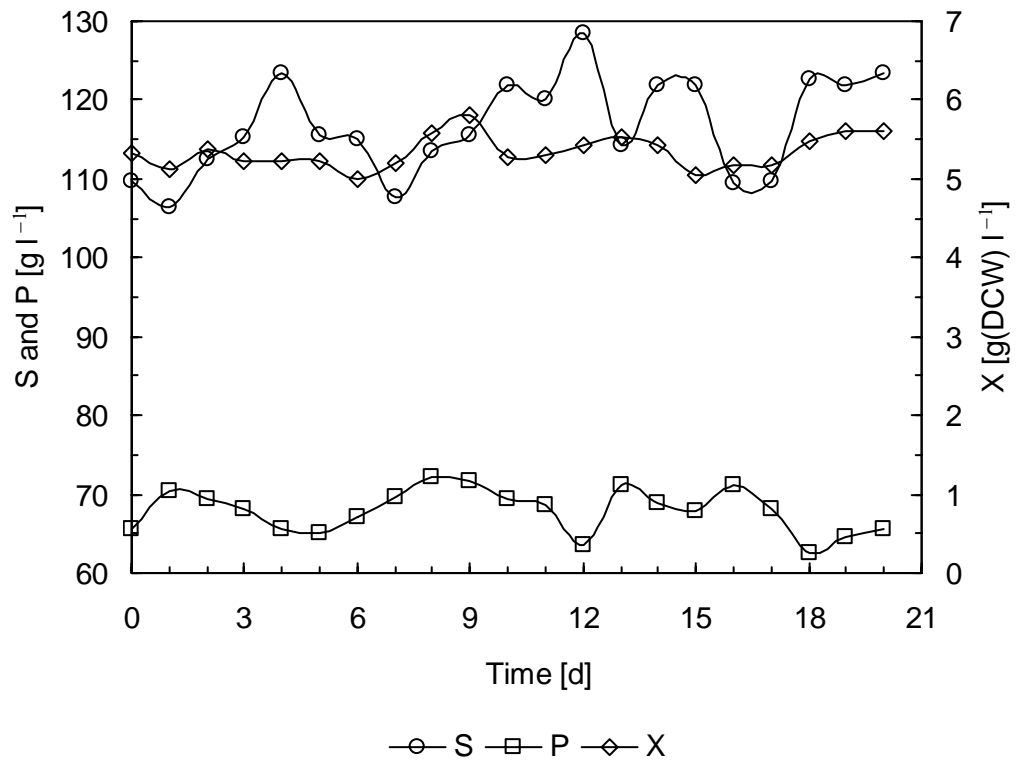


Figure 4.7 Oscillation profiles of the residual glucose, ethanol, and biomass of the continuous ethanol fermentation with *S. cerevisiae* ATCC4126 at the dilution rate of 0.027 h^{-1} . Initial glucose concentration in the medium: $S_0 = 280 \text{ g l}^{-1}$.

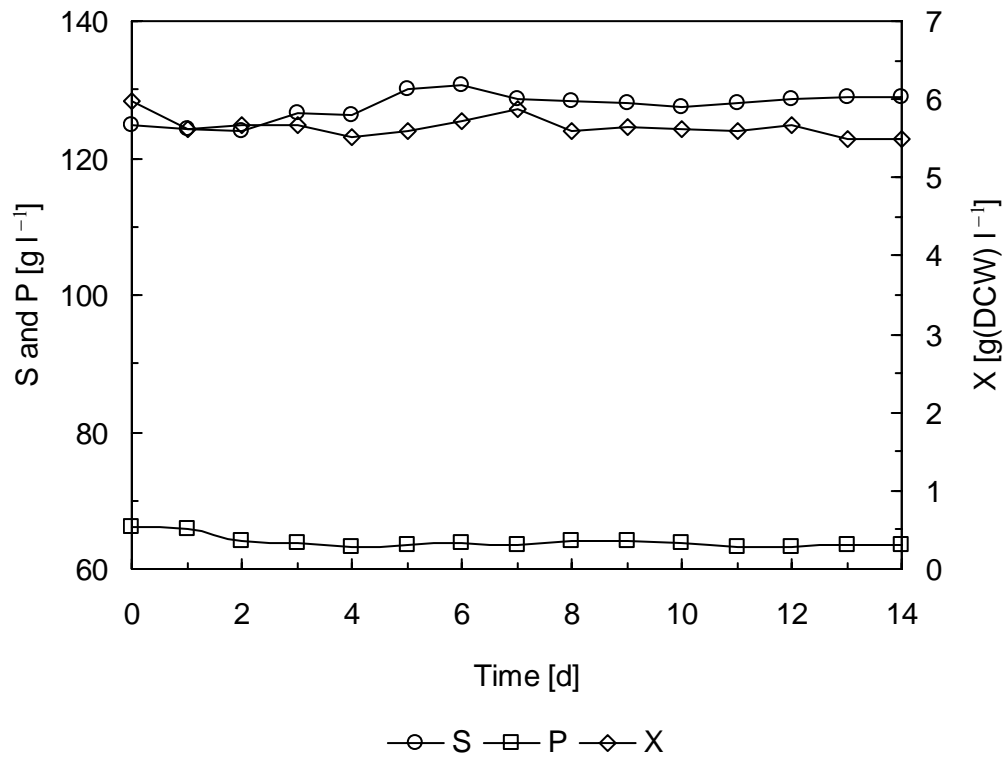


Figure 4.8 Oscillation profiles of the residual glucose, ethanol, and biomass of the continuous ethanol fermentation with *S. cerevisiae* ATCC4126 at the dilution rate of 0.036 h^{-1} . Initial glucose concentration in the medium: $S_0 = 280 \text{ g l}^{-1}$.

4.3.3 Evaluation of ethanol tolerance

The ethanol tolerance of *S. cerevisiae* ATCC4126 and *S. cerevisiae* 6508 as well as the self-flocculating yeast strain, SPSC, was examined by applying 15% and 18% ethanol shocks to their cultures for two hours, followed by the count of their viable cells. The higher the percentage of the viable cells, the better the ethanol tolerance of the strain will be. The experimental results are illustrated in Table 4.1.

Table 4.1 Ethanol tolerance of *S. cerevisiae* ATCC4126, *S. cerevisiae* 6508 and SPSC

Strains	Conditions	Viability
<i>S. cerevisiae</i> ATCC 4126	15% ethanol shock for 2 hours	96.4%
	18% ethanol shock for 2 hours	0
<i>S. cerevisiae</i> 6508	15% ethanol shock for 2 hours	98.7%
	18% ethanol shock for 2 hours	11.9%
SPSC	15% ethanol shock for 2 hours	97.3%
	18% ethanol shock for 2 hours	30.3%

The experimental data indicate that no significant difference in ethanol tolerance was observed for the three yeast strains when 15% ethanol shock was applied. However, when the concentration of ethanol shock was increased to 18%, *S. cerevisiae* 6508 and SPSC with their viable cell percentages of 11.9 % and 30.3% exhibited better ethanol tolerance, and no viable cells were detected for *S. cerevisiae* ATCC4126. These experimental results were in good agreement with our expectation that the ethanol tolerance of *S. cerevisiae* 6508 and SPSC was better than that of *S. cerevisiae* ATCC 4126.

Then, the impact of strains on oscillations was studied by comparing *S. cerevisiae* 6508 with *S. cerevisiae* ATCC 4126.

4.3.4 Continuous VHG ethanol fermentation with *S. cerevisiae* 6508

Four dilution rates, the same as those applied to *S. cerevisiae* ATCC 4126, were also applied to *S. cerevisiae* 6508 in order to compare its oscillation performance. The experimental results are illustrated in Figures 4.9-4.11.

At the dilution rate of 0.012 h^{-1} , oscillation was observed. The oscillation ranges were $106.2\sim 128.6 \text{ g l}^{-1}$, $62.8\sim 73.0 \text{ g l}^{-1}$, and $3.2\sim 5.0 \text{ g(DCW) l}^{-1}$ for residual glucose, ethanol, and biomass, and the corresponding absolute oscillation amplitudes were 22.4 g l^{-1} , 10.2 g l^{-1} , and $1.8 \text{ g(DCW) l}^{-1}$. The oscillation averages were 116.9 g l^{-1} , 67.6 g l^{-1} , and $4.1 \text{ g(DCW) l}^{-1}$ for residual glucose, ethanol, and biomass, and their relative oscillation amplitudes were $\pm 9.1\%$, $\pm 7.5\%$, and $\pm 21.9\%$. These oscillations in both their absolute and relative amplitudes were almost at the same scales as those observed for *S. cerevisiae* ATCC4126 at the same dilution rate except the average residual glucose was higher for *S. cerevisiae* 6508, and correspondingly, the average ethanol concentration was lower, which indicated the ethanol fermentability of this species was not good as that of *S. cerevisiae* ATCC 4126 for the VHG medium. Maybe, as an industrial strain, its fermentation potential could be better exploited when an industrial medium is used.

When the dilution rate of 0.021 h^{-1} was applied to this strain, the residual glucose increased to an average of 142.5 g l^{-1} , the ethanol decreased to an average of 60.3 g l^{-1} , and the biomass increased to an average of $6.9 \text{ g (DCW) l}^{-1}$. However, the oscillatory behavior observed at the dilution rate of 0.012 h^{-1} was significantly damped. For another two dilution rates, 0.027 h^{-1} and 0.036 h^{-1} , the continuous ethanol fermentation were at quasi-steady state, with very small fluctuations of residual glucose and ethanol, although the fluctuation of biomass was a little bigger.

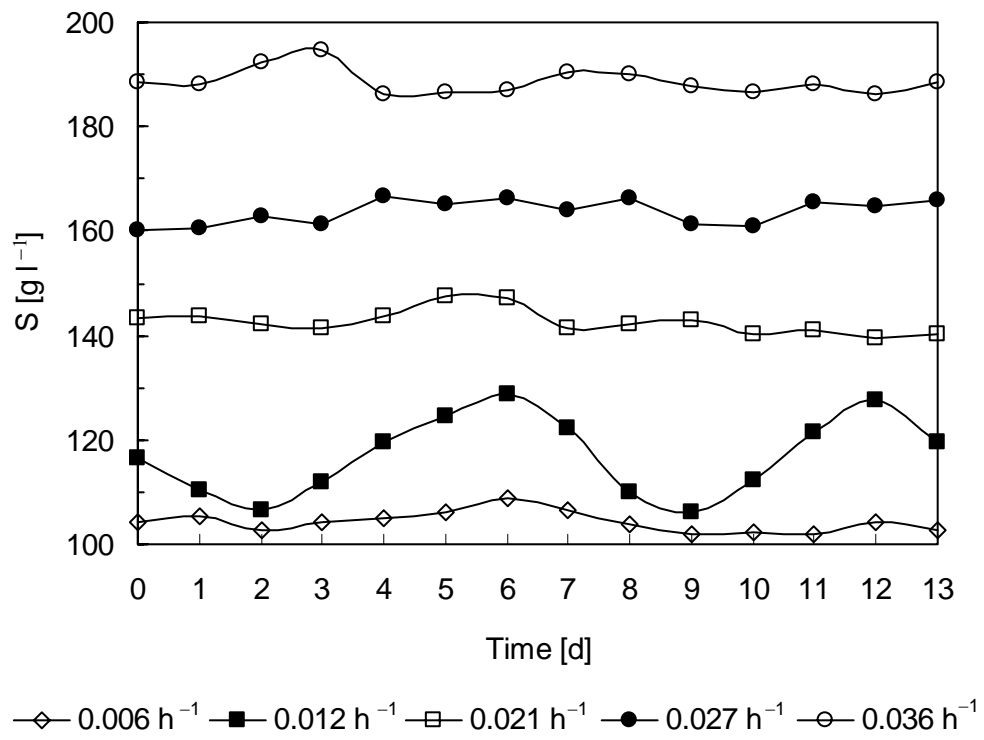


Figure 4.9 Residual glucose profiles of the continuous VHG ethanol fermentation with *S. cerevisiae* 6508. Initial glucose concentration in the medium $S_0 = 280 \text{ g l}^{-1}$.

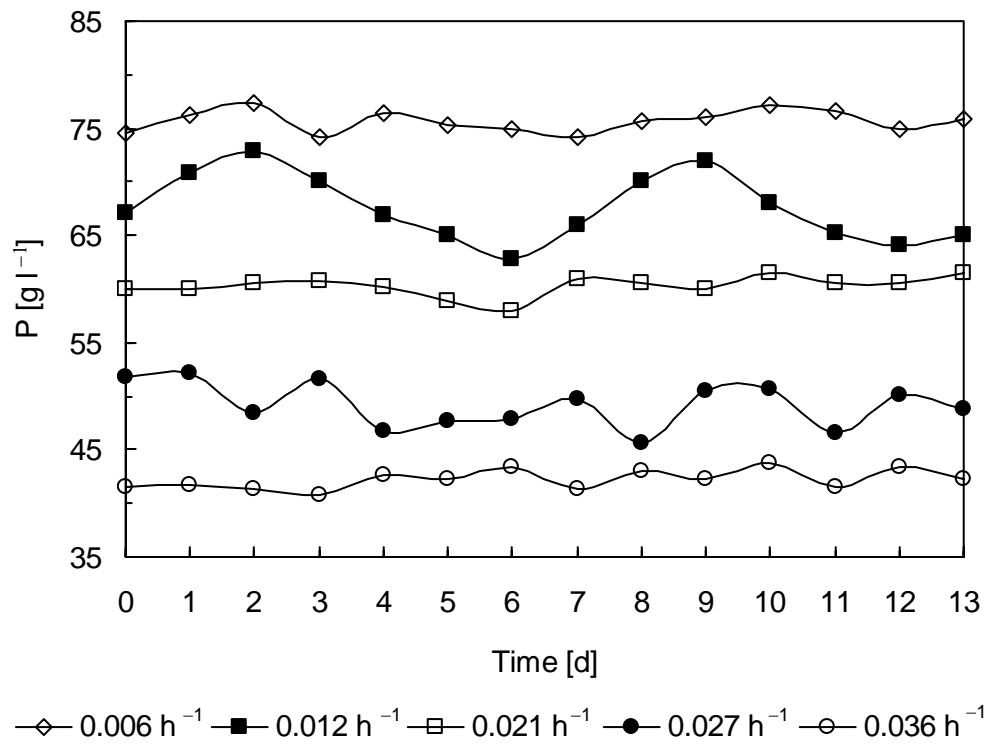


Figure 4.10 Ethanol profiles of the continuous VHG ethanol fermentation with *S. cerevisiae* 6508. Initial glucose concentration in the medium $S_0 = 280 \text{ g l}^{-1}$.

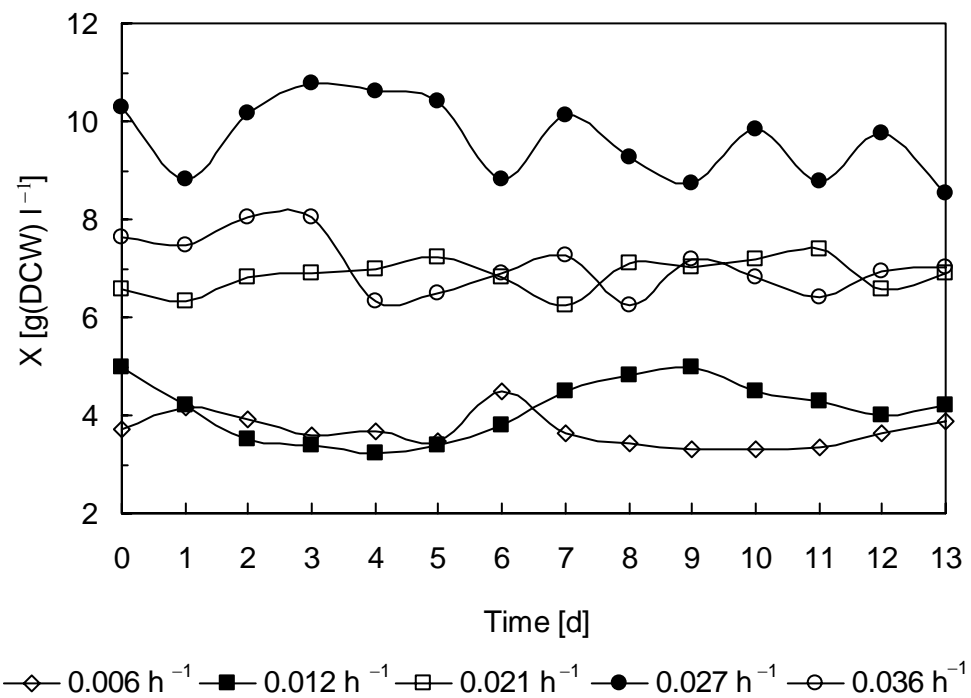


Figure 4.11 Biomass profiles of the continuous VHG ethanol fermentation with *S. cerevisiae* 6508. Initial glucose concentration in the medium $S_0 = 280 \text{ g l}^{-1}$.

For the four dilution rates applied to *S. cerevisiae* 6508, significant oscillation was observed only at the lowest dilution rate of 0.012 h^{-1} , and quasi-steady state was observed at the two higher dilution rates, which inspired us to exploit what could happen if the dilution rate was decreased to below 0.012 h^{-1} for this species. Then, the dilution rate of 0.006 h^{-1} was selected, and the experimental results are also illustrated in Figures 4.9-4.11.

At the dilution of 0.006 h^{-1} , the average residual glucose decreased to 104.3 g l^{-1} , the average ethanol increased to 75.7 g l^{-1} , and the average biomass decreased to $3.7 \text{ g(DCW) l}^{-1}$. The oscillation observed at the dilution of 0.012 h^{-1} was damped rather than exaggerated. The fluctuation ranges of residual glucose, ethanol, and biomass were $101.9\sim 108.9 \text{ g l}^{-1}$, $74.2\sim 77.3 \text{ g l}^{-1}$, and $3.3\sim 4.5 \text{ g(DCW) l}^{-1}$, making their absolute fluctuation amplitudes 7.0 g l^{-1} , 3.1 g l^{-1} , and $1.2 \text{ g(DCW) l}^{-1}$, and the relative fluctuation amplitudes $\pm 3.4\%$, $\pm 2.1\%$, and $\pm 16.2\%$. In fact, the fluctuations of both residual glucose and ethanol were close to their analytical errors, and they were at quasi-steady states!

The significant shift of the process state from oscillation at the dilution rate of 0.012 h^{-1} to quasi-steady state at the dilution rate of 0.006 h^{-1} seems in opposition to our previous mechanistic analysis because ethanol concentration at the lower dilution rate was higher and the corresponding ethanol inhibition was stronger. Following the mechanistic analysis that ethanol inhibition and the lag response of yeast cells to ethanol inhibition were the mechanistic reasons for the oscillation, the oscillation observed at the dilution rate of 0.012 h^{-1} should be exaggerated when the lower dilution rate of 0.006 h^{-1} was adopted and higher ethanol concentration was achieved. Similar phenomena were also observed in *S. cerevisiae* ATCC4126 although the impact of dilution rate on its oscillation was not so obvious when its dilution rate was decreased from 0.021 h^{-1} to 0.012 h^{-1} .

The growth of yeast cells is inhibited under ethanol fermentation, especially under the VHG condition. But, as a primary metabolite, ethanol production must be associated with yeast cell growth unless ethanol concentration achieves a level at which the growth of yeast cells

is completely inhibited. For these two yeast strains, *S. cerevisiae* ATCC4126 and *S. cerevisiae* 6508, the ethanol concentrations achieved under the dilution rates applied to them were not high enough to completely inhibit their growth, but exerted significant inhibition on their growth, and the generation times of their mother and daughter cells were extended. Dilution rate affects ethanol concentration of a continuous ethanol fermentation system as well as ethanol inhibition on yeast cells. Theoretically, a specific dilution rate range could exist, at which the rhythms of the mother and daughter cells could synchronize, and the oscillation similar to that observed in continuous aerobic cultures of *S. cerevisiae* could occur. This analysis seems to be reasonable in explaining the impact of dilution rate on the oscillation profiles observed for *S. cerevisiae* ATCC4126 and *S. cerevisiae* 6508.

For continuous aerobic cultures of *S. cerevisiae*, the synchronization of the mother and daughter cell cycles can be directly observed through regular microscope observations, or indirectly determined by quantitatively measuring the DNA distribution at the different budding stages through staining the yeast cells. Both results illustrated that the significant synchronization of the oscillations of the initial budding cells (DNA 1: 0), middle budding cells (DNA 0.5: 0.5), and late budding cells (1: 1) of *S. cerevisiae* occurred when the process oscillations were observed (Chen and McDonald, 1990; Beuse et al., 1998). In order to validate the aforementioned mechanistic speculation for the impact of dilution rate on the oscillation profiles, microscope observations were also performed, expecting to distinguish the morphology or variability difference among the different yeast cell populations under a continuous VHG ethanol fermentation condition. Unfortunately, neither quantitative nor qualitative correlations were observed. Obviously, new techniques or methods that can effectively distinguish different yeast cell populations under a VHG ethanol fermentation condition need to be developed.

From the point view of ethanol tolerance, the more tolerant a strain to ethanol inhibition, the narrower the oscillation dilution rate range of the strain will be. This is because an

ethanol-tolerant strain generally responds faster to ethanol concentration as well as ethanol inhibition (Casey and Ingledew, 1986) caused by the change of dilution rate and readily adapts to a new ethanol inhibition environment. The growth of the mother and daughter cells of the strain is more easily affected, and the synchronization of the mother and daughter cells occurring at the specific dilution rate is more easily interrupted, affecting the oscillation caused by this cell synchronization. This analysis is supported by the experimental data of the ethanol tolerance illustrated in Table 4.1 as well as by the experimental results of *S. cerevisiae* 6508 and *S. cerevisiae* ATCC4126. In fact, this analysis is in agreement with our previous mechanistic analysis rather than in opposition to it.

4.3 Conclusions

The LG medium supplemented with ethanol was fed into the fermentation system at the same dilution rate as that for the original LG medium, and the impact of externally added ethanol on oscillatory behavior of the fermentation system was studied. The experimental results illustrate that added ethanol also triggers oscillation.

Four dilution rates, 0.012 h^{-1} , 0.021 h^{-1} , 0.027 h^{-1} and 0.036 h^{-1} , were selected to study the impact of dilution rate on oscillatory behavior of *S. cerevisiae* ATCC4126. It was found that dilution rate affected oscillation profile. In addition to ethanol inhibition and lag response of yeast cells to ethanol inhibition, the synchronization of the mother and daughter cell rhythms that could happen at the specific dilution rate range in continuous ethanol fermentation was speculated to be responsible for this phenomenon.

An industrial strain *S. cerevisiae* 6508 was selected to study the impact of strain characteristics, especially its ethanol tolerance, on oscillatory behavior through comparison with the oscillatory behavior of the laboratory strain *S. cerevisiae* ATCC 4126. It was found that not only is the oscillatory dilution rate range of the industrial strain narrower, but it is

also less oscillatory than *S. cerevisiae* ATCC 4126 because of its better ethanol tolerance and faster response to ethanol inhibition. These inferences will be further investigated in the continuous ethanol fermentation with SPSC.

Chapter 5

Oscillations of Continuous Ethanol Fermentation with Self-flocculating Yeast in a Simulated Tanks-in-series System

A manuscript has been prepared for submission based on the work presented in this chapter.

5.1 Introduction

In Chapter 3, oscillations were observed in the continuous ethanol fermentation, and ethanol inhibition and the lag response of yeast cells to ethanol inhibition were proposed to be the mechanistic reasons for the oscillations of the CSTR, while the lethal effect of ethanol on yeast cells exaggerated the oscillations of the tubular bioreactors. In Chapter 4, the impacts of dilution rate and strain, especially the difference in ethanol tolerance between *S. cerevisiae* ATCC 4126 and an industrial strain *S. cerevisiae* 6508, on oscillation profiles were studied. The experimental results partly validated these mechanistic speculations, and at the same time, illustrated that the industrial strain was less oscillatory because of its better ethanol tolerance and faster response to ethanol inhibition.

In the fuel ethanol industry, tanks-in-series fermentation systems are widely used to alleviate ethanol inhibition through generating ethanol concentration difference among the tanks. Based on the aforementioned mechanisms, oscillations could occur in such kind of ethanol fermentation systems. On the other hand, self-flocculating yeast strains are superior to free yeast strains that have been used in the ethanol fermentation industry since its very beginning, because the biomass of a self-flocculating yeast is easier to be separated and

recovered by sedimentation at the end of fermentation, saving the energy consumption and capital investment for centrifuges required by the recovery of free yeast cells (Xu et al., 2005; Ge et al., 2006a, b, c). Moreover, as flocculation can effectively protect yeast cells from ethanol attack, a self-flocculating yeast strain tends to be more ethanol-tolerant than a free one (Hu et al., 2003), and the experimental data of ethanol tolerance in Table 4.1 also supports this point of view.

In this chapter, an industrial tanks-in-series fermentation system was experimentally simulated and long-term continuous ethanol fermentation was carried out using the self-flocculating yeast strain and industrial hydrolysate medium to further study the impact of strain on process oscillations as well as to explore more practical aspects of this fermentation system.

5.2 Materials and Methods

5.2.1 Strain, Medium, and Pre-culture

The self-flocculating yeast strain SPSC was provided by Ms. Ning Li, Department of Bioscience and Bioengineering, Dalian University of Technology, China. This strain was a fusant developed by the protoplast fusion technique from two parent yeast strains: *Saccharomyces cerevisiae* K2, an industrial strain with excellent ethanol fermentation performance but without self-flocculating ability, and *Schizosaccharomyces pombe*, a self-flocculating yeast strain with moderate ethanol fermentation performance. At present, SPSC with excellent ethanol fermentation performance as well as good self-flocculating ability is being used in the fuel ethanol production at BBKA, one of the biggest fuel ethanol producers in China. Its pre-culture medium in Erlenmeyer flasks was the same as that for *S. cerevisiae* ATCC 4126 and *S. cerevisiae* 6508, as described in Section 3.2.1. The media for

its initial culture in the fermentor and later for ethanol fermentation were different, and the hydrolysate of corn flour prepared by the two-stage enzymatic hydrolysis technology was used. It could be scientifically meaningful and practically useful that used the industrial media and a simulated tanks-in-series fermentation system that would be introduced below in Section 5.2.2 to exploit this species' potentials.

The preparation of corn flour hydrolysate was described below. Corn flour (dry-milled, germ-removed, and screened by 20 mesh screen) was donated by a local distiller. The enzymatic hydrolysis of the corn flour was carried out in a stirring tank with a working volume of 15 L. The corn flour was mixed with tap water at a ratio of 1:2. The α -amylase (commercial α -amylase, 20, 000 u ml⁻¹, donated by Novozymes) was added into the slurry at 0.05% (v/w) of the corn flour when the slurry was pre-heated to 55 °C by steam injected into the tank's jacket. The slurry was then heated to 95 °C and liquefied for 90 minutes. When the liquefaction was completed, the mash was cooled to 65 °C by pumping tap water into the jacket. The pH was adjusted to 4.5 by adding 98% H₂SO₄. The glucoamylase (commercial glucoamylase, 100, 000 u ml⁻¹, donated by Novozymes) was added into the mash at 0.15% (v/w) of the corn flour. After overnight saccharification, the DE (dextrose equivalent) value, the percentage of glucose to total sugar in the mash, could approach 90%, which was required by the ethanol fermentation with SPSC. The residue in the mash was removed by filtration and the liquor hydrolysate was collected for the seed culture and ethanol fermentation.

The hydrolysate was diluted by tap water to 120 ± 5 g l⁻¹ total sugar, supplemented with 2.0 g l⁻¹ (NH₄)₂HPO₄ and K₂HPO₄, respectively, and was used for the seed culture. Likewise the hydrolysate was adjusted by tap water to 220 ± 5 g l⁻¹ total sugar, supplemented with 0.5 g l⁻¹ (NH₄)₂HPO₄ and 0.15 g l⁻¹ K₂HPO₄, and was used for the continuous ethanol fermentation. These medium formulas were the same as those used at BBKA.

Flasks (3000 ml) were used as the medium storage tanks for the seed culture medium, in

which 1800 ml medium was contained. The seed culture medium was sterilized at 121°C for 15 minutes. Flasks (5000 ml) were used as the fermentation medium storage tanks. The empty flasks were sterilized at 121 °C for 15 minutes. Then, 4000 ml fermentation medium was added and the flasks were sterilized at 110 °C for 15 minutes. After sterilization, the fermentation medium was immediately cooled down to room temperature by immersing the flasks into water to avoid the formation of harmful by-products. Glucoamylase was sterilized by 0.2 µm membrane filtration and added into the sterilized fermentation medium at 0.15% (v/v) to compensate for the activity loss of the glucoamylase originally added but destroyed during the sterilization, so that a complete conversion of sugar to ethanol could be realized during the fermentation.

5.2.2 Bioreactor System

Although the tubular bioreactors illustrated in Figure 3.1 are suitable for the continuous ethanol fermentation using free yeast cells such as *S. cerevisiae* ATCC4126 and *S. cerevisiae* 6508, they cannot be used for the continuous ethanol fermentation with SPSC, because the self-flocculation of this species facilitates its sedimentation, easily generating dead zones and short-cut flows within the tubular bioreactors. In the ethanol fermentation industry, especially in large-scale fuel ethanol production, tanks-in-series bioreactor systems incorporated with seed tanks are widely used in order to guarantee the efficiency and reliability of these fermentation systems. Therefore, a simulated tanks-in-series fermentation system, as illustrated in Figure 5.1, was established for the continuous ethanol fermentation with SPSC.

Four small tanks, each with a working volume of 1000 ml, were used and operated as CSTRs. The first tank was designated as the seed tank through which healthy SPSC seed culture was continuously produced and transferred to the second tank as well as the whole fermentation system thereafter, guaranteeing the reliability of a long-term operation.

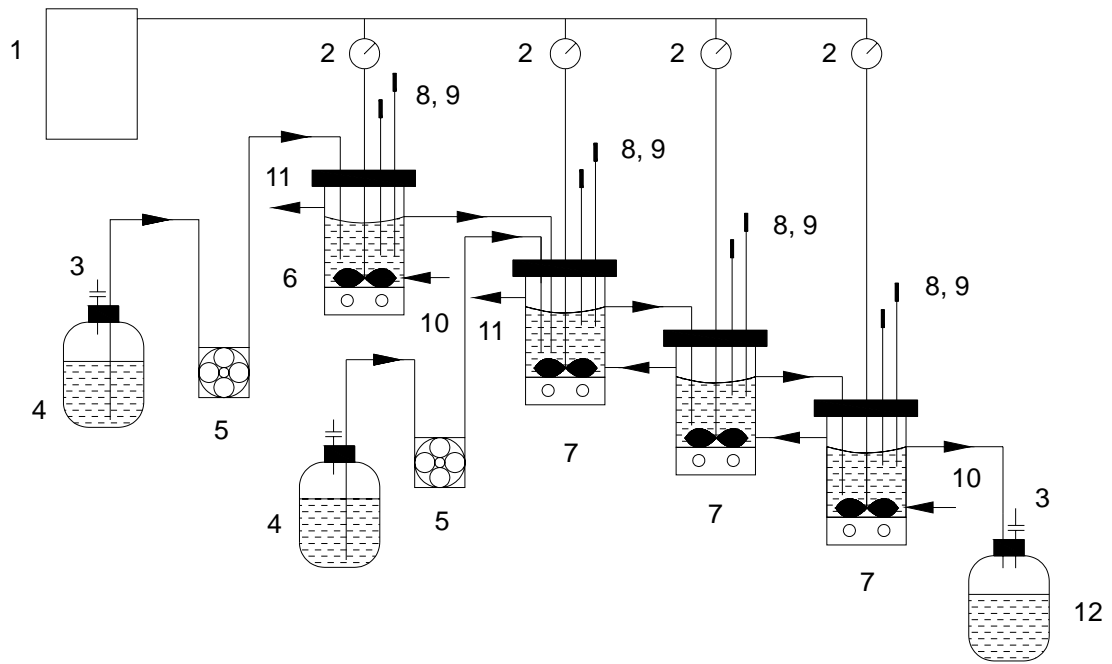


Figure 5.1 Diagram of the tanks-in-series bioreactor system for the continuous ethanol fermentation with a self-flocculating yeast strain SPSC and the hydrolysate of corn flour. 1 Air compressor, 2 Air flowmeters, 3 Filters, 4 Substrate storage tanks, 5 Peristaltic pumps, 6 Seed Fermentor, 7 Fermentors, 8, 9 Temperature and pH controlling units, 10 Thermostat water inlets, 11 Thermostat water outlets, 12 Effluent storage tank

The tanks containing 850 ml seed culture medium were sterilized at 121°C for 15 minutes, then cooled to room temperature and inoculated separately, each with 50 ml yeast flocs prepared through flask culture. After inoculation, batch culture was initiated. The temperature was controlled at $30 \pm 0.5^\circ\text{C}$ by pumping water into the tanks' jacket. The pH was controlled at 4.5 ± 0.2 by automatically adding ammonia water into the tanks, neutralizing acidic by-products produced by the yeast during fermentation as well as providing nitrogen nutrient. Air was aerated into each tank at the flowrate of 0.05 vvm. When the residual sugar within the tanks was lower than 1.0 g l^{-1} , the first tank was switched from batch to continuous mode by feeding the seed culture medium at the dilution rate of 0.017 h^{-1} . Meanwhile, continuous ethanol fermentations were switched on by feeding the fermentation medium into the second tank at different dilution rates to study the performance of this SPSC ethanol fermentation system. After the ethanol fermentation was initiated, the temperature of the fermentation system was controlled at $33 \pm 0.5^\circ\text{C}$, the pH was controlled at the same level as that for the seed culture, and the aeration of the second, third and fourth tanks was interrupted during the ethanol fermentation.

5.2.3 Analytical methods

Ethanol and biomass analysis were described in Section 3.2.3. The reducing and total sugar in the hydrolysate as well as in the fermented broth were analyzed by Fehling titration, but the samples for the total sugar analysis were hydrolyzed by HCl prior to the Fehling titration. A detailed analytical protocol can be found in the National Standard for Sugar Analysis GB/T 6194-86.

5.3 Results and Discussion

5.3.1 Continuous fermentation in the tanks-in-series system with the seed tank

Within a continuous operation of four months, the seed fermentor, which was fed with the low gravity hydrolysate medium containing 120 g l^{-1} sugar at a dilution rate of 0.017 h^{-1} , was at steady state, and its residual sugar, ethanol, and biomass were maintained at the levels of 3.0 g l^{-1} , 46.1 g l^{-1} , and $4.1 \text{ g(DCW) l}^{-1}$, with very small fluctuations.

Unlike the previous fermentations with *S. cerevisiae* ATCC4126 and *S. cerevisiae* 6508, the SPSC fermentation system was not interrupted when dilution rate adjustments were made in order to examine its long-term fermentation performance. Five days to three weeks were required for its system equilibrium, which depended on the dilution rate and was judged by matching the ethanol and residual sugar in the effluent from the last tank with the initial sugar in the media feeding into the seed fermentor as well as the fermentation system. Meanwhile, a backward sampling sequence starting with the last fermentor was adopted to minimize the potential influence of sampling on the fermentation system.

Because of the continuous inoculation from the seed fermentor and good nutrition provided by the hydrolysate, higher biomass concentrations were achieved within the fermentors. Therefore, higher dilution rates were applied, starting with 0.05 h^{-1} . After three weeks' system equilibrium from its inoculation, residual sugar, ethanol, and biomass were monitored, and the experimental results are illustrated in Figures 5.2~5.4.

Slight oscillations were observed for the first fermentor. The oscillation ranges of residual sugar, ethanol, and biomass were $24.0\sim 36.0 \text{ g l}^{-1}$, $71.4\sim 78.0 \text{ g l}^{-1}$, and $10.0\sim 12.8 \text{ g(DCW) l}^{-1}$, making the absolute oscillation amplitudes 12.6 g l^{-1} , 6.6 g l^{-1} , and $2.8 \text{ g(DCW) l}^{-1}$, respectively. The averages of residual sugar, ethanol, and biomass were 30.0 g l^{-1} , 74.6 g l^{-1} , and $11.3 \text{ g(DCW) l}^{-1}$, making the relative oscillation amplitudes $\pm 21.0\%$, $\pm 4.4\%$, and $\pm 12.4\%$. The oscillation periods were observed to be 8~10 days.

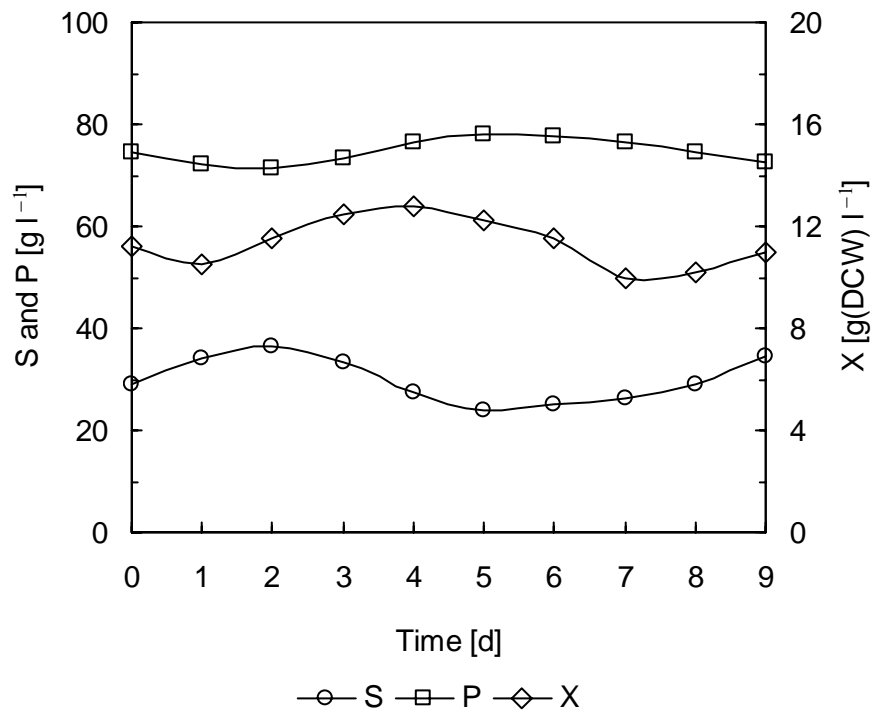


Figure 5.2 Performance of the first fermentor of the SPSC fermentation system at the dilution rate of 0.05 h^{-1} . Initial sugar in the hydrolysate medium: $S_0 = 220 \text{ g l}^{-1}$.

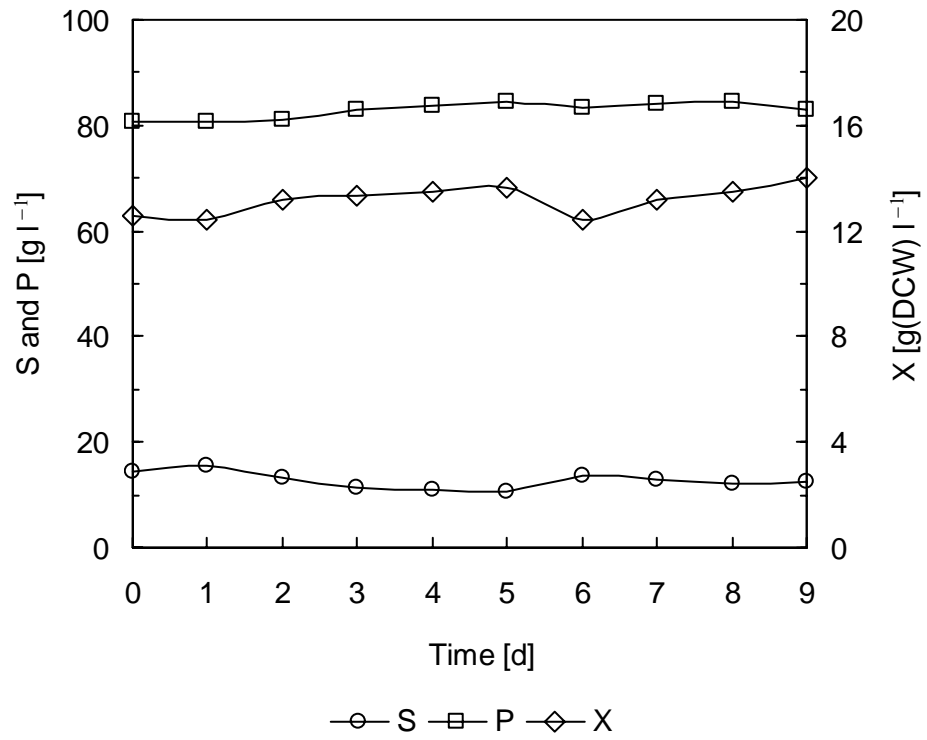


Figure 5.3 Performance of the second fermentor of the SPSC fermentation system at the dilution rate of 0.05 h^{-1} . Initial sugar in the hydrolysate medium: $S_0 = 220 \text{ g l}^{-1}$.

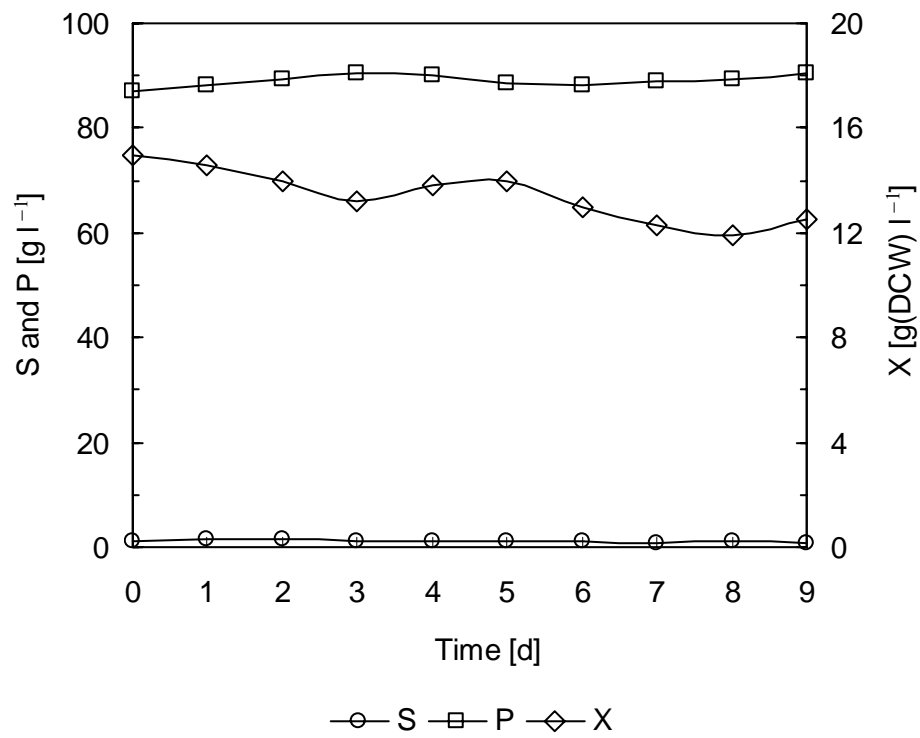


Figure 5.4 Performance of the third fermentor of the SPSC fermentation system at the dilution rate of 0.05 h^{-1} . Initial sugar in the hydrolysate medium: $S_0 = 220 \text{ g l}^{-1}$.

The oscillations observed in the first fermentor were damped in the second fermentor, with the corresponding oscillation ranges of 10.5~15.5 g l⁻¹, 80.5~84.3 g l⁻¹, and 12.4~14.0 g(DCW) l⁻¹ for residual sugar, ethanol, and biomass, and the absolute oscillation amplitudes of 5.0 g l⁻¹, 3.8 g l⁻¹, and 1.6 g(DCW) l⁻¹, respectively. The averages of residual sugar, ethanol, and biomass were 12.7 g l⁻¹, 82.8 g l⁻¹, and 13.2 g(DCW) l⁻¹, and correspondingly, the relative oscillation amplitudes were ±19.6%, ±2.3%, and ±6.0%. These experimental results indicated that quasi-steady states for ethanol and biomass were established. Because the average residual sugar was low, its relative oscillation amplitude was large. These quasi-steady states were further developed in the third fermentor.

At the dilution rate of 0.05 h⁻¹, the flowrate of the fermentation medium with 220 g l⁻¹ sugar was 50 ml h⁻¹. The seed fermentor was operated at the dilution rate of 0.017 h⁻¹, and the corresponding flowrate of the seed culture medium with 120 g l⁻¹ sugar was 17 ml h⁻¹. Therefore, the equivalent total sugar concentration that could be fermented into ethanol and CO₂ in the mixture feeding into the first fermentor was calculated to be 195 g l⁻¹. The average ethanol concentration in the final effluent from the third fermentor was 89.1 g l⁻¹, making an ethanol yield of 0.456 without deduction of the residual sugar but calibrated by the ethanol loss evaporated by the exhaust gas, or 89.2% of the theoretical ethanol-to-glucose yield of 0.511, almost at the same level as that is achieved in the industrial. The fact that more ethanol appeared in the third fermentor than consumed sugar could generate was attributed to the utilization of the organic acid byproducts produced during the main fermentation when the fermentable sugars were gradually depleted, which is a common phenomenon in the ethanol fermentation industry.

As the average residual sugar in the effluent from the third fermentor was only 1.1 g l⁻¹, the dilution rate was increased to 0.10 h⁻¹ to improve the ethanol productivity of the fermentation system, and ten days were allowed for the system equilibrium. Figures 5.5~5.7 show the experimental results.

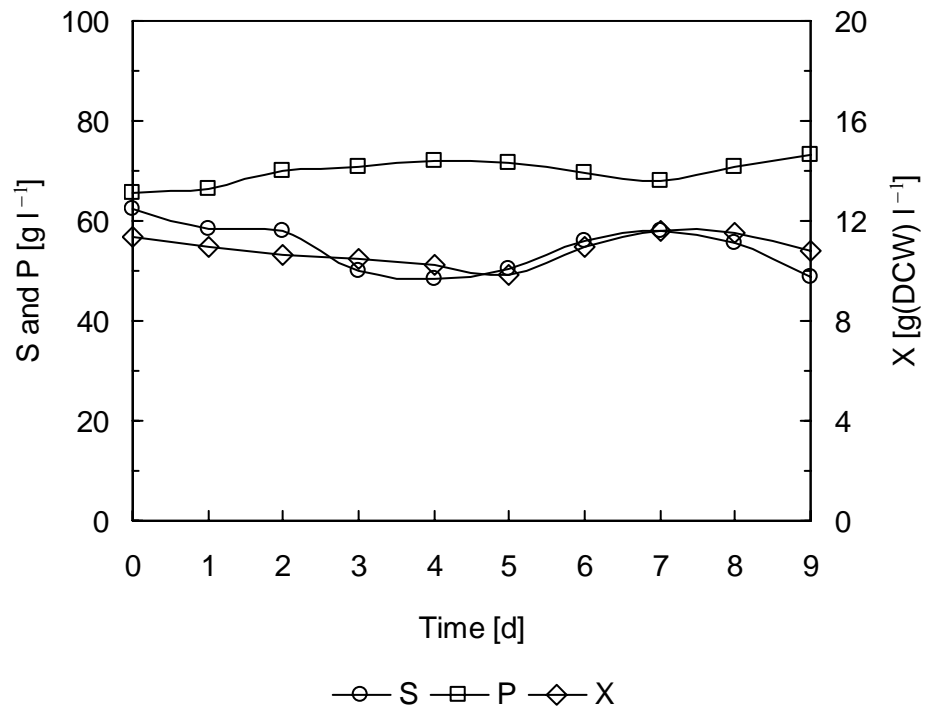


Figure 5.5 Performance of the first fermentor of the SPSC fermentation system at the dilution rate of 0.10 h^{-1} . Initial sugar in the hydrolysate medium: $S_0 = 220 \text{ g l}^{-1}$.

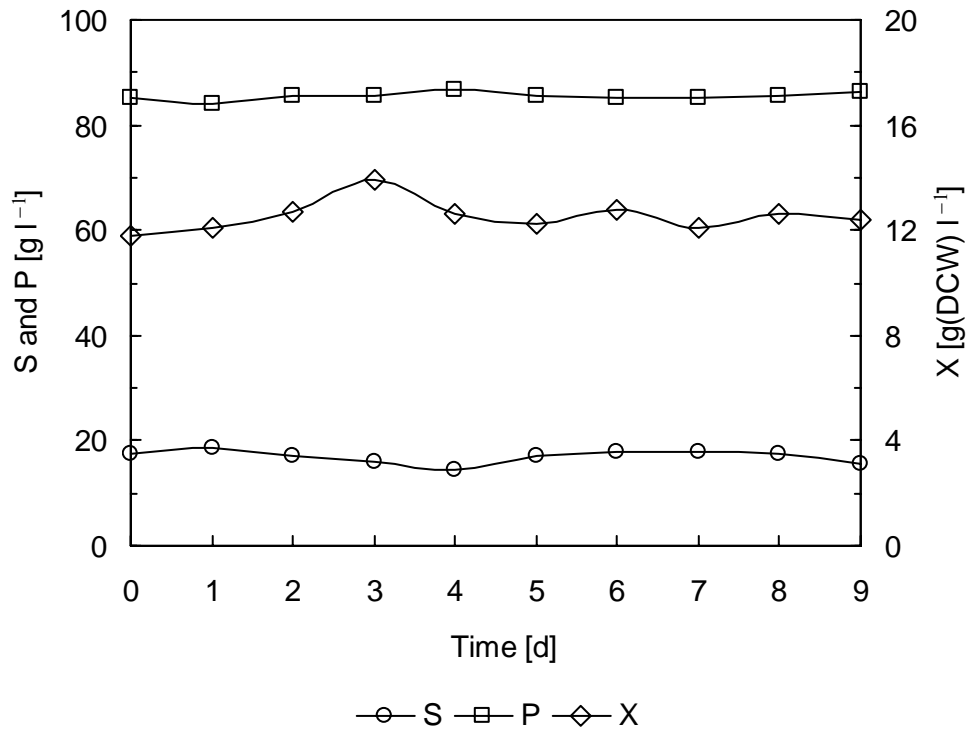


Figure 5.6 Performance of the second fermentor of the SPSC fermentation system at the dilution rate of 0.10 h^{-1} . Initial sugar in the hydrolysate medium: $S_0 = 220 \text{ g l}^{-1}$.

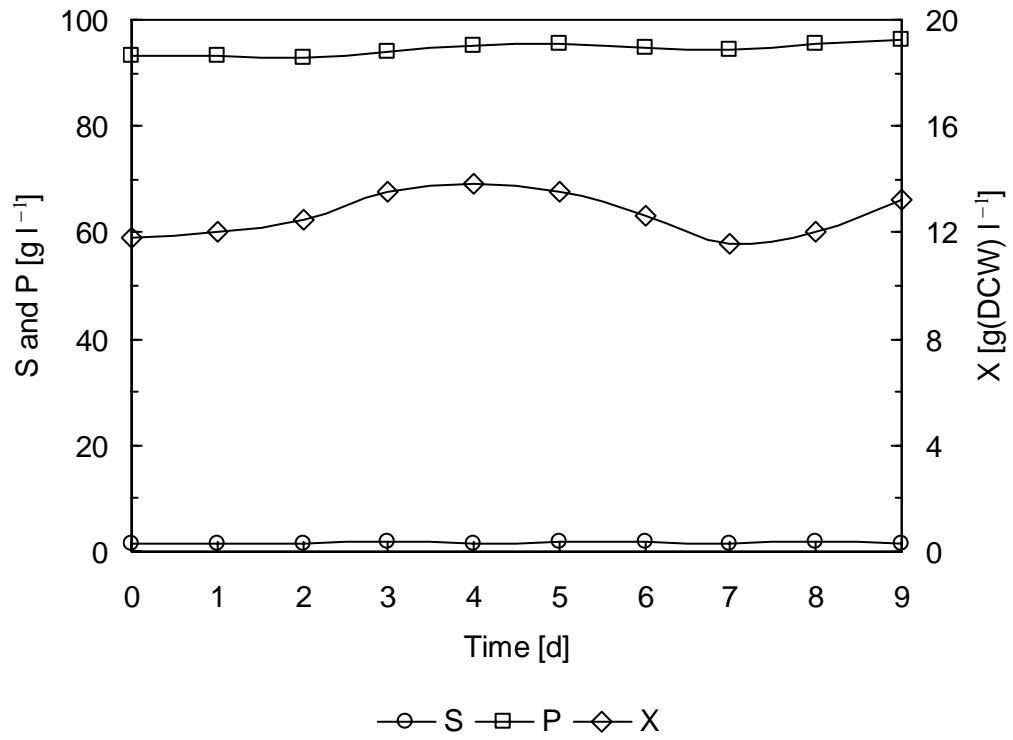


Figure 5.7 Performance of the third fermentor of the SPSC fermentation system at the dilution rate of 0.10 h^{-1} . Initial sugar in the hydrolysate medium: $S_0 = 220 \text{ g l}^{-1}$.

The first fermentor was observed to be oscillatory. The oscillation ranges of residual sugar, ethanol, and biomass were 48.6~62.5 g l⁻¹, 65.8~73.1 g l⁻¹, and 9.9~11.6 g(DCW) l⁻¹, making the absolute oscillation amplitudes be 13.9 g l⁻¹, 7.3 g l⁻¹, and 1.7 g(DCW) l⁻¹, respectively. The averages of residual sugar, ethanol, and biomass were 54.7 g l⁻¹, 69.8 g l⁻¹, and 10.9 g(DCW) l⁻¹, and correspondingly, the relative oscillation amplitudes were ±12.7%, ±5.2%, and ±7.8%. These oscillations were almost at the same scales as the oscillations observed at the dilution rate of 0.05 h⁻¹. For the second and third fermentors, no significant oscillations were observed.

When the fermentation system was operated at the dilution rate of 0.05 h⁻¹, the average residual sugar in the final effluent from the third fermentor was 1.1 g l⁻¹, and the average ethanol was 89.1 g l⁻¹. The ethanol productivity of the fermentation system was 1.72 g l⁻¹.h⁻¹*. At the dilution rate of 0.10 h⁻¹, the average ethanol concentration in the final effluent from the third fermentor increased to 94.5 g l⁻¹ because the dilution role of the seed culture in the fermentation medium was weakened, but the average residual sugar only slightly increased to 1.6 g l⁻¹, almost at the same level as that achieved at the dilution rate of 0.05 h⁻¹, making the ethanol productivity of the fermentation system increase to 3.42 g l⁻¹.h⁻¹. The fermentation potentials of the second and third fermentors were exploited.

As the residual sugar in the final effluent was still low, the dilution rate was increased to 0.15 h⁻¹, expecting that the productivity of the fermentation system could be further improved. Figures 5.8~5.10 illustrate the fermentation performance of the fermentation system at this dilution rate. One week was required for the system to be equilibrated.

* The ethanol productivity of the fermentation system was calculated by

$$q = \frac{F_t P_t - F_s P_s}{V_1 + V_2 + V_3}$$

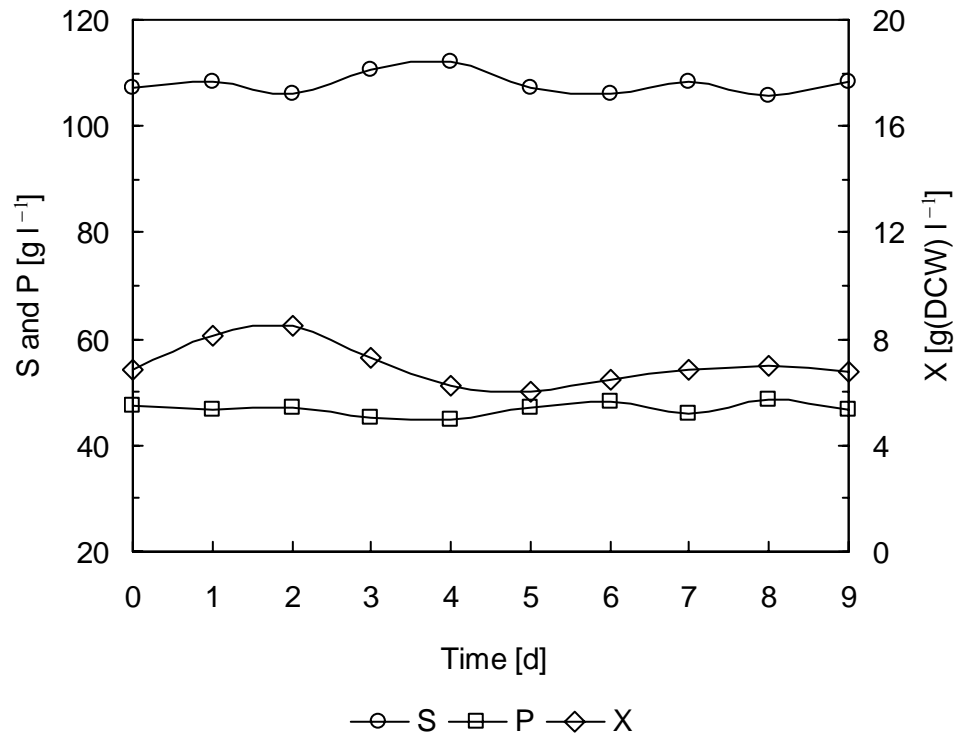


Figure 5.8 Performance of the first fermentor of the SPSC fermentation system at the dilution rate of 0.15 h^{-1} . Initial sugar in the hydrolysate medium: $S_0 = 220 \text{ g l}^{-1}$.

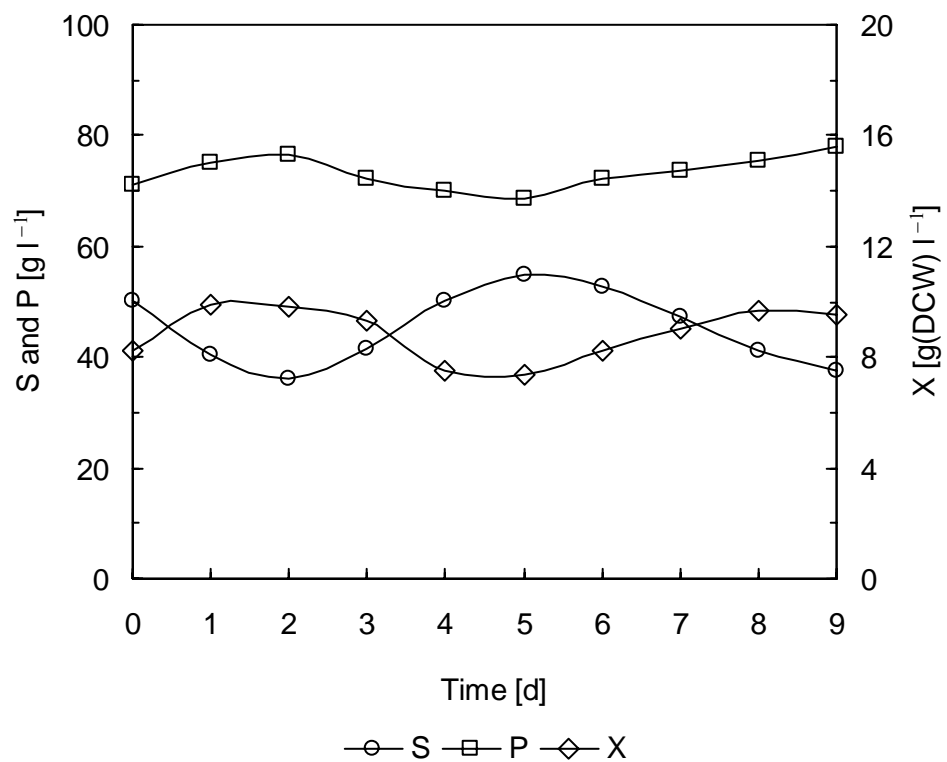


Figure 5.9 Performance of the second fermentor of the SPSC fermentation system at the dilution rate of 0.15 h^{-1} . Initial sugar in the hydrolysate medium: $S_0 = 220 \text{ g l}^{-1}$.

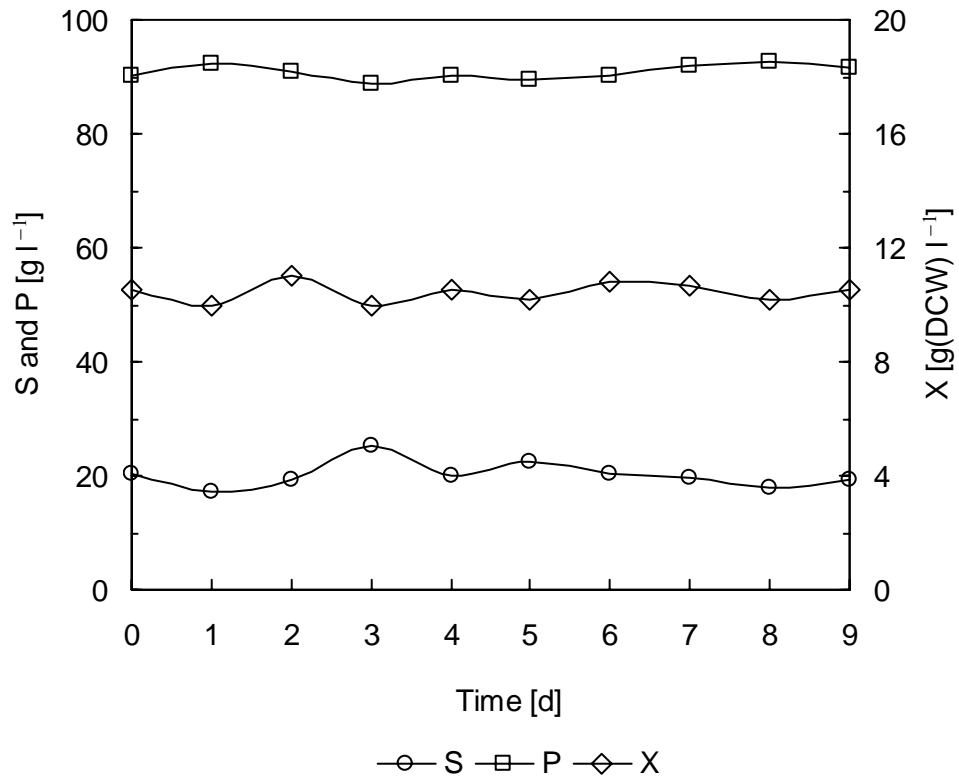


Figure 5.10 Performance of the third fermentor of the SPSC fermentation system at the dilution rate of 0.15 h^{-1} . Initial sugar in the hydrolysate medium: $S_0 = 220 \text{ g l}^{-1}$.

At this dilution rate, the average residual sugar of the first fermentor dramatically increased to 108.0 g l^{-1} , the average ethanol correspondingly decreased to 46.8 g l^{-1} , and the average biomass decreased to $7.0 \text{ g(DCW) l}^{-1}$. And quasi-steady states were developed for residual sugar, ethanol, and biomass because the ethanol concentration was too low to incite oscillations. However, oscillations were observed for the second fermentor. The oscillation ranges of residual sugar, ethanol, and biomass were $36.1\sim 55.0 \text{ g l}^{-1}$, $68.5\sim 77.8 \text{ g l}^{-1}$, and $7.4\sim 9.9 \text{ g(DCW) l}^{-1}$, and the corresponding absolute oscillation amplitudes were 18.9 g l^{-1} , 9.3 g l^{-1} and $2.5 \text{ g(DCW) l}^{-1}$. The averages of residual sugar, ethanol and biomass were 45.2 g l^{-1} , 73.3 g l^{-1} and $8.9 \text{ g(DCW) l}^{-1}$, giving the relative oscillation amplitudes of $\pm 20.9\%$, $\pm 6.3\%$, and $\pm 14.0\%$.

The shift of the oscillations from the first fermentor to the second is in good accordance with our previous mechanistic analysis. For the tanks-in-series ethanol fermentation system, the increase of dilution rate decreases the ethanol concentration of the front fermentors to values even below the critical ethanol concentration at which oscillations can be triggered, but the ethanol concentration of the rear fermentor correspondingly increases to values that are higher than the criterion, triggering the oscillations.

Affected by the oscillations of the second fermentor, the third fermentor also presented some kind of oscillations, but these oscillations were significantly damped. At this dilution rate, the average sugar in the final effluent from the third fermentor was 19.9 g l^{-1} , too high to be acceptable from the point view of industrial application. Therefore, the dilution rate was decreased to 0.12 h^{-1} , a value between the dilution rates of 0.10 h^{-1} and 0.15 h^{-1} , expecting a compromise between low residual sugar and the improvement of the ethanol productivity of the fermentation system.

After ten day's system equilibrium, the fermentation performance was evaluated, as illustrated in Figures 5.11~5.13.

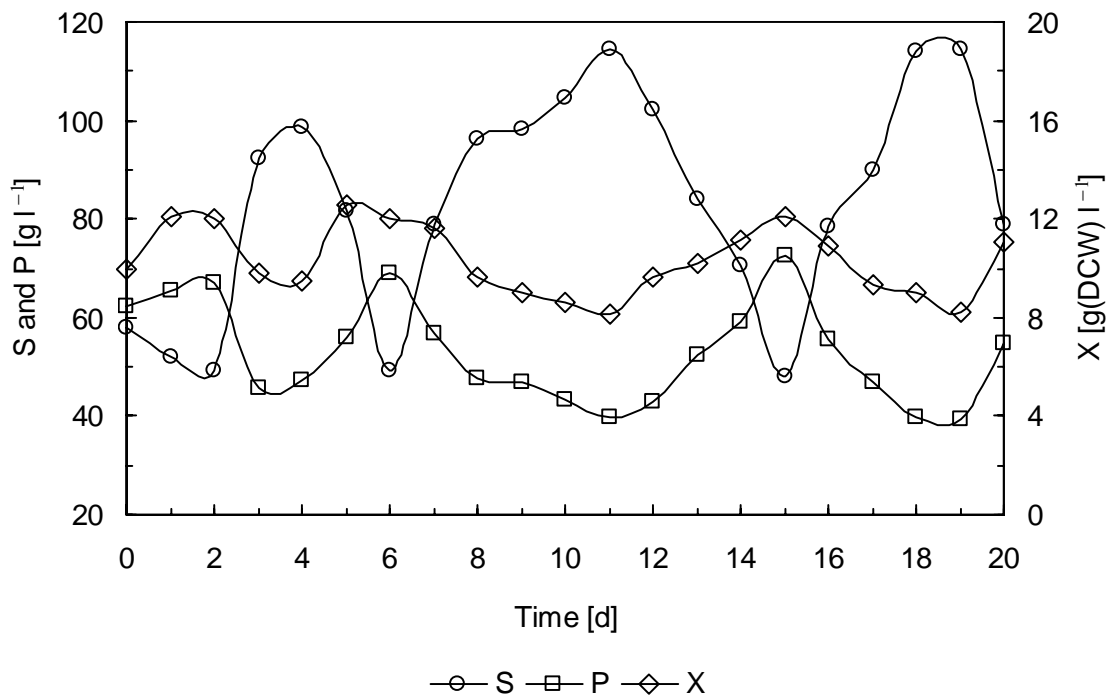


Figure 5.11 Performance of the first fermentor of the SPSC fermentation system at the dilution rate of 0.12 h^{-1} . Initial sugar in the hydrolysate medium: $S_0 = 220 \text{ g l}^{-1}$.

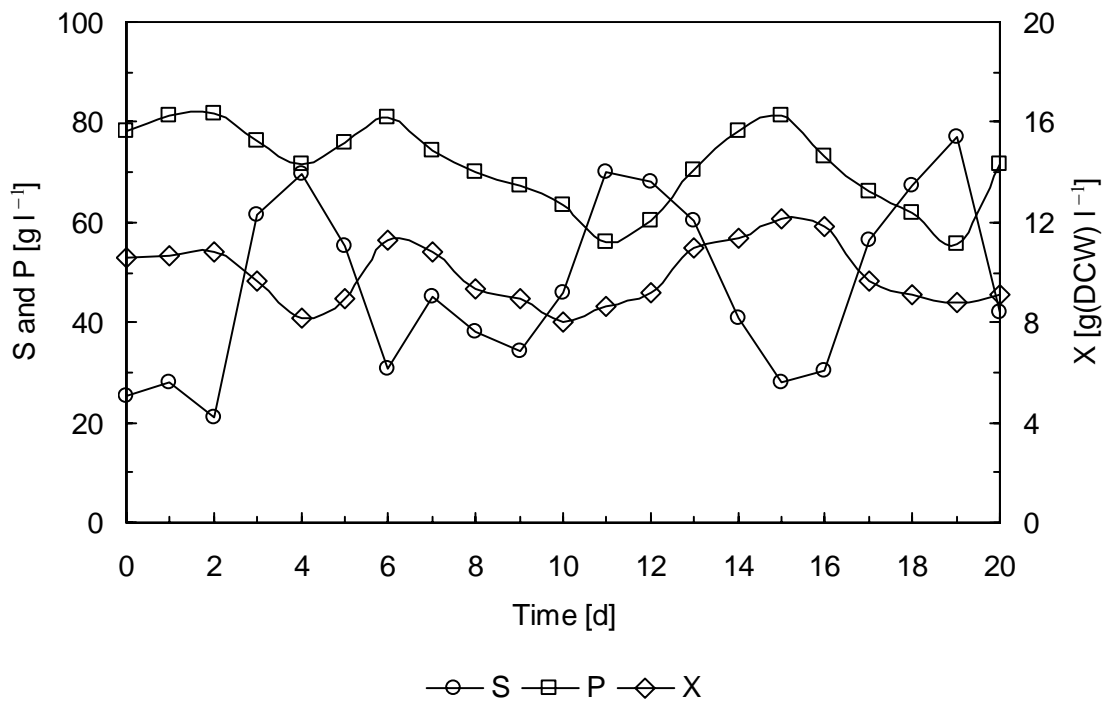


Figure 5.12 Performance of the second fermentor of the SPSC fermentation system at the dilution rate of 0.12 h^{-1} . Initial sugar in the hydrolysate medium: $S_0 = 220 \text{ g l}^{-1}$.

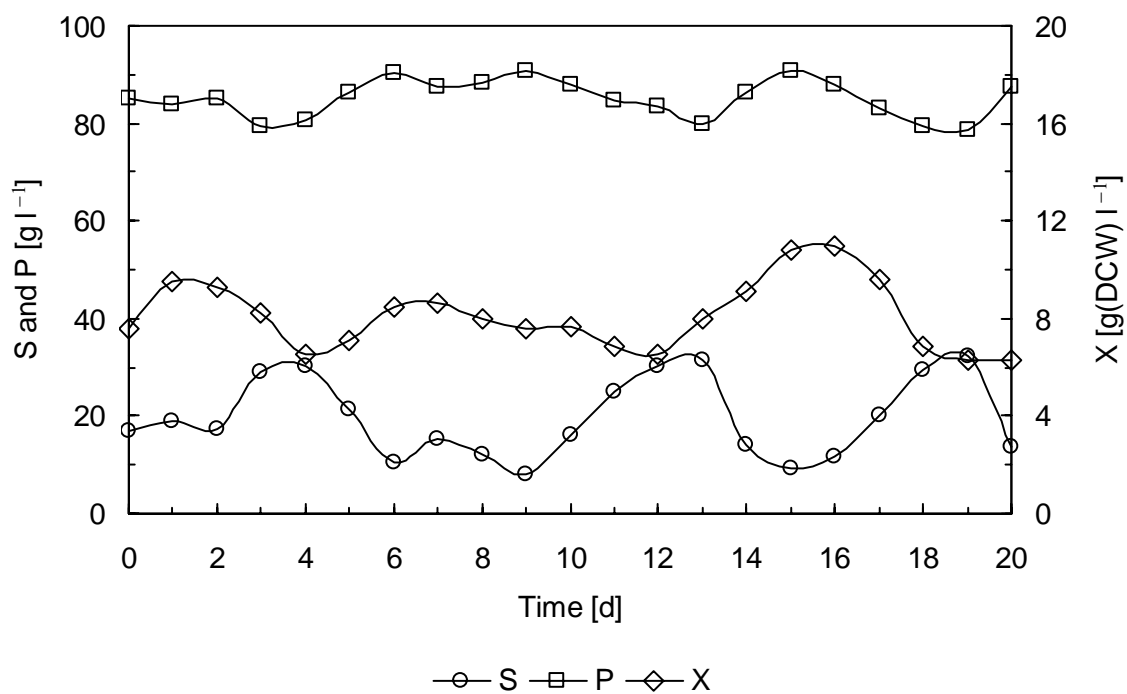


Figure 5.13 Performance of the third fermentor of the SPSC fermentation system at the dilution rate of 0.12 h^{-1} . Initial sugar in the hydrolysate medium: $S_0 = 220 \text{ g l}^{-1}$.

It was observed that exaggerated oscillations of residual sugar, ethanol and biomass occurred at this dilution rate occurred for the whole fermentation system. Therefore, the duration of this dilution was extended to three weeks to investigate these oscillations.

For the first fermentor, the oscillation ranges of residual sugar, ethanol, and biomass were 48.2~114.3 g l⁻¹, 39.5~72.4 g l⁻¹, and 6.3~11.0 g(DCW) l⁻¹, and the corresponding absolute oscillation amplitudes were 66.1 g l⁻¹, 32.9 g l⁻¹, and 4.7 g(DCW) l⁻¹. The oscillation averages of residual sugar, ethanol, and biomass were 83.5 g l⁻¹, 52.9 g l⁻¹, and 8.1 g (DCW) l⁻¹, and the relative oscillation amplitudes were ±39.6%, ±31.1%, and ±29.0%. Both the absolute and relative amplitudes were very large.

Influenced by the exaggerated oscillations of the first fermentor, the second and third fermentors were also oscillatory. The oscillation ranges of residual sugar, ethanol, and biomass were 21.1~77.2 g l⁻¹, 55.7~81.8 g l⁻¹, and 8.0 ~12.2 g(DCW) l⁻¹ for the second fermentor, and 8.1~32.4 g l⁻¹, 78.7~90.7 g l⁻¹, and 6.3 ~11.0 g(DCW) l⁻¹ for the third fermentor. The corresponding absolute oscillation amplitudes were 56.1 g l⁻¹, 26.2 g l⁻¹, and 4.2 g(DCW) l⁻¹ for the second fermentor, and 24.3 g l⁻¹, 12.0 g l⁻¹, and 4.4 g(DCW) l⁻¹ for the third fermentor. The averages of residual sugar, ethanol, and biomass were 47.4 g l⁻¹, 71.2 g l⁻¹, and 9.9 g(DCW) l⁻¹ for the second fermentor, and 19.7 g l⁻¹, 85.1 g l⁻¹, and 10.3 g(DCW) l⁻¹ for the third fermentor, making the relative oscillation amplitudes ±59.2%, ±18.4%, and ±21.2% for the second fermentor, and ±61.6%, ±7.1%, and ±21.4% for the third fermentor. These oscillations seriously compromised the fermentation performance of the whole fermentation system, making the residual sugar in the final effluent from the third fermentor higher, almost at the same level as that achieved at the higher dilution rate of 0.15 h⁻¹.

Figures 5.14-5.16 further compare the oscillation profiles of residual sugar, ethanol, and biomass of the three fermentors. It can be seen that the oscillations of the second and third fermentors were almost in phase with the oscillations of the first fermentor, indicating the

influences of the oscillations of the first fermentor on the behaviors of the second and third fermentors were so strong that the oscillation characteristics of their own if occurring might be masked. The oscillation periods were 8-10 days for the whole fermentation system.

Let us further examine the impact of the exaggerated oscillations on the fermentation performance of the system. As the dilution rate was decreased from 0.15 h^{-1} to 0.12 h^{-1} , the average fermentation time was increased to 25 h from 20 h, more sugar should be converted into ethanol, and lower residual sugar and higher ethanol should be achieved in the final effluent from the third fermentor. This effect seemed to occur only for the first fermentor with the decrease of its average residual sugar from 108.0 g l^{-1} at the dilution rate of 0.15 h^{-1} to 82.9 g l^{-1} at the dilution rate of 0.12 h^{-1} , and its average ethanol correspondingly increased to 52.9 g l^{-1} from 46.8 g l^{-1} . But for the second and third fermentors, their residual sugar and ethanol were almost the same as those previously achieved at the dilution rate of 0.15 h^{-1} , indicating the exaggerated oscillations occurring ahead in the first fermentor deteriorated the fermentation performance of these two fermentors thereafter. Therefore, these oscillations ought to be avoided or attenuated.

As the oscillatory behaviors previously observed at the dilution rate of 0.10 h^{-1} were much weaker than the oscillations observed at this dilution rate of 0.12 h^{-1} , why did such a small change in dilution rate cause such a large change in the process state? It was tested to determine if the process state previously observed at the dilution rate of 0.10 h^{-1} could be repeated after the fermentation system experienced these exaggerated oscillations. After ten days' system equilibrium, a duration of two weeks was maintained, and residual sugar, ethanol, and biomass were re-examined. The experimental data show the oscillatory behaviors of the fermentation system at the dilution rate of 0.10 h^{-1} were reproducible, except that the residual sugar of the second fermentor was slightly lower and the corresponding ethanol concentration was a little bit higher.

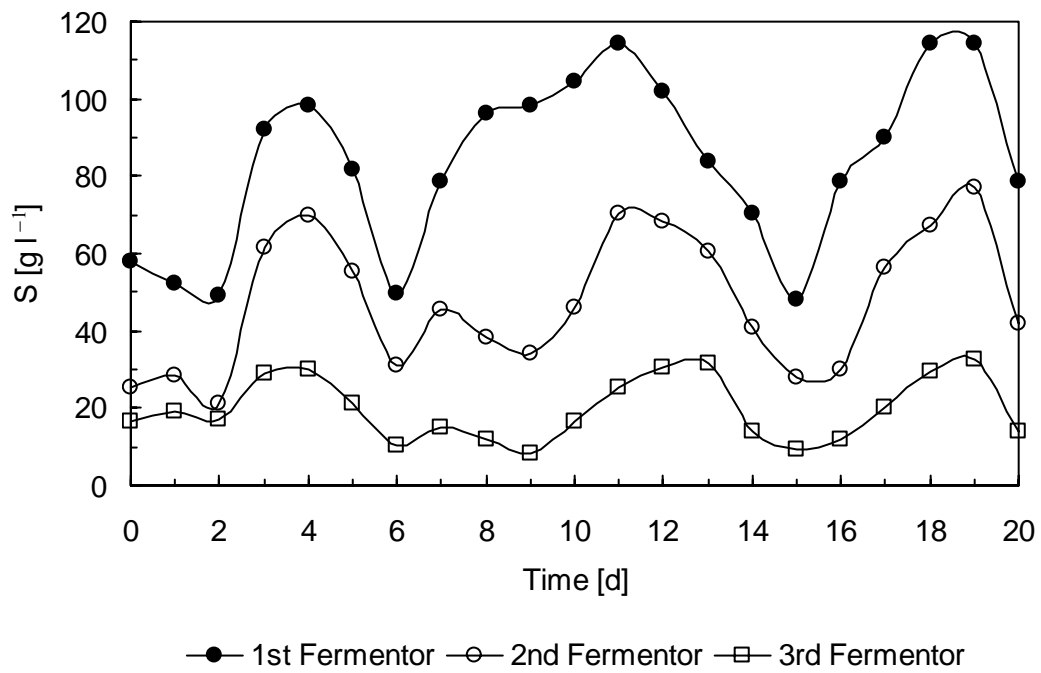


Figure 5.14 Residual sugar profiles of the SPSC fermentation system at the dilution of 0.12 h⁻¹. Initial total sugar of the hydrolysate medium: S₀ = 220 g l⁻¹.

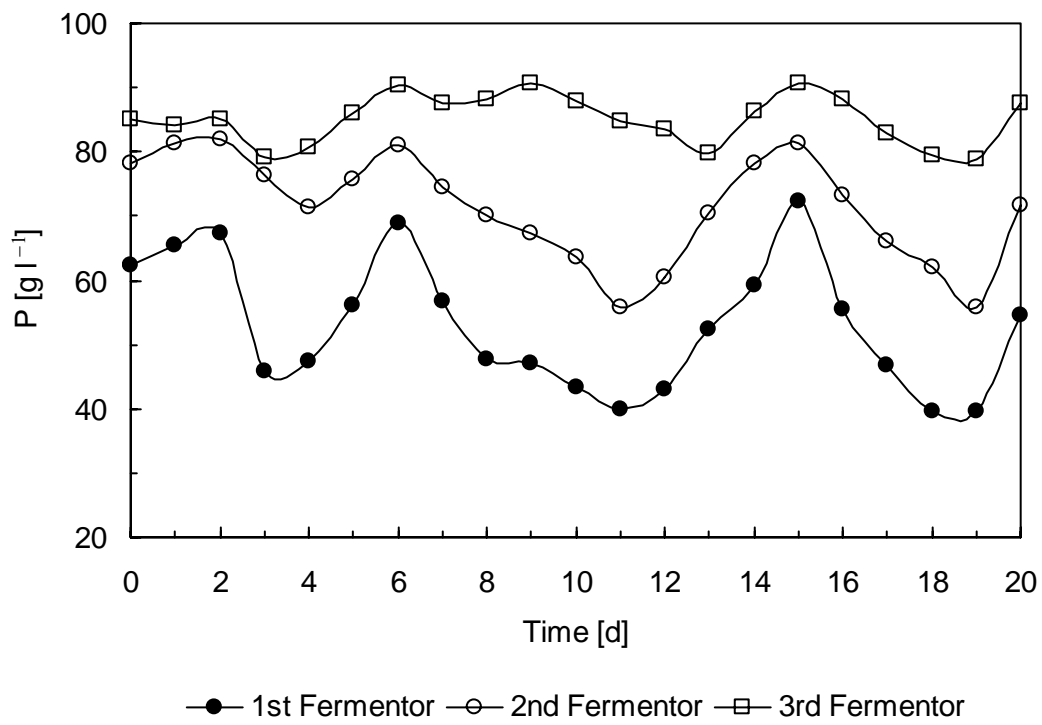


Figure 5.15 Ethanol profiles of the SPSC fermentation system at the dilution of 0.12 h^{-1} .

Initial total sugar of the hydrolysate medium: $S_0 = 220 \text{ g l}^{-1}$.

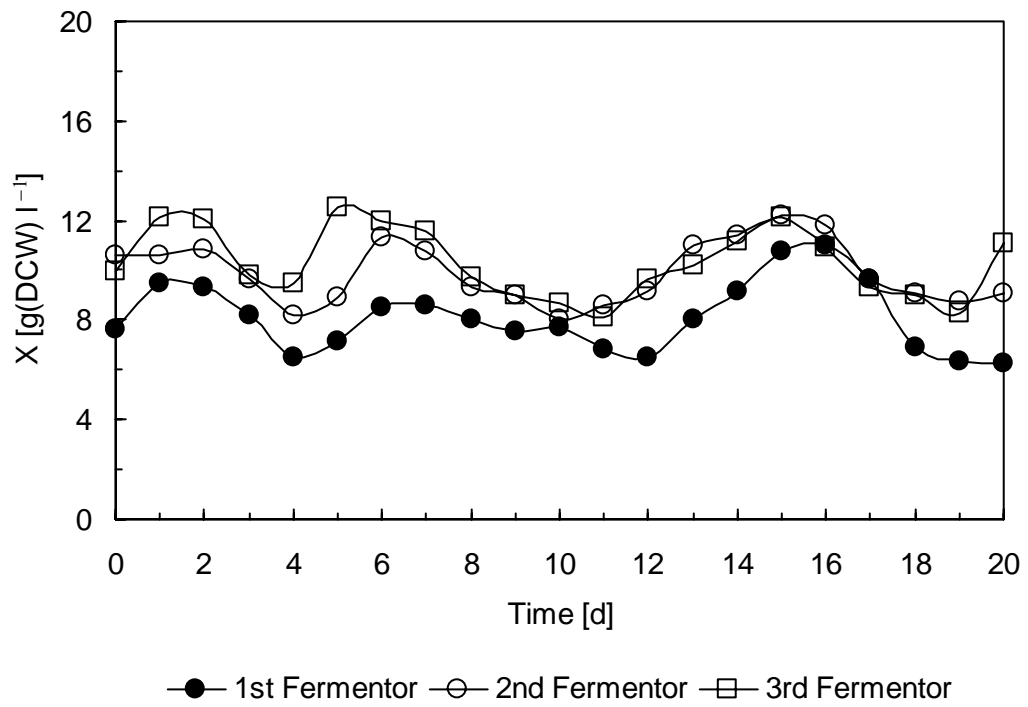


Figure 5.16 Biomass profiles of the SPSC fermentation system at the dilution of 0.12 h^{-1} .

Initial total sugar of the hydrolysate medium: $S_0 = 220 \text{ g l}^{-1}$.

Figures 5.17~5.19 illustrate the ethanol fermentation performance of this SPSC system within its whole running duration of four months, starting from the 22nd day after three weeks' system equilibrium from its first inoculation till the 119th day during which the four dilution rates: 0.05 h^{-1} , 0.10 h^{-1} , 0.15 h^{-1} , and 0.12 h^{-1} as well as the repeated dilution rate of 0.10 h^{-1} were examined.

Compared with the fermentations with *S. cerevisiae* ATCC4126 and *S. cerevisiae* 6508, the SPSC fermentation system was different. Firstly, its fermentation medium was the HG hydrolysate containing 220 g l^{-1} total sugar. Secondly, higher biomass concentrations were achieved within the three fermentors through the continuous inoculation from the seed fermentor, and thirdly, higher dilution rates were adopted.

From the mechanistic analysis: ethanol inhibition and the lag response of yeast cells to ethanol inhibition are the main reasons for the oscillations, the HG hydrolysate medium could not be the main reason for the unusual oscillatory behavior of the SPSC fermentation system, especially for those exaggerated oscillations observed at the dilution rate of 0.12 h^{-1} .

Dilution rate affects the oscillation profile of *S. cerevisiae* 6508 more significantly than *S. cerevisiae* ATCC 4126 because of their difference in ethanol tolerance. For SPSC, if the critical dilution rate of the oscillation of this tanks-in-series fermentation system was targeted among the selected four dilution rates, ranging from 0.05 h^{-1} to 0.15 h^{-1} , enhanced oscillation could happen, but the oscillation could not be so violent because the ethanol tolerance of this species was the best among the three strains with its remained viable yeast cell percentage of 30.3% after 2 hours 18% ethanol shock, making it least sensitive to the impact of a dilution rate change.

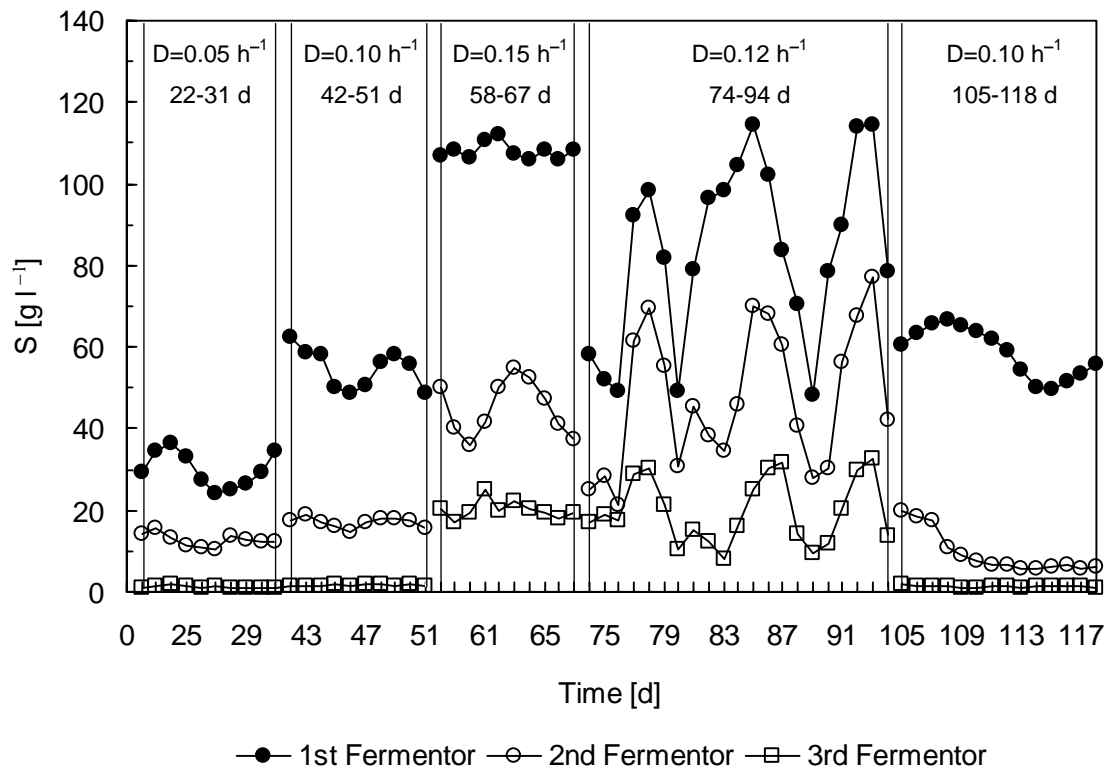


Figure 5.17 Residual sugar profiles of the SPSC fermentation system with the seed fermentor. Initial sugar in the hydrolysate medium: $S_0 = 220 \text{ g l}^{-1}$.

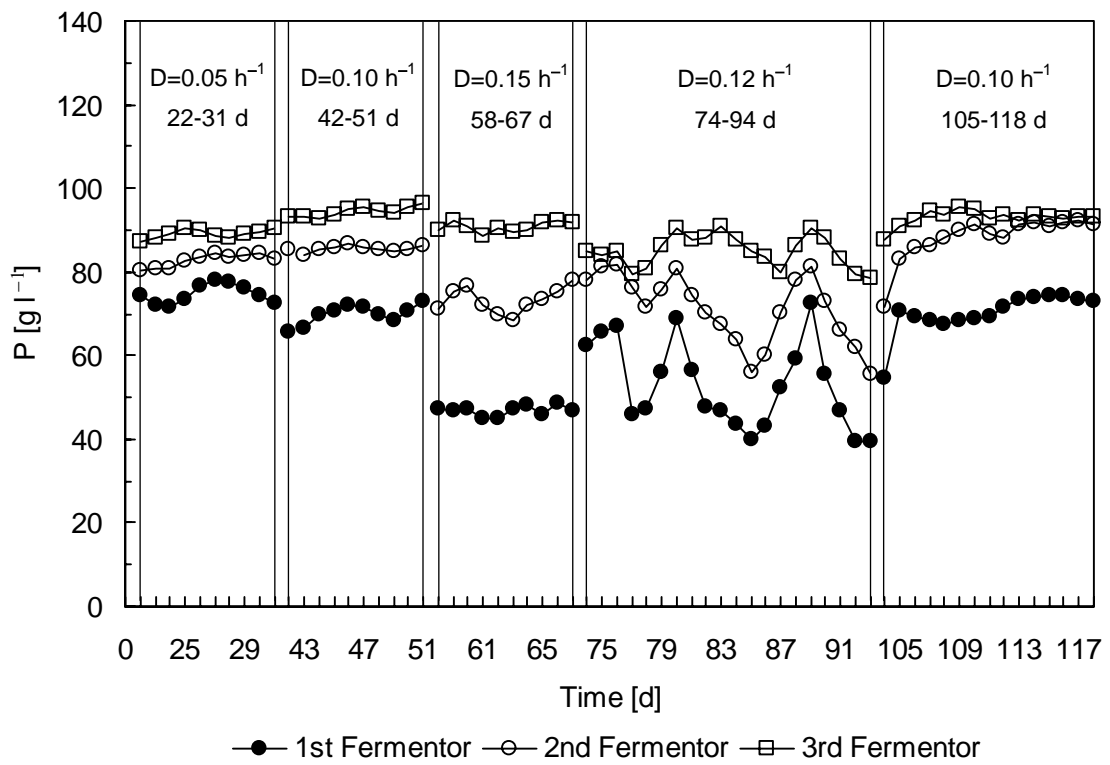


Figure 5.18 Ethanol profiles of the SPSC fermentation system with the seed fermentor.

Initial sugar in the hydrolysate medium: $S_0 = 220 \text{ g l}^{-1}$.

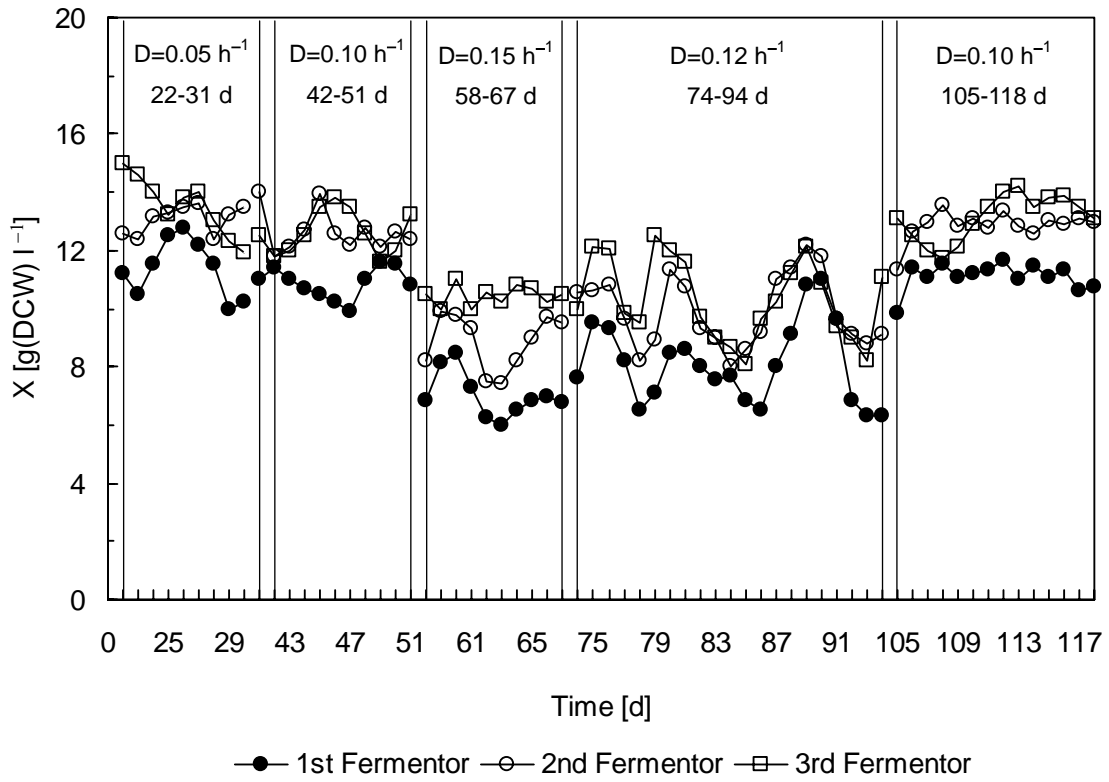


Figure 5.19 Biomass profiles of the SPSC fermentation system with the seed fermentor.

Initial sugar in the hydrolysate medium: $S_0 = 220 \text{ g l}^{-1}$.

Therefore, the seed fermentor affiliated with the fermentation system, through which much higher biomass concentrations were achieved for all three fermentors, could be the source triggering these violent oscillations. In order to validate this speculation, the seed fermentor was removed, and the same dilution rates were applied to the fermentation system. The self-balance of yeast cells could be established for each of the three fermentors during the new round continuous ethanol fermentation.

5.3.2 Continuous fermentation in the tanks-in-series system without the seed tank

The fermentation started with the dilution rate of 0.12 h^{-1} . After ten days' system equilibrium from its initial inoculation, the fermentation system was maintained for one month, and the experimental results are illustrated in Figures 5.20~5.22. It can be seen that although the fermentation system was still oscillatory, the exaggerated oscillations observed in the fermentation system with the seed fermentor were significantly damped.

For the first fermentor, the oscillation ranges of residual sugar, ethanol, and biomass were $84.0\sim 103.1 \text{ g l}^{-1}$, $53.5\sim 63.3 \text{ g l}^{-1}$, and $7.0 \sim 10.9 \text{ g(DCW) l}^{-1}$, and the corresponding absolute oscillation amplitudes were 19.1 g l^{-1} , 9.8 g l^{-1} , and $3.9 \text{ g(DCW) l}^{-1}$. The oscillation averages of residual sugar, ethanol, and biomass were 90.7 g l^{-1} , 59.9 g l^{-1} , and $8.9 \text{ g(DCW) l}^{-1}$, making the corresponding relative oscillation amplitudes be $\pm 10.5\%$, $\pm 8.2\%$, and $\pm 21.9\%$.

Table 5.1 compares the oscillation characteristics of the first fermentor with and without the seed fermentor. As can be seen, the oscillations previously observed for the fermentation system with the seed fermentor were significantly damped. The absolute oscillation amplitudes of residual sugar and ethanol decreased to 19.1 g l^{-1} and 9.8 g l^{-1} from 66.1 g l^{-1} and 32.9 g l^{-1} , while the relative oscillation amplitudes of residual sugar and ethanol decreased to $\pm 10.5 \%$ and $\pm 8.2\%$ from $\pm 39.6\%$ and $\pm 31.1\%$.

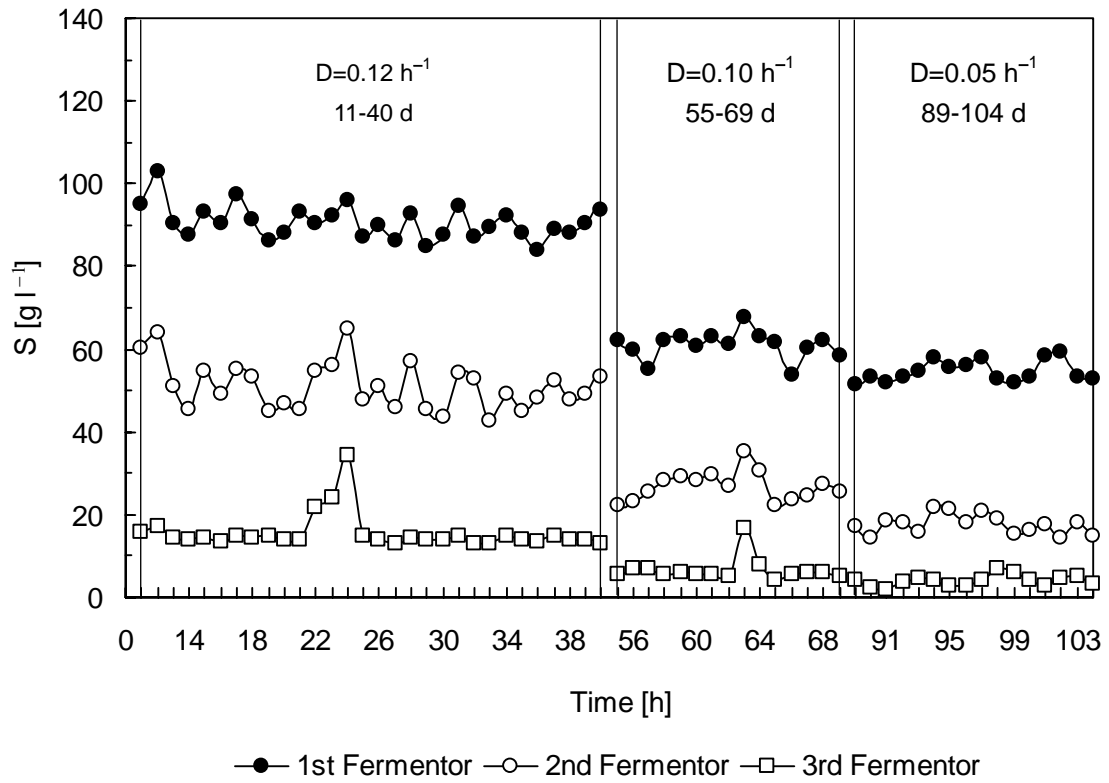


Figure 5.20 Residual sugar profiles of the SPSC fermentation system without the feed fermentor. Initial sugar in the medium: $S_0 = 220 \text{ g l}^{-1}$.

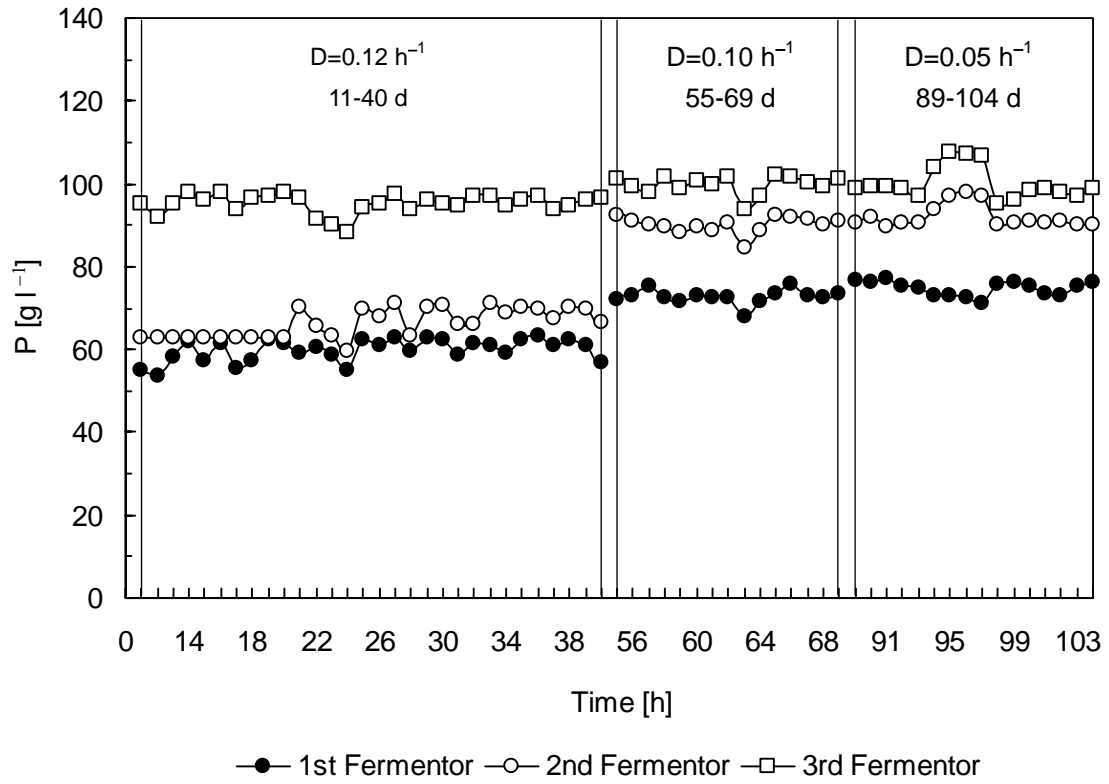


Figure 5.21 Ethanol profiles of the SPSC fermentation system without the feed fermentor.

Initial sugar in the medium: $S_0 = 220 \text{ g l}^{-1}$.

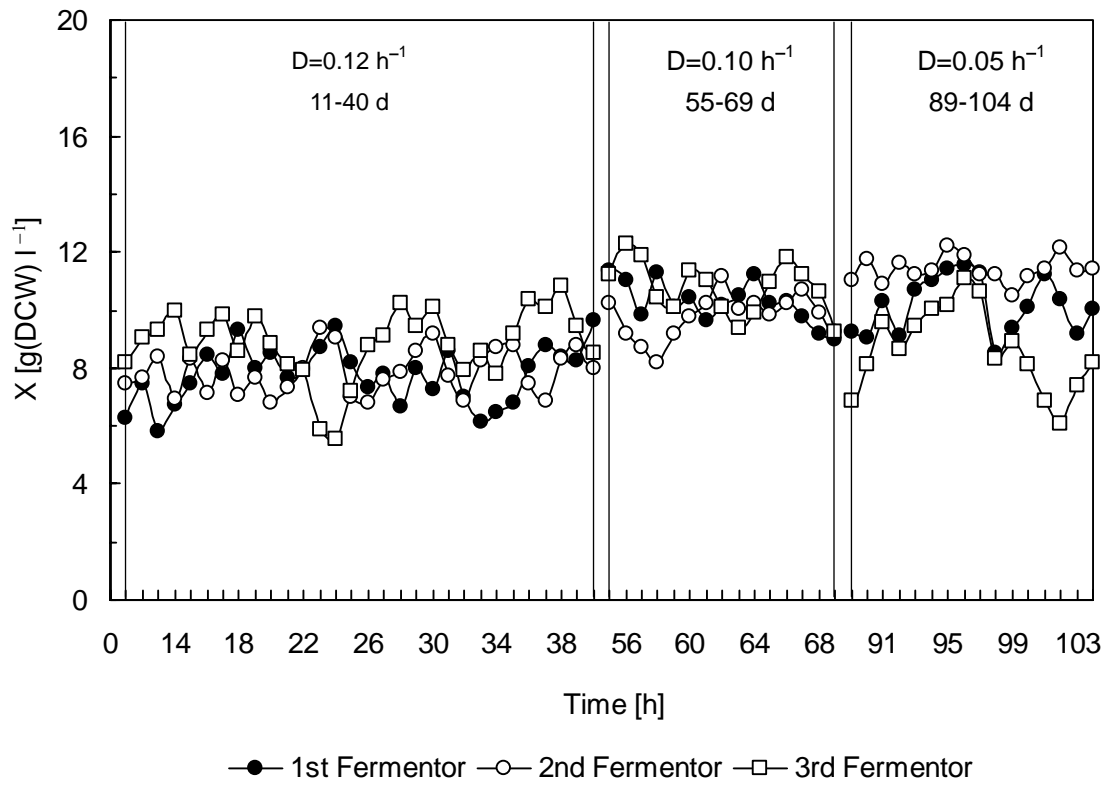


Figure 5.22 Biomass profiles of the SPSC fermentation system without the feed fermentor.

Initial sugar in the medium: $S_0 = 220 \text{ g l}^{-1}$.

Table 5.1 Comparison of the oscillation parameters of the first fermentor, $D = 0.12 \text{ h}^{-1}$

Parameters		Fermentation systems	
		with seed fermentor*	without seed fermentor
Residual sugar	Average, g l^{-1}	83.5	90.7
	Absolute amplitude, g l^{-1}	66.1	19.1
	Relative amplitude, %	± 39.6	± 10.5
Ethanol	Average, g l^{-1}	52.9	59.9
	Absolute amplitude, g l^{-1}	32.9	9.8
	Relative amplitude, %	± 31.1	± 8.2
Biomass	Average, g(DCW) l^{-1}	8.1	8.8
	Absolute amplitude, g(DCW) l^{-1}	4.7	5.4
	Relative amplitude, %	± 29.0	± 21.9

* The sugar in the mixture of the fermentation medium and the seed culture feeding into the first fermentor was calculated to be 207 g l^{-1} when the seed medium containing 120 g l^{-1} sugar was fed into the seed fermentor at the dilution rate of 0.17 h^{-1} , while the fermentation medium containing 220 g l^{-1} sugar was fed into the first fermentor after the seed fermentor was removed.

The analytical error of the biomass measurement for SPSC was much larger than that for *S. cerevisiae* ATCC 4126 and *S. cerevisiae* 6508 because of the self-flocculating of this strain, which facilitated sedimentation of the yeast cells and significantly affected the sampling accuracy for its biomass measurement. For *S. cerevisiae* ATCC 4126 and *S. cerevisiae* 6508, the analytical error of their yeast cell biomass measurement was validated to be less than 5%, but as high as 15% analytical error was observed for SPSC. Therefore, that the damping in the biomass oscillation was not significant as those in residual sugar and ethanol might be caused by a large analytical error for the biomass measurement.

The process states of another two dilution rates, 0.10 h^{-1} and 0.05 h^{-1} , were further re-examined after the fermentation system experienced 15 and 20 days' transition periods after the corresponding dilution rate adjustments. The oscillatory behaviors previously observed for the fermentation system with the seed fermentor were also damped to some extent. These experimental results indicated the seed fermentor was the source of the oscillation amplification.

The reason for the oscillation amplification of the seed fermentor could be the role of the seed fermentor in inoculating the fermentation system with healthy seed culture, and correspondingly generating two cell populations within the fermentation system: the newly inoculated cells and the cells previously existed and already adapted to the fermentation system. At a specific dilution rate range, the synchronization of the growth rhythms of these two cell populations, similar to that of the mother and daughter cells that was speculated for the impact of dilution rate on the oscillation profiles of *S. cerevisiae* ATCC 4126 and *S. cerevisiae* 6508 in Chapter 4, could occur and enhance the oscillation triggered by ethanol inhibition and the lag response of yeast cells to ethanol inhibition. Much higher biomass concentrations achieved within the three fermentors of the SPSC fermentation system increased the probability of this kind of synchronization of the two cell populations.

Although the seed fermentor amplified the oscillation of the SPSC fermentation system, its role in improving the sugar conversion under strong ethanol inhibition by continuously providing a healthy seed culture to the fermentation system was very significant. At the dilution rates of 0.10 h^{-1} and 0.05 h^{-1} , the average residual sugar concentrations in the final effluent increased to 6.5 g l^{-1} and 4.0 g l^{-1} after the seed fermentor was removed, comparing with the average residual sugar concentrations as low as only 1.6 g l^{-1} and 1.1 g l^{-1} when the seed fermentor was incorporated. Therefore, a seed culture system is necessary in the industry to achieve complete sugar conversion, which is the prerequisite to achieve high ethanol yield and save the cost of raw material consumption.

In fact, the oscillations of residual sugar, ethanol, and biomass do exist in the industry, especially in those front or middle fermentors of the cascade fermentation systems, but these oscillations are assumed to be caused by the fluctuations of the operating parameters such as sugar concentration, medium flowrate, temperature, pH, and so on, although the computerized control system that is widely used in the industry has actually controlled these operating parameters very precisely, ultimately eliminating their disturbances on the fermentation process. Our experimental results and analysis for the reasons triggering these oscillations could be meaningful to reevaluate the process state of continuous ethanol fermentation.

On the other hand, an average fermentation time as long as 40-60 hours is currently required for fermenting the medium containing sugar of 16-22% (w/v) and achieving the ethanol concentration of 10-13% (v/v). Such a long fermentation time effectively damps the oscillation that is occurring in the front or middle fermentors of a cascade fermentation system, and quasi-steady state can be achieved for the final effluent from the last fermentor. Without doubt, the productivity of such an ethanol fermentation system has been significantly compromised, and more effective oscillation attenuation strategies need to be developed.

5.4 Conclusions

Four dilution rates: 0.05, 0.10, 0.15, and 0.12 h^{-1} were selected to study the oscillatory behavior of the continuous ethanol fermentation with the self-flocculating yeast strain SPSC in the simulated tanks-in-series bioreactor system. The experimental results illustrated that oscillations triggered by ethanol inhibition and the lag response of yeast cells to ethanol inhibition also occurred.

Amplified oscillations were observed at the dilution rate of 0.12 h^{-1} , and the reason was speculated to be due to the continuous inoculation from the seed fermentor to the fermentation system, through two yeast cell populations: the newly inoculated seed cultures and the yeast cells already existing within the fermentors and adapted to the fermentation environment, and the synchronization of the two different yeast cell populations that could occur and enhance the oscillations triggered by ethanol inhibition and the lag response of yeast cells to ethanol inhibition. This mechanistic speculation was validated by removing the seed fermentor from the fermentation system and the corresponding damping of the exaggerated oscillations.

The oscillations increased the residual sugar in the final effluent, decreased the ethanol yield that was calculated based on the sugar fed into the fermentation system without the deduction of the residual, and negatively affected the ethanol fermentation performance of the fermentation system. Therefore, attenuation strategies should be developed.

Chapter 6

Oscillation Attenuation Strategies and Mechanisms

A manuscript has been prepared for submission based on the work presented in this chapter.

6.1 Introduction

Chapter 5 demonstrated that oscillations decreased the ethanol productivity of the SPSC fermentation system. On the other hand, as discussed in the Chapter 1, the cost from raw material consumption could be as high as 60% of the total production cost for the fuel ethanol from starch materials and therefore, the residual sugar concentration at the end of fermentation is strictly controlled at an extremely low level of 0.1~0.2 % (w/v) in the industry, guaranteeing a sugar conversion of more than 99.0% for the medium with an initial total sugar concentration of 22.0% (w/v) and correspondingly, an ethanol yield of more than 90% of its theoretical sugar-to-ethanol value, 0.511. The studies in Chapter 3 also illustrated that oscillations occurring in the continuous ethanol fermentation increased the residual sugar concentration, which definitely decreased the ethanol yield that is calculated based on the total sugar fed into the fermentation system, without deduction of the residual sugar.

Although oscillations have not been reported for industrial plants, an average fermentation time as long as 60 hours is required to the ferment medium containing sugar of no more than 22.0% (w/v) in order to achieve the designated residual sugar concentration, which effectively attenuates the oscillations that are happening within the front and middle tanks in the tanks-in-series fermentation systems, as discussed in Chapter 5. This extended

fermentation time sacrifices the ethanol productivity of the fermentation systems as well as increases the probability of contamination. Without doubt, new strategies that can more effectively attenuate these oscillations should be developed.

In Chapter 3, the oscillations of the bioreactor system were attenuated after the tubular bioreactors were packed with the Intalox ceramic saddles, and the mechanisms were speculated to be related to the backmixing alleviation for the packed tubular bioreactors as well as the yeast cell immobilization in the packing. In this chapter, the backmixing performance of this bioreactor system and the impact of yeast cell immobilization on oscillation attenuation were experimentally studied to validate these mechanistic speculations.

6.2 Materials and Methods

6.2.1 Strain, Medium, and Pre-culture

Microorganism, medium, and pre-culture were described in Section 3.2.

6.2.2 Packing selection

As yeast cell immobilization was speculated to be one of the mechanisms for the oscillation attenuation achieved in the tubular bioreactors packed with the Intalox ceramic saddles, the main consideration for selecting packings to experimentally validate this mechanistic speculation was their difference in immobilizing yeast cells. In addition to the Intalox ceramic saddles, 10×10×10 mm polyurethane particles, 5 × 5 ×10 mm wood chips, and $\phi 10 \times 10$ mm Raschig rings made of 80 mesh stainless steel wire mesh were selected.

The polyurethane particles, with good porosity and high specific surface area, immobilized yeast cells by adsorption and entrapment, and yeast cells could be adsorbed onto the inner

surface as well as entrapped into the inside space of the pores, achieving very high cell density. The wood chips immobilized yeast cells mainly by surface adsorption, and a moderate yeast cell immobilization effect was expected. On the other hand, as the Intalox ceramic saddles immobilized yeast cells in the same mechanism as the wood chips, the oscillation attenuation achieved by the Intalox ceramic saddles should be reproducible in the wood chips if the oscillation attenuation was caused by a specific yeast cell immobilization mechanism. The Raschig rings with a smooth surface were not expected to immobilize yeast cells very well.

6.2.3 Bioreactor system

The same bioreactor system as illustrated in Figure 3.1 was used. The working volumes of the tubular bioreactors were measured to be 400, 410, 420 ml when packed with the polyurethane particles; 320, 330, 340 ml when packed with the wood chips; 580, 590, and 600 ml when packed with the Raschig rings. The inoculation procedures of these packed tubular bioreactors were the same as those applied to the tubular bioreactors backed with the Intalox ceramic saddles, which were described in Section 3.2.2.

In order to measure the concentrations of residual glucose, ethanol, and biomass along the axial directions of the tubular bioreactors and evaluate their mixing performance, two sampling sections were designated equally along their axial directions, and stainless steel sample tubes ($\phi 2.6 \times 0.3 \text{ mm}$) were inserted into each tubular bioreactor from its top, approaching two sampling sections, respectively, as illustrated in Figure 6.1.

The samples were taken through a peristaltic pump, and the sampling flowrate was controlled to be lower than the flowrate of the medium feeding into the system. The concentration gradients across the radial directions of the tubular bioreactors were considered to be negligible because the ratio of the height to diameter of the tubular bioreactors was as high as 20.

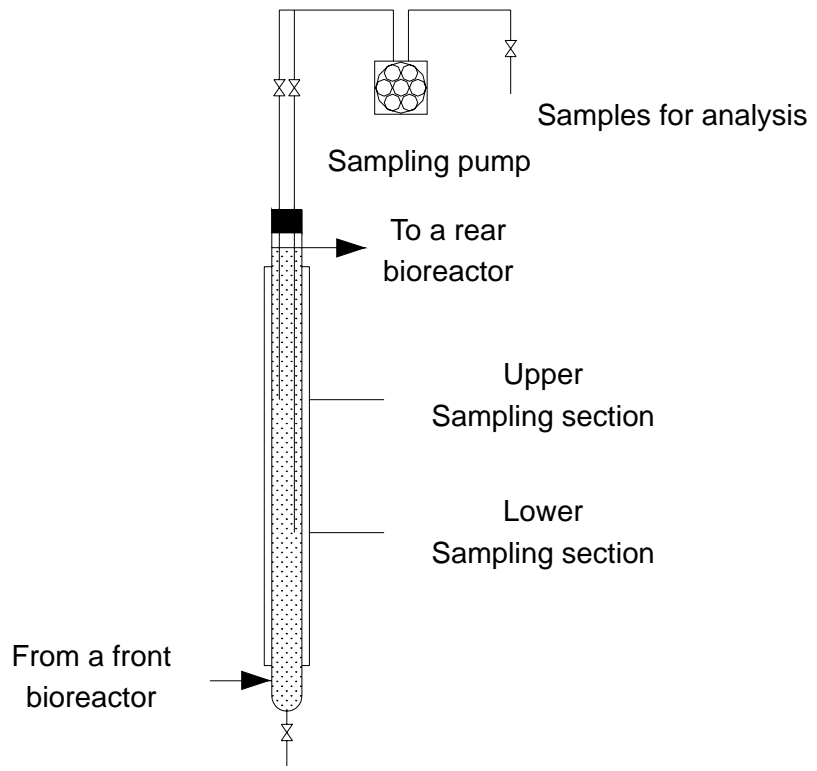


Figure 6.1 Sampling diagram along the axial direction of a tubular bioreactor.

6.2.4 Analytical methods

6.2.4.1 Glucose, ethanol and biomass analysis

The analysis for glucose, ethanol, and biomass were described in Sections 3.2.3 and 4.2.3.

6.2.4.2 RTD analysis

Residence time distribution (RTD) was measured for the bioreactor system in order to evaluate its mixing performance because of the difficulties of sampling the packed tubular bioreactors along their axial directions. Xylose, which *S. cerevisiae* species cannot metabolize, was selected as a tracer and added into the medium at the concentration of 20 g l⁻¹ for the RTD analysis. Xylose was analyzed by HPLC (Waters™600 Controller and Waters™ 600 Pump; Detector: Waters 410 Differential Refractometer; Column: Aminex® HPX-87H, 300×7.8mm; Eluant: 0.005 mol l⁻¹ H₂SO₄, flow rate: 0.4ml min⁻¹; Data treatment software: Waters Millennium 32).

6.2.4.3 Evaluation of yeast cell immobilization effect

Yeast cells immobilized onto the surface of the wood chips, the Intalox ceramic saddles, and the Raschig rings were washed off, collected, and measured at the end of the experiments. The polyurethane particles were dried and balanced before they were packed into the tubular bioreactors, and re-dried and re-balanced after washing. It was assumed that residual sugar and other soluble components were completely washed out so that the yeast cells retained could be estimated by the net mass increase. After these treatments, the total yeast cell concentrations within the tubular bioreactors were evaluated.

6.2.4.4 Variability analysis of immobilized yeast cells

Yeast cell variability was analyzed immediately after the cells were collected. The method was described in Section 3.2.3.

6.3 Results and Discussion

6.3.1 Mixing performance of the empty columns

For the bioreactor system illustrated in Figure 3.1, the substrate inhibition from the VHG medium was effectively alleviated because of the well-mixed performance of the CSTR in which the VHG medium was diluted immediately after it was fed into the bioreactor. The ethanol inhibition could also be mitigated as the fermented broth went through the tubular bioreactors if the mixing performance of these tubular bioreactors was significantly deviated from CSTR and close to a PFR model. From the point view of ethanol fermentation kinetics, such a bioreactor system should be suitable for continuous VHG ethanol fermentation and good ethanol fermentation performance should be achieved.

On the other hand, ethanol inhibition and the lag response of yeast cells to ethanol inhibition were confirmed to be the mechanistic reasons for the oscillations observed for the CSTR, and the lethal effect of high concentration ethanol on yeast cells was for the exaggerated oscillations of the tubular bioreactors. The oscillations of the CSTR should be effectively attenuated if the mixing performance of the tubular bioreactors significantly were deviated from a CSTR mode and effective ethanol concentration gradients developed within these tubular bioreactors.

In order to further validate these speculations, the concentrations of residual glucose, ethanol, and biomass were measured along the axial directions of these tubular bioreactors, and the experimental results are illustrated in Figures 6.2~6.4. It can be seen that the axial concentration gradients for residual glucose and ethanol could not be established within the tubular bioreactors because no significant concentration differences between the two sampling sections were observed for both residual glucose and ethanol, indicating the effect of ethanol inhibition alleviation initially assumed for these tubular bioreactors could not be achieved.

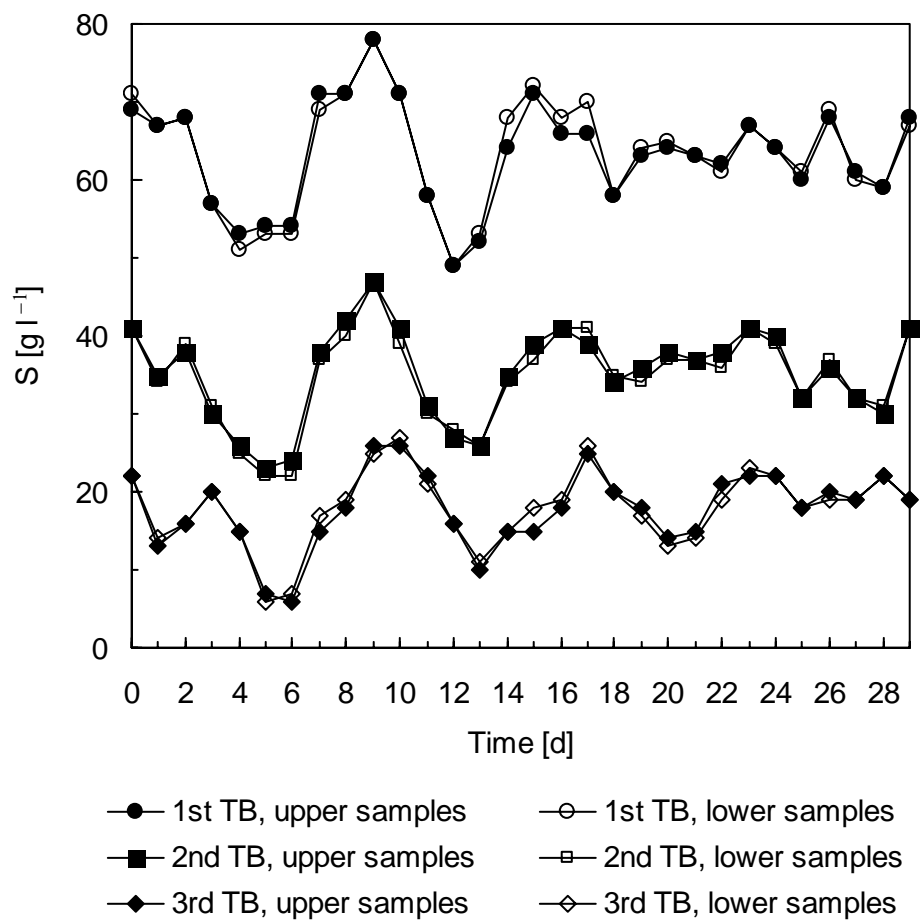


Figure 6.2 Residual glucose concentrations along the axial directions of the tubular bioreactors. The VHGM medium containing 280 g l^{-1} glucose was fed into the CSTR at the dilution rate of 0.027 h^{-1} .

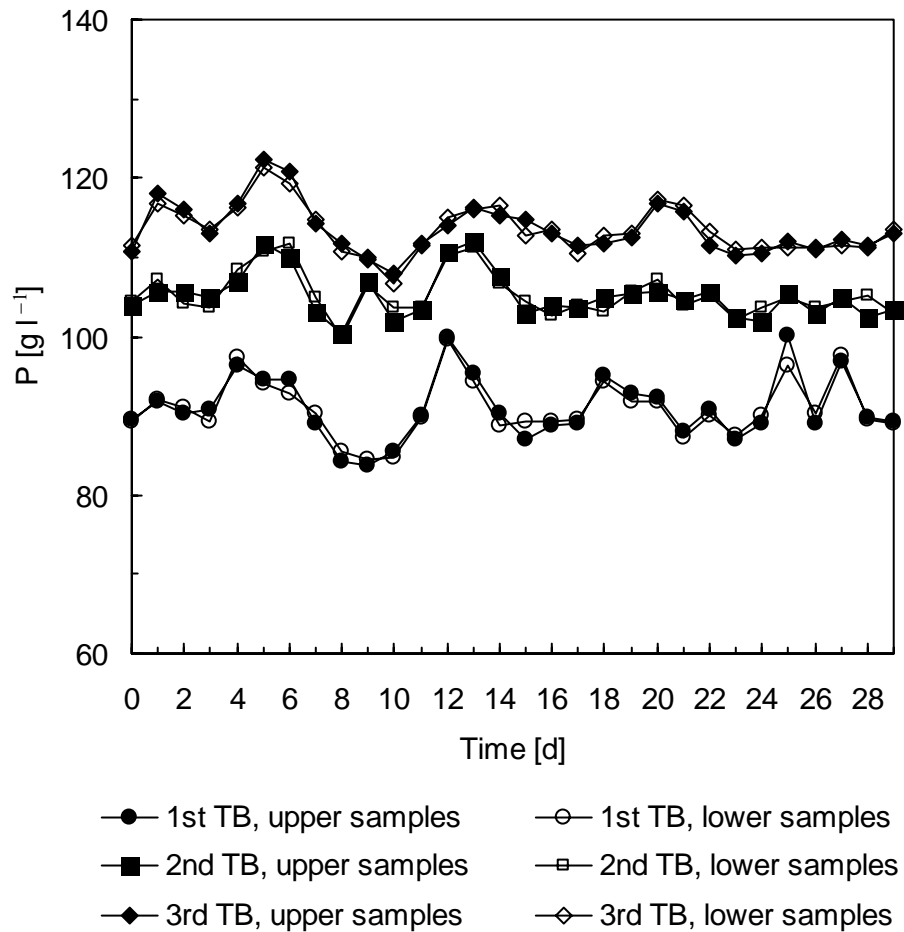


Figure 6.3 Ethanol concentrations along the axial directions of the tubular bioreactors. The VHG medium containing 280 g l^{-1} glucose was fed into the CSTR at the dilution rate of 0.027 h^{-1} .

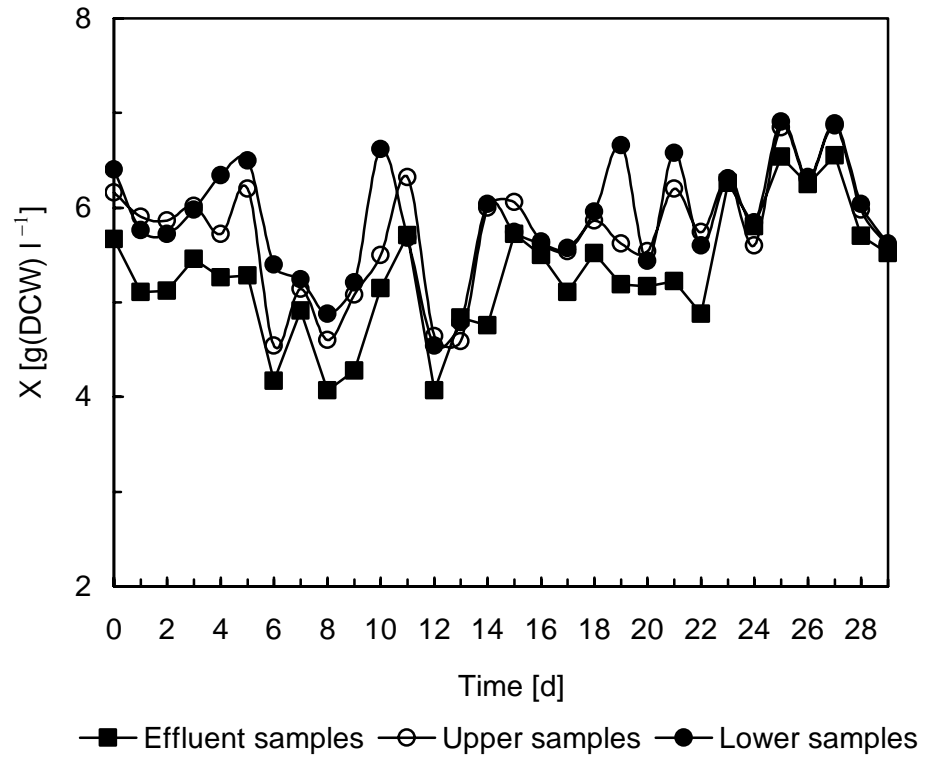


Figure 6.4 Biomass concentrations along the axial direction of the first tubular bioreactor.

The VHG medium containing 280 g l⁻¹ glucose was fed into the CSTR at the dilution rate of 0.027 h⁻¹.

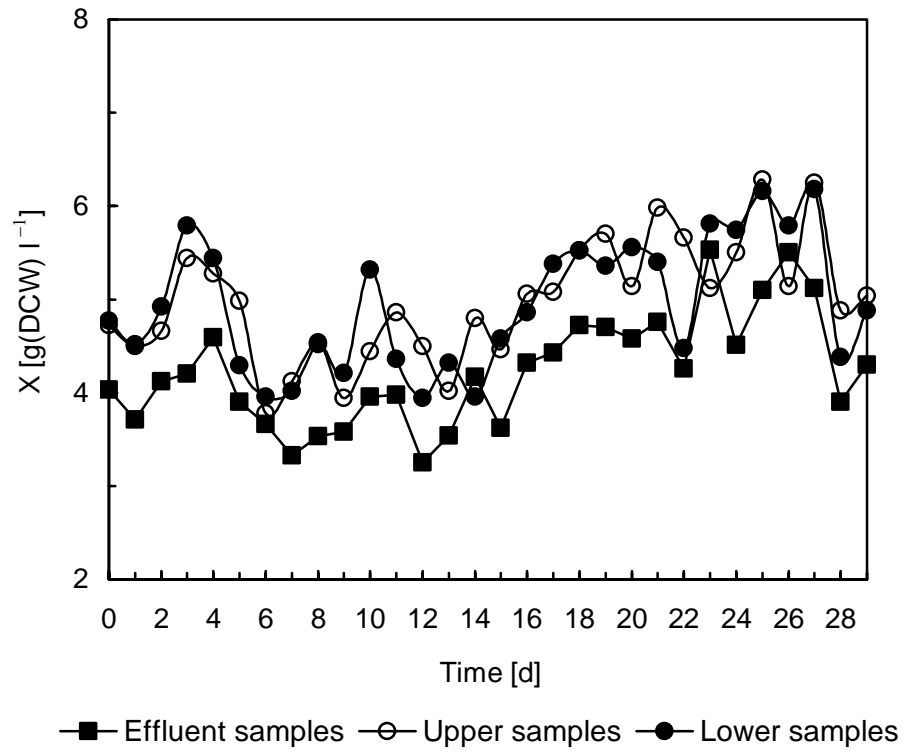


Figure 6.5 Biomass concentrations along the axial direction of the second tubular bioreactor.

The VHG medium containing 280 g l^{-1} glucose was fed into the CSTR at the dilution rate of 0.027 h^{-1} .

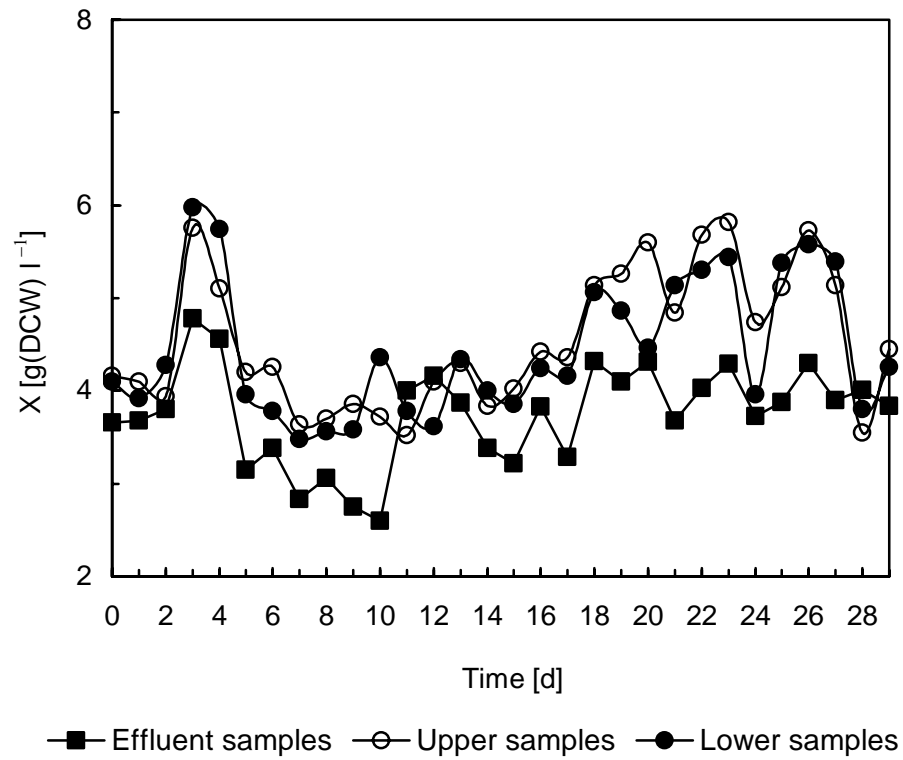


Figure 6.6 Biomass concentrations along the axial direction of the third tubular bioreactor.

The VHG medium containing 280 g l^{-1} glucose was fed into the CSTR at the dilution rate of 0.027 h^{-1} .

The reasons were analyzed to be: 1) given the average working volume of 600 ml for the tubular bioreactors and the medium flowrate of 40 ml h⁻¹ at the dilution rate of 0.027 h⁻¹ for the CSTR, the average residence time of the tubular bioreactors was about 15 hours, too long to counteract the backmixing of ethanol and glucose caused by their molecular diffusions; 2) CO₂ produced within the first tubular bioreactor during the fermentation as well as the aeration of the second and third tubular bioreactors to prevent yeast cells from settling further worsened the backmixing of these tubular bioreactors.

The biomass gradient was observed through direct observations as well as the measurements of the biomass concentrations along the axial directions of the tubular bioreactors, as illustrated in Figures 6.4~6.6, because the mixing provided by CO₂ within the first tubular bioreactor and the aeration at a rate of 0.005 vvm for the second and third tubular bioreactors was not enough to suspend the yeast cells uniformly.

Although the biomass gradient existed within the tubular bioreactors, its impact on the residual glucose conversion and ethanol production was negligible, that is, the biomass gradient did not correspondingly generate concentration gradients for residual glucose and ethanol. This could be explained by: 1) the biomass gradient within the tubular bioreactors was dynamic because of the disturbance from CO₂ produced during the fermentation for the first tubular bioreactor and the aeration for the second and third tubular bioreactors; and 2) the viability of the yeast cells within the tubular bioreactors was very low because of the lethal effect of high ethanol concentration, especially on the yeast cells within the second and third tubular bioreactors, making the fermentation rates too low to build up the concentration gradients for residual glucose and ethanol under the conditions of relatively rapid molecular diffusions, which was supported by the previous research involving the evaluation of yeast cell lysis and viability loss for the tubular bioreactors (Bai et al., 2004b).

6.3.2 Exploration of attenuation mechanisms

Although the packing occupied volume in the tubular bioreactors, decreased their effective working volume, and shortened their average fermentation time, the fermentation performance was improved after they were packed with the Intalox ceramic saddles, and the oscillations were significantly attenuated, as illustrated in Figures 3.9~3.11. Exploring the corresponding mechanisms could help develop more effective strategies to attenuate the oscillations which are happening in continuous ethanol fermentations in the industry, but are currently attenuated by the extension of average fermentation time.

The packing could exert the following impacts: 1) partitioning the tubular bioreactors into small reaction chambers and affecting their mixing performance; 2) immobilizing yeast cells as the yeast cells deposited onto the surface of the packing were retained within those small chambers; and 3) shifting the dilution rate of the tubular bioreactors when the same medium flow rate was applied to the bioreactor system.

6.3.2.1 Impact of the packing on the backmixing of the tubular bioreactors

After the tubular bioreactors were packed, the sampling tubes could not be positioned precisely at the sampling points as previously done for the empty columns, and samples could not be collected along the axial directions of the tubular bioreactors to evaluate their mixing performance directly. Therefore, the RTD of the bioreactor system was measured by applying the step-input-response technique using xylose as a tracer, which was added into the medium feeding into the tank at a concentration of 20 g l^{-1} .

Figures 6.7~6.10 show the normalized xylose concentration responses in the effluents from each bioreactor, i.e., the F curves, through which the variances of the RTDs were calculated to be 0.95 for the tank, 0.64 for the tank and first packed tubular bioreactor, 0.52 for the tank, the first and second packed tubular bioreactor, and 0.33 for the whole bioreactor system.

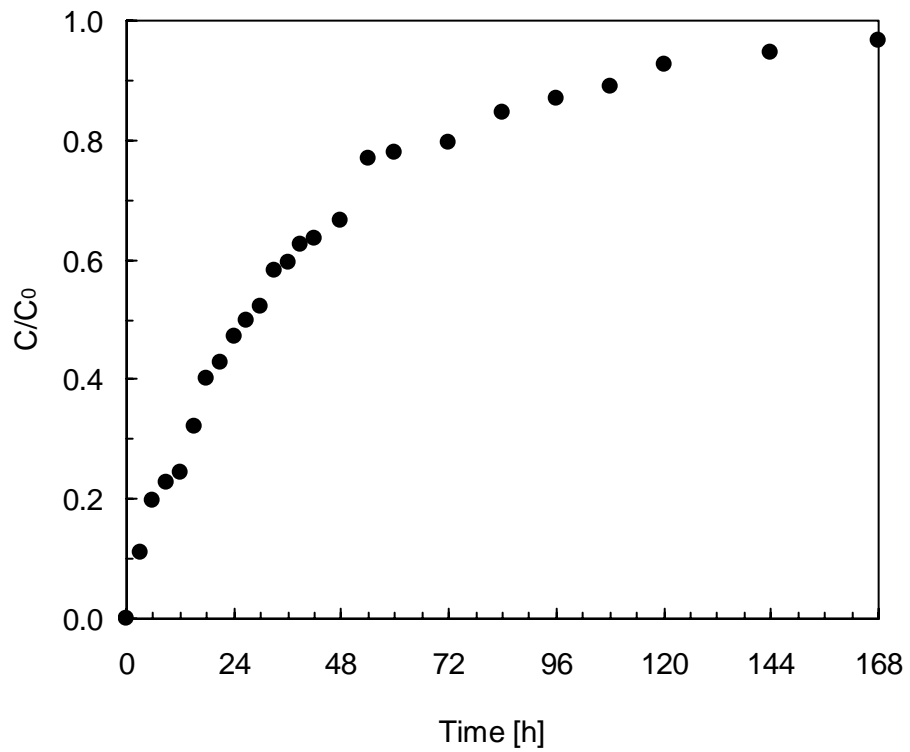


Figure 6.7 Response of the tank to the step input. Xylose was used as a tracer and added into the VHG medium at a concentration of 20 g l^{-1} . The VHG medium containing 280 g l^{-1} glucose was fed into the tank fermentor at the dilution rate of 0.027 h^{-1} .

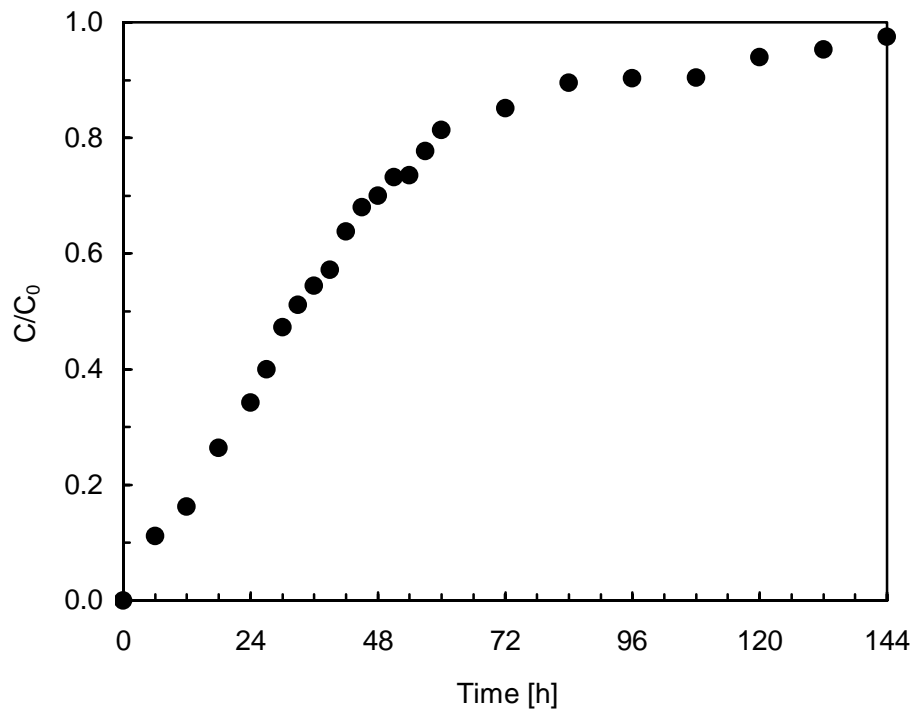


Figure 6.8 Response of the tank and first tubular bioreactor to the step input. Xylose was used as a tracer and added into the VHG medium at a concentration of 20 g l^{-1} . The VHG medium containing 280 g l^{-1} glucose was fed into the tank fermentor at the dilution rate of 0.027 h^{-1} .

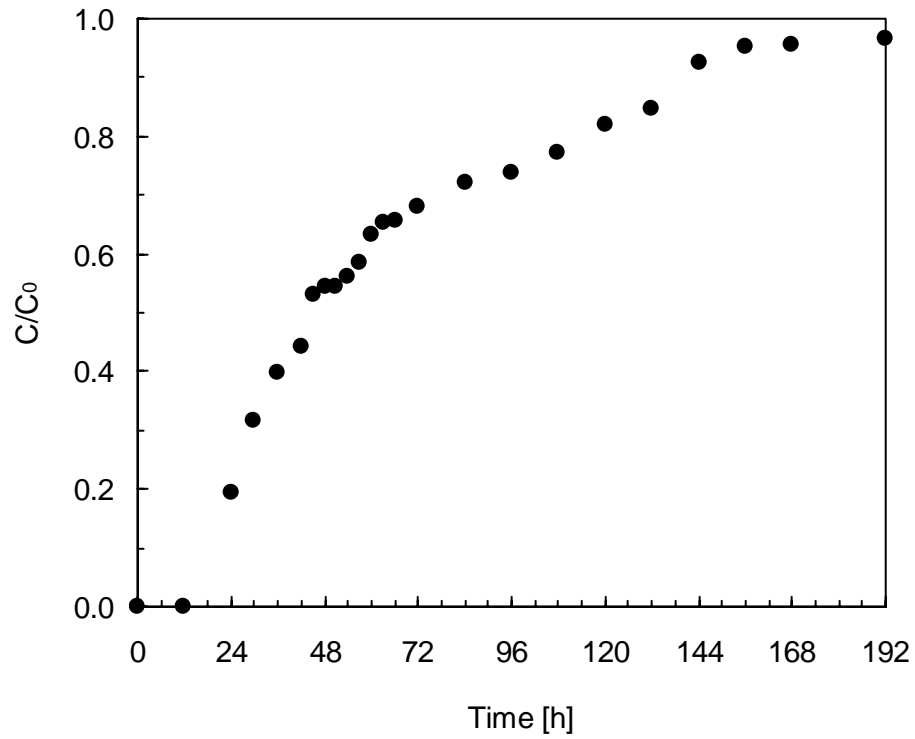


Figure 6.9 Response of the tank, first and second tubular bioreactors to the step input. Xylose was used as a tracer and added into the VHG medium at a concentration of 20 g l^{-1} . The VHG medium containing 280 g l^{-1} glucose was fed into the tank fermentor at the dilution rate of 0.027 h^{-1} .

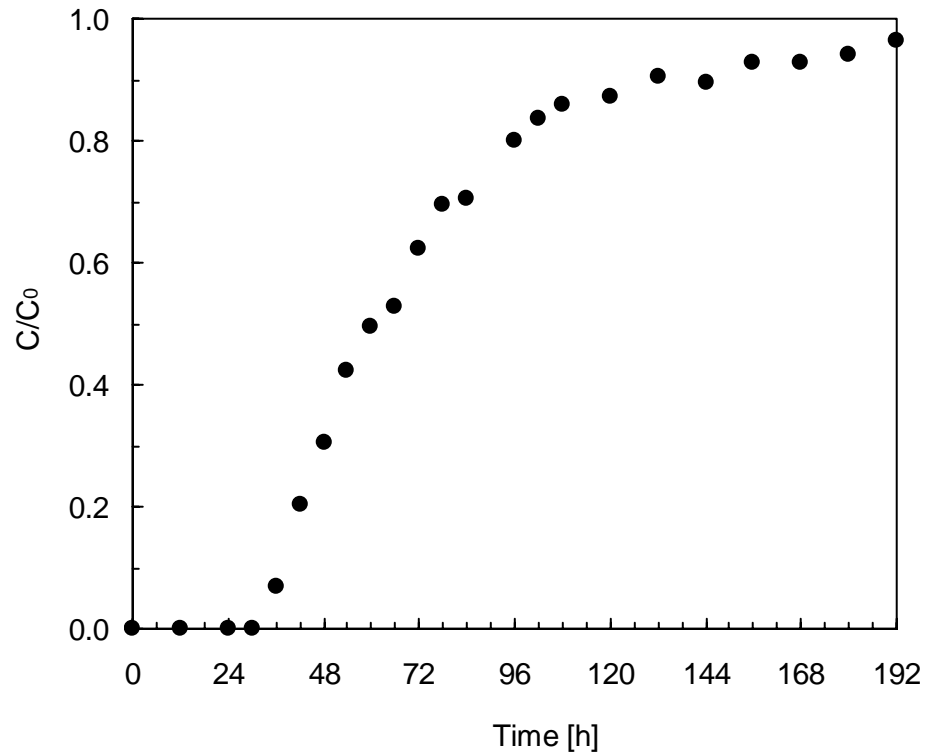


Figure 6.10 Response of the whole bioreactor system to the step input. Xylose was used as a tracer and added into the VHG medium at a concentration of 20 g l^{-1} . The VHG medium containing 280 g l^{-1} glucose was fed into the tank fermentor at the dilution rate of 0.027 h^{-1} .

The variance of the RTD for an ideal CSTR is 1.0. The variance of the RTD for the tank fermentor was measured to be 0.95, very close to that of an ideal CSTR. Thus, the tank fermentor could be treated as an ideal CSTR.

If the packed tubular bioreactors were assumed to be CSTRs, the variances of the RTDs were calculated to be 0.70 for the combined tank and first packed tubular bioreactor, 0.55 for the tank, first and second packed tubular bioreactors, and 0.46 for the whole bioreactor system, including the tank and three packed tubular bioreactors. The experimentally measured variances were 0.64, 0.52, and 0.33, respectively, very close to these theoretical predictions, indicating the mixing performance of the packed tubular bioreactors was close to a CSTR model and the concentration gradients for residual glucose and ethanol still could not be built up within these packed tubular bioreactors. Therefore, the improvement of their ethanol fermentation performance and the attenuation of their oscillatory behaviors were not from the impact of the packing on the mixing performance of the tubular bioreactors. In fact, an average residence time around 10 hours was still too long to build up the concentration gradients for the residual glucose and ethanol along the axial directions of these tubular bioreactors because the molecular diffusions of glucose and ethanol overtook the potential impact of the packing on the mixing performance of the tubular bioreactors by partitioning them into countless small reaction chambers.

6.3.3.2 Yeast cell immobilization and its impact on oscillation attenuation

When the tubular bioreactors were packed, yeast cells deposited onto the packing surface could be retained and immobilized within the small chambers created by the packing. In order to evaluate the impact of the potential yeast cell immobilization on the fermentation performance, the biomass concentrations in the effluents from the packed bioreactors were measured and compared with the biomass concentrations measured in the effluents from the empty columns. The experimental results are illustrated in Figures 6.11~6.13.

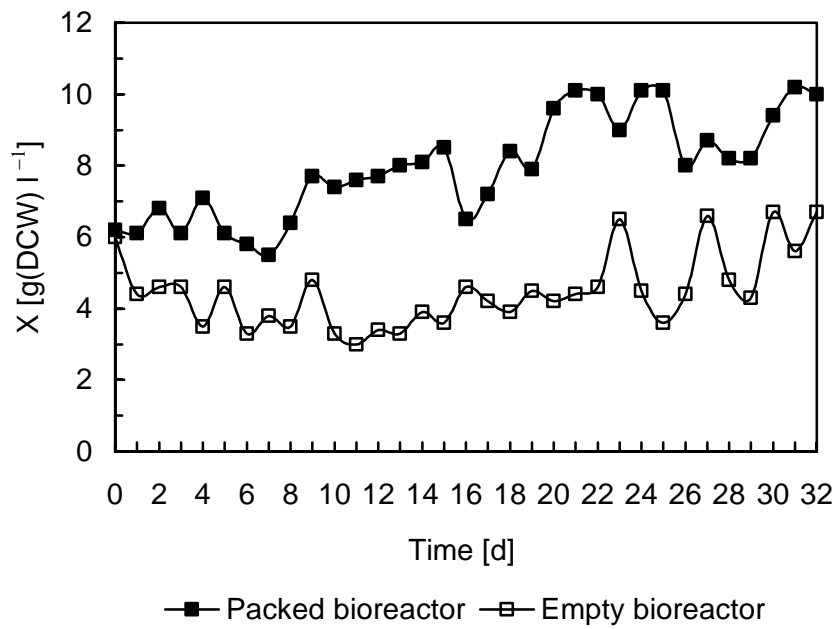


Figure 6.11 Biomass in the effluent from the first tubular bioreactor before and after it was packed with the Intalox ceramic saddles. The VHGM medium containing 280 g l⁻¹ glucose was fed into the tank at a dilution rate of 0.027 h⁻¹.

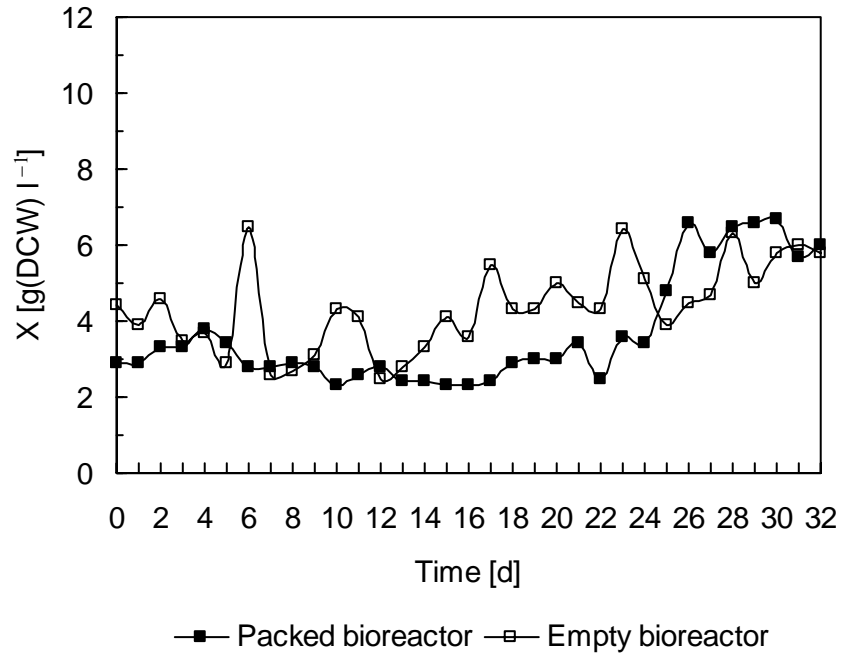


Figure 6.12 Biomass in the effluent from the second tubular bioreactor before and after it was packed with the Intalox ceramic saddles. The VHG medium containing 280 g l⁻¹ glucose was fed into the tank at a dilution rate of 0.027 h⁻¹.

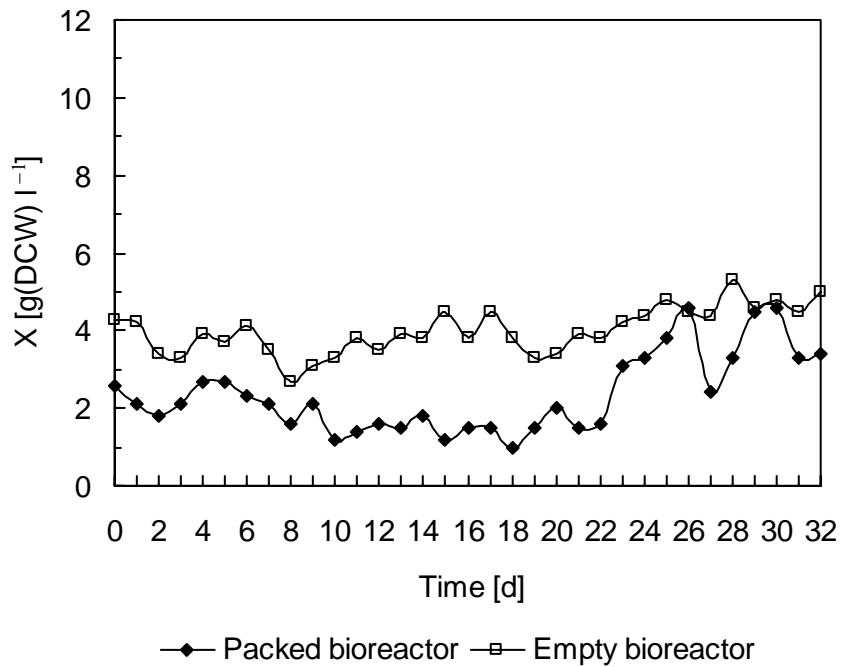


Figure 6.13 Biomass in the effluent from the third tubular bioreactor before and after it was packed with the Intalox ceramic saddles. The VHG medium containing 280 g l^{-1} glucose was fed into the tank at a dilution rate of 0.027 h^{-1} .

Figure 6.11 shows that the biomass concentration in the effluent of the first tubular bioreactor was higher after it was packed, indicating the growth of yeast cells was improved, through which more ethanol was produced, the fermentation performance of the bioreactor was improved, and the oscillatory behavior of the bioreactor was damped. At the end of the operation, the broth within the bioreactor was drained, and the biomass concentration was measured to be $11.0 \text{ g(DCW) l}^{-1}$, almost the same level as the biomass concentration around $10.0 \text{ g(DCW) l}^{-1}$ measured in the effluent of the bioreactor toward the end of the experiment, whereas the yeast cells attached onto the packing surface were collected and measured to be only 2.3 g(DCW) in total after the packing was washed. This was equivalent to $4.9 \text{ g(DCW) l}^{-1}$ based on the bioreactor's working volume of 470 ml , indicating the yeast cells were slightly immobilized within this bioreactor because of its high residual glucose concentration and ethanol fermentation productivity which generated enough CO_2 to stir and prevent yeast cells from depositing onto the packing surface.

On the other hand, Figure 6.12 shows the biomass concentration in the effluent of the second packed tubular bioreactor was lower than the biomass concentration detected in the effluent of the empty column, and also lower than the biomass concentration in the effluent out of the first packed tubular bioreactor, indicating more yeast cells were retained and immobilized within this bioreactor as the CO_2 generated by fermentation was not enough to stir, suspend, and wash yeast cells out of the bioreactor. A similar situation also happened for the third packed tubular bioreactor, as illustrated in Figure 6.13.

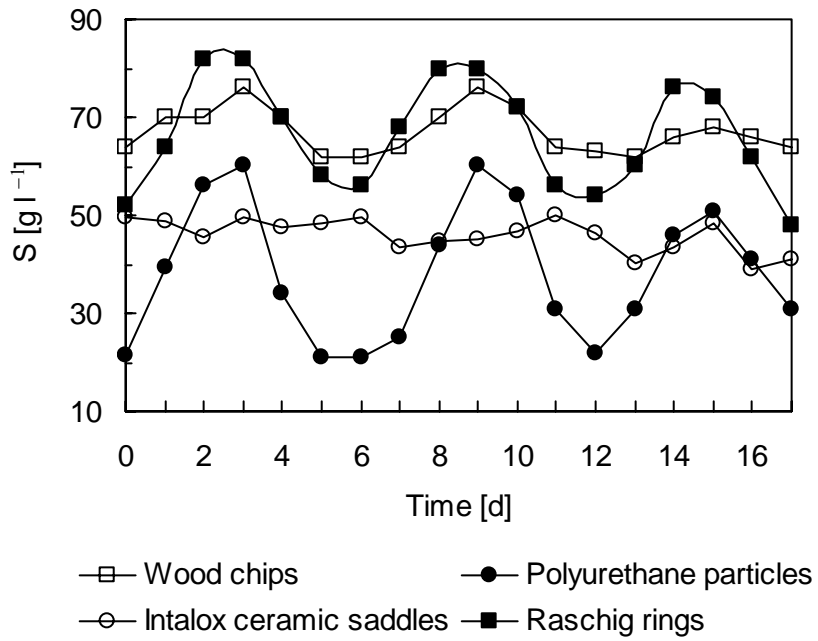
The biomass concentrations in the broth within the second and third packed bioreactors were measured to be $21.3 \text{ g(DCW) l}^{-1}$ and $32.5 \text{ g(DCW) l}^{-1}$ at the end of their operations, much higher than the biomass concentration in the broth within the first tubular bioreactor. The high biomass concentrations compensated for the viability loss of the yeast cells under the high ethanol and poor nutritional conditions within these two bioreactors, improving their ethanol fermentation performance as well as attenuating their oscillations, especially

under the situation when ethanol was mainly produced by the maintenance metabolism rather than by the growth of yeast cells within these two bioreactors, as discussed in Chapter 3.

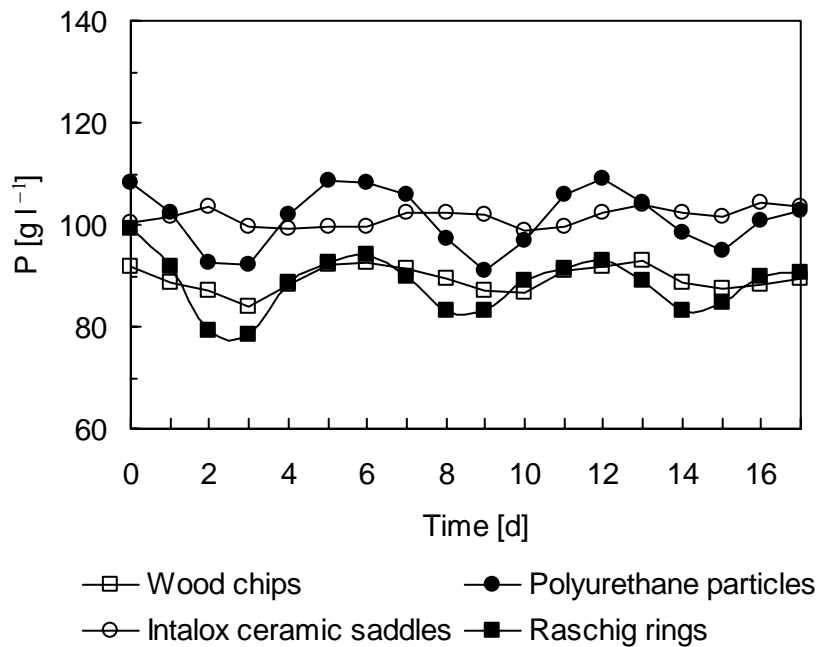
6.3.3.3 Impact of cell immobilization methods on oscillation attenuation

In order to further explore the impact of yeast cell immobilization on the performance of the tubular bioreactors as well as on the oscillation attenuation, 10×10×10 mm porous polyurethane particles which immobilized yeast cells through adsorption and entrapment (Amin et al., 1987; Lorene et al., 1987), and 5 × 5 ×10 mm wood chips (Moo-Young et al., 1984) which immobilized yeast cells by the same mechanism (adsorption) as the Intalox ceramic saddles, were selected. The experimental results are illustrated in Figures 6.14~6.16.

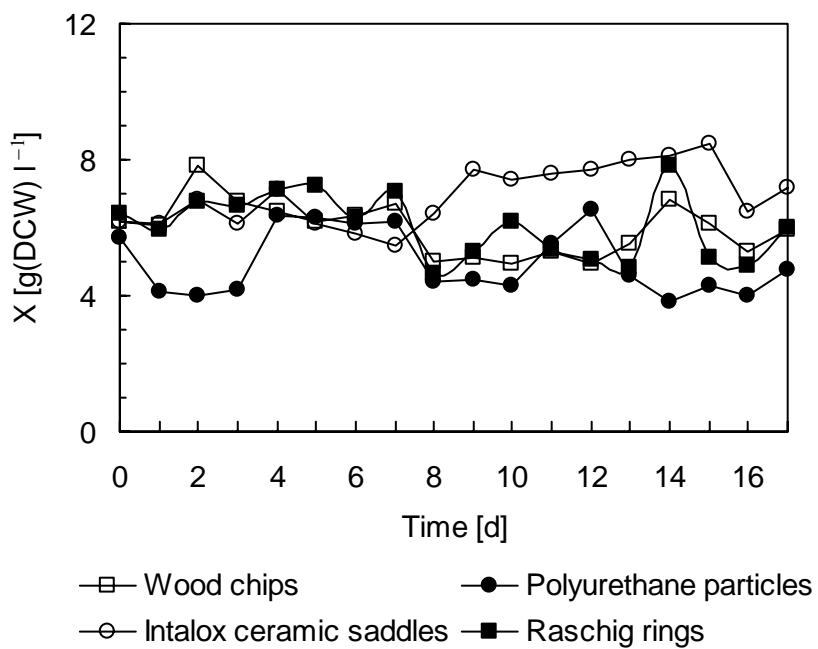
Table 6.1 further illustrates the yeast cell immobilization effects of these packings. As can be seen, the best yeast cell immobilization effect was obtained by the porous polyurethane particles, and the total yeast cell concentrations of 60.1, 71.7, and 108.7 g (DCW) l⁻¹ were achieved for the first, second, and third tubular bioreactors, compared with the average yeast cell concentrations of only 5.0, 1.7, and 0.8 g (DCW) l⁻¹ detected in the effluents from the corresponding bioreactors. A yeast cell mass balance was established for the first tubular bioreactor because the yeast cell concentration in the effluent out of it was almost equal to that in the effluent into it. The yeast cell concentration as high as twelve-fold that in the effluent was obtained within the bioreactor as the result of the yeast cell immobilization. For the second and third tubular bioreactors, although yeast cell mass balances were not achieved since the yeast cell concentrations in the inlet streams were higher than those in the effluents, the impact of the imbalances of yeast cell biomass on their fermentation performance was negligible, because the viability of the yeast cells within the second and third tubular bioreactors was extremely low (see Table 6.2).



(a) Residual glucose

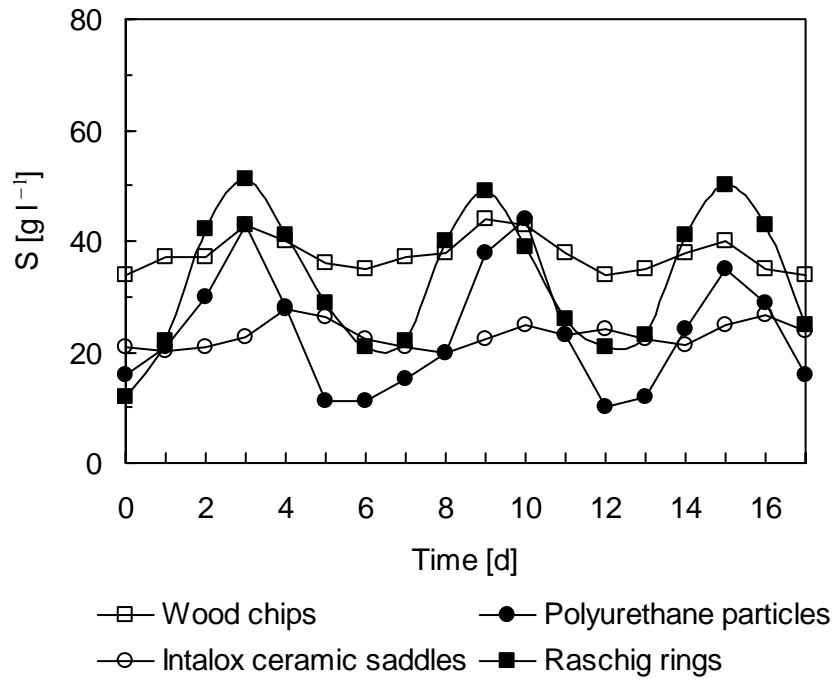


(b) Ethanol

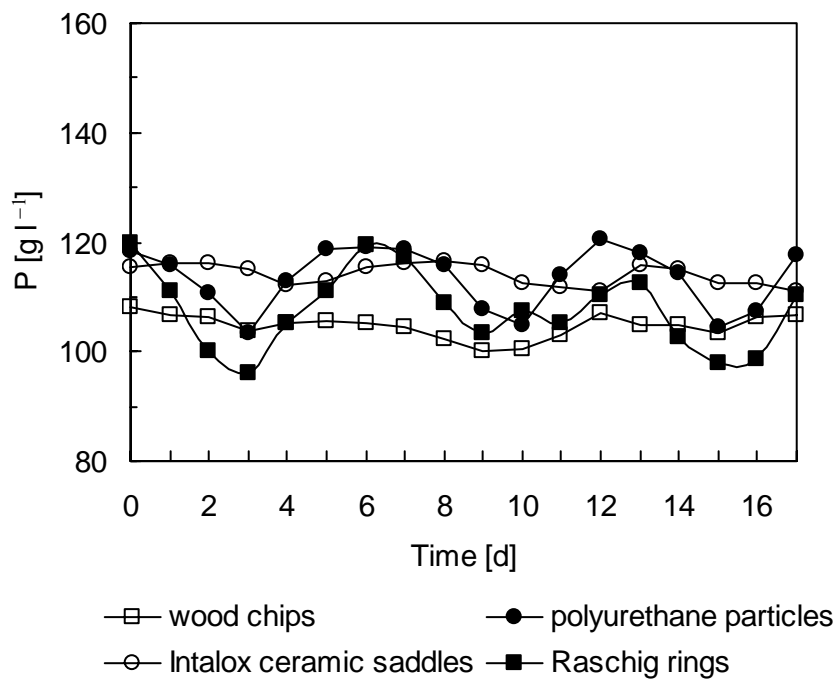


(c) Biomass

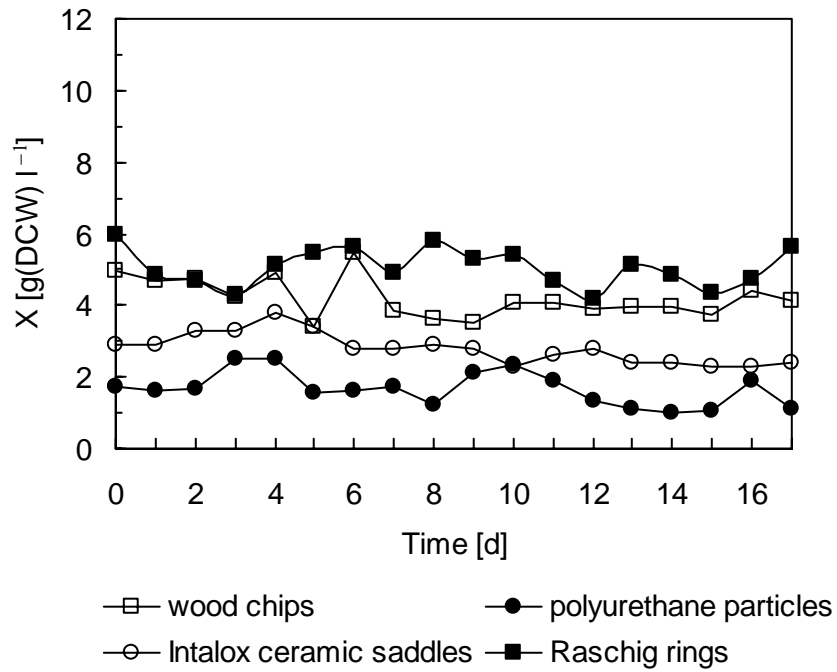
Figure 6.14 Impact of the packings on the fermentation performance of the first tubular bioreactor. The VHG medium containing 280 g l^{-1} glucose was fed into the tank at a dilution rate of 0.027 h^{-1} .



(a) Residual glucose

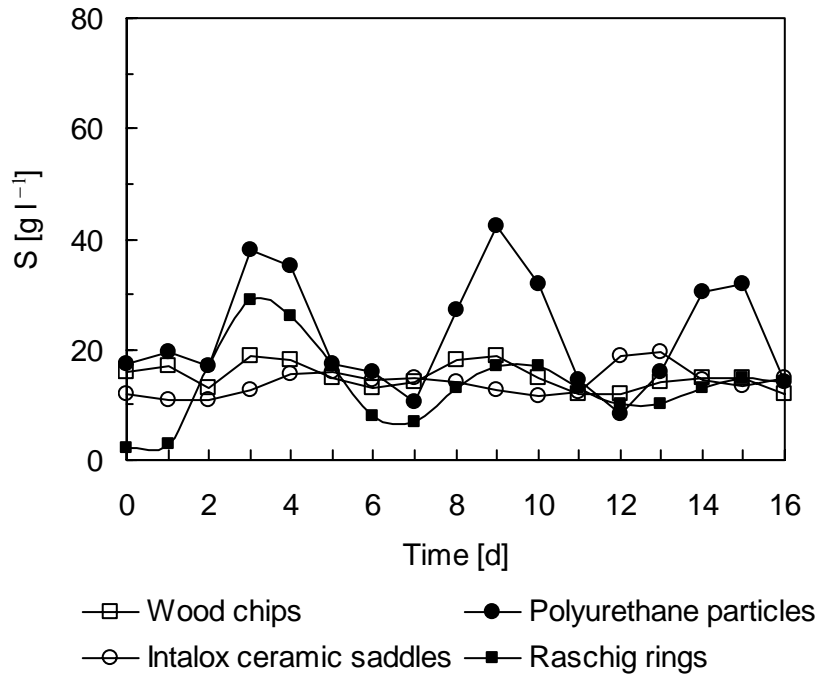


(b) Ethanol

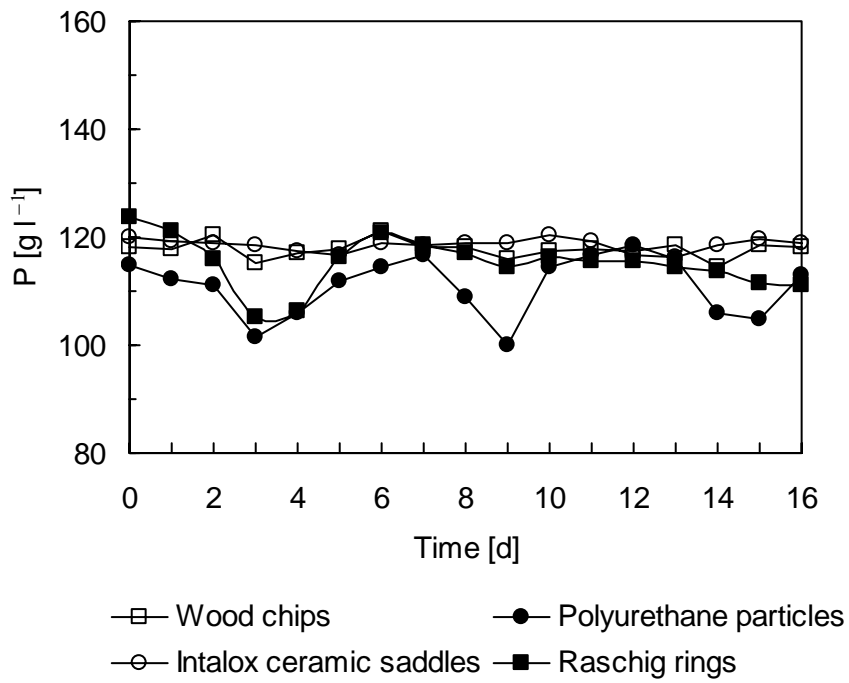


(c) Biomass

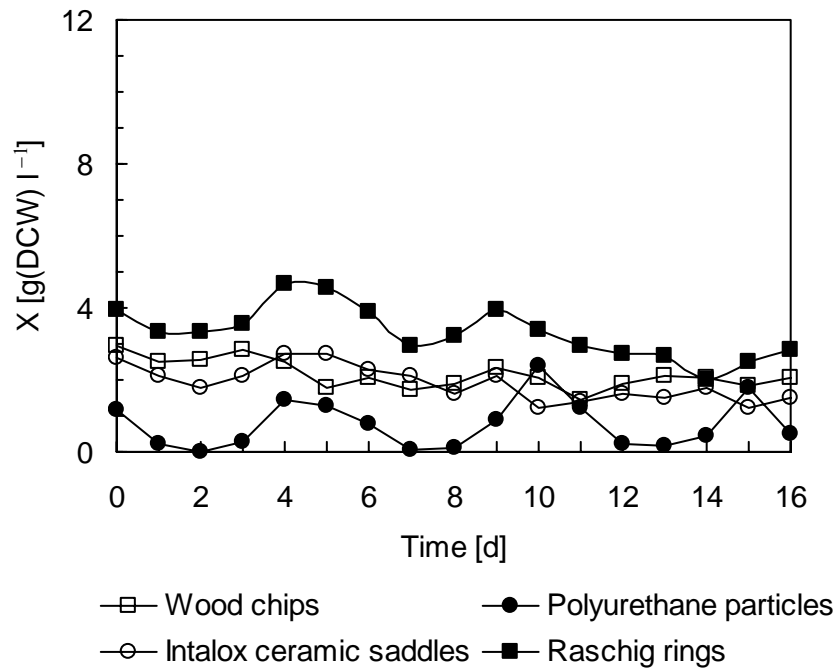
Figure 6.15 Impact of the packings on the fermentation performance of the second tubular bioreactor. The VHGM medium containing 280 g l⁻¹ glucose was fed into the tank at a dilution rate of 0.027 h⁻¹.



(a) Residual glucose



(b) Ethanol



(c) Biomass

Figure 6.16 Impact of the packings on the fermentation performance of the third tubular bioreactor. The VHG medium containing 280 g l^{-1} glucose was fed into the tank at a dilution rate of 0.027 h^{-1} .

Table 6.1 Impact of the packings on yeast cell immobilization effects

Tubular bioreactors (TBs)		Packings	Wood chips	Polyurethane particles	Ceramic saddles
TB1	Cells in the broth, g(DCW) l ⁻¹		12.0	29.9	11.0
	Cells deposited onto the surfaces or occluded into the pores of the packings, g(DCW)		4.5	12.9	2.3
	Total cell concentration *, g(DCW) l ⁻¹		25.3	60.1	16.0
TB2	Cells in the broth, g(DCW) l ⁻¹		11.4	44.5	21.3
	Cells deposited onto the surface or occluded into the pores of the packings, g(DCW)		5.0	11.1	3.0
	Total cell concentration *, g(DCW) l ⁻¹		26.4	71.7	27.6
TB3	Cells in the broth, g(DCW) l ⁻¹		17.5	71.9	32.5
	Cells deposited onto the surface or occluded into the pores of the packings, g(DCW)		5.6	14.8	3.1
	Total cell concentration *, g(DCW) l ⁻¹		35.1	108.7	39.3

* Total cell concentration: $X_T = X_1 + X_2$, where X_1 is the cell concentration in the broth, and X_2 is the cell concentration generated by the cells deposited onto the surface or adsorbed into the pore of the packings.

Table 6.2 Impact of the packings on fermentation performance and yeast cell viability*

Tubular bioreactors		Packings	Wood chips	Polyurethane particles	Ceramic saddles
		TB1	Average residual glucose, g l ⁻¹		66.7
Average ethanol, g l ⁻¹			89.5	101.2	102.3
Cell viability, %	Within TB1		42.6 ^{+7.8} _{-12.8}	22.7 ^{+3.1} _{-4.8}	32.5 ^{+9.0} _{-10.8}
	In effluent		40.1 ^{+6.4} _{-10.2}	26.8 ^{+7.8} _{-4.8}	29.6 ^{+10.3} _{-14.7}
TB2	Average residual glucose, g l ⁻¹		37.0	23.7	22.5
	Average ethanol, g l ⁻¹		104.9	113.5	114.6
	Cell viability, %	Within TB2	19.5 ^{+6.4} _{-4.6}	4.7 ^{+1.9} _{-1.8}	7.9 ^{+2.7} _{-3.3}
		In effluent	25.6 ^{+4.6} _{-5.9}	10.2 ^{+1.9} _{-2.2}	12.8 ^{+2.2} _{-2.2}
TB3	Average residual glucose, g l ⁻¹		14.6	22.8	14.0
	Average ethanol, g l ⁻¹		117.7	111.0	118.4
	Cell viability, %	Within TB3	9.8 ^{+1.8} _{-2.7}	0.8 ^{+0.2} _{-0.3}	4.9 ^{+2.0} _{-1.5}
		In effluent	15.2 ^{+4.9} _{-3.3}	3.4 ^{+0.8} _{-0.7}	7.1 ^{+3.4} _{-1.8}

* The average analytical errors for the yeast cell viability were observed to be +27.1% and -28.1%, and the data illustrated in Table 6.2 were the averages of triplicate counting samples.

The significant oscillations of residual glucose and ethanol were observed for all the three tubular bioreactors packed with the polyurethane particles, as illustrated in Figures 6.14~6.16. The averages of the residual glucose and ethanol of the third tubular bioreactor were 22.8 g l^{-1} and 111.0 g l^{-1} , but their oscillation ranges were as big as $8.5\sim 42.5 \text{ g l}^{-1}$ and $99.9\sim 118.5 \text{ g l}^{-1}$, making the corresponding absolute oscillation amplitudes as high as 34.0 g l^{-1} and 18.6 g l^{-1} , almost the same levels as those observed for the empty column, although a significantly lower average residual glucose of 38.3 g l^{-1} was achieved for the first tubular bioreactor.

On the other hand, moderate yeast cell immobilization was observed for the wood chips as well as for the Intalox ceramic saddles. The total yeast cell concentrations in the broth within the first, second, and third bioreactors were 25.3 , 26.4 , and $35.1 \text{ g (DCW) l}^{-1}$ when the bioreactors were packed with the wood chips, and 16.0 , 27.6 , and $39.3 \text{ g (DCW) l}^{-1}$ when the bioreactors were packed with the Intalox ceramic saddles. The average yeast cell concentrations in the effluents from the first, second, and third tubular bioreactors were 6.0 , 4.2 , and $2.2 \text{ g (DCW) l}^{-1}$ when the bioreactors were packed with the wood chips, and 7.6 , 2.9 , and $1.9 \text{ g (DCW) l}^{-1}$ when the bioreactors were packed with the Intalox ceramic saddles.

However, the oscillations of these tubular bioreactors were effectively attenuated when they were packed with the wood chips and the Intalox ceramic saddles, and a pseudo-steady state was observed for the third tubular bioreactor, because the fluctuation ranges of its residual glucose were only $1.5\sim 3.0 \text{ g l}^{-1}$ when packed with the wood chips and $1.0\sim 3.0 \text{ g l}^{-1}$ when packed with the Intalox ceramic saddles.

In order to further explore the mechanistic reason for the oscillation attenuation caused by the wood chips and the Intalox ceramic saddles, but not by the polyurethane particles, the viability of the yeast cells within the packed bioreactors was examined at the end of these

experiments, and it was found that the percentages of the viable cells were significantly lower when the tubular bioreactors were packed with the porous polyurethane particles, especially for the third tubular bioreactor within which almost no viable yeast cells were detected, although the yeast cell concentration was as high as $108.7 \text{ g (DCW) l}^{-1}$, as illustrated in Table 6.2.

When the empty columns were employed, the second and third columns were aerated in order to prevent the yeast cells from settling. Although an aeration rate of 0.005 vvm was extremely low, it was enough to improve the viability of the yeast cells suffering from the toxicity of high concentration ethanol (Ryu et al., 1984; Alfenore et al., 2004), resulting in a high viable cell percentage (about 40%) in the effluent from the third tubular bioreactor. The aeration for the second and third tubular bioreactors was interrupted after they were packed, making the viable cell percentages within the bioreactors decrease dramatically. However, the high yeast cell concentrations resulting from the immobilization effects of the packings compensated for this impact, much better ethanol fermentation performance was achieved, and the oscillations were effectively attenuated after the bioreactors were packed with the wood chips and the Intalox ceramic saddles.

Compared with the porous polyurethane particles, the wood chips and the Intalox ceramic saddles had a common characteristic, that is, the yeast cells loosely deposited and immobilized onto their surfaces, making the dead cells easily detached and washed out of the bioreactors. Although the polyurethane particles immobilized many more yeast cells, the renewal of the yeast cells that were immobilized within their inner pores by adsorption and entrapment was very difficult, and even impossible, which was supported by the much lower viable yeast cell percentages, 22.7%, 4.7% and 0.8%, respectively, for the first, second, and third bioreactors packed with the polyurethane particles, comparing with the viable yeast cell percentages of 42.6%, 19.5% and 9.8% within the bioreactors packed with the wood chips, and 32.5%, 7.9% and 4.9% within the bioreactors packed with the Intalox

ceramic saddles. In fact, almost no viable yeast cells were detected within the third bioreactor packed with the polyurethane particles, which was in good accordance with the glucose conversion of this bioreactor, 23.7 g l⁻¹ in the effluent from the second tubular bioreactor into it and 22.8 g l⁻¹ in the effluent out of it. The lower viable yeast cell percentages significantly affected the performance of the second and third tubular bioreactors, making the bioreactors lose their ability to attenuate the oscillations.

The viable yeast cell percentages within the first tubular bioreactor packed with the wood chips and the Intalox ceramic saddles were measured to be 42.6% and 32.5%, while the viable yeast cell percentages in the effluents were 40.1% and 29.5%, almost at the same levels with the viable cell percentages inside the bioreactor, indicating that dead yeast cells could be proportionately washed out of the bioreactor. However, the viable yeast cell percentage within the first tubular bioreactor was measured to be 22.7% when it was packed with the polyurethane particles, not only significantly lower than the viable yeast cell percentages when the bioreactor was packed with the wood chips and the Intalox ceramic saddles, but also lower than the viable yeast cell percentage of 26.8% detected in its own effluent, which meant viability-lost yeast cells were retained within the pores of the polyurethane particles and could not be readily washed out of the bioreactor. For the second and third bioreactors, although higher viable yeast cell percentages were detected in the effluents of the bioreactors packed with all the three packings, the largest difference in the viable yeast cell percentages was observed between the effluent and broth within the bioreactors when the bioreactors were packed with the polyurethane particles, indicating more viable yeast cells were washed out than remained inside the bioreactors.

The significant difference in the viability of the immobilized yeast cells generated by the different mechanisms of yeast cell immobilization gives a reasonable explanation for the role of the wood chips and the Intalox ceramic saddles in attenuating the oscillatory behaviors of the tubular bioreactors.

In order to further validate the impact of yeast cell immobilization, the packing, $\phi 10 \times 10$ mm Raschig rings made of 80 mesh stainless steel wire mesh with smooth surface that yeast cells could not deposit onto, was selected. No yeast cell immobilization was observed for the bioreactors packed with this packing, and the ethanol fermentation performance and oscillatory behavior of the tubular bioreactors were not significantly affected, almost the same as those observed for the empty column system, supporting the inference that the oscillation attenuation was from the yeast cell immobilization.

6.3.3.4 Impact of dilution rate shift on oscillation attenuation

As the void fraction of the packings was different, the real working volume of the tubular bioreactors was changed after they were packed. When the medium dilution rate of the CSTR was maintained at the same as that for the empty column system, the real dilution rates of the tubular bioreactors were changed, correspondingly. In order to examine the impact of the shift of dilution rate on the oscillations, $\phi 10$ mm smooth surface glass beads which could not immobilize yeast cells, but made the packed tubular bioreactors have the same working volumes as those packed with the wood chips were selected. No significant improvement in ethanol fermentation performance as well as oscillation attenuation were observed for the tubular bioreactors packed with the glass beads, which ruled out the significant impact of the shift of dilution rate.

6.4 Conclusions

When the tubular bioreactors were packed with the Intalox ceramic saddles, the oscillations previously observed for the empty column system were effectively attenuated. Through the RTD analysis and the comparisons with other packings: the wood chips, the polyurethane particles as well as the Raschig rings, the following conclusions are made:

1. The packings were inefficient in reducing axial backmixing in the tubular bioreactors because of the lower dilution rate, and correspondingly, longer average residence time required by the fermentation system. Therefore, the alleviation of ethanol inhibition through establishing concentration gradients within the tubular bioreactors is not applicable for this bioreactor system.
2. The packings improved the VHG ethanol fermentation performance of the tubular bioreactors and attenuated the oscillations, and the corresponding mechanism was shown to be the yeast cell immobilization effect of the packings. However, only the packing which loosely immobilizes yeast cells on its outside surface to make the immobilized yeast cells easily renewed during fermentation can achieve such a effect.
3. Although the packings decreased the working volumes of the tubular bioreactors, and correspondingly, increased their dilution rates, the shifts of the dilution rates did not significantly affect the oscillation profiles of the tubular bioreactors.

Chapter 7

Kinetics and Dynamic Simulations

Part of this chapter was published in *Biotechnol Biopro Eng*, 2005, 10, 115-121.

7.1 Introduction

Oscillations increased residual sugar at the end of fermentation, negatively affecting the ethanol yield that is calculated based on the sugar fed into the fermentation system without deduction of the residual. Some packing, which can loosely immobilize yeast cells, making immobilized yeast cells easily renewed, and ensure their proper viability, can attenuate the oscillations. On the other hand, process intervention can be applied to prevent oscillations from occurring or minimize their negative impact if the oscillations can be simulated and predicted in advance.

Kinetics is the very basis for process optimization and control. Although continuous ethanol fermentation kinetics were studied as early as in the 1960s (Aiba et al. 1968), most kinetic expressions currently available are instantaneous for batch fermentation and steady-state for continuous fermentation. Reports on the literatures are lacking for VHG ethanol fermentation kinetics, characterized by both substrate and product inhibitions as well as sustainable oscillations.

As the oscillations were observed to be symmetrical above and below their averages, the concept of pseudo-steady state was applied to such an oscillatory system. In this chapter, the pseudo-steady state kinetic models of continuous ethanol fermentation are first established for yeast cell growth and ethanol production. Then, based on the mechanistic

analysis that shows that ethanol inhibition and the lag response of yeast cells to ethanol inhibition cause the oscillations, a time delay taking into account the impact of a previous ethanol concentration history on the current yeast cell growth and ethanol production was proposed and incorporated into the pseudo-steady state kinetic models. Finally, the dynamic behavior of continuous VHG ethanol fermentation is simulated, which not only provides the basis for developing the strategies to minimize the oscillation in advance, but also further supports the mechanistic explanation for the oscillations.

7.2 Materials and Methods

7.2.1 Strain, medium, and pre-culture

Microorganism, media, and pre-culture were described in Section 3.2.1.

7.2.2 Bioreactor system

The 1500 ml Bioflo fermentor illustrated in Figure 3.1 was used, and its operating parameters including temperature, pH, stirring speed, and aeration rate were the same as described in Section 3.2.2.

7.2.3 Analytical methods

The analytical methods for glucose, ethanol, and biomass were described in Section 3.2.3.

7.3 Models

7.3.1 Pseudo-steady state kinetic models

The Monod model is widely used to express the relationship between specific growth rate and limiting substrate concentration.

$$\mu = \mu_{max} \frac{S}{K_s + S} \quad (7.1)$$

This well-known Monod model is only applicable when the presence of toxic metabolic products plays no inhibitory role. For ethanol fermentation, especially for VHG fermentation, ethanol significantly inhibits yeast cell growth as well as ethanol production. Therefore, Equation (7.1) needs to be modified to include the influence of ethanol inhibition.

$$\mu = f(S, P) \quad (7.2)$$

Many previous studies have revealed that yeast cell growth is inhibited by ethanol in a noncompetitive manner similar to that of enzymatic reactions (Aiba *et al.* 1968; Luong, 1985). In this case, only the maximum specific growth rate is affected by ethanol concentration.

$$\mu = \mu_i \frac{S}{K_s + S} \quad (7.3)$$

The dependence of μ_i on ethanol concentration can be correlated using a generalized nonlinear equation (Levenspiel 1980).

$$\mu_i = \mu_{max} \left(1 - \frac{P}{P_{max}}\right)^\alpha \quad (7.4)$$

Substrate inhibition can be treated by introducing a substrate inhibition constant into the corresponding kinetic expression (Andrews 1968).

$$\mu = \mu_{max} \frac{S}{K_s + S + S^2 / K_I} \quad (7.5)$$

Combining Equations (7.3), (7.4) and (7.5), a model reflecting both substrate and product inhibitions can be developed.

$$\mu = \mu_{max} \frac{S}{K_S + S + S^2/K_I} \left(1 - \frac{P}{P_{max}}\right)^\alpha \quad (7.6)$$

When the dilution rate is controlled at a relatively lower level during continuous ethanol fermentation, especially for low gravity media, the limiting substrate concentration is undetectable, and the specific growth rate predicted by Equation (7.6) is zero, but the growth of yeast cells does happen as the broth containing yeast cells is continuously produced. This discrepancy in Equation (7.6) needs to be further addressed by adding an experimental parameter μ_0 that equals the dilution rate at which the limiting substrate concentration falls below a detection limit.

$$\mu = \mu_{max} \frac{S}{K_S + S + S^2/K_I} \left(1 - \frac{P}{P_{max}}\right)^\alpha + \mu_0 \quad (7.7)$$

Ethanol is a typical primary metabolite of yeast cells under an anaerobic condition, and its production is tightly associated with the growth of yeast cells, so that a similar kinetic model for ethanol production can be developed.

$$v = Y_{E/X} \mu = Y_{E/X} \left[\mu_{max} \frac{S}{K_S + S + S^2/K_I} \left(1 - \frac{P}{P_{max}}\right)^\alpha + \mu_0 \right] \quad (7.8)$$

As biomass concentration is generally expressed on a dry cell weight basis, viable cells cannot be quantitatively distinguished from non-viable or dead ones. This complicated biological phenomenon can be taken into account by modifying the model parameters of Equations (7.7) and (7.8), but the maximum ethanol concentration for yeast cell growth and ethanol formation should be the same if the ethanol produced by the maintenance metabolism of yeast cells is negligible. Thus, we have:

$$\mu = \mu_{max} \frac{S}{K_S + S + S^2/K_I} \left(1 - \frac{P}{P_{max}}\right)^\alpha + \mu_0 \quad (7.9)$$

$$v = v_{max} \frac{S}{K_S^* + S + S^2/K_I^*} \left(1 - \frac{P}{P_{max}}\right)^\beta + v_0 \quad (7.10)$$

For a fermentor operating as a CSTR, biomass mass balance gives:

$$\frac{dX}{dt} = \mu X - DX \quad (7.11)$$

Under a pseudo-steady state condition in which the fluctuation of biomass concentration is symmetrical above and below the average value, we have:

$$\frac{dX}{dt} \approx 0 \quad (7.12)$$

Therefore,

$$D \approx \mu \quad (7.13)$$

Mass balance for ethanol gives:

$$\frac{dP}{dt} = v X - DP \quad (7.14)$$

Similarly

$$\frac{dP}{dt} \approx 0 \quad (7.15)$$

Thus,

$$v = \frac{DP}{X} \quad (7.16)$$

The specific rates for yeast cell growth and ethanol production can be determined by controlling the medium dilution rate, measured biomass and ethanol concentration for a continuous fermentation system.

7.3.2 Dynamic models

For the oscillations observed in continuous ethanol fermentation with *Z. mobilis*, Li et al. elucidated that the ethanol concentration change rate history rather than the ethanol concentration history, the time period in which the species had experienced, was the main reason for the oscillations (Li et al., 1995), and based on this mechanistic analysis, they developed corresponding dynamic models in which the lag response of the species to the ethanol concentration change rate history was incorporated (Daugulis et al., 1997; McLellan et al., 1999).

However, for the oscillations observed in continuous ethanol fermentation with *S. cerevisiae*, the aforementioned analysis makes no sense because the oscillation periods observed to be as long as one week, even more, made any component concentration gradients negligible, but the influence of the ethanol concentration itself, the history of ethanol concentration, was more significant.

The lag response of yeast cells to ethanol concentration history can be modeled by introducing a weight function, and thus, the dynamic specific growth rate, Ω , can be expressed as (Daugulis et al., 1997):

$$\Omega = \int_{-\infty}^t \mu(t) \Big|_{t=\tau} \cdot \theta(\tau) d\tau \quad (7.17)$$

Because ethanol production is tightly associated with the growth of yeast cells, a dynamic specific ethanol production rate, Φ , can be similarly defined as:

$$\Phi = \int_{-\infty}^t \nu(t) \Big|_{t=\tau} \cdot \theta(\tau) d\tau \quad (7.18)$$

And the weight function for the ethanol concentration history $\theta(\tau)$ is:

$$\theta(\tau) = \omega^2 (t - \tau) \cdot e^{-\omega(t-\tau)} \quad (7.19)$$

where τ is the time in history and t is the current time. The maximum of $\theta(\tau)$ occurs at $\tau = t - 1/\omega$, that is, $1/\omega$ hours prior to the current time t . In other words, the ethanol concentration which happened at $1/\omega$ hours before has most significant influence on current status, and the model parameter ω indicates the magnitude of the time lag for the delayed response of yeast cells to ethanol inhibition effect. Such a time delay effect recognizes that yeast cells do not respond immediately to the ethanol inhibition exerted on them, but require a period of time to adjust their intracellular metabolism to adapt such an ethanol inhibition environment.

A dynamic mass balance for biomass, glucose, and ethanol gives:

$$\frac{dX}{dt} = X(\Omega - D) \quad (7.20)$$

$$\frac{dS}{dt} = D(S_0 - S) - \frac{1}{Y_{P/S}} \Phi X \quad (7.21)$$

$$\frac{dP}{dt} = -DP + \Phi X \quad (7.22)$$

Equations (7.17) and (7.18) give:

$$\frac{d\Omega}{dt} = \omega(V_G - \Omega) \quad (7.23)$$

where the intermediate variable V also is a weighted average of the previous ethanol concentration history with the weight $\sigma(\tau)$:

$$V_G = \int_{-\infty}^t \mu(\tau) \cdot \sigma(\tau) d\tau \quad (7.24)$$

and

$$\sigma(\tau) = \omega \cdot e^{-\omega(t-\tau)} \quad (7.25)$$

therefore,

* The detailed mathematical derivation is given in Appendix C.

$$\frac{dV_G}{dt} = \omega(\mu - V_G) \quad (7.26)$$

Similarly, Equations (7.18) and (7.19) give:

$$\frac{d\Phi}{dt} = \omega(V_P - \Phi) \quad (7.27)$$

and the intermediate variable V_P is expressed as:

$$V_P = \int_{-\infty}^t v(\tau) \cdot \sigma(\tau) d\tau \quad (7.28)$$

therefore,

$$\frac{dV_P}{dt} = \omega(v - V_P) \quad (7.29)$$

Equations (7.20) ~ (7.23), (7.26), (7.27) and (7.29), together with the pseudo-steady kinetic models: Equations (7.9) and (7.10), can be used to simulate the dynamic process of continuous VHG ethanol fermentation.

7.4 RESULTS AND DISCUSSION

7.4.1 Pseudo-steady state kinetics

The media containing glucose 120, 200, and 280 g l⁻¹ were fed into the CSTR at different dilution rates to generate various glucose, ethanol, and biomass concentration scenarios, as illustrated in Table 7.1, through which the pseudo-steady state kinetic parameters in Equations (7.9) and (7.10) were evaluated using the nonlinear least-squares method. A function (lsqnonlin) in MATLAB (Appendix D1) was used to solve this problem by fitting the experimental data with a 95% confidence, and the results are illustrated in Table 7.2.

Table 7.1 Pseudo-steady state kinetic data of continuous fermentation by *S. cerevisiae* ATCC 4126*

$S_0 = 120 \text{ g l}^{-1}$, steady state						
$\mu_{exp.} \text{ h}^{-1}$	0.027	0.050	0.083	0.100	0.116	0.140
$\mu_{cal.} \text{ h}^{-1}$	0.038	0.039	0.084	0.098	0.117	0.144
$S \text{ g l}^{-1}$	0	0.14	17.3	20.2	32.5	44.7
$P \text{ g l}^{-1}$	58.2	52.2	44.3	40.8	38.4	32.5
$X \text{ g l}^{-1}$	6.33	7.43	4.96	4.73	4.63	4.23
$v_{exp.} \text{ h}^{-1}$	0.262	0.351	0.741	0.862	0.962	1.075
$v_{cal.} \text{ h}^{-1}$	0.246	0.252	0.748	0.819	0.986	1.145
$S_0 = 200 \text{ g l}^{-1}$, pseudo-steady state						
$\mu_{exp.} \text{ h}^{-1}$	0.027	0.040	0.067	0.100	0.120	0.146
$\mu_{cal.} \text{ h}^{-1}$	0.023	0.044	0.065	0.105	0.116	0.133
$S \text{ g l}^{-1}$	36.5	61.4	86.8	110.7	118.8	129.0
$P \text{ g l}^{-1}$	82.5	68.3	56.8	41.3	37.3	32.1
$X \text{ g l}^{-1}$	4.0	4.8	4.6	4.1	4.4	4.0
$v_{exp.} \text{ h}^{-1}$	0.500	0.575	0.832	1.020	1.017	1.172
$v_{cal.} \text{ h}^{-1}$	0.632	0.593	0.773	1.007	1.074	1.161
$S_0 = 280 \text{ g l}^{-1}$, pseudo-steady state						
$\mu_{exp.} \text{ h}^{-1}$	0.018	0.027	0.053	0.080	0.106	
$\mu_{cal.} \text{ h}^{-1}$	0.023	0.030	0.044	0.082	0.116	
$S \text{ g l}^{-1}$	96.8	117.2	143.9	175.3	213.2	
$P \text{ g l}^{-1}$	82.5	76.0	65.2	45.2	31.5	
$X \text{ g l}^{-1}$	3.7	4.0	4.3	3.6	3.5	
$v_{exp.} \text{ h}^{-1}$	0.401	0.513	0.803	1.004	0.954	
$v_{cal.} \text{ h}^{-1}$	0.509	0.595	0.739	1.021	1.244	

* The ethanol production concentration P was calibrated by taking into account the ethanol evaporation loss by exhaust gas.

Table 7.2 Values of the pseudo-steady state kinetic parameters

μ_{\max} (h^{-1})	K_S (g l^{-1})	K_I (g l^{-1})	μ_0	α	P_{\max} (g l^{-1})
0.471	10.78	293.2	0.0378	3.86	167.0
ν_{\max}	K_S^* (g l^{-1})	K_I^* (g l^{-1})	ν_0	β	
1.95	22.95	1.81×10^3	0.246	1.66	

The maximum ethanol concentration for both yeast cell growth and ethanol fermentation P_{\max} was estimated to be 167.0 g l^{-1} , much higher than those previously reported values (Converti et al. 1985, Luong 1985, Thatipamala et al. 1992), but very near to the 23% (v) upper limit achieved by Kelsall et al. (1999). The parameters K_S and K_S^* were higher, which means the substrate affinity is poor, and correspondingly, the viability of yeast cells is lower under the inhibitions from substrate and product. K_I and K_I^* are relatively smaller compared with S^2 , indicating substrate inhibition cannot be neglected when substrate concentration is high, especially for the growth of yeast cells. $\alpha = 3.86$ and $\beta = 1.66$ illustrate that ethanol inhibition is much stronger on yeast cell growth than on ethanol fermentation. The reason for the relatively large confidence intervals is the relatively small number of the samples as well as the broad experimental conditions, especially the medium gravities.

Substituting Equations (7.9) and (7.10) with these model parameters gives the pseudo-steady kinetic expressions.

For growth:

$$\mu = \frac{0.471S}{10.78 + S + S^2/293.2} \left(1 - \frac{P}{167.0}\right)^{3.86} + 0.0378 \quad S \leq K_S \quad (7.30a)$$

and

$$\mu = \frac{0.471S}{10.78 + S + S^2/293.2} \left(1 - \frac{P}{167.0}\right)^{3.86} \quad S > K_S \quad (7.30b)$$

For fermentation:

$$v = \frac{1.95S}{22.95 + S + S^2/1.81 \times 10^3} \left(1 - \frac{P}{167.0}\right)^{1.66} + 0.246 \quad S \leq 2K_S^* \quad (7.31a)$$

and

$$v = \frac{1.95S}{22.95 + S + S^2/1.81 \times 10^3} \left(1 - \frac{P}{167.0}\right)^{1.66} \quad S > 2K_S^* \quad (7.31b)$$

As no kinetic data are available from other sources for the same strain and medium composition, the models cannot be further validated to be universal. In fact, almost no cell growth and fermentation kinetic models can be directly used to predict and simulate kinetic behavior of other cell culture and fermentation systems outside the conditions at which the models were developed and the model parameters were evaluated, and some modifications are always required to incorporate the specificities of each individual system. That's why many cell culture and fermentation kinetic models established by researchers cannot be directly used in the corresponding industrial process design. Generally speaking, kinetic models can provide some qualitative analysis to the corresponding industrial process design as well as to the plant operation, like the current situation of the ethanol fermentation industry in which the process design still to a very large extent depends on the experience accumulated in the past, as well as some qualitative understanding of yeast cell growth and

ethanol fermentation kinetic characteristics.

Equations (7.9) and (7.10) could be applicable for other continuous ethanol fermentation systems in which the inhibitions of substrate and product present, either one of them or both, after the model parameters illustrated in Table 7.2 are modified according to the specificities of the corresponding fermentation systems such as the characteristics of strains, the composition of media, and any difference in operating parameters.

Figures 7.1 and 7.2 compare the model calculated values, μ_{cal} and v_{cal} , with the experimental data, μ_{exp} and v_{exp} , by applying the linear correlation: $y = x$ (Devore and Farnum, 1999), and the corresponding coefficients $R^2 = 0.9744$ for the growth of yeast cells and $R^2 = 0.9289$ for ethanol production indicate these models properly correlate the pseudo-steady state kinetic data of *S. cerevisiae* ATCC 4126 under the experimental conditions.

With the pseudo-steady state kinetic expressions in hand, the dynamic models of Equations (7.20) ~ (7.23), (7.26), (7.27) and (7.29) are ready to be solved by the multi-response nonlinear regression estimation method using MATLAB, and the model parameter ω , the weighted history of ethanol inhibition on both yeast cell growth and ethanol production, can be evaluated.

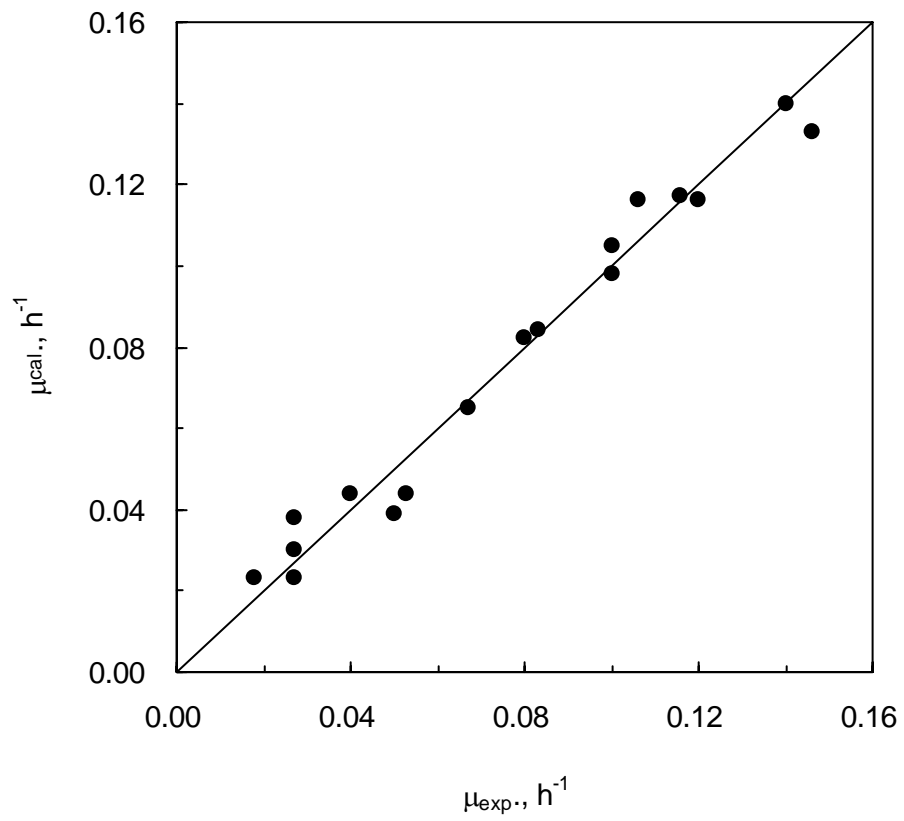


Figure 7.1 Comparison of the experimental data with the model predictions for yeast cell growth (A linear correlation $y = x$, $R^2 = 0.9744$)

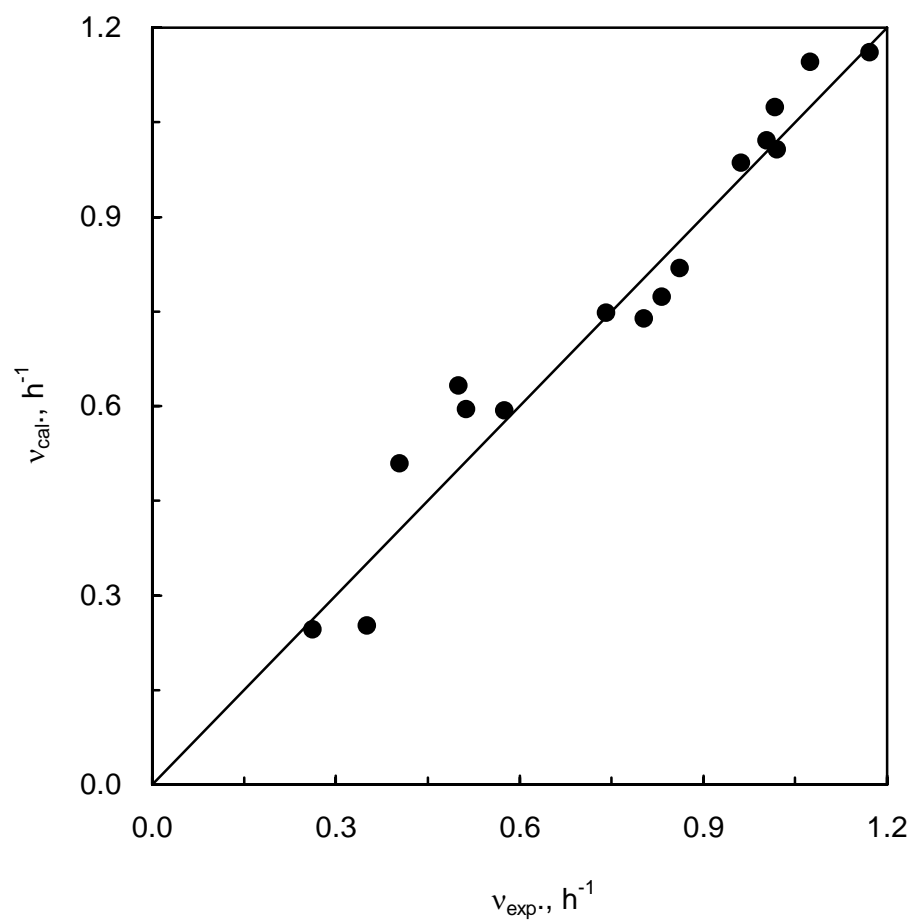


Figure 7.2 Comparison of the experimental data with the model predictions for ethanol production (A linear correlation $y = x$, $R^2 = 0.9289$)

7.4.2 Dynamic simulations

Although oscillations occurred during the continuous VHG ethanol fermentation, the ethanol production yield $Y_{P/S}$ which was calculated based on the glucose consumed was constant as illustrated in Figure 3.6 and Appendix A. Two groups of experimental data were obtained independently. One group in Table 7.3 was used to evaluate the dynamic model parameter ω , the weighted inhibition history of ethanol concentration on both yeast cell growth and ethanol fermentation, by solving the ordinary differential equations (7.20) ~ (7.23), (7.26), (7.27) and (7.29), and fitting the experimental data. An ODE solver (ode113) in MATLAB was used to solve these ordinary differential equations, and the complete program is illustrated in Appendix D2.

The estimated value of ω is 0.0612 ± 0.0064 with a 95% confidence, and the quantity of $1/\omega$ is 16.3 hours, indicating that the ethanol concentration at 16.3 hours prior to the current time exerts the strongest inhibitory effect on yeast cell growth as well as on ethanol production. This time scale is roughly equivalent to half of the average generation time (25.6 h) of yeast cells when the VHG medium was fed into the fermentation system at a dilution rate of 0.027 h^{-1} . Meanwhile, it was reported a 5.8 hours time delay for the continuous ethanol fermentation with *Z. mobilis* (Daugulis et al., 1997), which is shorter than that of the continuous ethanol fermentation with *S. cerevisiae*. This comparison seems reasonable because *S. cerevisiae* metabolizes slower than *Z. mobilis*, and correspondingly, a longer time delay for its response to ethanol inhibition is required.

The dynamic behaviors of residual glucose, ethanol, and biomass were simulated for continuous ethanol fermentation fed with the VHG medium ($S_0 = 280 \text{ g l}^{-1}$) at a dilution rate of $D = 0.027 \text{ h}^{-1}$. The simulation results were compared with the experimental data illustrated in Figure 3.2, as illustrated in Figure 7.3.

Table 7.3 Dynamic data of continuous VHG ethanol fermentation by *S. cerevisiae* ATCC 4126, $S_0 = 280 \text{ g l}^{-1}$ and $D = 0.027 \text{ h}^{-1}$.

Time h	Glucose g l^{-1}	Ethanol g l^{-1}	Biomass g(DCW) l^{-1}	Time h	Glucose g l^{-1}	Ethanol g l^{-1}	Biomass g(DCW) l^{-1}
0	104.2	79.0	3.5	264	120.0	78.5	4.3
24	114.2	76.7	4.1	288	112.6	78.5	4.3
48	120.1	73.8	3.5	312	100.1	82.1	4.7
72	130.6	66.9	3.1	336	106.8	77.0	4.6
96	118.5	70.1	3.6	360	112.2	78.1	3.6
120	102.0	80.3	4.5	384	120.2	73.1	3.5
144	98.3	82.4	4.1	408	122.8	68.3	3.6
168	106.1	80.4	4.2	432	112.9	68.0	4.5
192	110.8	76.4	3.8	456	106.2	73.7	3.9
216	124.2	72.0	3.8	480	110.3	74.8	4.0
240	130.6	66.9	3.8	–	–	–	–

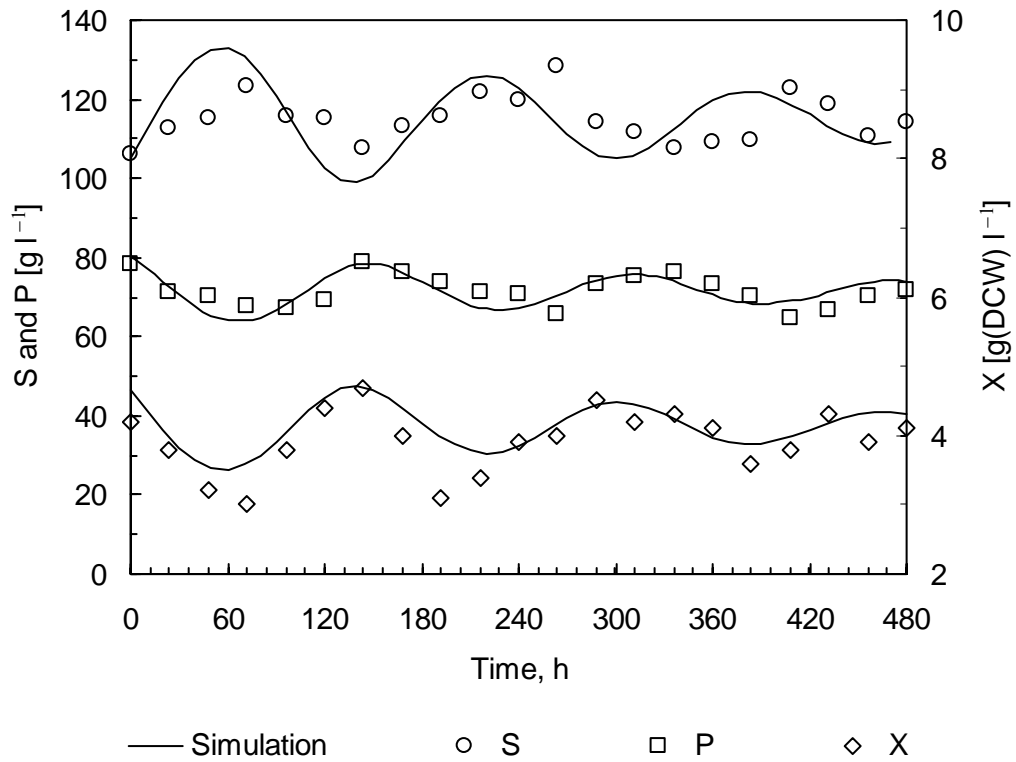


Figure 7.3 Dynamic simulations of the oscillations of residual glucose, ethanol, and biomass for continuous VHG fermentation with *S. cerevisiae* ATCC 4126. The VHG medium containing 280 g l⁻¹ glucose was fed into the tank at a dilution rate of 0.027 h⁻¹.

As can be seen, the simulations of residual glucose and ethanol fit the experimental data well within 20 days, about three oscillation periods, which further validates the lag response of yeast cells to ethanol inhibition. A relatively large deviation for the simulation of biomass indicates some discrepancies between the biomass concentration measured on the dry cell weight basis and the fermentability of yeast cells under the VHG condition, and more reliable biomass measurement needs to be applied.

Equations (7.17) and (7.18) exhibit time delay effects across the whole time scale. Obviously, it contradicts the fact that the lag response of yeast cells to ethanol inhibition is developed gradually after the fermentation is set up. In order to obtain good simulation results, the simulations before time zero were cut off. The initial time was selected by an iterative method so that the simulation results could better match the experimental data illustrated in Figure 3.2, starting at a proper zero time. A prior time of 300 hours achieved best simulation results for the oscillations of residual glucose and ethanol.

Mathematically, Equations (7.17) and (7.18) give self-attenuated simulations when time is further extended and the lag response of yeast cells to ethanol inhibition predicted by the equations is accumulated, which indicates that more mathematical and biochemical considerations need to be incorporated into the models, making it more practical.

7.5 Conclusions

A pseudo-steady state assumption was applied to the oscillatory ethanol fermentation process, and the corresponding kinetic models for both yeast cell growth and ethanol fermentation were correlated.

The concept of dynamic specific rates incorporating the effect of ethanol inhibition history on yeast cell growth as well as on ethanol fermentation was proposed. Furthermore, the

dynamic model consisting of the differential equations for the mass balance of the oscillatory fermentation system was formulated, and the model parameter, ω , the weighted history of ethanol inhibition, was evaluated.

Finally, the dynamic behaviors of residual glucose, ethanol, and biomass were simulated for the continuous VHG ethanol fermentation under the conditions of $S_0 = 280 \text{ g l}^{-1}$ and $D = 0.027 \text{ h}^{-1}$, and compared with the corresponding experiment data to evaluate the effectiveness of the dynamic model. Not only can this dynamic model provide the basis for developing strategies to predict these oscillations in advance, but also further validate our speculations on oscillation mechanisms.

Chapter 8

Conclusions and Recommendations

8.1 Conclusions

In this thesis, a continuous VHG ethanol fermentation process using strains of *S. cerevisiae* was studied. A bioreactor system composed of a CSTR and three tubular bioreactors in series was used to examine the oscillatory behaviors of fermentation parameters that occurred under certain conditions. The following can be concluded:

1. The oscillatory behaviors in the continuous VHG ethanol fermentation are due to ethanol inhibition and the lag response of yeast cells to this inhibition. Also, there is a lethal effect of high ethanol concentration on yeast cells toward the end of the fermentation, which further exaggerate the oscillations.
2. Ethanol tolerance affects oscillation profiles and industrial strains with better ethanol tolerance are less oscillatory because they can respond faster to ethanol inhibition and more easily adapt to an ethanol inhibition environment.
3. The reason for the exaggerated oscillations observed at specific dilution rates for the continuous ethanol fermentation with the self-flocculating yeast strain SPSC and the tanks-in-series fermentation system is the continuous inoculation from the seed fermentor.
4. The packing could not significantly reduce backmixing in the tubular bioreactors. The yeast cell immobilization in the packing was the main reason for the improvement of ethanol fermentation performance as well as the attenuation of the oscillations. However, only a packing which immobilizes yeast cells loosely,

making the cells easily renewed so that the overall viability can be maintained, can achieve such effects.

5. A dynamic kinetic model was developed by incorporating the time delay impact that reflects the history of ethanol concentration inhibition and the lag response of yeast cells into the pseudo-steady kinetic models. The dynamic behavior of the continuous VHG ethanol fermentation was simulated at designated conditions, which not only provides the basis for developing intervention strategies, but also further supports the mechanistic analysis for the oscillations.

8.2 Recommendations

The thesis presents some new understanding of the oscillatory behavior occurring in the continuous VHG ethanol fermentation with *S. cerevisiae*. The following is recommended for future work to further improve the mechanistic understanding as well as develop strategies for process design and control.

1. The mechanisms triggering the oscillatory behavior in the continuous VHG ethanol fermentation must have an intracellular metabolic basis. Therefore, more research needs to be done to reveal the intrinsic connection between the oscillatory behaviors of extracellular fermentation parameters and the corresponding responses of intracellular metabolisms, identifying key enzymes affected by ethanol inhibition, regulating metabolic pathways, and crossover metabolites, as well as understanding how the shifts of intracellular metabolisms can affect the oscillatory behaviors of extracellular parameters.
2. The impact of dilution rate on oscillation profiles was hypothesized to be the potential synchronization of the growth rhythms of the mother and daughter cells. However, reliable techniques that can effectively characterize and distinguish the

mother and daughter cells under the VHG condition need to be developed to support this mechanistic analysis.

3. In addition to attenuation using modified bioreactor designs, process intervention based on dynamic simulation is another strategy, which might be more suitable for large scale ethanol fermentation processes in which fermentors with working volumes of thousands of cubic meters are used. These fermentors are likely too large to be packed and operated economically. Although some preliminary work has been done in this thesis, a more universal kinetic and dynamic model that can be used to predict and simulate the process under various conditions is still not available, because of the complexity and remaining uncertainty of the mechanisms triggering and affecting the oscillations. More work is needed to further elucidate the mechanisms and develop mathematical models to correlate the corresponding mechanistic analysis, which could then be used to develop control strategies using dilution rate adjustment, for example.

References

- Ahrens K, Menzel K, Zeng AP, Deckwer WD (1998) Kinetic, dynamic, and pathway studies of glycerol metabolism by *Klebsiella pneumoniae* in anaerobic continuous culture: III. Enzyme and fluxes of glycerol dissimilation and 1,3-propanediol formation. *Biotechnol Bioeng*, 59: 544-552.
- Aiba S, Shoda M, Nagatani M (1968) Kinetics of product inhibition in alcohol fermentation. *Biotechnol Bioeng*, 10: 845-864.
- Alfenore S, Cameleyre X, Benbadis L, Bideaux C, Uribelarrea JL, Goma G, Molina-Jouve C, Guillouet SE (2004) Aeration strategy: a need for very high ethanol performance in *Saccharomyces cerevisiae* fed-batch process, *Appl Microbiol Biotechnol*, 63, 537-542.
- Amin G, Doelle HW, Greefield PF (1987) Ethanol production from sucrose by immobilized *Zymomonas mobilis* cells in polyurethane foam, *Biotechnol Lett*, 9, 225-228.
- Andrews JF (1968) A mathematical model for the continuous culture of micro-organisms utilizing inhibitory substrates. *Biotechnol. Bioeng*, 10: 707–723.
- Bai FW, Chen LJ, Anderson WA and Moo-Young M (2004a) Parameter oscillations in very high gravity medium continuous ethanol fermentation and their attenuation on multi-stage packed column bioreactor system. *Biotechnol Bioeng*, 88: 558-566.
- Bai FW, Chen LJ, Zhang Z, Anderson WA and Moo-Young M (2004b) Continuous ethanol production and evaluation of yeast cell lysis and viability loss under very high gravity medium conditions, *J Biotechnol*, 110: 287-293.
- Bailey JE, Ollis DF (1986) *Biochemical engineering fundamentals*, 2nd, McGraw-Hill Book

Company, Singapore

Bailey JE (1991) Toward a science of metabolic engineering. *Sciences*, 252, 1668-1675.

Bayrock DP, Ingledew WM (2001) Application of multistage continuous fermentation for production of fuel alcohol by very-high-gravity fermentation technology, *J Indust. Microbiol. Technol*, 27: 87-93.

Bazua CD, Wilke CR (1977) Ethanol effects on kinetics of a continuous fermentation with *Saccharomyces-cerevisiae*. *Biotechnol Bioeng Symp*, 7: 105-118.

Bellgardt KH (1994a) Analysis of synchronous growth of yeast. Part I: Development of a theoretical model for sustained oscillations. *J Biotechnol*, 35: 19-33.

Bellgardt KH (1994b) Analysis of synchronous growth of yeast. Part II: Comparison of model prediction and experimental data. *J Biotechnol*, 35: 35-49.

Beuse M, Bartling R, Kopmann A, Diekmann H, Thoma M (1998) Effect of the dilution rate on the mode of oscillation in continuous cultures of *Saccharomyces cerevisiae*. *J. Biotechnol.*, 61: 15-31.

Beuse M, Kopmann A, Diekmann H, Thoma M (1999) Oxygen, pH value, and carbon source induced changes of the mode of oscillation in synchronous continuous culture of *Saccharomyces cerevisiae*. *Biotechnol. Bioeng.*, 63: 410-417.

Boon B, Laudelout H (1962) Kinetics of nitrite oxidation by *Nitrobacter winogradskyi*. *Biochem J*, 85: 440-447.

Borzani W (2001) Variation of the ethanol yield during oscillatory concentrations changes in undisturbed continuous ethanol fermentation of sugar-cane blackstrap molasses. *World J Microbiol Biotechnol*, 17: 253-258.

- Bothast RJ, Schlicher MA (2005) Biotechnological processes for conversion of corn into ethanol. *Appl Microbiol Biotechnol*, 67: 19-25.
- Bruce LJ, Axford DB, Ciszek B, Daugulis AJ (1991) Extractive fermentation by *Zymomonas mobilis* and the control of oscillatory behavior. *Biotechnol Lett*, 13: 291-296.
- Bungay HR. Confessions of a bioenergy advocate. *Trends Biotechnol* 2004; 22: 67-71.
- Cartwright CP, Veazey FJ, Rose AH (1987) Effect of ethanol on activity of the plasma-membrane ATPase in and accumulation of glycine by *Saccharomyces cerevisiae*. *J Gen Microbiol*, 133: 857-865.
- Casey GP, Ingledew WM (1986) Ethanol tolerance in yeasts. *Crit Rev Microbiol*, 13: 219-280.
- Chen CI, McDonald KA (1990a) Oscillatory behavior of *Saccharomyces cerevisiae* in continuous culture: I. Effects of pH and nitrogen levels. *Biotechnol. Bioeng*, 36: 19-27.
- Chen CI, McDonald KA (1990b) Oscillatory behavior of *Saccharomyces cerevisiae* in continuous culture: II. Analysis of cell synchronization and metabolism. *Biotechnol. Bioeng*, 36: 28-38.
- Chen LJ, Xu YL, Bai FW, Anderson WA, Moo-Young M (2005) Observed quasi-steady kinetics of yeast cell growth and ethanol formation under very high gravity fermentation condition. *Biotechnol Bioproc Eng*, 10: 115-121.
- Converti A, Perego P, Borghi MD, Parisi F, Ferraiolo G (1986) Kinetic considerations about the study of alcoholic fermentations of starch hydrolysate. *Biotechnol Bioeng*. 28: 711-717.

- Conway T (1992) The Entner-Doudoroff pathway: history, physiology and macular biology. FEMS Microbiol Rev, 103: 1-28.
- Cysewski GR, Wilke CR (1977) Rapid ethanol fermentations using vacuum and cell recycle. Biotechnol Bioeng, 19: 1125-1143.
- D'Amore T, Stewart GG (1987) Ethanol tolerance of yeast. Enzyme Microb Technol, 9: 322-330.
- Danø S, Sørensen PG, Hynne F (1999) Sustained oscillations in living cells. Nature, 402: 320-322.
- Daugulis AJ, McLellan PJ, Li J (1997) Experimental investigation and modeling of oscillatory behavior in the continuous culture of *Zymomonas mobilis*. Biotechnol Bioeng, 56: 99-105.
- Desimone MF, Degrossi J, D'Aquino M, Diaz LE (2002) Ethanol tolerance in free and sol-gel immobilized *Saccharomyces cerevisiae*, Biotechnol Lett, 24: 1557-1559.
- Devantier R, Pedersen S, Olsson L (2005) Characterization of very high gravity ethanol fermentation of corn mash, effect of glucoamylase dosage, pre-saccharification and yeast strain. Appl Microbiol Biotechnol, 68: 622-629.
- Devantier R, Scheithauer B, Villas-Boas SG, Pedersen S, Olsson L (2005) Metabolite profiling for analysis of yeast stress response during very high gravity ethanol fermentation. Biotechnol Bioeng, 90: 703-714.
- Devore J and Farnum N (1999) Chapter 11 Inferential methods in regression and correlation, Applied statistics for engineers and sciences, Duxbury Press, USA
- Duboc P, Marison I, Stockar U (1996) Physiology of *Saccharomyces cerevisiae* during cell

cycle oscillations. J. Biotechnol., 51: 57-72.

Fieschko J, Humphrey RE (1983) Effects of temperature and ethanol concentration on the maintenance and yield coefficient of *Zymomonas mobilis*. Biotechnol Bioeng, 25, 1655-1660.

Ge XM, Zhao XQ, Bai FW (2005) Online monitoring and characterization of flocculating yeast cell flocs during continuous ethanol fermentation. Biotechnol Bioeng, 90, 523-531.

Ge XM, Zhang L, Bai FW (2006a) Impacts of temperature, pH, divalent cations, sugars and ethanol on the flocculating of SPSC01. Enzyme Microbial Technol, 39, 783-787.

Ge XM, FW Bai (2006b) Intrinsic kinetics of continuous ethanol fermentation using a self-flocculating fusant yeast strain SPSC01. J Biotechnol, 124, 363-372.

Ge XM, Zhang L, Bai FW (2006c) Impact of the floc size distributions on observed substrate uptake and product formation rates. Enzyme Microbial Technol, 39, 289-295.

Ghommidh C, Vaija J, Bolarinwa S, Navarro JM (1989) Oscillatory behavior of *Z. mobilis* in continuous cultures: a simple stochastic model. Biotechnol Letts, 11: 659-664.

Ghose TK, Roychoudhury PK, Ghosh P (1983) Simultaneous saccharification and fermentation (SSF) of lignocellulosics to ethanol under vacuum cycling and step feeding. Biotechnol Bioeng, 16: 377-381.

Ghosh A, Chance B (1964) Oscillations of glycolytic intermediates in yeast cells. Biochem Biophys Res Commun, 16: 174-181.

Ghosh A, Chance B, Pye EK (1971) Metabolic coupling and synchronization of NADH

- oscillations in yeast cell populations. Arch Biochem Biophys, 145: 319-331.
- Goffeau A, Barrell BG, Bussey H et al.(1996) Life with 6000 genes. Science, 274: 546-567.
- Groot WJ, Sikkenk CM, Waldram RH, van der Lans RGJM, Luyben KchAM (1992a)
Kinetics of ethanol production by baker's yeast in an intergrated process of fermentation and microfiltration. Biopro Eng, 8: 39-47.
- Groot WJ, Kraayenbrink MR, Waldram RH, van der Lans RGJM, Luyben KchAM (1992b)
Ethanol production in an integrated process of fermentation and ethanol recovery by pervaporation. Bioprocess Eng, 8: 99-111.
- Guijarro JM, Lagunas R (1984) *Saccharomyces cerevisiae* does not accumulate ethanol against a concentration gradient. J Bacteriol, 160: 874-878.
- Hartwell LH, Unger MW (1977) Unequal division in *Saccharomyces cerevisiae* and its implications for the control of cell division. J Cell Biol, 75: 422-435.
- Ho NWY, Chen Z, Brainard AP (1998) Genetically engineered *S. cerevisiae* capable of effective cofermentation of glucose and xylose. Appl Environ Microbiol, 64: 1852-1859.
- Holzberg I, Finn RK, Steinkraus KH (1967) A kinetic study of the alcoholic fermentation of grape juice. Biotechnol Bioeng, 9: 413-427.
- Hu CK, Bai FW, An LJ (2005) Effect of the flocculating of a self-flocculating yeast on its ethanol tolerance and corresponding mechanisms, Chinese J Biotechnol, 21: 123-128.
- Huang SY, Chen JC (1988) Analysis of the kinetics of ethanol fermentation with *Zymomonas mobilis* considering temperature effect. Enzyme Microb Technol, 10: 431-439.

- Ikegami T, Yanagishita H, Kitamoto D, Negishi H, Haraya K, Sano T (2002) Concentration of fermented ethanol by pervaporation using silicalite membranes coated with silicone rubber, *Desalination*, 149: 49-54.
- Ingledeu WM (1999) Alcohol production by *Saccharomyces cerevisiae*: a yeast primer. In *The alcohol textbook*, 3rd, Nottingham University Press, UK.
- Jarzebski AB (1992) Modeling of oscillatory behavior in continuous ethanol fermentation. *Biotechnol Lett*, 14: 137-142.
- Jirku V (1999) Whole cell immobilization as a means of enhancing ethanol tolerance. *J Ind Microbiol Biotechnol*, 22: 147-151.
- Jöbses IML, Egberts GTC, Luyben KCAM, Roels JA (1986) Fermentation kinetics of *Zymomonas mobilis* at high ethanol concentrations: oscillations in continuous cultures. *Biotechnol Bioeng*, 18: 868-877.
- Jones RP (1989) Biological principles for the effects of ethanol. *Enzyme Microb Technol*, 11: 130-153.
- Jones RP, Ingledeu WM (1994a) Fuel ethanol production: appraisal of nitrogenous yeast foods for very high gravity wheat mash fermentation. *Process Biochem*, 29: 483-488.
- Jones AM, Ingledeu WM (1994b) Fuel alcohol production: assessment of selected commercial proteases for very high gravity wheat mash fermentation. *Enzyme Microbiol Technol*, 16: 683-687.
- Jones AM, Ingledeu WM (1994c) Fuel alcohol production: optimizing of temperature for efficient very-high-gravity fermentation. *Appl Environ Microbiol*, 60: 1048-1051.
- Kelsall DR, Lyons TP (1999) Grain dry milling and cooking for alcohol production:

designing for 23% ethanol and maximum yield. In The alcohol textbook, 3rd, Nottingham University Press, UK.

Kierstan M, Bucke C (1977) The immobilization of microbial cells, subcellular organells, and enzyme in calcium alginate gels. *Biotechnol Bioeng*, 14: 387-397.

Larue F, Lafon-Lafourcade S, Ribereau-Gayon P (1984) Relationship between the inhibition of alcoholic fermentation by *Saccharomyces cerevisiae* and the activities of hexokinase and alcohol dehydrogenase. *Biotechnol Lett*. 6: 687-692

Lee CW, Chang HN (1987) Kinetics of ethanol fermentation in membrane cell recycle fermentor. *Biotechnol Bioeng*, 29: 1105-1112.

Lee JH, Woodard JC, Pagan RJ (1981) Vacuum fermentation for ethanol production using strains of *Z. mobilis*. *Biotechnol Lett*, 3: 177-182.

Lee KJ, Tribe DE, Rogers PL (1979) Ethanol production by *Zymomonas mobilis* in continuous culture at high glucose concentrations. *Biotechnol Lett*, 1: 421-426.

Levenspiel O (1980) The Monod equation: A revisit and a generalization to product inhibition situations. *Biotechnol Bioeng*, 22: 1671-1687.

Levenspiel O (1999) The tanks-in-series models, In chemical reaction engineering, 3rd, New York, John Wiley & Sons.

Li J, McLellan PJ, Daugulis AJ (1995) Inhibition effects of ethanol concentration history and ethanol concentration change rate on *Zymomonas mobilis*. *Biotechnol Lett*, 17: 321-326.

Lin YH, Bayrock DP, Ingledew WM (2002) Evaluation of *Saccharomyces cerevisiae* grown in a multi-stage chemosta environment under increasing levels of glucose. *Biotechnol*

Lett, 24: 449-453.

Lorenz O, Haulena F, Rose G (1987) Immobilization of yeast cells in polyurethane ionomers. *Biotechnol Bioeng*, 29, 388-391.

Luong JHT (1985) Kinetics of ethanol inhibition in alcohol fermentation. *Biotechnol Bioeng*, 17: 280-285.

Madigan MT, Martinko JM, Parker J (2000) Nutrition and metabolism. In: Brock biology of microbiology, 9rd, Prentice-Hall, NJ.

Madsen MF, DanøS, Sørensen PG (2005) On the mechanisms of glycolytic oscillations in yeast. *FEBS J*, 272: 2648-2660.

Menzel K, Zeng AP, Biebl H, Deckwer WD (1996) Kinetic, dynamic, and pathway studies of glycerol metabolism by *Klebsiella pneumoniae* in anaerobic continuous culture: I the phenomena and characterization of oscillation and hysteresis, *Biotechnol Bioeng*, 52: 549-560.

Menzel K, Ahrens K, Zeng AP, Deckwer WD (1998) Kinetic, dynamic, and pathway studies of glycerol metabolism by *Klebsiella pneumoniae* in anaerobic continuous culture: IV. Enzyme and fluxes of pyruvate metabolism, *Biotechnol Bioeng*, 60: 617-626.

McLellan PJ, Daugulis AJ, Li J (1999) The incidence of oscillatory behavior in the continuous fermentation of *Zymomonas mobilis*. *Biotechnol Prog*, 15: 667-680.

Moo-Young M, Lamptey J, Robinson CW (1980) Immobilization of yeast cells on various supports for ethanol fermentation. *Biotechnol Lett*. 2: 541-548.

Nagashima M, Azuma M, Noguchi S, Inuzuka K, Samejima H (1984) Continuous ethanol

fermentation using immobilized yeast cells. *Biotechnol Bioeng.* 26: 992-9977.

Nagodawithana TW, Steinkraus KH (1976) Influence of the rate of ethanol production and accumulation on the viability of *Saccharomyces cerevisiae* in rapid fermentation. *Appl Environ Microbiol*, 31: 158-162.

O'Brien DJ, Craig JC (1996) Ethanol production in a continuous fermentation membrane pervaporation system. *Appl Microbiol Biotechnol*, 44: 699-704.

O'Brien DJ, Roth LH, McAloon AJ (2000) Concentration of fermented ethanol by pervaporation using silicalite membranes coated with silicone rubber: a preliminary economic analysis. *J Membr Sci*, 166: 105-111.

Pascual C, Alonso A, Garcia I, Roman C, Kotyk A (1988) Effect of ethanol on glucose transport, key glycolytic enzymes, and proton extrusion in *Saccharomyces cerevisiae*. *Biotechnol Bioeng*, 32: 374-378.

Patnaik PR (2003) Oscillatory metabolism of *Saccharomyces cerevisiae*: an overview of mechanisms and models. *Biotechnol. Adv.*, 21: 183-192.

Porto MM, Lafforgue C, Strehaiano P, Goma G (1987) Fermentation coupled with microfiltration: kinetics of ethanol fermentation with cell cycle. *Biopro Eng*, 2: 65-68.

Rasch, M. et al., (2002) Characterization and modeling of oscillatory behavior related to reuterin production by *Lactobacillus reuteri*. *Int. J. Food Microbiol.*, 73: 383-394.

Reddy LVA, Reddy OVS (2005) Improvement of ethanol production in very high gravity fermentation by horse gram (*Dolichos biflorus*) flour supplementation. *Lett Appl Microbiol*, 41: 440-444.

Reddy LVA, Reddy OVS (2006) Rapid and enhanced production of ethanol in very high

- gravity (VHG) sugar fermentation by *Saccharomyces cerevisiae*: role of finger millet (*Eleusine coracana L*) flour. *Process Biochem*, 41: 726-729.
- Roffler SR, Blanch HW, Wilke CR (1984) *In situ* recovery of fermentation products. *Trends Biotechnol*, 2: 129-136.
- Rosa MF, Sá-Correia I (1992) Ethanol tolerance and activity of plasma membrane ATPase in *Kluyveromyces marxianus* and *Saccharomyces cerevisiae*. *Enzyme Microb Technol*, 14: 23-27.
- Ryu DDY, Kim YJ, Kim JH (1984) Effect of air supplement on the performance of continuous ethanol fermentation system. *Biotechnol Bioeng*, 26: 12-16.
- Salguerio SP, Sá-Correia I, Novais JM (1988) Ethanol induced-leakage in *Saccharomyces cerevisiae*: kinetics and relationship to yeast ethanol tolerance and alcohol fermentation productivity. *Appl Environ Microbiol*, 54: 903-909.
- Sprenger GA (1996) Carbohydrate metabolism in *Zymomonas mobilis*: a catabolic highway with some scenic routes. *FEMS Microbiol Lett*, 145: 301-307.
- Stevsberg N, Lawfors HG, Martin N, Beveridge T (1986) Effect of growth temperature on the morphology and performance of *Z. mobilis* ATCC 29191 in batch and continuous culture. *Appl Microbiol Biotechnol*, 25: 116-123.
- Swings J, Deley J (1977) The biology of *Zymomonas mobilis*. *Bacteriol Rev*, 41: 1-46.
- Taylor F, Kurantz MJ, Goldberg N, McAloon AJ, Craig JC (2000) Dry-grind process for fuel ethanol by continuous fermentation and stripping. *Biotechnol Prog*, 16: 541-547.

- Thatipamala R, Rohani S, Hill GA (1992) Effects of high product and substrate inhibitions on the kinetics and biomass and product yields during ethanol batch fermentation. *Biotechnol Bioeng.* 40: 289-297.
- Thomas KC, Ingledew WM (1992) Production of 21% (v/v) ethanol by fermentation of very high gravity (VHG) wheat mashes. *J Ind Microbiol*, 10: 61-68.
- Thomas KC, Ingledew WM (1990) Fuel alcohol production: effects of free amino nitrogen on fermentation of very-high-gravity wheat mash. *Appl Environ Microbiol*, 56: 2046-2050.
- Thomas KC, Hynes SH, Ingledew WM (1996) Practical and theoretical considerations in the production of high concentration of alcohol by fermentation. *Process Biochem*, 31: 321-331.
- Thomas KC, Hynes SH, Ingledew WM (1994) Effects of particulate materials and osmoprotectants on very-high-gravity ethanolic fermentation. *Appl Environ Microbiol*, 60: 1519-1524.
- Wolf J, Heinrich R (2000) Effect of cellular interaction on glycolytic oscillations in yeast: a theoretical investigation. *Biochem J*, 345: 321-334.
- Yang RYK, Su J (1993) Improvement of chemostat performance via nonlinear oscillations. Part I: Operation strategy. *Biopro Eng*, 9, 97-102.
- You KM, Rosenfield CL, Knipple DC (2003) Ethanol tolerance in the yeast *Saccharomyces cerevisiae* is dependent on cellular oleic acid content. *Appl Environ Microbiol*, 69: 1499-1503.

Zeng AP, Menzel K, Deckwer WD (1996) Kinetic, dynamic, and pathway studies of glycerol metabolism by *Klebsiella pneumoniae* in anaerobic continuous culture: II. Analysis of metabolic rates and pathway under oscillation and steady-state conditions, *Biotechnol Bioeng*, 52: 561-571

Appendixes

Appendix A: Evaluation of ethanol yield under oscillations

Ethanol yield was calculated based on the experimental data illustrated in Figure 3.2 and illustrated in Appendixes table A.

Appendixes table A

Day	CSTR	TB1	TB2	TB3	Day	CSTR	TB1	TB2	TB3
0	0.443	0.430	0.450	0.438	20	0.416	0.427	0.431	0.450
1	0.452	0.431	0.430	0.438	21	0.432	0.423	0.432	0.442
2	0.427	0.430	0.430	0.454	22	0.447	0.422	0.428	0.438
3	0.425	0.428	0.430	0.435	23	0.443	0.430	0.429	0.438
4	0.431	0.422	0.427	0.413	24	0.433	0.426	0.430	0.437
5	0.408	0.421	0.428	0.443	25	0.429	0.422	0.428	0.432
6	0.419	0.430	0.428	0.424	25	0.423	0.425	0.429	0.431
7	0.456	0.429	0.430	0.427	27	0.421	0.435	0.427	0.423
8	0.457	0.428	0.428	0.430	28	0.428	0.415	0.433	0.425
9	0.448	0.425	0.428	0.429	29	0.442	0.425	0.432	0.425
10	0.451	0.425	0.428	0.418	30	0.442	0.426	0.432	0.424
11	0.441	0.423	0.428	0.422	31	0.451	0.425	0.429	0.424
12	0.432	0.425	0.428	0.422	32	0.453	0.429	0.430	0.427
13	0.441	0.421	0.429	0.422	33	0.445	0.425	0.430	0.432
14	0.449	0.425	0.431	0.436	34	0.439	0.420	0.429	0.437
15	0.442	0.425	0.430	0.440	35	0.444	0.416	0.428	0.435
16	0.429	0.425	0.431	0.447	36	0.419	0.418	0.430	0.443
17	0.411	0.418	0.430	0.445	37	0.426	0.423	0.429	0.444
18	0.410	0.423	0.430	0.450	38	0.429	0.425	0.431	0.443
19	0.413	0.429	0.439	0.449	39	0.441	0.422	0.428	0.443

Appendix B: Validation of the reproducibility of oscillations

In order to validate the reproducibility of the oscillatory behaviors, the averages, oscillation peaks and troughs were compared for the CSTR and the tubular bioreactors based on the experimental data independently collected, as illustrated in Appendixes table B.

Appendixes table B

Bioreactors		Glucose/ethanol oscillation averages g l^{-1}	Glucose/ethanol oscillation peaks g l^{-1}	Glucose/ethanol oscillation troughs g l^{-1}
CSTR	Fig.3.2 (40 days' duration)	117.2/70.3	129.7/76.1	106.3/64.4
	Tab. 7.3 (20 day's duration)	113.1/75.1	130.0/82.4	98.0/66.9
1st TB	Fig.3.3 (40 days' duration)	60.1/93.4	78.1/98.9	50.0/85.1
	Figs.6.2-6.3 (30 days' duration)	63.2/91.0	78.0/100.1	49.0/83.7
2nd TB	Fig.3.4 (40 days' duration)	31.7/106.8	45.0/114.0	20.2/100.4
	Figs.6.2-6.3 (30 days' duration)	35.0/105.2	47.0/112.0	23.0/100.4
3rd TB	Fig.3.5 (40 days' duration)	17.9/113.9	31.8/121.9	8.3/105.4
	Figs.6.2-6.3 (30 days' duration)	17.8/113.5	26.0/122.4	6.0/107.9

Appendix C: Mathematical Derivation of Equations (7.23) and (7.26)

$$\Omega = \int_{-\infty}^t \mu(t) \Big|_{t=\tau} \cdot \theta(\tau) d\tau \quad (7.17)$$

$$\theta(\tau) = \omega^2 (t - \tau) \cdot e^{-\omega(t-\tau)} \quad (7.19)$$

Substituting Equation (7.19) into Equation (7.17):

$$\begin{aligned} \Omega &= \int_{-\infty}^t \mu(\tau) \cdot \omega^2 (t - \tau) \cdot e^{-\omega(t-\tau)} d\tau \\ &= \omega^2 \cdot e^{-\omega t} \cdot \int_{-\infty}^t \mu(\tau) \cdot (t - \tau) \cdot e^{\omega\tau} d\tau \\ &= \omega^2 \cdot e^{-\omega t} \cdot \int_{-\infty}^t [\mu(\tau) \cdot e^{\omega\tau} \cdot t - \mu(\tau) \cdot e^{\omega\tau} \cdot \tau] d\tau \\ &= \omega^2 \cdot e^{-\omega t} \cdot \left[t \cdot \int_{-\infty}^t \mu(\tau) \cdot e^{\omega\tau} d\tau - \int_{-\infty}^t \mu(\tau) \cdot e^{\omega\tau} \cdot \tau d\tau \right] \\ \frac{d\Omega}{dt} &= \omega^2 \cdot (-\omega) \cdot e^{-\omega t} \cdot \left[t \cdot \int_{-\infty}^t \mu(\tau) \cdot e^{\omega\tau} d\tau - \int_{-\infty}^t \mu(\tau) \cdot e^{\omega\tau} \cdot \tau d\tau \right] \\ &\quad + \omega^2 \cdot e^{-\omega t} \cdot \frac{d \left[t \cdot \int_{-\infty}^t \mu(\tau) \cdot e^{\omega\tau} d\tau - \int_{-\infty}^t \mu(\tau) \cdot e^{\omega\tau} \cdot \tau d\tau \right]}{dt} \\ &= \omega^2 \cdot (-\omega) \cdot e^{-\omega t} \left[t \cdot \int_{-\infty}^t \mu(\tau) \cdot e^{\omega\tau} d\tau - \int_{-\infty}^t \mu(\tau) \cdot e^{\omega\tau} \cdot \tau d\tau \right] \\ &\quad + \omega^2 \cdot e^{-\omega t} \cdot \left[\int_{-\infty}^t \mu(\tau) \cdot e^{\omega\tau} d\tau + t \cdot \mu(t) \cdot e^{\omega t} - \mu(t) \cdot e^{\omega t} \cdot t \right] \\ &= \omega^2 \cdot (-\omega) \cdot e^{-\omega t} \cdot \left[t \cdot \int_{-\infty}^t \mu(\tau) \cdot e^{\omega\tau} d\tau - \int_{-\infty}^t \mu(\tau) \cdot e^{\omega\tau} \cdot \tau d\tau \right] \\ &\quad + \omega^2 \cdot e^{-\omega t} \cdot \int_{-\infty}^t \mu(\tau) \cdot e^{\omega\tau} d\tau \\ &= (-\omega) \cdot \left[\int_{-\infty}^t \omega^2 \cdot (t - \tau) \cdot \mu(\tau) \cdot e^{-\omega(t-\tau)} \cdot d\tau \right] + \omega \cdot \int_{-\infty}^t \mu(\tau) \omega \cdot e^{-\omega(t-\tau)} d\tau \\ &= -\omega \cdot \Omega + \omega \cdot V_G \\ &= \omega(V_G - \Omega) \end{aligned} \quad \dots\dots\dots(7.23)$$

where

$$V_G = \int_{-\infty}^t \mu(\tau) \cdot \sigma(\tau) d\tau \quad (7.24)$$

$$\sigma(\tau) = \omega \cdot e^{-\omega(t-\tau)} \quad (7.25)$$

Similarly, for Equations (7.24) and (7.25), substituting Equation (7.25) into Equation (7.24):

$$\begin{aligned} V_G &= \int_{-\infty}^t \mu(\tau) \cdot \omega \cdot e^{-\omega(t-\tau)} d\tau \\ &= \int_{-\infty}^t \mu(\tau) \cdot \omega \cdot e^{-\omega t} \cdot e^{\omega\tau} d\tau \\ &= \omega \cdot e^{-\omega t} \cdot \int_{-\infty}^t \mu(\tau) \cdot e^{\omega\tau} d\tau \end{aligned}$$

and

$$\begin{aligned} \frac{dV_G}{dt} &= \omega \cdot \left\{ (-\omega) \cdot e^{-\omega t} \cdot \int_{-\infty}^t \mu(\tau) \cdot e^{\omega\tau} d\tau + e^{-\omega t} \cdot \frac{d\left[\int_{-\infty}^t \mu(\tau) \cdot e^{\omega\tau} d\tau\right]}{dT} \right\} \\ &= \omega \cdot \left\{ -\int_{-\infty}^t \omega \cdot \mu(\tau) \cdot e^{-\omega(t-\tau)} d\tau + e^{-\omega t} \cdot \mu(t) \cdot e^{\omega t} \right\} \\ &= \omega[\mu(t) - V_G] \end{aligned}$$

(7.26)

Appendix D: MATLAB Programs

D1 Evaluation of Pseudo-steady State Kinetic Parameters

```
function f = cal_Mu(x)
global Mu_final;
global Mu_exp;
global S;
global P;

Pm = 167;

Mu_max = x(1);
Ks = x(2);
Ki = x(3);
Mu0 = x(4);
alf = x(5);

Mu_cal = (Mu_max.*S./(Ks+S+S.^2./Ki)).*(1-P/Pm).^alf;

for i = 1:length(S)
    if S(i)<=Ks
        Mu_cal(i) = Mu_cal(i)+Mu0;
    end
end

f = Mu_cal-Mu_exp;
```

```
Mu_final = Mu_cal;
```

```
-----
```

```
function find_parameters_Mu
```

```
global Mu_final;
```

```
global Mu_exp;
```

```
global S;
```

```
global P;
```

```
Mu_exp = [0.027  0.05  0.083  0.1 0.116  0.14  0.027  0.04  
0.067  0.1 0.12  0.146  0.018  0.027  0.053  0.08  0.106];
```

```
S = [0  0.14  17.3  20.2  32.5  44.7  36.5  61.4  86.8  
110.7  118.8  129 96.8  117.2  143.9  175.3  213.2];
```

```
P = [58.2  52.2  44.3  40.8  38.4  32.5  82.5  68.3  56.8  
41.3  37.3  32.1  82.5  76  65.2  45.2  31.5];
```

```
Mu_max_0 = 0.5;
```

```
Ks_0 = 10;
```

```
Ki_0 = 300;
```

```
Mu0_0 = 0.027;
```

```
alf_0 = 4;
```

```
parameter0 = [Mu_max_0; Ks_0; Ki_0; Mu0_0; alf_0];
```

```

[parameters,resnorm,residual,exitflag,output,lambda,jacobian]=
lsqnonlin(@cal_Mu,parameter0,[0.01,0.1,100,0,0],[1,100,10000,0.04,
10]);

%Show results =====
Mu_max__and__confidence_interval=parameters(1)
Ks__and__confidence_interval=parameters(2)
Ki__and__confidence_interval=parameters(3)
Mu0__and__confidence_interval=parameters(4)
alf__and__confidence_interval=parameters(5)

plot(Mu_exp,Mu_final,'o');

r2=corr2(Mu_exp,Mu_final)^2

%Mu_max_0=0.5; Ks_0=10; Ki_0=300; Mu0_0=0.027; alf_0=4;
%Mu_max__and__confidence_interval = 0.4617  0.2792  0.6442
%Ks__and__confidence_interval = 10.7818  -1.2452  22.8087
%Ki__and__confidence_interval = 293.2348  6.1898  580.2798
%Mu0__and__confidence_interval = 0.0378  0.0259  0.0496
%alf0__and__confidence_interval = 3.8552  3.2571  4.4534
%r2 = 0.9744

```

```

function f = cal_v(x)
global v_final;
global v_exp;
global S;
global P;

Pm = 167;

vmax = x(1);
Ks = x(2);
Ki = x(3);
v0 = x(4);
beta = x(5);

v_cal = (vmax.*S./(Ks+S+S.^2./Ki)).*(1-P/Pm).^beta;

for i = 1:length(S)
    if S(i)<=2*Ks
        v_cal(i)=v_cal(i)+v0;
    end
end

f = v_cal-v_exp;
v_final = v_cal;

```

```

function find_parameters_v
global v_final;
global v_exp;
global S;
global P;

v_exp = [0.248  0.351  0.741  0.863  0.962  1.076  0.557  0.569
0.827  1.007  1.017  1.172  0.401  0.513  0.804  1.004
0.954];

S = [0  0.14  17.3  20.2  32.5  44.7  36.5  61.4  86.8
110.7  118.8  129 96.8  117.2  143.9  175.3  213.2];

P = [58.2  52.2  44.3  40.8  38.4  32.5  82.5  68.3  56.8
41.3  37.3  32.1  82.5  76  65.2  45.2  31.5];

vmax_0 = 1.5; Ks_0 = 30; Ki_0 = 2000; v0_0 = 0.248; beta_0 = 1;

parameter0 = [vmax_0; Ks_0; Ki_0; v0_0; beta_0];

[parameters,resnorm,residual,exitflag,output,lambda,jacobian]=
lsqnonlin(@cal_v,parameter0,[0.1,1,1000,0,0],[10,100,1000000,0.4,1
0]);

%Show results =====
vmax__and__confidence_interval=parameters(1)

```

```

Ks__and__confidence_interval=parameters(2)
Ki__and__confidence_interval=parameters(3)
v0__and__confidence_interval=parameters(4)
beta__and__confidence_interval=parameters(5)

plot(v_exp,v_final,'o');
r2=corr2(v_exp,v_final)^2

%vmax_0=1.5; Ks_0=30; Ki_0=2000; v0_0=0.248; beta_0=1;
%vmax__and__confidence_interval = 1.9487 0.8206 3.0769
%Ks__and__confidence_interval = 22.9544 -8.4374 54.3461
%Ki__and__confidence_interval = 0.1813*1.0e+004 -0.7791*1.0e+004
1.1416*1.0e+004
%v0__and__confidence_interval = 0.2459 0.1250 0.3667
%beta__and__confidence_interval = 1.6583 1.1465 2.1702
%r2 = 0.9289

```

D2 Dynamic Simulations

```
function f = odeoscillation(t,y)
```

```
global w;
```

```
global Mu_max;
```

```
global Ks;
```

```
global Ki;
```

```
global U0;
```

```
global Pm;
```

```
global alf;
```

```
global Qpmax;
```

```
global Ksp;
```

```
global Kip;
```

```
global Q0;
```

```
global beta;
```

```
global D;
```

```
global S0;
```

```
global Yps;
```

```
X = y(1);
```

```
S = y(2);
```

```
P = y(3);
```

```

Z = y(4);
V = y(5);
Zp = y(6);
Vp = y(7);

Mu = (Mu_max*S/(Ks+S+S^2/Ki))*(1-P/Pm)^alf+U0;
Qp = (Qpmax*S/(Ksp+S+S^2/Kip))*(1-P/Pm)^beta+Q0;

g(1) = (Z-D)*X;
g(2) = (S0-S)*D-Zp*X/Yps;
g(3) = Zp*X-D*P;
g(4) = w*(V-Z);
g(5) = w*(Mu-V);
g(6) = w*(Vp-Zp);
g(7) = w*(Qp-Vp);

f = g';

-----

function f = show_oscillation(x)

global w;

global y_final;
global t_exp;
global S_exp;

```

```

global P_exp;
global X_exp;

w = x(1);

t0 = x(2);

X0 = x(3);
S0 = x(4);
P0 = x(5);

Z = 0;
V = 0;
Zp = 0;
Vp = 0;

y0 = [X0; S0; P0; Z; V; Zp; Vp];

t_left = [t0:2:-2];
t = [t_left, t_exp];

[t, y] = ode113(@odeoscillation, t, y0);

ya = length(t_left)+1;
yb = length(y);
fx = X_exp'-y(ya:yb,1);

```

```

fs = S_exp'-y(ya:yb,2);
fp = P_exp'-y(ya:yb,3);

weight_x = 92;
%Determined according to values of S, P and X
weight_s = 3.2;
%Determined according to values of S, P and X
weight_p = 4.8;
%Determined according to values of S, P and X

f = [weight_x*fx; weight_s*fs; weight_p*fp];

y_final=y;

```

```

-----

function optimum_oscillation
global y_final;
global t_exp;
global S_exp;
global P_exp;
global X_exp;
global Mu_max;
global Ks;
global Ki;
global U0;
global Pm;

```

```
global alf;
global Qpmax;
global Ksp;
global Kip;
global Q0;
global beta;
global D;
global S0;
global Yps;

Mu_max = 0.462*0.868;
% Evaluated by Function "find_parameters.m"

Ks = 10.8;
Ki = 293.2;
% Evaluated by Function "find_parameters.m"

U0=0;
% Because Cs > Ks
alf = 3.86;
Pm = 167;

Qpmax = 1.95*0.853;
% Evaluated by Function "find_parameters_v.m"
Ksp = 23.0;
Kip = 1751.7;
```

```

% Evaluated by Function "find_parameters_v.m"
Q0 = 0;
% Because Cs > 2Ks
beta = 1.66;

D = 0.027;
S0 = 280;
%Yps = 0.465;
Yps = 0.45;

t_exp = [0 24 48 72 96 120 144 168 192 216 240 264 288 312 336 360 384
408 432 456 480];

S_exp = [104.2 114.2 120.1 130.6 118.5 102.0 98.3 106.1 110.8 124.2
130.6 120.0 112.6 100.1 106.8 112.2 120.2 122.8 112.9 106.2 110.3];

P_exp = [79.0 76.7 73.8 66.9 70.1 80.3 82.4 80.4 76.4 72.0 66.9
78.5 78.5 82.1 77.0 78.1 73.1 68.3 68.0 73.7 74.8];

X_exp = [3.5 4.1 3.5 3.1 3.6 4.5 4.1 4.2 3.8 3.8 3.8 4.3 4.3
4.7 4.6 3.6 3.5 3.6 4.5 3.9 4.0];

w0 = 0.06;
t0_0 = -300;
X_0 = 10;
S_0 = 90;

```

```

P_0 = 80;

x0 = [w0, t0_0, X_0, S_0, P_0];

[x,resnorm,residual,exitflag,output,lambda,jacobian]=
lsqnonlin(@show_oscillation,x0,[0,-1000,1,1,1],[1,-1,30,150,100]);
betaci = nlparci(x,residual,jacobian);

%Show results =====
w = x(1)
confidence_interval_w = betaci(1,:)% 95% confidence interval of w

t0 = x(2);
t_left = [t0:2:-2];

y0 = [x(3);x(4);x(5);0;0;0;0];
t = [t_left,[0:10:480]];
[t,y] = ode113(@odeoscillation,t,y0);

ya = length(t_left)+1;
yb = length(y(:,1));

subplot(2,1,1);
plot([0:10:480],y(ya:yb,2),'-',t_exp,S_exp(:),'o',[0:10:480],y(ya:
yb,3),'-',t_exp,P_exp(:),'o');
xlabel('time t');

```

```
ylabel('S and P');

subplot(2,1,2);
plot([0:10:480],y(ya:yb,1),'-',t_exp,X_exp(:),'o');
xlabel('time t');
ylabel('X');

y(ya:yb,1:3)

%w = 0.0612
%confidence_interval_w = 0.0560 0.0663
```
